THE *WISE* LIGHT CURVES OF POLARS

Thomas E. Harrison[1] and Ryan K. Campbell[2]

[1] Department of Astronomy, New Mexico State University, Box 30001, MSC 4500, Las Cruces, NM 88003-8001, USA; tharriso@nmsu.edu
[2] Department of Physics & Astronomy, Humboldt State University, 1 Harpst St., Arcata, CA 95521, USA; Ryan.Campbell@humboldt.edu

ABSTRACT

We have extracted the *WISE* (Wide-field Infrared Survey Explorer) single-exposure data for a sample of 72 polars, which are highly magnetic cataclysmic variables (CVs). We combine these data with both published and unpublished optical and infrared data to explore the origins of the large amplitude variations seen in these systems. In nearly every case, we find evidence for cyclotron emission in the *WISE* bandpasses. We find that the derived magnetic field strengths for some polars are either too high, or cyclotron emission from lower field components, located spatially coincident to the main accreting poles, must be occurring. We have also estimated field strengths for a number of polars where no such values exist. In addition, contrary to expectations, we find that emission from the fundamental cyclotron harmonic ($n = 1$) appears to be nearly always present when the magnetic field is of the appropriate strength that it falls within a *WISE* bandpass. We find that the light curves for RBS 490, an ultrashort-period (46 minutes) CV, suggest that it is a polar. Modeling its spectrum indicates that its donor star is much hotter than expected. Nearly all of the detected polars show 11.5 μm ("*W*3 band") excesses. The general lack of variability seen in the *W*3 bandpass light curves for higher-field polars demonstrates that these excesses are probably not due to cyclotron emission. There is circumstantial evidence that these excesses can be attributed to bremsstrahlung emission from their accretion streams. Reduction of the *Spitzer* 24 μm image of V1500 Cyg shows that it appears to be located at the center of a small nebula.

Key words: infrared: stars – novae, cataclysmic variables – stars: magnetic field

1. INTRODUCTION

Cataclysmic variables (CVs) are short-period binary systems consisting of a white dwarf primary that is accreting material via Roche-lobe overflow from a low-mass, late-type secondary star. CVs can be divided into two main classes: magnetic and nonmagnetic. In magnetic systems, the primary white dwarf has a strong magnetic field (0.5 MG $\leqslant B \leqslant$ 240 MG). In "polars," the magnetic field of the white dwarf is strong enough to capture the accretion stream close to the secondary star. In "intermediate polars" (IPs), the magnetic field of the white dwarf is believed to be weaker ($B \leqslant 8$ MG) and is insufficient to completely prevent the formation of an accretion disk. In polars, the white dwarf and secondary star rotate synchronously with the orbital period. In IPs, the spin periods of the white dwarfs are much shorter than the orbital period. Additionally, there is a small family of "asynchronous polars" that have properties that make them more similar to polars than IPs, but in which the white dwarf spins at a slightly different rate than the orbital period.

Analyzing the *WISE* (Wide-field Infrared Survey Explorer) and *Spitzer* data for two polars observed with *Herschel*, AM Her and EF Eri, Harrison et al. (2013b) found that the midinfrared "excesses" in both systems, previously attributed to circumbinary dust emission, could be fully explained by cyclotron emission. The *WISE* light curves for both sources exhibited large, orbitally modulated variations that were similarly phased to large-amplitude variations in their near-IR light curves. Phase-resolved near-IR spectroscopy showed that the large-amplitude, periodic variations visible in the *JHK* light curves of AM Her and EF Eri arose from the changing viewing angle to their cyclotron emitting regions that occur over each orbital revolution (Campbell 2008). Harrison et al. proposed that significant emission from the lowest cyclotron harmonics ($n \leqslant 3$) must be present in both EF Eri and AM Her. The

conditions found in the accretion region of polars are such that the lowest harmonics are generally expected to be optically thick, and thus large orbital modulations would not be expected. The accretion rate in EF Eri is very low (see Schwope et al. 2007), and thus one could envision a scenario where the lowest harmonics in this polar might be optically thin. AM Her, however, was in a *high state* when observed by *WISE*, and thus the presence of a large-amplitude, orbitally modulated flux at 11.5 μm, presumably from the $n = 1$ cyclotron harmonic, was completely unexpected. This suggests that the accretion onto polars is much more complicated than assumed in many of the simple models developed for these systems.

The value of the *WISE* light curve data to explore the cyclotron emission from polars has led us to extract data for all such systems identified in the Downes et al. (2001) catalog. We combine these data with additional optical and infrared observations to examine their light curve morphologies. As we discuss below, it is often possible to constrain magnetic field strengths from multiband photometry due to the nature of cyclotron emission. In addition, the field strengths for many polars have been previously estimated, and we can use the *WISE* light curve data to ascertain whether emission from the lowest harmonics are present in some of those systems. In the next section we discuss the data sets employed in this paper, in Section 3 we discuss the results for the individual objects, and in Section 4 we present our conclusions.

2. DATA

We have used the online version of the Downes et al. (2001) catalog of CVs to construct our list of program polars. A number of the objects in this catalog are listed as having questionable classifications. In addition, some of the objects have been reclassified since the original publication of that work. To this

list we add the two systems V379 Vir and V479 And, objects that might be polars and that have interesting properties. We have searched the *WISE* and *Spitzer* databases for all of these objects. For each detected source, we examined the *WISE* images to ensure that the cataloged midinfrared point source was the true counterpart of the optically identified polar.

We have also extracted ground-based data, such as infrared observations from the Two Micron All-Sky Survey (2MASS) Point Source catalog (Skrutskie et al. 2006), the Deep Near Infrared Survey (DENIS) (*IJK* bands, Epchtein et al. 1994), and the UKIRT Infrared Deep Sky Survey (UKIDSS) (*YJHK* bands, Lawrence et al. 2007). To these we add visual wavelength data from the Sloan Digital Sky Survey (SDSS; York et al. 2000) and the AAVSO Photometric All-sky Survey (APASS; Henden & Munari 2014). In addition, we have extracted optical and infrared light curves for a number of polars from published sources to allow us to attempt to understand the *WISE* light curves. We also present new (or previously unpublished) infrared or optical photometry for several sources. To this we add phase-resolved near-infrared spectroscopy. While most of these spectroscopic data have been previously published (Campbell 2008), we re-reduced those data to attempt to improve the quality of the resultant spectra.

2.1. The WISE Observations

The *WISE* mission (Wright et al. 2010) surveyed the entire sky in four wavelength bands: 3.4, 4.6, 12, and 22 μm. The two short bandpasses ("*W1*" and "*W2*") are similar to the two short *Spitzer* Infrared Array Camera (IRAC) bandpasses (hereafter, "*S1*" and "*S2*"). The 12 μm channel ("*W3*," $\lambda_{\rm eff} = 11.56\ \mu$m), is similar to that of the *IRAS* 12 μm bandpass, and the 22 μm ("*W4*"; $\lambda_{\rm eff} = 22.09\ \mu$m) bandpass closely resembles the *Spitzer* MIPS 24 μm channel (Jarret et al. 2011). Because of the scanning nature of its orbit, every object was observed by *WISE* on at least 12 separate occasions. Thus, it is possible to generate light curves using the "single-exposure" observations from the *WISE* mission. We have extracted both the light curve data and the "AllWISE" point-source fluxes for the program polars using the IRSA website (http://irsa.ipac.caltech.edu/). Table 1 lists the AllWISE point-source catalog fluxes for the program polars whether they were detected by *WISE* or not. The objects are arranged alphabetically by variable star name if it exists, and then alphabetically by their current (survey-based) designations.

Unlike the magnitudes presented in the AllWISE point-source catalog, the single exposure source light curves can have defects due to a number of effects.[3] There are also slight offsets between the mean magnitudes derived from the single-exposure data and the final AllWISE point-source catalog fluxes, due to enhancements in the calibration of the individual light curve data used in the latter. In addition to the main four-band survey data, a small subset of the polars were observed during the "three-band Cryo" survey[4] of the *WISE* mission. In the following we discuss the single-exposure light curve data for the program objects using the order of Table 1. For some sources, we will be constructing spectral energy distributions

(SEDs). When we do so, we will use the AllWISE mean magnitudes.

Although a large number of polars were detected in the AllWISE survey, not all of these were bright enough to produce usable light curves in the single-exposure data. Some of the objects have light curves that do no show anything of interest. We denote all of the objects that have light curves presented in the following by a notation in the final column of Table 1. The *WISE* light curve data for AM Her and EF Eri have been presented in Harrison et al. (2013b).

2.2. Spitzer Data

In addition to the *WISE* data, we have searched the *Spitzer* data archive[5] for observations of the program polars. While the majority of these data have been presented elsewhere, we decided to perform our own reduction because the calibration of *Spitzer* data has changed since the time when the original observations were reduced and published. With the exception of V1500 Cyg, all of the *Spitzer* observations consist of IRAC 3.5 to 8 μm photometry (Fazio et al. 2004). V1500 Cyg was also observed at 24 μm with Multiband Imaging Photometer for *Spitzer* (MIPS; Rieke et al. 2004). To achieve *mean* flux densities for the IRAC and MIPS data, we have used MOsaicker and Point source EXtractor (MOPEX; Makovoz et al. 2006). Several sources (e.g., V1500 Cyg) were too faint to be identified with MOPEX. In those cases, we used IRAF to perform aperture photometry on the targets and several nearby, brighter field stars. The MOPEX values for these brighter field stars were then used to calibrate the IRAF photometry. For V347 Pav, we used IRAF to generate a light curve from the *Spitzer* observations, using the mean flux density from the reduction of the total data set and using MOPEX to calibrate the result. Because of its faintness, we generated a light curve for V379 Vir using MOPEX by coadding three successive images and then extracting a flux density. To construct light curves, we put the flux densities derived using MOPEX onto the IRAC magnitude system.[6] *Spitzer* data for the program polars are listed in Table 2.

2.3. Near-infrared Photometry and Spectroscopy

For a number of sources, we have obtained *JHK* light curves using Simultaneous Quad Infrared Imaging Device (SQIID)[7] on the KPNO 2.1 m telescope. SQIID obtained data in four near-IR channels simultaneously. These data, when combined with the *WISE* light curves, can be used to provide insight on the magnetic field strength because cyclotron emission is strongly wavelength dependent (see below). In addition, however, we can use the combined data sets to construct ellipsoidal light curve models to constrain the orbital inclinations using the Wilson–Devinney code (Wilson & Devinney 1971). For details on applying this code to *WISE* and *Spitzer* light curves, see Section 3.6 in Harrison et al. (2013b).

Near-IR spectra were obtained using SpeX[8] at the *Infrared Telescope Facility* ("IRTF") on Mauna Kea. SpeX has a 1024 × 1024 Raytheon Aladdin 3 InSb detector, allowing spectroscopy from 0.6 to 5.0 μm. The low-resolution prism

---

[3] See http://wise2.ipac.caltech.edu/docs/release/allsky/expsup/sec4_4a.html
[4] See http://wise2.ipac.caltech.edu/docs/release/3band/

[5] http://irsa.ipac.caltech.edu/data/SPITZER/docs/spitzerdataarchives/
[6] http://irsa.ipac.caltech.edu/data/SPITZER/docs/irac/iracinstrumenthandbook/17/
[7] http://www.noao.edu/kpno/sqiid/
[8] http://irtfweb.ifa.hawaii.edu/~spex/

Table 1
WISE Magnitudes for Polars

Name	W1	W2	W3	W4	Light Curve?
AI Tri	13.639 ± 0.025	13.327 ± 0.032	11.823 ± 0.278	…	Y
AM Her	10.544 ± 0.023	10.167 ± 0.020	9.041 ± 0.025	7.976 ± 0.129	N
AN UMa	14.590 ± 0.029	14.073 ± 0.040	12.107 ± 0.330	…	Y
AP CrB	13.653 ± 0.025	13.376 ± 0.031	12.369 ± 0.248	…	Y
AR UMa	13.122 ± 0.024	12.882 ± 0.025	…	…	Y
BL Hyi	12.659 ± 0.023	12.053 ± 0.021	10.082 ± 0.046	…	Y
BY Cam	12.173 ± 0.024	11.598 ± 0.021	9.981 ± 0.057	…	Y
CD Ind	12.708 ± 0.023	12.197 ± 0.022	10.918 ± 0.096	…	Y
CE Gru	17.150 ± 0.123	16.253 ± 0.194	…	…	N
CP Tuc	15.267 ± 0.038	15.168 ± 0.079	…	…	Y
CV Hyi	15.378 ± 0.034	14.772 ± 0.050	10.871 ± 0.089	…	N (Blend)
CW Hyi	14.901 ± 0.029	14.347 ± 0.035	12.651 ± 0.338	…	Y
DP Leo	16.282 ± 0.074	16.064 ± 0.200	…	…	N
EF Eri	14.188 ± 0.027	13.529 ± 0.029	11.440 ± 0.111	…	N
EG Lyn	16.451 ± 0.071	16.142 ± 0.189	…	…	N
EK UMa	…	…	…	…	…
EP Dra	15.543 ± 0.030	14.995 ± 0.041	13.128 ± 0.322	…	Y
EQ Cet	15.412 ± 0.041	14.639 ± 0.064	…	…	Y
EU Cnc	…	…	…	…	…
EU UMa	16.949 ± 0.116	16.451 ± 0.248	…	…	N
EV UMa	17.479 ± 0.133	17.356 ± 0.424	…	…	N
FH UMa	…	…	…	…	…
FL Cet	15.003 ± 0.033	14.781 ± 0.067	12.080 ± 0.285	…	Y
GG Leo	15.595 ± 0.048	14.981 ± 0.083	…	…	Y
HS Cam	15.187 ± 0.033	14.364 ± 0.044	…	…	Y
HU Aqr	13.769 ± 0.026	13.412 ± 0.033	11.592 ± 0.253	…	Y
HY Eri	16.149 ± 0.115	15.788 ± 0.184	…	…	N (Blend)
IW Eri	13.061 ± 0.024	12.329 ± 0.022	11.183 ± 0.122	…	Y
LW Cam	16.200 ± 0.058	15.308 ± 0.082	…	…	N
MN Hya	15.389 ± 0.037	14.658 ± 0.055	…	…	Y
MR Ser	13.718 ± 0.025	13.228 ± 0.030	11.502 ± 0.197	…	Y
QQ Vul	12.685 ± 0.025	12.393 ± 0.025	11.017 ± 0.118	…	Y
QS Tel	13.757 ± 0.027	13.515 ± 0.032	…	…	Y
RS Cae	17.386 ± 0.108	17.253 ± 0.350	…	…	N
ST LMi	13.490 ± 0.025	13.236 ± 0.030	11.834 ± 0.273	…	Y
UW Pic	13.809 ± 0.026	13.243 ± 0.026	11.152 ± 0.110	…	Y
UZ For	14.350 ± 0.027	13.924 ± 0.035	…	…	Y
VV Pup	13.736 ± 0.026	13.231 ± 0.030	11.769 ± 0.234	…	Y
VW For	16.456 ± 0.053	16.730 ± 0.214	…	…	N
VY For	14.508 ± 0.028	14.229 ± 0.037	12.940 ± 0.445	…	Y
V347 Pav	14.259 ± 0.029	13.872 ± 0.035	…	…	Y
V349 Pav	14.998 ± 0.032	14.367 ± 0.043	12.415 ± 0.370	…	Y
V379 Vir	14.754 ± 0.033	13.827 ± 0.041	…	…	N
V381 Vel	15.746 ± 0.045	15.442 ± 0.095	…	…	N
V388 Peg	14.852 ± 0.033	14.694 ± 0.059	…	…	N
V393 Pav	15.379 ± 0.038	14.998 ± 0.068	…	…	Y
V479 And	15.288 ± 0.037	15.220 ± 0.079	…	…	Y
V516 Pup	15.424 ± 0.038	15.219 ± 0.065	12.446 ± 0.339	…	Y
V834 Cen	12.528 ± 0.023	11.970 ± 0.022	10.105 ± 0.042	8.367 ± 0.177	Y
V884 Her	12.783 ± 0.024	12.432 ± 0.023	10.848 ± 0.096	…	Y
V895 Cen	13.199 ± 0.024	13.054 ± 0.030	12.522 ± 0.339	…	Y
V1007 Her	15.897 ± 0.039	15.139 ± 0.057	…	…	Y
V1033 Cen	12.646 ± 0.025	12.637 ± 0.026	…	…	N
V1043 Cen	11.755 ± 0.023	11.531 ± 0.022	10.351 ± 0.054	…	Y
V1309 Ori	13.255 ± 0.025	12.986 ± 0.026	11.653 ± 0.253	…	Y
V1432 Aql	12.785 ± 0.024	12.337 ± 0.025	11.254 ± 0.165	…	Y
V1500 Cyg	…	…	…	…	…
V2301 Oph	11.268 ± 0.023	10.747 ± 0.020	9.584 ± 0.051	8.517 ± 0.369	Y
V4738 Sgr	…	…	…	…	…
WW Hor	15.356 ± 0.034	15.065 ± 0.059	…	…	Y
WX LMi	12.284 ± 0.022	12.086 ± 0.022	11.313 ± 0.160	…	Y
HS0922+1333	12.374 ± 0.023	12.179 ± 0.024	11.812 ± 0.319	…	N
RBS490	15.354 ± 0.039	14.305 ± 0.043	11.421 ± 0.168	…	Y
RXJ0154.0–5947	14.621 ± 0.112	14.300 ± 0.157	10.763 ± 0.322	…	N (Blend)

Table 1
(Continued)

Name	W1	W2	W3	W4	Light Curve?
RXJ0425.6–5714	17.883 ± 0.102	…	…	…	N
RXJ0502.8+1624	13.894 ± 0.027	13.474 ± 0.037	11.703 ± 0.280	…	Y
RXJ0649.8–0737	14.238 ± 0.028	13.968 ± 0.043	…	…	Y
RXJ0749.1-0549	15.697 ± 0.046	15.492 ± 0.111	…	…	N
RXJ0859.1+0537	15.197 ± 0.037	14.743 ± 0.069	…	…	N
RXJ0953.1+1458	15.913 ± 0.056	15.294 ± 0.103	…	…	N
RXJ1002–1925	16.412 ± 0.064	15.825 ± 0.120	…	…	N
RXJ1007.5–2017	15.187 ± 0.036	14.659 ± 0.060	…	…	N
RXJ2316–0527	14.970 ± 0.035	14.575 ± 0.057	…	…	N
RXSJ060033.1–270918	15.170 ± 0.036	14.936 ± 0.060	…	…	Y
2QZ142256.3–022108	16.347 ± 0.066	16.218 ± 0.206	…	…	N
2QZJ142438.9–022739	15.539 ± 0.044	15.154 ± 0.083	…	…	N
2XMM J183219.3–084030	…	…	…	…	…

Table 2
Spitzer Data for Polars

Object	Obs. Date (MJD)	3.6 μm (mJy)	4.5 μm (mJy)	5.8 μm (mJy)	8.0 μm (mJy)	Phase
AN UMa	54598.86656	0.39 ± 0.01	…	0.30 ± 0.03	…	0.25
AR UMa	54099.40347	2.21 ± 0.01	1.41 ± 0.01	1.00 ± 0.01	0.51 ± 0.01	0.68
AR UMa	54229.74969	1.69 ± 0.01	1.17 ± 0.01	0.83 ± 0.01	0.39 ± 0.01	0.89
CP Tuc	56272.08636	0.28 ± 0.01	0.21 ± 0.01	…	…	0.38
FL Cet	56586.02561	0.09 ± 0.01	0.07 ± 0.01	…	…	0.57, 0.24
GG Leo	53496.63113	0.24 ± 0.01	0.17 ± 0.01	0.19 ± 0.01	0.18 ± 0.02	0.86
MR Ser	53456.22639	1.69 ± 0.03	1.10 ± 0.03	1.43 ± 0.01	1.11 ± 0.01	0.54
ST LMi	55337.16746	2.70 ± 0.02	1.77 ± 0.02	1.58 ± 0.02	0.95 ± 0.02	0.33
VV Pup	53335.27798	0.70 ± 0.01	0.55 ± 0.01	0.35 ± 0.01	0.26 ± 0.01	0.71
V347 Pav	53601.67867	0.88 ± 0.01	0.69 ± 0.01	0.67 ± 0.01	0.64 ± 0.01	0.36
V379 Vir	54285.19149	0.27 ± 0.01	0.27 ± 0.01	0.23 ± 0.01	0.16 ± 0.01	(Mean)
V1043 Cen	53957.13551	5.99 ± 0.03	4.38 ± 0.03	3.33 ± 0.03	1.71 ± 0.02	0.75
V1309 Ori	54006.60187	1.32 ± 0.01	0.89 ± 0.01	0.72 ± 0.01	0.29 ± 0.01	0.87
V1500 Cyg	53665.25482	0.15 ± 0.02	0.13 ± 0.03	…	…	0.69/0.83
V1500 Cyg	52976.56661	0.22 ± 0.03	0.20 ± 0.03	0.17 ± 0.04	0.19 ± 0.03	0.85/0.26

mode produces spectra covering the wavelengths $0.6 \leqslant \lambda \leqslant$ 2.5 μm at an average resolving power of $R \sim 250$. However, because angular dispersion is a function of refractive index, the resolving power varies by a factor of two, from $R = 150$ at 0.8 μm to $R = 350$ at 2.5 μm. Most of these spectra have been presented in Campbell (2008). We include them here because we have re-reduced these data in an attempt to achieve a better telluric correction to aid in cyclotron harmonic identification.

2.4. Optical Light Curves

We have used the New Mexico State University (NMSU) 1.0 m telescope to obtain light curves for several polars. The NMSU 1.0 m telescope is equipped with an E2V 2048x2048 CCD with standard Johnson–Cousins *BVRI* filters. All of these data were processed in the normal way, and differential light curves for the program objects were generated by comparison with four nearby field stars. The light curves were put on the standard system either by using Landolt standards to calibrate the differential photometry reference stars, or through the use of APASS[9], or other sources of data for the reference stars.

---

[9] http://www.aavso.org/apass

3. THE *WISE* LIGHT CURVES OF POLARS

In Figure 1 we present a color–color plot for the polars in Table 1 that have detections in the first three *WISE* bands. It is clear that the majority of polars have colors that are much redder than main sequence stars in both of these colors. We find that nearly all of the polars with the reddest $(W1 - W2)$ colors are those where cyclotron emission is present in the *W3* bandpass. Most of the polars have extreme $(W2 - W3)$ colors that are difficult to explain. We will explore the possible origin of these 11.5 μm excesses in Section 4.1.

Before we examine the data for the individual objects, we feel it is valuable to quickly review the behavior of cyclotron emission. For magnetic field strengths typically found in polars, the cyclotron spectrum transitions from optically thick to thin at optical or near-IR wavelengths, making complex radiative transfer calculations necessary to model the emitted spectrum. In the accretion column, the plasma is dispersive and birefringent. Ramaty (1969) showed that in the large Faraday rotation limit of such a plasma, it is possible to decouple the radiative transfer into two magnetoionic modes (ordinary and extraordinary). In this case, the radiative transfer equation reduces to $I_{o,e} = I_{RJ} [1 - \exp(-\tau_{o,e})]$, where the o and e indicate the ordinary and extraordinary modes, respectively.
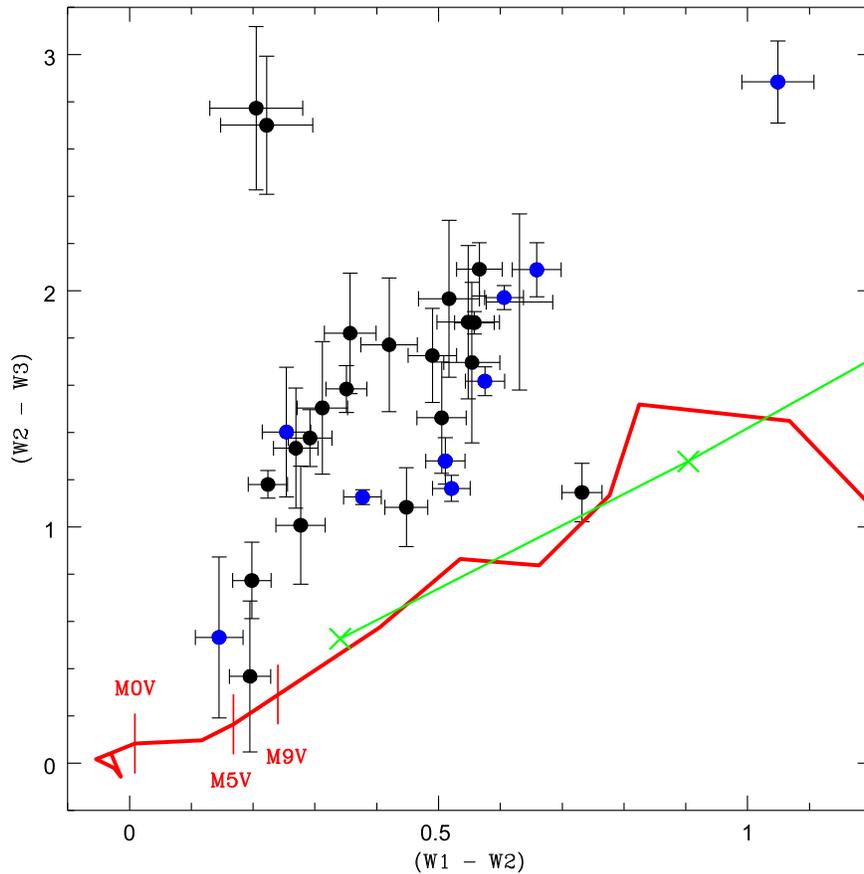
Figure 1. *WISE* color–color plot for the sources in Table 1. Plotted in red are the colors of main sequence stars and brown dwarfs. We note the position of an M0V, an M5V, and an M9V along this relationship. The green line is the color that blackbodies have in this diagram, with the "X" marking temperatures of 2000 K (left) and 1000 K (right). A blue dot indicates a polar where the derived field strength puts the fundamental cyclotron harmonic in the *W*3 band (see Section 4.1).

The total intensity is taken to be the sum of the ordinary and extraordinary modes.

The optical depth, τ, can be parameterized in terms of a dimensionless optical depth (or "size") parameter Λ: $\tau_{o,e} = \Lambda \phi_{o,e}$, where $\Lambda = l\omega_p^2/(c\omega_c)$, l is the path length through the plasma, ω_p is the plasma frequency, $\omega_p = (4\pi Ne^2/m)^{1/2}$, and ω_c is the frequency of the cyclotron fundamental, $\omega_c = eB/mc$, with m being the relativistic mass of the gyrating particles. In the above formulation, the dimensionless absorption coefficient $\phi_{o,e}$ is dependent on B, the magnetic field strength, Θ, the viewing angle with respect to the magnetic field, and T, the isothermal temperature of the emitting slab. By integrating the emissivity of the gyrating electrons over an assumed relativistic Maxwellian distribution, Chanmugam & Dulk (1981) produced a general formulation of the cyclotron absorption coefficients.

These constant-lambda, "CL," models, so called because the emergent radiation is assumed to be due to a single path through a slab of uniform optical depth parameter, Λ, have been used with great success in characterizing the magnetic fields of the white dwarfs in polars (numerous examples will be cited below). We employ the CL code used by Campbell (2008, originally developed by Schwope 1990) to produce model cyclotron spectra. More advanced and realistic prescriptions for calculating cyclotron spectra have been constructed, such as that by Fischer & Beuermann (2001), but for the purposes of attempting to explain broadband photometry, CL models are adequate.

CL cyclotron models depend on four distinct global variables mentioned previously: B, T, Θ, and $\log \Lambda$. Because altering those four parameters causes complex, quasi-degenerate changes in the spectra produced, we briefly examine the influence of each parameter on the emergent spectrum in preparation for the discussion of the individual objects that follows. The magnetic field strength is the most independent of the four parameters used because increasing B merely shifts the position of each harmonic blueward (see Figure 2). Increasing the plasma temperature has two main effects. Primarily, it causes the harmonics to grow. But as they bleed upward they eventually "saturate" at the Rayleigh–Jeans limit (proportional to λ^{-4}), effectively becoming a blackbody source. Because the lower harmonics saturate first, higher harmonics contribute ever more of the total flux with increasing temperature (see Figure 3). Also, because the humps are the product of an ensemble of electrons emitting over a temperature distribution, higher temperatures increasingly populate the wings of the relativistic Maxwellian, broadening each harmonic as a result. Unfortunately, each of these effects can also be reproduced by increasing $\log \Lambda$, as shown in Figure 4. Because the temperature does produce a small systematic shift in the position of the harmonics, it is possible in theory to decouple the effects of temperature and the size parameter. However, in practice, identifying this shift is difficult, principally because neither the temperature nor Λ is truly single valued in a real polar accretion column.
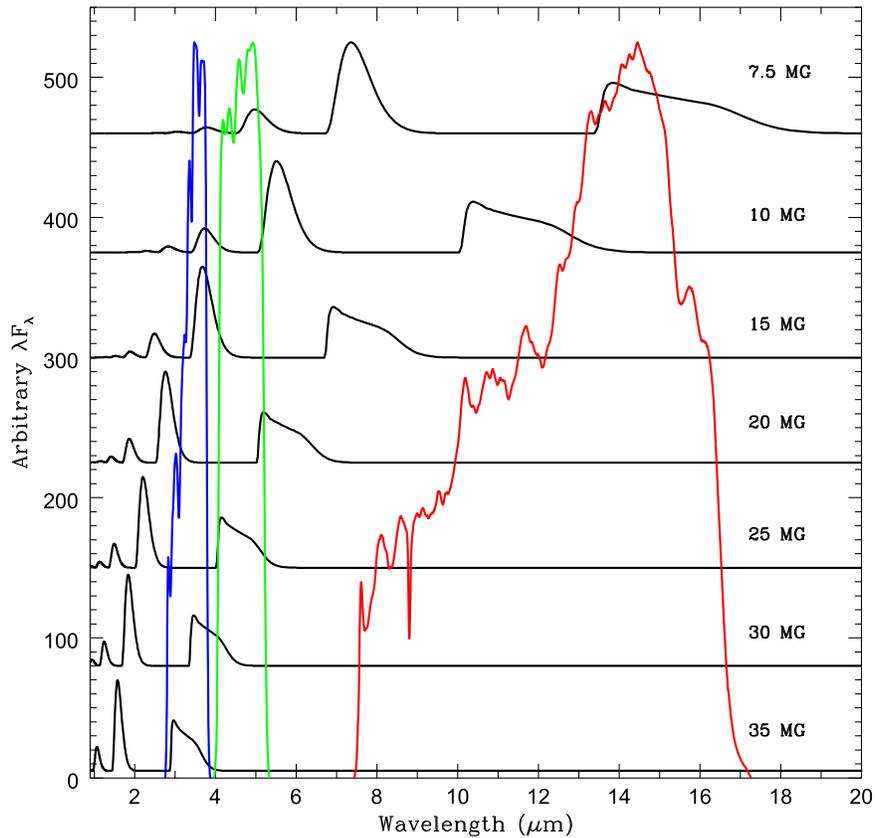
Figure 2. Position of cyclotron harmonics as a function of the magnetic field strength (labeled) in the infrared. The *W1* (blue), *W2* (green), and *W3* (red) bandpasses are plotted.

Finally, varying the viewing angle changes the spectrum in two ways. First, viewing angles near 90° produce "peaky" harmonics with the higher orders pumped up. Also, as the viewing angle decreases from 90° (see Figure 5), the harmonics shift blueward. This viewing-angle-induced shift then creates a periodic motion in the position of the harmonics over the orbit as the viewing angle ranges between its minimum and maximum values. In nearly every polar, the viewing angle dramatically changes over an orbital period. This also induces periodic variations in the observed polarization. The maximum circular polarization occurs when the viewer looks down the accretion "column." However, the optical depth at this time is a minimum, and thus the total circularly polarized and cyclotron fluxes are both low. As the accretion region rotates toward the limb, the circular polarization decreases, but the cyclotron flux increases. During this time, the linear polarization tends toward a maximum. In the following, we will occasionally use such information to help in deducing the origin of the variations seen in the *WISE* data.

As discussed in the introduction, Harrison et al. (2013b) postulated that the large amplitude variations seen in the longest-bandpass *Spitzer* and *WISE* light curves of AM Her and EF Eri could be attributed to emission from the $n = 1$ cyclotron harmonic. As noted above, the maximum observed cyclotron emission generally occurs when our viewing angle to the magnetic field is closest to 90°. This, however, is *not* true for the cyclotron fundamental. In Figure 6, we plot the angular emission of the first three harmonics for two cases: cool and optically thin ($kT = 5$ keV, $\log \Lambda = -5$) and hotter and more optically thick ($kT = 10$ keV, $\log \Lambda = 0$). Emission from the

fundamental should be antiphased to the higher harmonics. In cool, optically thin cases, emission from the $n = 1$ harmonic varies by a factor of two ($\Delta m = 0.75$ mag) over the possible range in viewing angles. As the optical depth increases, less and less emission occurs in the plane perpendicular to the magnetic field. For the case shown in the right-hand panel of Figure 6, the ratio is nearly six. Thus, we should expect to see the $n = 1$ emission to be antiphased to that from the higher harmonics, and its variation over an orbit should increase with increasing optical depth.

As demonstrated by Figure 2, there will be certain field strengths where a single harmonic can fall into a *WISE* bandpass, which will then show up as single-band variability. There are also certain field strengths (e.g., $B \simeq 15, 30$ MG) where a cyclotron harmonic can span the two shorter wavelength bandpasses, allowing for similar levels of variability at both wavelengths. Even given the broadening and wavelength shifting of the harmonics noted above, we should not see strong, orbitally modulated cyclotron variations in the *WISE* bandpasses for any polar where the field strength is in excess of $B = 60$ MG. The combination of *WISE* light curves along with phase-resolved, ground-based visual or near-IR data can allow for surprisingly tight constraints on possible field strengths if emission from the lower harmonics is present.

Given the rapidly declining blackbody fluxes of the hotter sources in polars, it should often be possible to detect ellipsoidal variations in the *WISE* bandpasses that are due to the orbital motion of the distorted donor star. For several polars, we have used the *WISE* light curves in combination with ground-based data to model the ellipsoidal variations using the
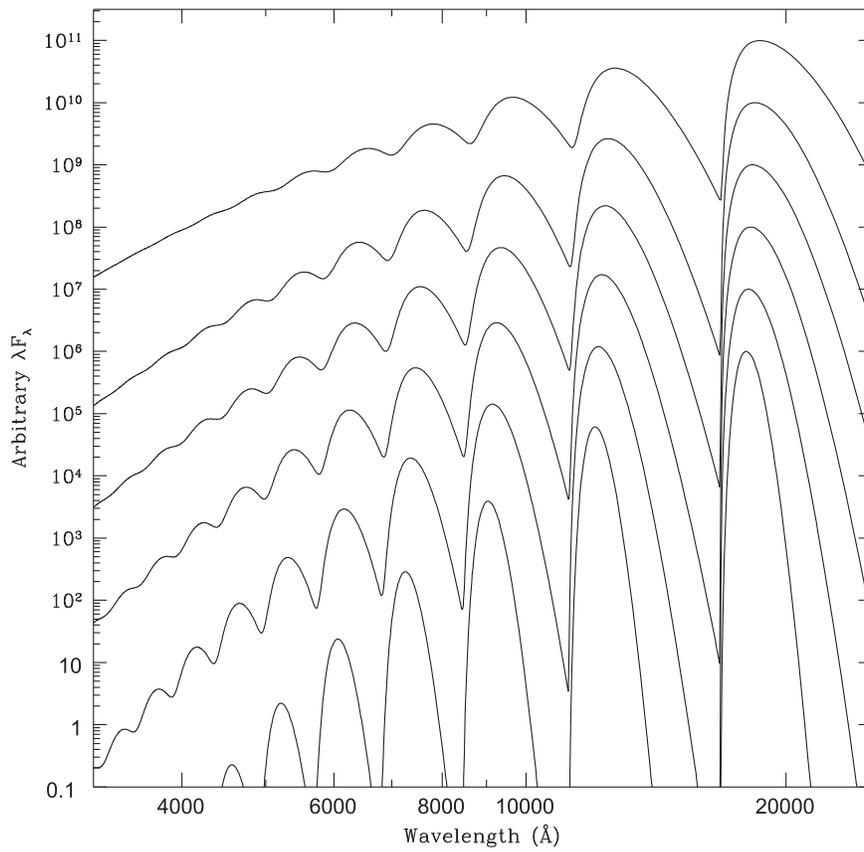
Figure 3. Effect of changing the temperature of the shock from 2 keV (bottom) to 15 keV (top), in 2 keV increments, except for the final step of 5 keV going from 10 to 15 keV. These models are for a 30 MG field, where $\log \Lambda = 3$, and the viewing angle was $\theta = 75°$.
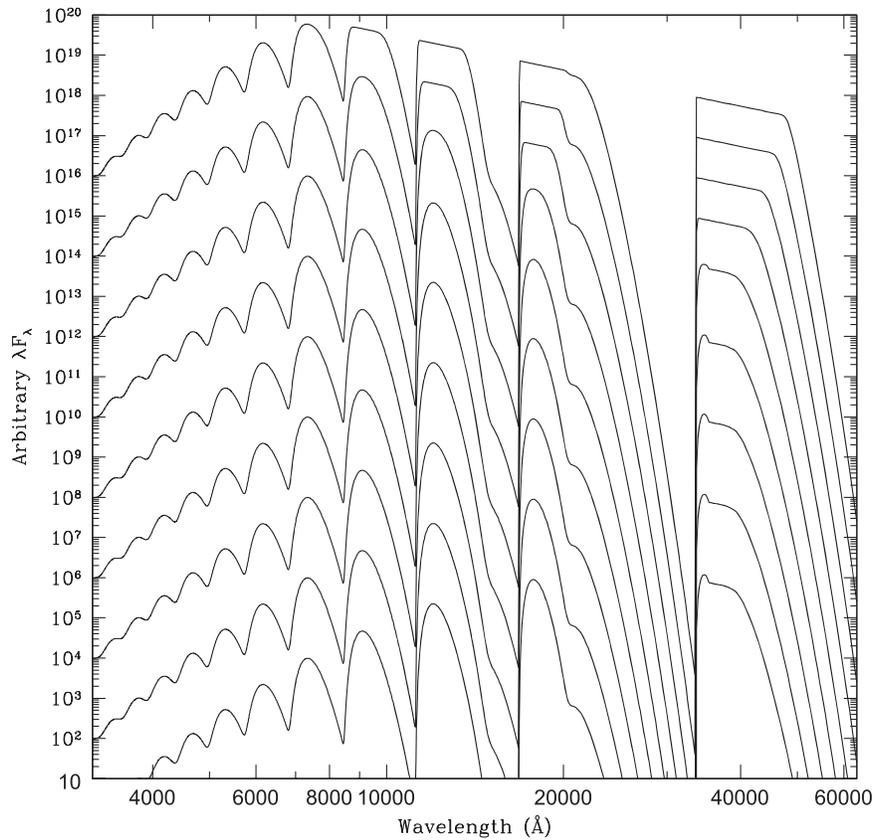
Figure 4. Effect of changing the size parameter ($\log \Lambda$) from -3 on the bottom to $+5$ on top in steps of 1 for a field with $B = 30$ MG, $T = 5$ keV, and $\theta = 75°$.
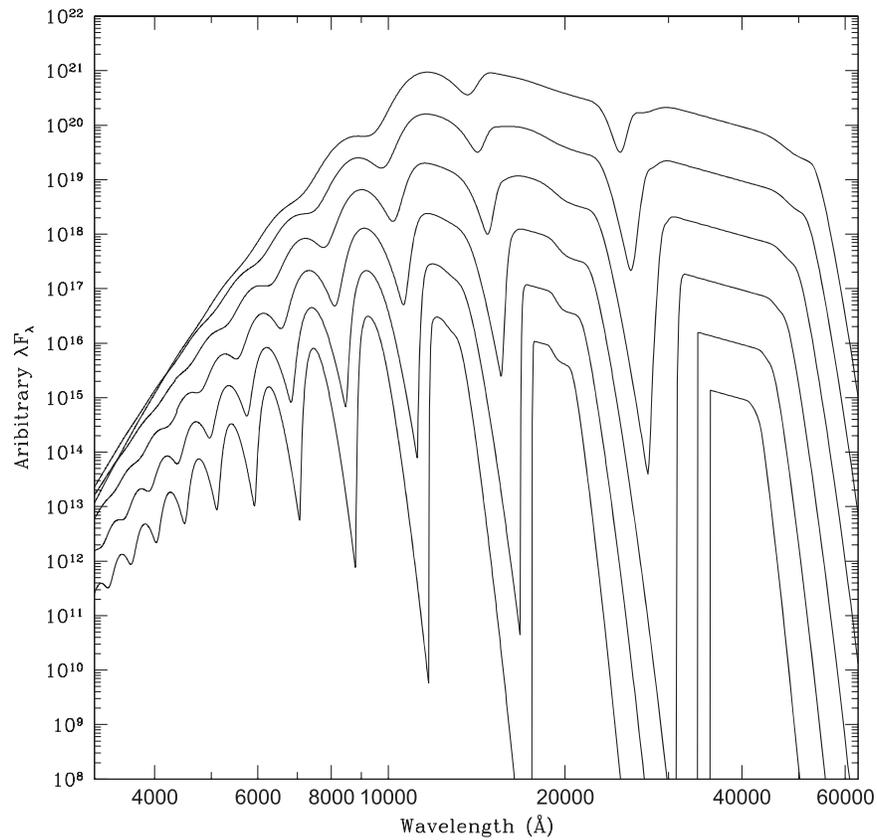
Figure 5. Change in the shape of the cyclotron harmonics as a function of the viewing angle θ, from 80° (bottom) to 30° (top) in 10 degree increments for a 30 MG field, with $T = 5$ keV and $\Lambda = 3$.
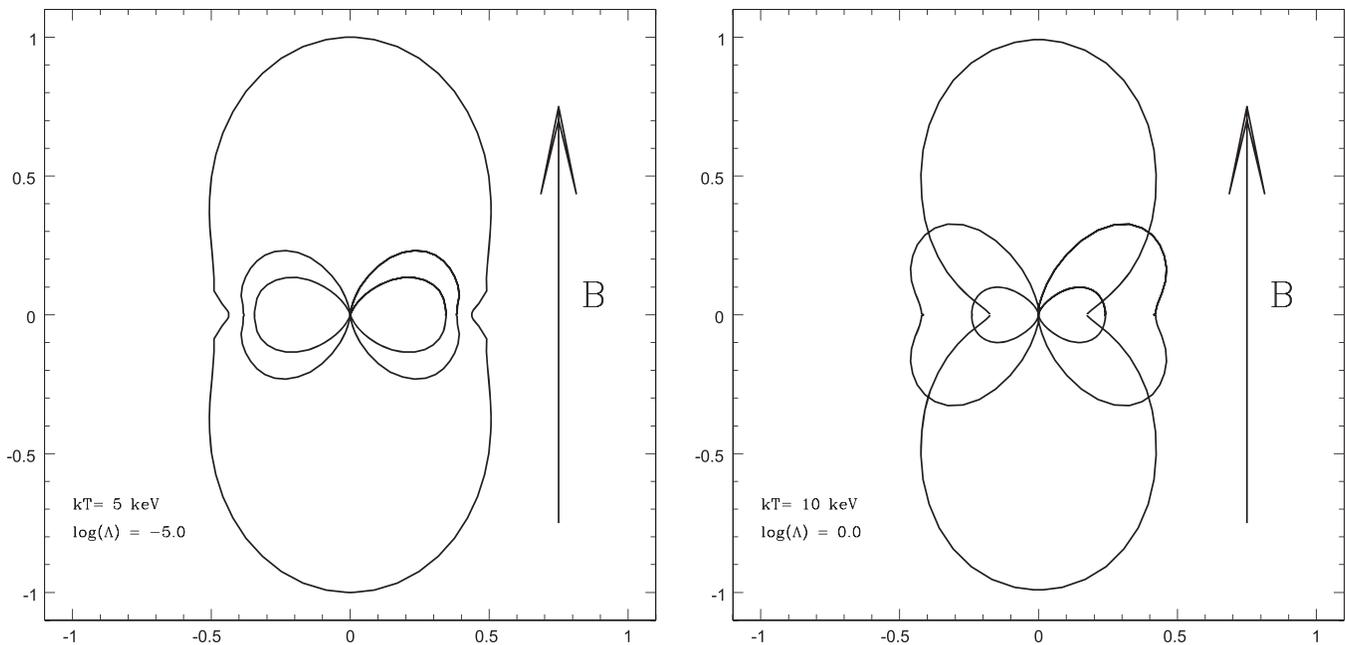
Figure 6. Angular distribution of cyclotron emission for the first three harmonics. The $n = 1$ harmonic emits preferentially along the axis of the magnetic field. As the optical depth increases (right-hand panel), cyclotron emission from the fundamental becomes increasingly antiphased with the higher harmonics (though note that the $n = 2$ harmonic now has increased emission along the magnetic field axis).

Wilson–Devinney code WD2010.[10] Such modeling can be useful in constraining the temperatures of the stellar components, as well as the binary orbital inclination.

One of the great difficulties with ascertaining the origin of the observed variability in the sample of polars is that almost none of the ground-based (or *Spitzer*) data overlaps the observational epoch of the *WISE* data. Unfortunately, many polars are visually faint, so little monitoring has been attempted

---

[10] ftp://ftp.astro.ufl.edu/pub/wilson/lcdc2010/

by organizations such as the AAVSO. We have used AAVSO or other visual estimates that we extracted from the literature to attempt to ascertain whether a polar observed by *WISE* was in a high or low state. This has only been partially successful. Sometimes, a discontinuous SED, after properly accounting for any cyclotron emission given the system's magnetic field strength, can be used to identify whether a polar was in a high or low state when observed by *WISE*. But for most of the sample of objects discussed below, we do not know their outburst states. In the following, we present a discussion of the data for all of the detected objects in the order in which they appear in Table 1.

3.1. AI Tri

Schwarz et al. (1998) present visual light curves for AI Tri that showed that, when in its high or intermediate state (their "regular mode"), the system has a single maximum and minimum during each orbit. The X-ray light curve of AI Tri also showed large variations with minima at roughly the same phase as the optical data, but with a distinctly more complex morphology. Traulsen et al. (2010) present an updated ephemeris for the *V*-band minima of AI Tri. In this ephemeris, as was true for that originally derived by Schwarz et al., the light curve minima are offset from the spectroscopic (binary) phase by +0.191. With this phasing, the source has *R*- and *I*-band maxima near binary phase 0.3. Similarly sized variations were also observed in the *B* and *V* bands, with the total amplitude of the variations of order $\Delta V = 0.7$ mag. The *W*1 and *W*2 light curves presented in Figure 7 are essentially identical to each other and closely resemble the regular-mode *V*-band data in both amplitude and phasing.

Since some of the variability of AI Tri at visual wavelengths is attributed to cyclotron emission, the *WISE* light curves presumably also arise from cyclotron emission. Schwarz et al. assign the observed cyclotron humps in their optical spectrum to the $n = 4$–6 harmonics for a field with $B = 38 \pm 2$ MG. As demonstrated in Figure 2, getting significant cyclotron emission in the *W*2 band requires a field strength of less than 38 MG. As noted above, the appearance and location of cyclotron harmonic emission depends on a number of parameters, but after the field strength, the main parameter that causes a shift in the wavelength of the peak emission from a harmonic is the viewing angle: as one works from large viewing angles to small, the harmonics broaden and move blueward. This is opposite to what is needed. To try to allow such a field strength to explain the *W*2 light curve requires very broad harmonics with a long wavelength tail, and this is best achieved with a high temperature. Schwarz et al. (1998) present CL cyclotron models for their spectra with a temperature of 20 keV. But the cyclotron emission from a 38 MG field with $kT = 20$ keV has almost no cyclotron emission in *W*2. Thus, the field strength has to be lower than 38 MG.

We obtained a single low-resolution spectrum of AI Tri with SpeX at the IRTF on 2005 September 1, where the orbital phase was $\phi = 0.57$. This spectrum, shown in Figure 8, was obtained about halfway from light curve maximum to minimum. If the field strength was 38 MG, there should be cyclotron harmonics near 0.9 and 1.4 μm. No such features are seen. In contrast, a 32 MG field would have the $n = 2$

harmonic at 1.67 μm and the $n = 3$ harmonic at 1.11 μm. As described below, we believe the light curve minimum is when the line-of-sight angle to the accreting pole is most favorable and thus has a smaller viewing angle (θ). In Figure 8, we plot a cyclotron model with $B = 32$ MG, $kT = 5.2$ keV (see below), $\log \Lambda = 3$, and $\theta = 65°$. It appears that the $n = 3$ harmonic for a field with 32 MG is present in this spectrum, though the same cannot be said for $n = 2$. A 32 MG field strength is also consistent with the broad 8200 Å emission feature noted by Schwarz et al. (see their Figure 13). In modeling their polarimetry, Katajainen et al. (2001) found a field strength of 32–33 MG for the main accretion pole. This field strength places the broad $n = 1$ harmonic straddling both the *W*1 and *W*2 bands, potentially explaining their light curves.

To investigate this possibility, we constructed the SED of AI Tri shown in Figure 9. In this figure, we have plotted the extreme ranges in variability of the source in the *WISE* bands, centered on the mean fluxes listed in Table 1. These are indicated by the filled circles that are connected by a thin solid line. In addition to the *WISE* data, we add the $UBV(RI)_J$ light curve data from Katajainen et al. (2001), plotted in a similar fashion. The amplitude of the variations seen in the *WISE* data suggests that AI Tri was in a bright or intermediate state, as were the five-color data from Katajainen et al. (note that those light curves were obtained simultaneously). To this SED we add the single-epoch *JHK* data from 2MASS and the far-ultraviolet (FUV) and near-ultraviolet (NUV) data from *GALEX* (see Table 3). The 2MASS data were obtained at binary phase 0.48, which is close to the maxima in the light curves, while the *GALEX* observations occurred at phase 0.90, or close to the light curve minimum. We observed AI Tri at APO on 2014 October 30 to obtain *JHK* data (at Table 4) at phase zero (the AAVSO database indicates the system had *V* ~ 16 at this time). SDSS photometry for this object also exists (see Table 3), and those data were obtained near the light curve minimum ($\phi = 0.90 \pm 0.02$). All five SDSS magnitudes (not plotted) are consistent with the minima of the $UBV(RI)_J$ data set. The plotted data have been dereddened assuming $A_V = 0.18$, derived from the hydrogen column (1.5×10^{20} cm^{-2}) used in the X-ray modeling by Traulsen et al. with the relationship from Predehl & Schmitt (1995). Note that even this small amount of visual extinction is important for the *GALEX* fluxes (see Yuan et al. 2013).

The variability in the UV is important for modeling the SED. Traulsen et al. used the Optical Monitor on *XMM* to obtain a light curve in the UVM2 filter ($\lambda_{eff} = 2310$ Å). The UVM2 filter has a similar effective wavelength as the *GALEX* NUV band, though the latter has twice the bandpass. The UVM2 light curve of AI Tri showed 1.5 mag of variability with a sharp minimum at light curve phase 0.05. The *GALEX* data were obtained on the decline to this minimum, and the NUV flux is nearly identical to the UVM2 flux at that phase. Thus, we dereddened the UVM2 fluxes using the relationship for the *GALEX* NUV bandpass to help constrain the SED.

We downloaded and reduced the *XMM* data for AI Tri to allow us to use XSPEC (Arnaud et al. 1996) in an attempt to model the SED for this object from 5 Å to 11.3 μm. Traulsen et al. (2010) have presented and modeled the *XMM* data for AI Tri, and we use their results to engender a simpler XSPEC
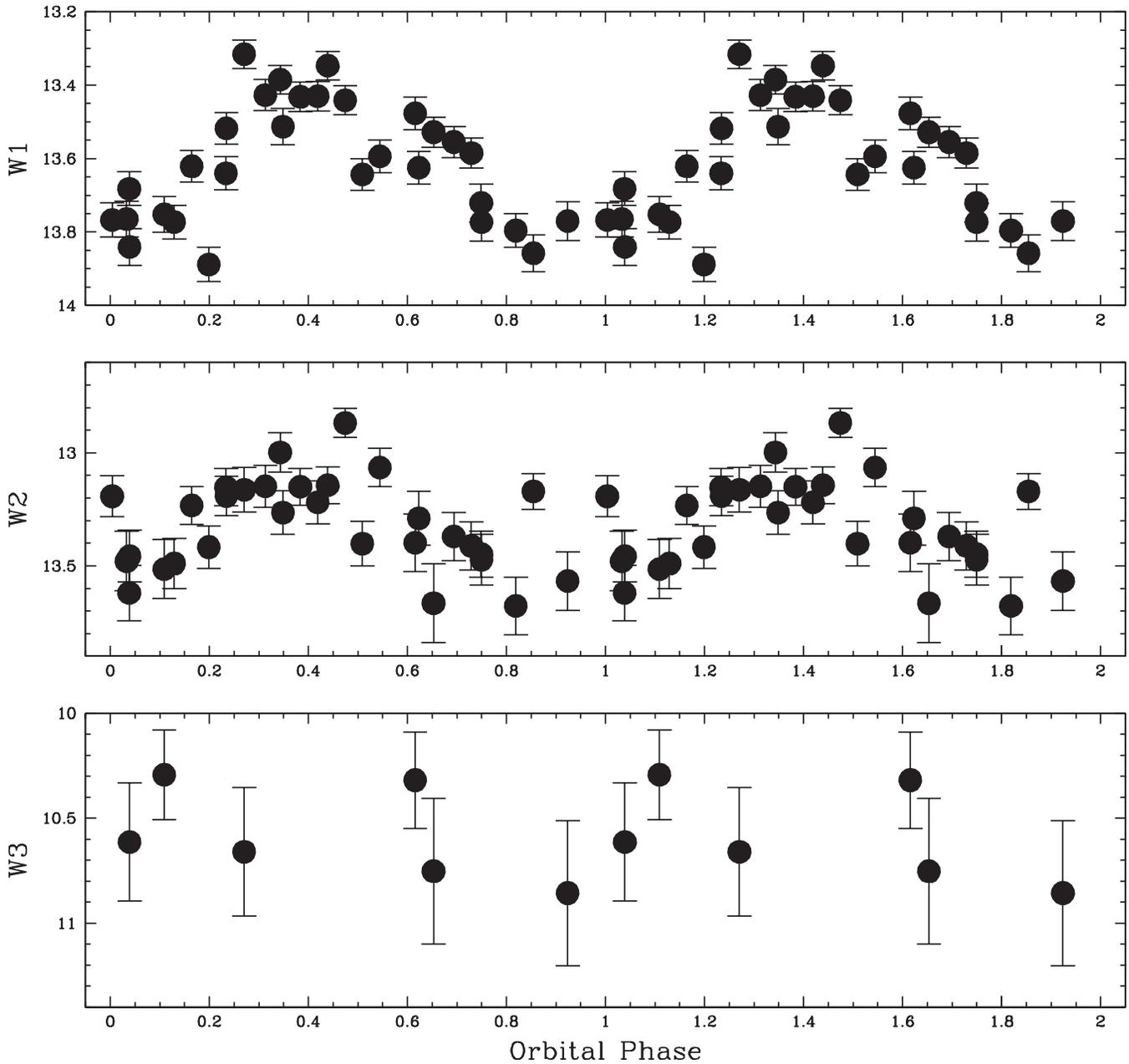
Figure 7. *WISE* light curve of AI Tri phased to the ephemeris of Traulsen et al. (2010). In this, and in all of the *WISE* light curves that follow, we repeat the light curve over two orbital cycles for clarity.

model for these data. We modeled the 2005 August 22 "bright phase 1" epoch of the *XMM* data set for AI Tri, as defined by Traulsen et al. Instead of the multitemperature hot blackbody component they used, we employed a single-temperature (39.5eV) blackbody in combination with a thermal bremsstrahlung component ($kT = 5.2$ keV), both absorbed by the hydrogen column noted above. Because of the rather low signal-to-noise ratio (S/N) of the high-energy portion of this data set, we were able to achieve a similar quality of fit with this simpler model, even though there were several weak emission lines visible in the *XMM* data that were better modeled with the "mekal" plasma model in XSPEC, as used by Traulsen et al. The *XMM* data points are plotted in Figure 9 as "×" symbols, and the final XSPEC model for this X-ray-bright phase is in blue.

Schwarz et al. (1998) estimate a distance for AI Tri of $d = 620 \pm 100$ pc using the secondary star color–surface brightness relationship of Ramseyer (1994). Using a white dwarf with $T = 23{,}000$ K (Traulsen et al.) and a secondary star with $T = 3200$ K (Schwarz et al.), we added these two additional blackbody components into XSPEC to generate a model that covers the spectral range from the X-ray to the mid-IR. At first, we normalized both blackbody spectral components to 620 pc. Such a normalization did not work in that *all of the minimum light fluxes* were well above the model SED. Given the sharp UV minimum, we then attempted a normalization of the white dwarf to reproduce this flux. This sets a lower limit to the distance of 450 pc. As we find below, this closer distance allows us to construct a reasonable model for the observed fluxes and variability exhibited by AI Tri. Although this distance is quite discrepant with that derived
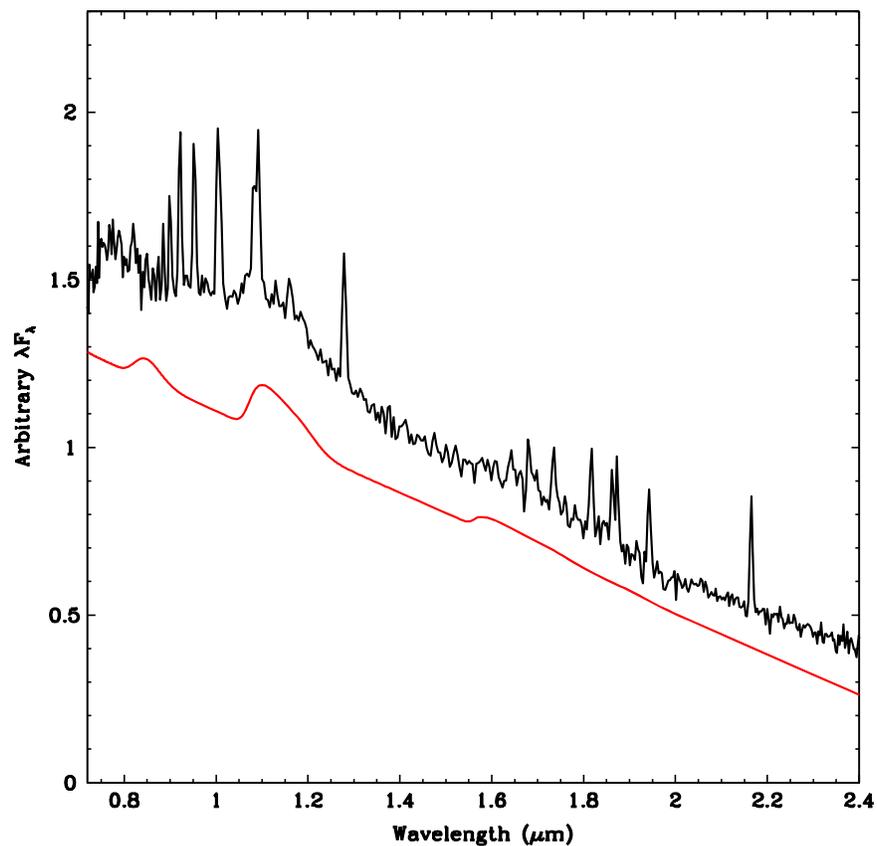
Figure 8. SpeX spectrum for AI Tri, and the red curve represents a cyclotron model (log $\Lambda = 3$, $kT = 5.2$ keV, $\theta = 65°$) for $B = 32$ MG.
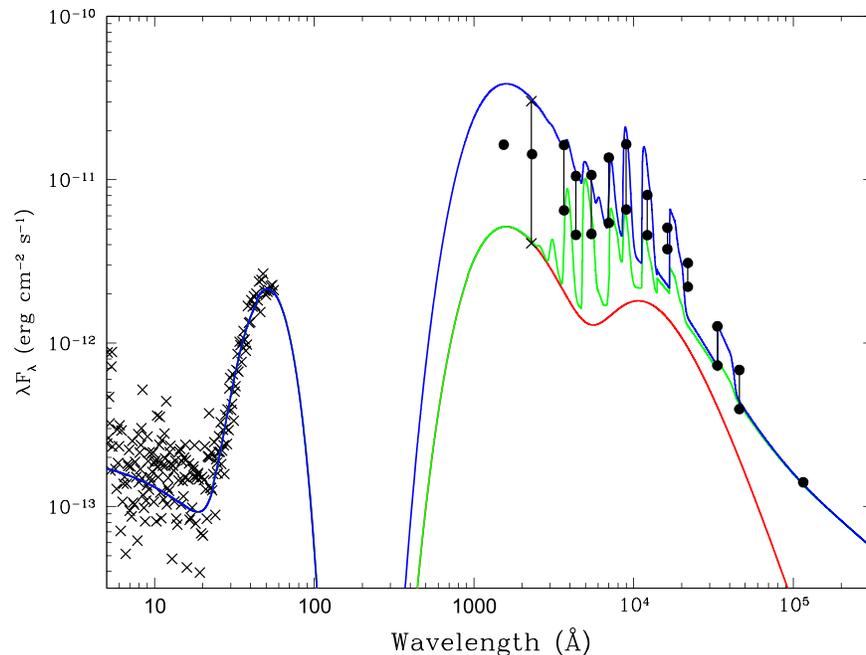
Figure 9. SED of AI Tri. As described in the text, the blue curve is the peak of the bright phase, and the green curve is the faint phase. To both of these we have added cyclotron models. The "×" symbols are from *XMM* observations, and the solid circles are from *WISE*, *GALEX*, and ground-based data. Two data points at any one wavelength, connected by a line segment, represent the observed variability in that bandpass. The *JHK* data are from 2MASS and APO and were obtained at the light curve maximum and minimum, respectively. The *UBVRI* data are from Katajainen et al. (2001). The red curve represents the sum of the emission from just the white dwarf and secondary star.

by Schwarz et al., they fit an M2 template to the red portion of their minimum light spectrum, and, as we show below, there appears to be significant cyclotron contamination in the red end of the optical spectrum during minimum light. In concert, our estimate ignores any contribution from hot spots to the minimum light flux of the white dwarf.

Table 3
GALEX and SDSS Data for Polars

Object	FUV	NUV	u	g	r	i	z	Phase/SDSS Date
AI Tri	16.72 ± 0.03	16.48 ± 0.02	16.65 ± 0.01	16.82 ± 0.01	16.56 ± 0.01	16.18 ± 0.01	15.92 ± 0.01	0.90
AN UMa	18.08 ± 0.09	18.27 ± 0.03	15.37 ± 0.01	15.44 ± 0.01	15.60 ± 0.01	15.70 ± 0.01	15.63 ± 0.01	2002.9500
"	...	...	15.81 ± 0.01	15.74 ± 0.01	15.82 ± 0.01	15.84 ± 0.01	16.63 ± 0.01	2003.1768
AP CrB	16.97 ± 0.06	17.34 ± 0.02	17.62 ± 0.01	17.50 ± 0.01	17.68 ± 0.01	16.99 ± 0.01	16.27 ± 0.01	2003.3303
"	...	...	17.59 ± 0.01	17.54 ± 0.01	17.70 ± 0.01	16.95 ± 0.01	16.21 ± 0.01	2003.4750
AR UMa	14.92 ± 0.02	14.82 ± 0.01	15.44 ± 0.01	15.51 ± 0.01	15.55 ± 0.01	15.57 ± 0.01	15.16 ± 0.01	2003.2256
BL Hyi	18.01 ± 0.07	17.63 ± 0.04	...	...	...	...	...	...
BY Cam	15.68 ± 0.02	15.60 ± 0.01	...	...	...	...	...	...
CD Ind	17.59 ± 0.05	17.79 ± 0.03	...	...	...	...	...	...
CV Hyi	20.83 ± 0.17	20.64 ± 0.13	...	...	...	...	...	...
EG Lyn	19.79 ± 0.18	19.95 ± 0.14	19.64 ± 0.04	19.53 ± 0.01	18.55 ± 0.01	18.59 ± 0.01	18.82 ± 0.05	2000.3154
EG Lyn	...	...	20.19 ± 0.05	19.83 ± 0.02	19.36 ± 0.02	19.30 ± 0.02	19.20 ± 0.06	2000.3207
"	...	...	20.50 ± 0.09	20.26 ± 0.03	20.08 ± 0.04	19.96 ± 0.04	19.59 ± 0.11	2000.3374
EP Dra	17.63 ± 0.04	17.97 ± 0.04	...	...	...	...	...	...
EQ Cet	19.32 ± 0.11	19.09 ± 0.06	...	...	...	...	...	...
EU UMa	17.32 ± 0.05	17.31 ± 0.05	17.57 ± 0.01	17.60 ± 0.01	17.70 ± 0.01	17.80 ± 0.01	17.55 ± 0.01	2004.9567
FL Cet	19.79 ± 0.03	19.55 ± 0.02	16.03 ± 0.01	15.42 ± 0.01	15.34 ± 0.01	15.60 ± 0.01	15.70 ± 0.01	1998.7335
"	...	...	16.87 ± 0.01	16.64 ± 0.01	16.54 ± 0.01	16.79 ± 0.01	16.78 ± 0.01	1998.8727
"	...	...	17.37 ± 0.01	16.56 ± 0.01	16.27 ± 0.01	16.27 ± 0.01	16.39 ± 0.01	2001.8652
"	...	...	15.97 ± 0.01	15.99 ± 0.01	16.13 ± 0.01	16.16 ± 0.01	16.07 ± 0.01	2002.0372
"	...	...	15.82 ± 0.01	15.20 ± 0.01	15.06 ± 0.01	15.14 ± 0.01	15.42 ± 0.01	2002.7580
"	...	...	15.60 ± 0.01	15.22 ± 0.01	15.24 ± 0.01	15.34 ± 0.01	15.40 ± 0.01	2002.7773
"	...	...	16.17 ± 0.01	15.82 ± 0.01	15.72 ± 0.01	15.89 ± 0.01	15.94 ± 0.01	2002.8261
"	...	...	16.16 ± 0.01	16.26 ± 0.01	15.50 ± 0.01	15.60 ± 0.01	15.92 ± 0.01	2002.8290
"	...	...	15.93 ± 0.01	15.91 ± 0.01	15.83 ± 0.01	15.92 ± 0.01	16.04 ± 0.01	2002.8507
"	...	...	16.03 ± 0.01	15.51 ± 0.01	15.65 ± 0.01	15.58 ± 0.01	15.65 ± 0.01	2003.0009
"	...	...	19.03 ± 0.01	17.86 ± 0.01	16.94 ± 0.01	16.77 ± 0.01	16.99 ± 0.01	2003.7383
"	...	...	19.04 ± 0.01	17.83 ± 0.01	16.99 ± 0.01	16.74 ± 0.01	16.94 ± 0.01	2003.7409
"	...	...	19.15 ± 0.02	18.05 ± 0.01	17.45 ± 0.01	17.29 ± 0.01	17.27 ± 0.01	2003.8091
"	...	...	19.52 ± 0.03	19.31 ± 0.01	19.02 ± 0.01	18.79 ± 0.01	18.67 ± 0.03	2003.8856
"	...	...	19.44 ± 0.03	19.36 ± 0.01	19.16 ± 0.01	18.87 ± 0.01	18.63 ± 0.03	2003.9075
"	...	...	19.25 ± 0.02	18.28 ± 0.01	17.75 ± 0.01	17.61 ± 0.01	17.50 ± 0.02	2004.9477
"	...	...	18.48 ± 0.02	17.91 ± 0.01	17.05 ± 0.01	17.16 ± 0.01	17.47 ± 0.01	2007.8857
GG Leo	18.86 ± 0.08	18.91 ± 0.04	17.12 ± 0.01	17.23 ± 0.01	16.89 ± 0.01	16.87 ± 0.01	16.93 ± 0.01	2002.1936
HS Cam	18.73 ± 0.10	18.48 ± 0.06	16.97 ± 0.01	17.43 ± 0.01	17.14 ± 0.01	17.05 ± 0.01	17.10 ± 0.01	2004.7980
"	...	...	17.40 ± 0.01	17.54 ± 0.01	17.50 ± 0.01	17.43 ± 0.01	17.15 ± 0.01	2004.9509
MR Ser	...	...	17.44 ± 0.01	17.24 ± 0.01	17.35 ± 0.01	17.04 ± 0.01	16.37 ± 0.01	2004.3898
Object	FUV	NUV	u	g	r	i	z	Phase/SDSS Date
ST LMi	16.51 ± 0.04	16.55 ± 0.02	17.97 ± 0.01	17.60 ± 0.01	17.58 ± 0.01	17.00 ± 0.01	16.24 ± 0.01	2004.9731
"	...	...	17.97 ± 0.01	17.58 ± 0.01	17.58 ± 0.01	17.10 ± 0.01	16.32 ± 0.01	2005.0527
"	...	...	17.93 ± 0.01	17.56 ± 0.01	17.56 ± 0.01	17.71 ± 0.01	16.36 ± 0.01	2005.0962
UW Pic	18.01 ± 0.05	18.11 ± 0.04	...	16.43 ± 0.24	16.08 ± 0.33	...	...	APASS
UZ For	18.25 ± 0.08	18.45 ± 0.06	...	...	...	...	...	...
VY For	18.10 ± 0.09	18.29 ± 0.04	...	...	...	...	...	...
V347 Pav	17.98 ± 0.05	17.62 ± 0.03	...	...	...	...	...	...
V349 Pav	19.36 ± 0.10	19.17 ± 0.06	...	...	...	...	...	...

Table 3
(Continued)

Object	FUV	NUV	u	g	r	i	z	Phase/SDSS Date
V381 Vel	...	18.77 ± 0.02	...	...	...	...	...	...
V388 Peg	19.r0 ± 0.12	19.13 ± 0.06	17.90 ± 0.01	18.22 ± 0.01	18.10 ± 0.01	17.78 ± 0.01	17.44 ± 0.01	2008.8273
V393 Pav	20.24 ± 0.16	19.63 ± 0.07	...	...	...	...	...	...
V479 And	18.95 ± 0.08	18.32 ± 0.04	17.58 ± 0.01	17.45 ± 0.01	17.07 ± 0.01	16.85 ± 0.01	16.78 ± 0.01	2002.7583
"	...	...	18.18 ± 0.01	17.84 ± 0.01	17.34 ± 0.01	17.16 ± 0.01	16.78 ± 0.01	2008.8196
V884 Her	15.36 ± 0.02	15.68 ± 0.02	...	13.22 ± 0.16	13.21 ± 0.28	13.09 ± 0.23	...	APASS
V1007 Her	19.18 ± 0.10	19.67 ± 0.10	...	...	...	...	...	...
V1043 Cen	17.00 ± 0.05	16.68 ± 0.02	...	16.10 ± 0.18	15.42 ± 0.07	14.70 ± 0.10	...	APASS
V1309 Ori	...	...	15.96 ± 0.01	15.96 ± 0.01	15.58 ± 0.01	15.34 ± 0.01	15.20 ± 0.01	1998.8895
"	...	...	15.92 ± 0.01	15.82 ± 0.01	15.57 ± 0.01	15.37 ± 0.01	15.16 ± 0.01	1998.8785
"	...	...	16.00 ± 0.01	16.02 ± 0.01	15.62 ± 0.01	15.44 ± 0.01	15.21 ± 0.01	1998.8922
"	...	...	15.33 ± 0.01	15.28 ± 0.01	15.16 ± 0.01	15.01 ± 0.01	14.92 ± 0.01	2002.1029
"	...	...	16.22 ± 0.01	15.93 ± 0.01	15.59 ± 0.01	15.39 ± 0.01	15.22 ± 0.01	2004.7761
V1432 Aql	16.36 ± 0.02	16.38 ± 0.02	...	...	...	...	...	...
V2301 Oph	17.21 ± 0.03	17.52 ± 0.02	18.11 ± 0.01	17.90 ± 0.01	17.62 ± 0.01	17.11 ± 0.01	16.51 ± 0.01	2005.4330
WX LMi	20.92 ± 0.03	19.49 ± 0.01	18.27 ± 0.02	17.35 ± 0.01	17.12 ± 0.01	15.58 ± 0.01	14.99 ± 0.01	2003.0863
"	...	...	18.21 ± 0.01	17.57 ± 0.01	17.06 ± 0.01	15.55 ± 0.01	14.90 ± 0.01	2003.0866
"	...	...	18.32 ± 0.02	17.70 ± 0.01	16.59 ± 0.01	15.91 ± 0.01	14.92 ± 0.01	2003.3131
HS9022+1333	21.71 ± 0.26	20.03 ± 0.08	19.06 ± 0.02	18.14 ± 0.01	17.32 ± 0.01	15.88 ± 0.01	14.98 ± 0.01	2006.0162
RXJ0154.0–5947	19.83 ± 0.12	19.69 ± 0.08	...	...	...	...	...	...
RXJ0859.1+0537	19.96 ± 0.18	20.01 ± 0.14	18.03 ± 0.01	17.69 ± 0.01	18.00 ± 0.01	17.61 ± 0.01	17.10 ± 0.01	2002.1935
"	...	...	18.03 ± 0.01	17.69 ± 0.01	18.00 ± 0.01	17.61 ± 0.01	17.10 ± 0.01	2002.1935
RXJ0953.1+1458	20.49 ± 0.25	20.26 ± 0.17	20.21 ± 0.04	19.24 ± 0.01	18.44 ± 0.01	18.27 ± 0.01	17.93 ± 0.02	2005.8658
"	...	...	20.49 ± 0.06	20.37 ± 0.02	20.39 ± 0.03	19.66 ± 0.03	18.74 ± 0.03	2006.0845
RXJ1002–1925	18.24 ± 0.08	17.51 ± 0.04	...	16.93 ± 0.08	16.00 ± 0.08	15.59 ± 0.23	...	APASS
RXJ2316–0527	17.09 ± 0.05	17.32 ± 0.03	19.85 ± 0.06	19.88 ± 0.02	19.59 ± 0.02	18.50 ± 0.01	17.60 ± 0.02	2009.7423
1RXSJ06003- 2709	19.32 ± 0.10	19.32 ± 0.06	...	...	...	...	...	...

Object	FUV	NUV	u	g	r	i	z	Phase/SDSS Date
2QZJ142256.3–022108	20.21 ± 0.04	20.21 ± 0.03	19.51 ± 0.03	19.83 ± 0.02	19.33 ± 0.01	18.98 ± 0.01	18.73 ± 0.04	2001.3943
"	...	...	21.18 ± 0.11	21.35 ± 0.05	20.51 ± 0.03	19.93 ± 0.03	19.44 ± 0.07	2007.2862
"	...	...	21.46 ± 0.13	21.54 ± 0.05	20.89 ± 0.04	20.06 ± 0.03	19.40 ± 0.06	2007.2999
"	...	...	22.05 ± 0.32	21.91 ± 0.09	21.28 ± 0.08	20.27 ± 0.05	19.68 ± 0.12	2007.1987
2QZJ142438.9–022739	19.73 ± 0.16	19.64 ± 0.11	18.08 ± 0.01	18.13 ± 0.01	17.81 ± 0.01	17.15 ± 0.01	16.98 ± 0.01	2001.3941
"	...	...	17.65 ± 0.01	17.94 ± 0.01	17.72 ± 0.01	17.17 ± 0.01	16.71 ± 0.01	2001.4543
"	...	...	19.76 ± 0.05	19.55 ± 0.01	19.61 ± 0.02	19.04 ± 0.02	18.46 ± 0.04	2007.1987
"	...	...	19.71 ± 0.04	19.55 ± 0.01	19.67 ± 0.02	19.30 ± 0.02	18.61 ± 0.04	2007.2862
"	...	...	19.83 ± 0.04	19.59 ± 0.01	19.63 ± 0.02	19.12 ± 0.01	18.37 ± 0.03	2007.2999
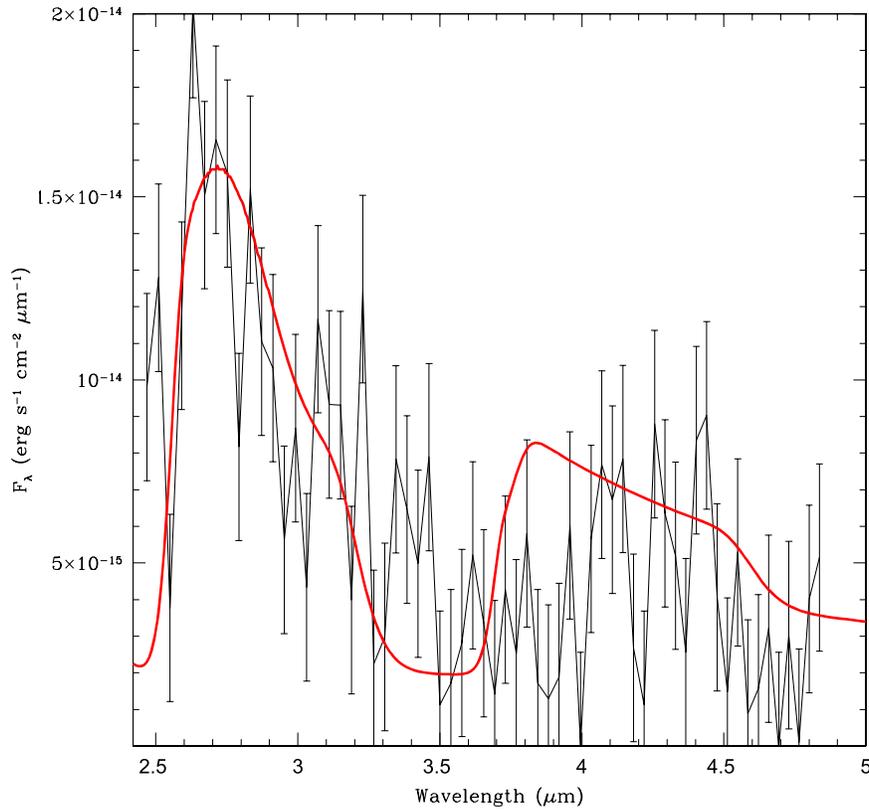
Figure 10. ISOPHT-S spectrum for AM Her. The red line is a cyclotron model with $B = 12.8$ MG. The cyclotron hump centered near 2.8 μ is due to the $n = 3$ harmonic, with $n = 2$ at 3.9 μm.

The sum of the fluxes from the two stellar components is plotted in red in Figure 9. Note that the mid-IR SEDs of late-type dwarfs are slightly fainter than the simple extrapolation of a blackbody normalized to optical/near-IR photometry (see AM Her, below). This is also almost certainly true for the UV/optical spectra of magnetic white dwarfs (see Gänsicke et al. 2001). Given the uncertainties inherent in modeling this *nonsimultaneous* data set, these small differences are not important. Fixing the distance of AI Tri so that the white dwarf represents 100% of the flux at the UVM2 minimum requires it to have $M_V = 8.6$, close to the expected value for such an object (Krzesinski et al. 2009). This, in turn, fixes the secondary star so that it has $K \sim 14.8$.

As the *WISE* light curves show, the source varies by about 0.6 mag in *W*1 and *W*2, but is constant in *W*3 to within the error bars. Given the light curve morphology and amplitude, we ascribe the variability in *W*1 and *W*2 to cyclotron emission. We explored a wide range of cyclotron models for AI Tri and found that the best fit to the *RIJHK* and *WISE* data were models with $B = 32 \pm 1$ MG. To create the observed amplitude of the *WISE* variations, assuming a shock with $kT = 5.2$ keV found in the X-ray fitting, we needed to keep the viewing angle high ($\theta = 75°$) and log $\Lambda = 3$. Note that such a model, when added to the bright phase SED (blue), does an excellent job of explaining the maximum light *JHK* photometric points (when properly accounting for their actual bandpasses).

As shown in Figure 9, the sum of the white dwarf and red dwarf blackbodies, and cyclotron emission from a 32 MG field, cannot explain the *W*3 flux. In the following, we will encounter quite a few other polars where the *W*3 luminosity is higher than

expected. In some cases (e.g., BL Hyi), the *W*3 light curves show large amplitude variations that suggest low magnetic field cyclotron emission. For most of the sources, however, the *W*3 flux is quite stable. One could invoke a cool dust shell to explain this excess, but we have chosen to use a thermal bremsstrahlung source. This emission could come from the accretion stream, absorption from which was used to explain features in both the X-ray and polarization light curves of AI Tri. Harrison et al. (2013b) and Harrison (2014) have not found any evidence to support dust shell interpretations for the mid-IR excesses of CVs. With the addition and normalization of this source inside XSPEC, we add the result to our 32 MG cyclotron spectrum to produce a model SED that reproduces the bright phase red/infrared fluxes.

There is no single component CL model, however, that can explain the variability observed at all wavelengths. To get the large cyclotron component needed to peak in the *I* and *J* bands, while having sufficient cyclotron emission to explain the *W*1 and *W*2 variability, requires $kT \sim 5$ keV, high viewing angles ($\theta > 60°$), and log $\Lambda \sim 3$. In such a model, one cannot pump up the harmonics with $n > 5$ to the level needed to explain the minimum light fluxes observed in the *U*, *B*, and V bands. Katajainen et al. (2001) noted that the circular polarization had both positive and negative maxima, indicating two-pole accretion. They suggested that the other, secondary pole had a magnetic field strength of $B = 40$–41 MG, while noting that most two-pole accretors (e.g., VV Pup, see below) have much larger differences in field strengths between the two poles. A field strength of 40 MG is much too low, however, to reproduce the variability in the bluest fluxes. In addition, it
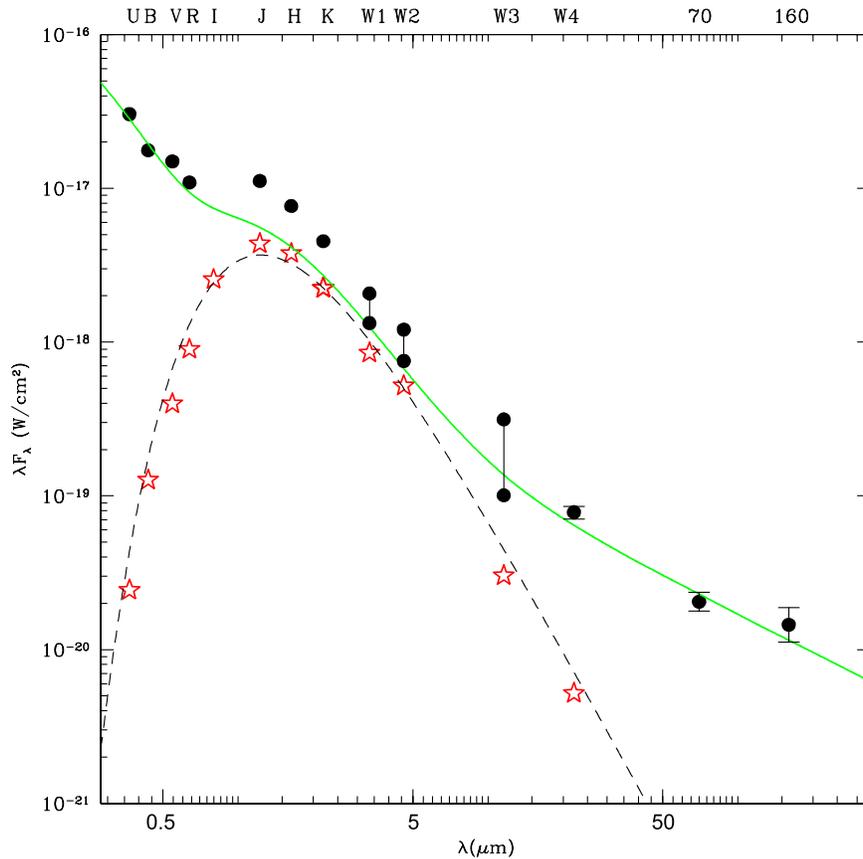
Figure 11. High-state SED of AM Her with the revised *Herschel* flux densities at 70 and 160 μm (see Figure 5 in Harrison et al. 2013b). The red star symbols represent the SED of the M4V secondary star in AM Her, and the dashed line represents a 3000 K blackbody. As in AI Tri, the minimum and maximum *WISE* fluxes are plotted and connected by a line segment. As described in the text, the green line is the sum of hot and cool blackbodies plus a bremsstrahlung component.

would add significant light to the minimum light fluxes in the red and infrared. We find that a field with $B = 73$ MG, with parameters identical to the 32 MG field used above, does an excellent job of reproducing the minimum light observations (green curve in Figure 9).

With this model it is possible to explain the observations of AI Tri. The sharp UV minimum appears to correspond to a brief self-eclipse of the 32 MG pole. At this time, the cyclotron emission from this pole essentially disappears, creating the W1 and W2 minima. However, emission from the secondary 73 MG pole never disappears and thus produces shallower minima than one would expect if the stellar components were the only sources of light in the system. Our model also appears to be consistent with the polarimetric light curves. The *UBV* (negative) circular polarization during minimum light comes from the 73 MG pole, and the smaller extrema suggest an orientation to the 73 MG pole that is unfavorable (closer to the limb). This is also consistent with a diminished or negligible UV flux that is due to foreshortening. Such an orientation, however, is favorable for producing strong cyclotron emission. This emission is greatly diluted but does not disappear, as the main accreting pole comes into view, and the UV/optical flux rises because of the transit of the main hot spot or shock region into a favorable viewing geometry. This results in the rise to the maximum in the positive circular polarization, followed by its decline into the self-eclipse.

As discussed above, if the W1 and W2 light curves result from $n = 1$ cyclotron emission, their maxima should not be exactly phased to the emission from the higher harmonics. This offset does not appear to be true for the *WISE* light curves of AI Tri. The *R*- and *I*-band light curves shown in Schwarz et al. peak at binary phase $\phi = 0.25$, very similar to that of the W1 data set (though the W1 light curve does exhibit considerable variability exactly at this phase). The best explanation for this apparent contradiction, while remaining consistent with our model, is that the emission from the $n = 1$ harmonic is mostly shaped by the self-eclipse of the accretion region of the 32 MG pole. The visual bands are strongly influenced by changing hot spot emission, and thus their variability is only partially due to cyclotron emission. So while all of the light curves appear to have similar phasing of their maxima, one must first remove the hot spot flux before we can estimate the component due to cyclotron emission. As shown in Figure 7 of Schwarz et al., both the *B* and *V* bands have more sinusoidal light curves when compared to those at *R* and *I*, suggesting that the emission from the hot spot dominates in the blue, as is found in our model.

As discussed by Bailey et al. (1983), a viewing angle where the observer looks directly down the accretion column produces nearly 100% circularly polarized flux. In V834 Cen, their observations showed that the polarization reached 30% at its maximum. If the viewing angle was similar in AI Tri, we should expect much higher polarization maxima than the $\sim$6% observed by Katajainen et al. (2001). The reason for the lower values of the peak of the circular polarization can also be
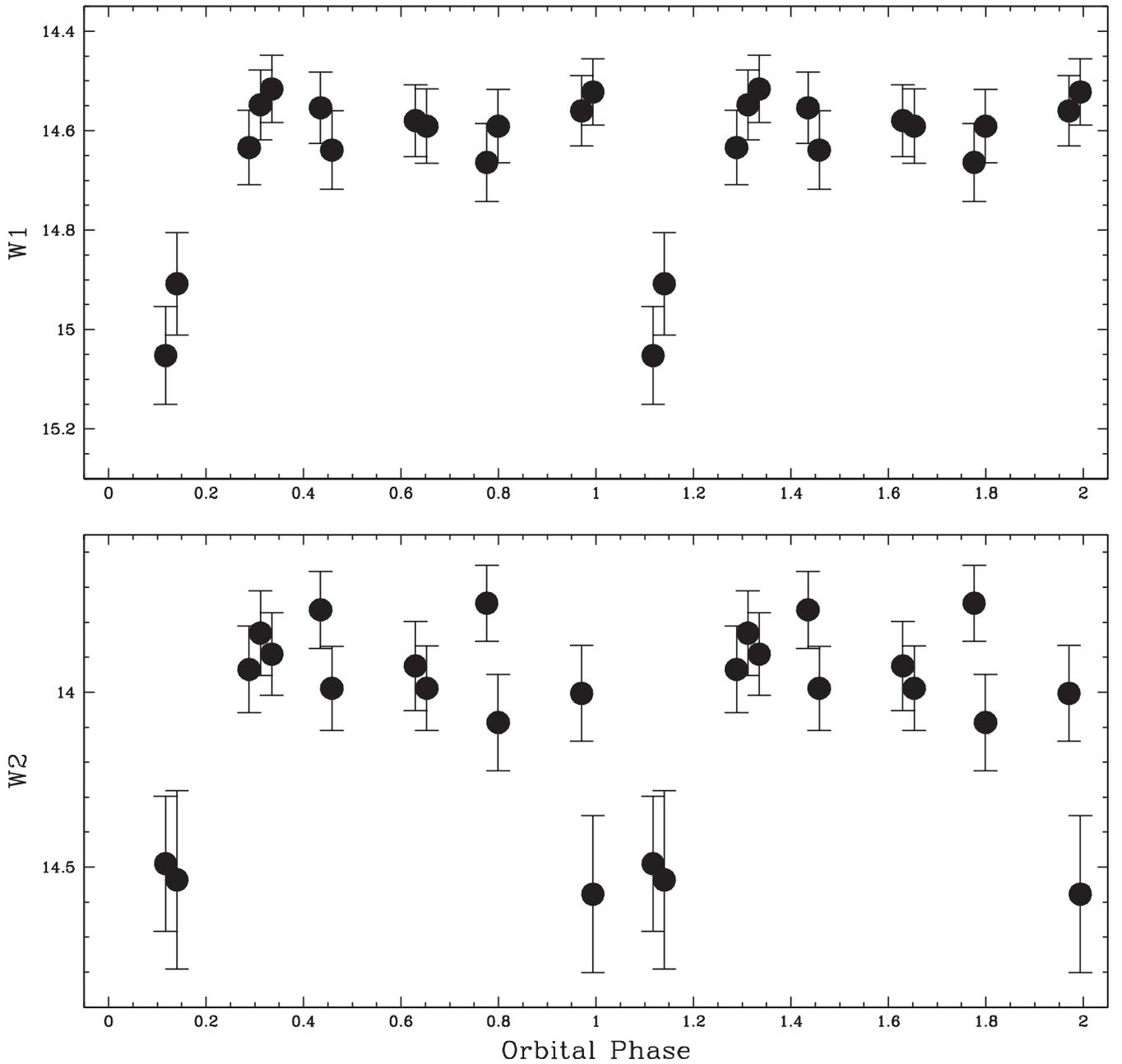
Figure 12. Light curves of AN UMa phased to the ephemeris of Bonnet-Bidaud et al. (1996).

explained by dilution due to the strong optical continuum emission from the hot spot that coincides with the polarization maxima. The *B*-band flux, presumably dominated by the hot spot, increases by $\sim$0.7 mag, so the undiluted polarization would be considerably larger than that observed.

While we have sketched out a model that can explain the observations, modeling cyclotron emission with broadband photometry can only provide weak constraints on the geometry of, and the conditions within, the cyclotron emission regions. This exercise was conducted for AI Tri to demonstrate that the addition of *WISE* light curves can lead to increased insight into the behavior of polars. Phase-resolved near-IR spectroscopy of AI Tri would be extremely useful to confirm the field strength of the primary pole. The secondary star would also be much more prominent in the *K* band during the light curve minimum. Even *JHK* light curves would be helpful in evaluating the

model we have just proposed, but it will require phase-resolved optical spectra covering the entire visual window over a full orbital cycle to generate a more robust model of this system.

3.2. AM Her

Harrison et al. (2013b) have already presented the *WISE* light curves of AM Her, the prototype polar. The somewhat sparse *WISE* light curves of AM Her show large amplitude variations in the *W*1 through *W*3 bands. These variations appear to be identically phased to the *JHK* light curves, which have been shown to be due to orbitally modulated cyclotron emission from a $B = 13.8$ MG field (Campbell et al. 2008a). As shown in Figure 2, the *W*3 band is broad enough to encompass some emission from the $n = 1$ harmonic for $B = 13.8$ MG. However, a lower field strength ($B \approx 12$ MG) appears to be needed to
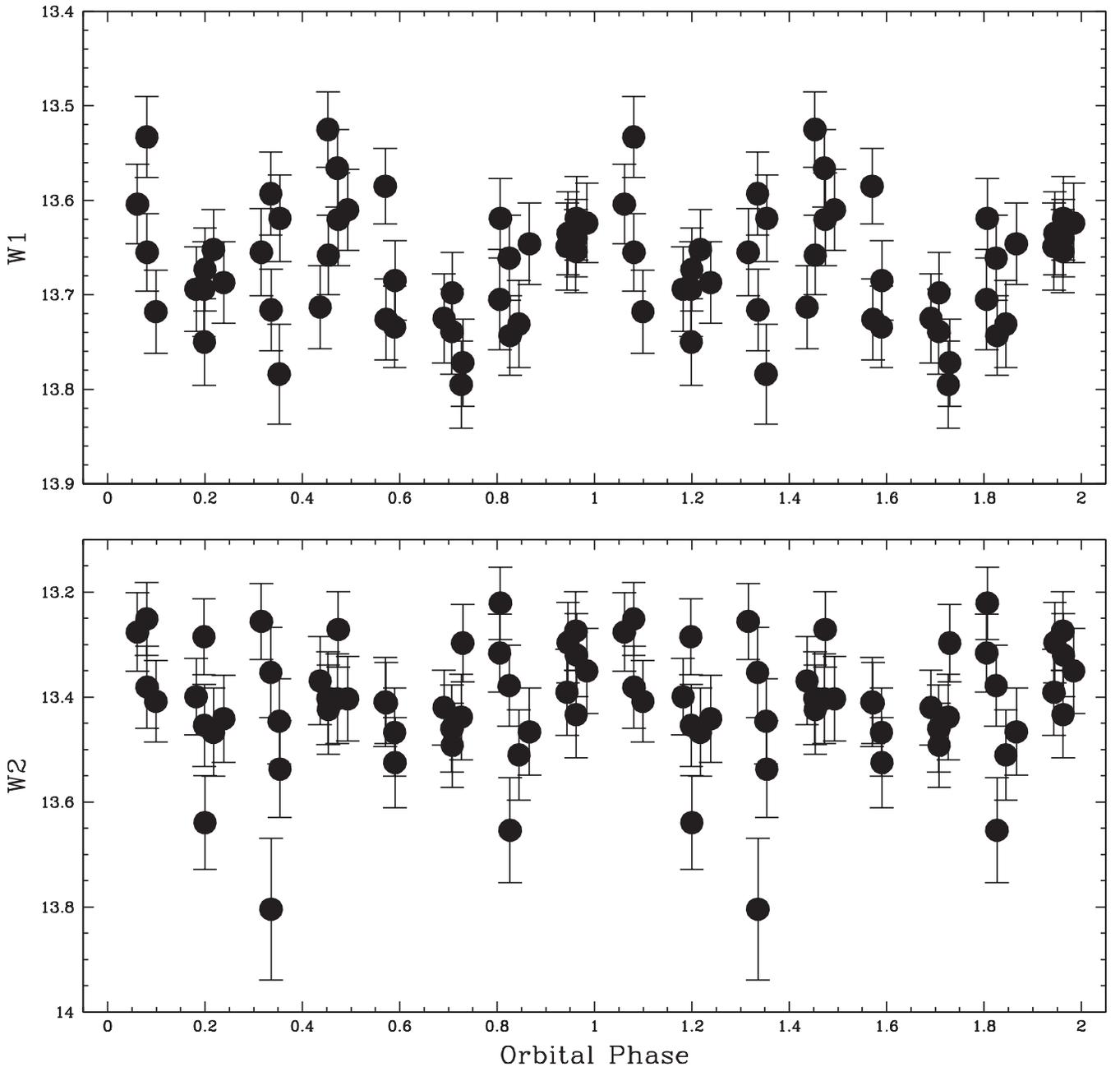
Figure 13. Light curves of AP CrB phased to the ephemeris of Thorstensen & Fenton (2002).

better center the $n = 1$ harmonic in the $W3$ band to create the very large amplitude variations seen in this bandpass. As noted in Harrison et al., AM Her was in a high state when observed with *WISE*. The fact that the $W3$-band light curve showed variations with an amplitude of $\Delta W3 \sim 1.6$ mag from the $n = 1$ harmonic *during* a high state clearly shows that the common assumption that the lowest harmonics are always optically thick at this time is certainly false. Perhaps the $n = 1$ emission comes from a region farther from the core of the accretion column, where the field strength is lower and the material more optically thin.

This hypothesis is fortified by a low-resolution spectrum obtained with ISOPHT-S[11] on the *Infrared Space Observatory*

(*ISO*). Shown in Figure 10, the ISOPHT-S data cover the spectral region from 2.47 to 4.87 μm. While this spectrum, obtained on 1996 September 14, has a very low S/N (CVs were generally much too faint to be detected with *ISO*), it certainly appears to show the $n = 3$ harmonic from a 12.8 MG field. AM Her was in a high state at the time of this observation.

The *Herschel* observations of AM Her also occurred during a high state, and the 70 and 160 μm PACS fluxes were consistent with the extension of a simple power law from the *WISE* data. Harrison et al. ascribe this excess to a combination of blackbody and thermal bremsstrahlung emission. With improvements to the calibration of the *Herschel* PACS photometry, including a recently updated aperture-correction table (Balog et al. 2014) and improved user familiarity (see

---

[11] http://iso.esac.esa.int/manuals/HANDBOOK/pht_hb/
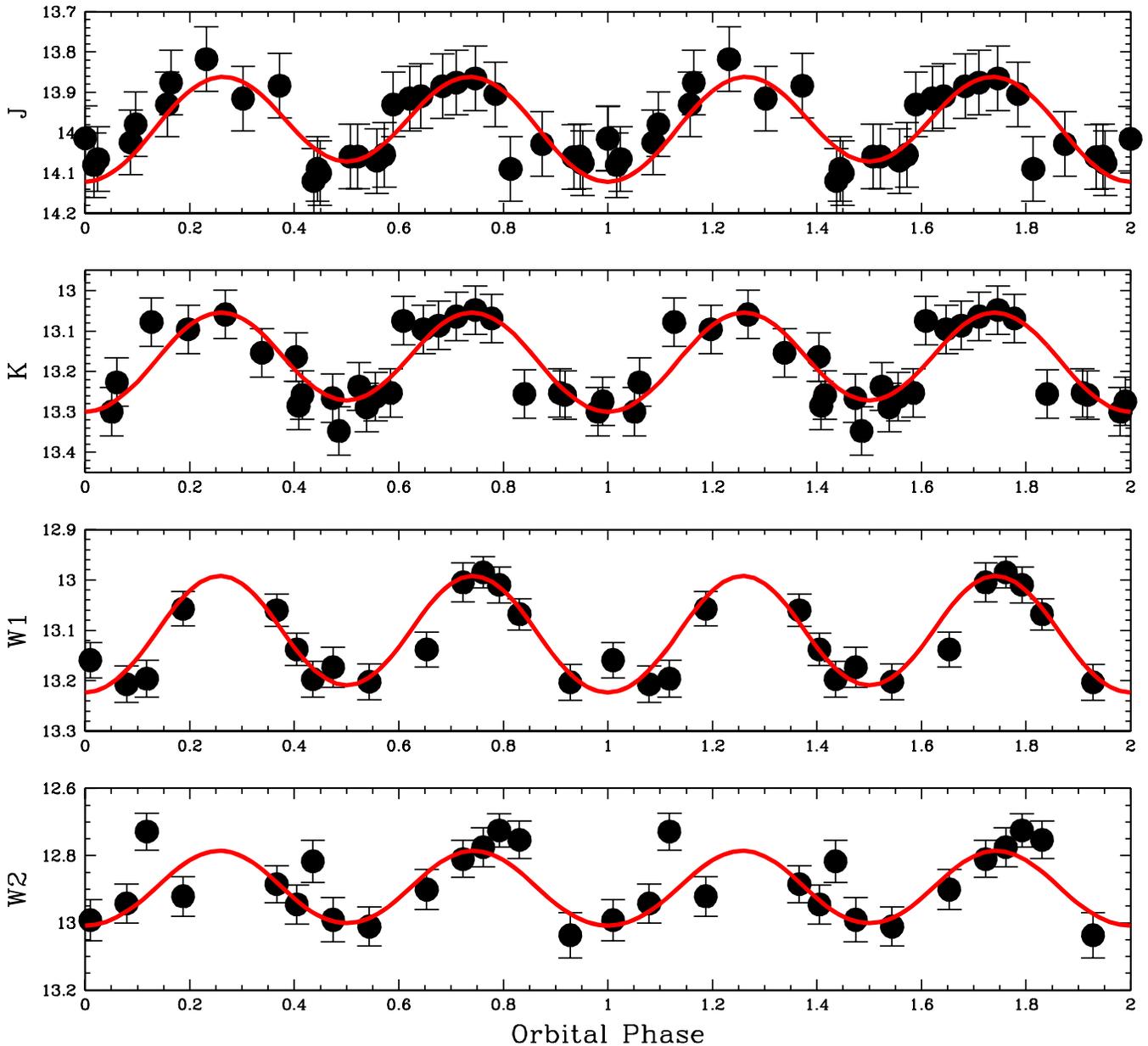
Figure 14. Light curves of AR UMa phased to the ephermeris of Schmidt et al. (1996). The solid red line is an ellipsoidal variation model, with $i = 65°$, as described in the text.

Harrison et al. 2014), we have re-reduced the data for AM Her and present the revised photometry in Table 5. The large change in fluxes is due to the use of a much smaller aperture (3″) to extract the point-source flux, as compared to the default value used by Harrison et al. (2013b). It is important to note that the position of the 70 μm source is located almost 3″ north of the nominal position of AM Her, whereas the 160 μm source is within 1″ of that position. Typically, the astrometry from the *Herschel* PACS data is good to ⩽ 2″ (Ibar et al. 2010).

With the new values for the PACS data, we revised the AM Her SED plot in Harrison et al. (2013b) and modeled it using XSPEC assuming a hot white dwarf, a cool secondary star, and a thermal bremsstrahlung component (see Figure 11). As in AI Tri, we plot the observed ranges in the *WISE* magnitudes. The flux and spectral type of the secondary in AM Her are well known, and here we plot its SED (red stars) using the *WISE* colors of an M4V normalized to its *K* magnitude. As noted above, blackbody curves overestimate the fluxes of late-type dwarfs in the mid-IR. In addition to the data, we plot a 3000 K blackbody (dashed line) normalized to the donor star's *K*-band flux. The *W*1 flux from an M4V is below this curve, due to the large water vapor absorption feature in this bandpass, and the *W*3 and *W*4 stellar fluxes are only about 68% of that of the blackbody model. If this deficit was properly accounted for, the XSPEC model would pass through the minimum *W*3 flux, while remaining consistent with the *W*4 flux. Unfortunately, we do not have any information on the variability of AM Her in *W*4 or in the *Herschel* PACS bandpasses. Note that extrapolation of the model spectrum to radio frequencies implies that the free–free component must turn over if it is to be consistent with the
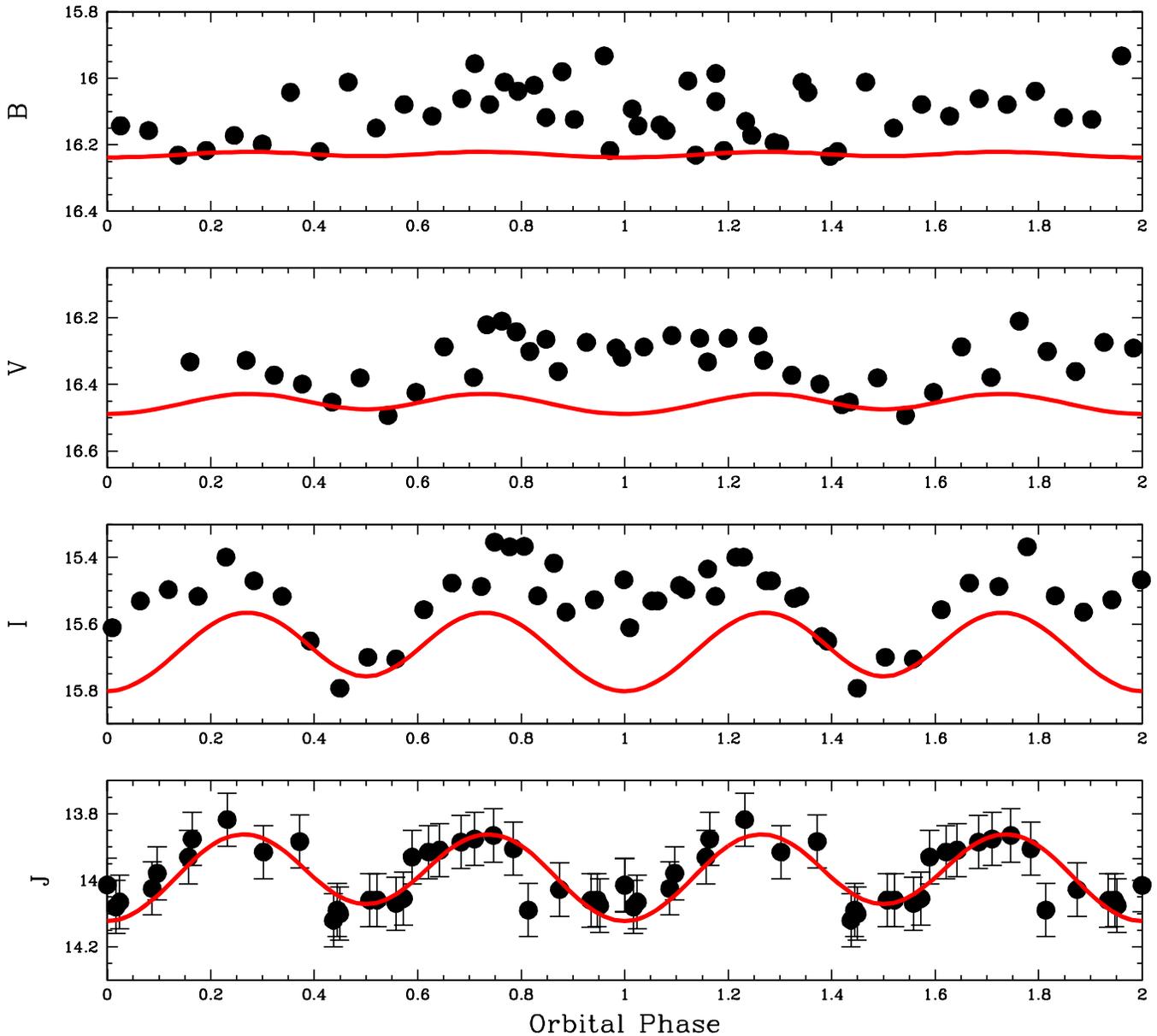
Figure 15. *BVIJ* light curves of AR UMa as in Figure 14. For clarity, we repeat the *J*-band light curve in this figure.

high-state 4.8 GHz flux density of 0.69 mJy observed by Chanmuam & Dulk (1982).

3.3. AN UMa

Bonnet-Bidaud et al. (1996) present optical photometry and spectroscopy of AN UMa and derive an ephemeris for this system. They found that there might be a higher-order term, suggesting possible asynchronism. Their optical photometry indicated a broad minimum that in the X-ray corresponded to a bright "spike." The *WISE* light curves, presented in Figure 12, show a deep, short-lived minimum at the same phase as those seen in the optical, though there appears to have been a small shift in phase in the nineteen years since the establishment of the ephemeris. Outside of this minimum, the light curves are consistent with little variation. Bonnet-Bidaud et al. believe the optical minima are due to a grazing eclipse of the accreting pole. The depth of the minima in the mid-IR suggests that there is probably strong cyclotron emission present in both bands

because a simple hot spot eclipse is unlikely to create such large minima at these wavelengths. This is consistent with the $B = 32$ MG field strength found by Campbell et al. (2008b).

AN UMa was serendipitously observed by *Spitzer* at a time when the AAVSO database suggests AN UMa had $v \sim 16$, about 1 mag below its brightest recorded levels. The *Spitzer* observations occurred at $\phi = 0.25$, and the $3.6\,\mu$m ("S1") flux density is in agreement with the *W*1 light curve. The 2MASS data for AN UMa was obtained in a similar outburst state at an orbital phase of $\phi = 0.23$.

3.4. AP CrB

Gänsicke et al. (2004) and Schwope et al. (2006) both argue that the magnetic field strength in AP CrB is above 100 MG. Thorstensen & Fenton (2002) present an ephemeris for AP CrB and assume that the light curve minimum was due to the secondary star (i.e., phase 0.0). *WISE* observed this source 42 times, and while the source is slightly variable, the only real
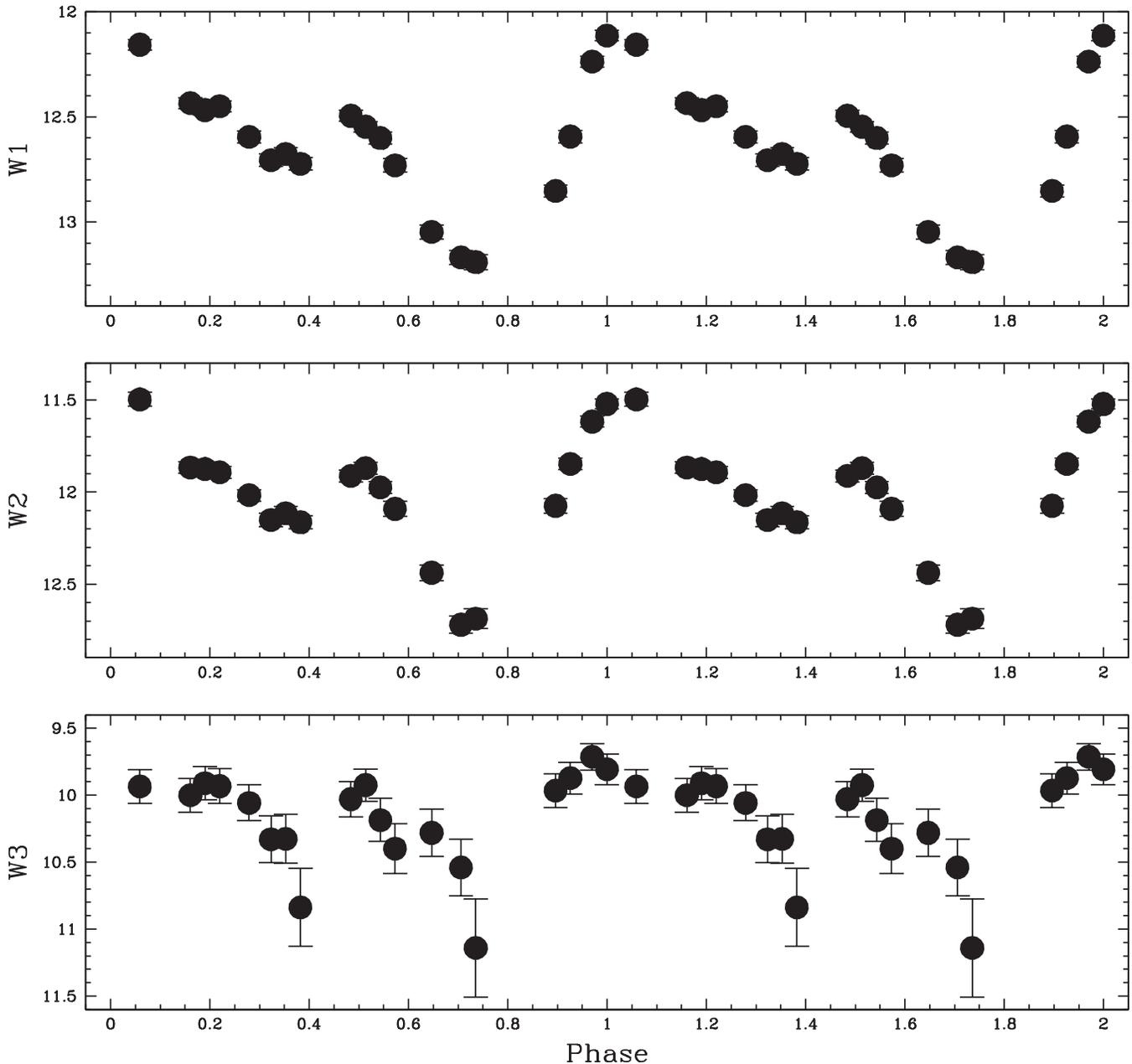
Figure 16. Light curves of BL Hyi, phased to the ephemeris of Wolff et al. (1999), where phase zero is defined as the onset of the bright phase.

features are weak minima near $\phi = 0.2$ and 0.7 in the $W1$ light curve (see Figure 13). These could be due to ellipsoidal variations because the offset in the phasing is within the error bars of the ephemeris for AP CrB.

3.5. AR UMa

Ferrario et al. (2003) believe AR UMa harbors a white dwarf with a very high field strength, with an average surface field of $B \sim 155$ MG. Such a high field strength precludes cyclotron emission in the *WISE* bandpasses. The *WISE* light curves appear to be dominated by ellipsoidal variations. Combining the *WISE* data with the *J*- and *K*-band data from Howell et al. (2001), and with the ephemeris of Schmidt et al. (1996), we can use WD2010 to explore ellipsoidal models for this system. Gänsicke et al. (2001) estimate the primary star

temperature to be $T_{WD} \approx 20,000$ K. Harrison et al. (2005) estimate a spectral type of M5.5V for the secondary star. Using these input parameters, we ran a large number of light curve models for AR UMa and find that the best-fitting model has $T_{WD} = 15,000$ K, $T_{RD} = 3000$ K, and $i = 65°$. This model is indicated by the red lines in Figure 14. The inclination we find is slightly lower than that found by Howell et al., but it is higher than that of Schmidt et al. (1996). We note that Hubeny (1988) obtained $T_{WD} = 15,000$ K from UV spectral modeling, in agreement with our value. The minima at phase 0.5 are extremely sensitive to the temperatures of the two stellar components.

In Figure 15, we present the *BVI* light curves of AR UMa obtained with the NMSU 1 m (and repeat the *J*-band light curve from Figure 14) with the same ellipsoidal model as derived for the infrared. It is clear that there is cyclotron
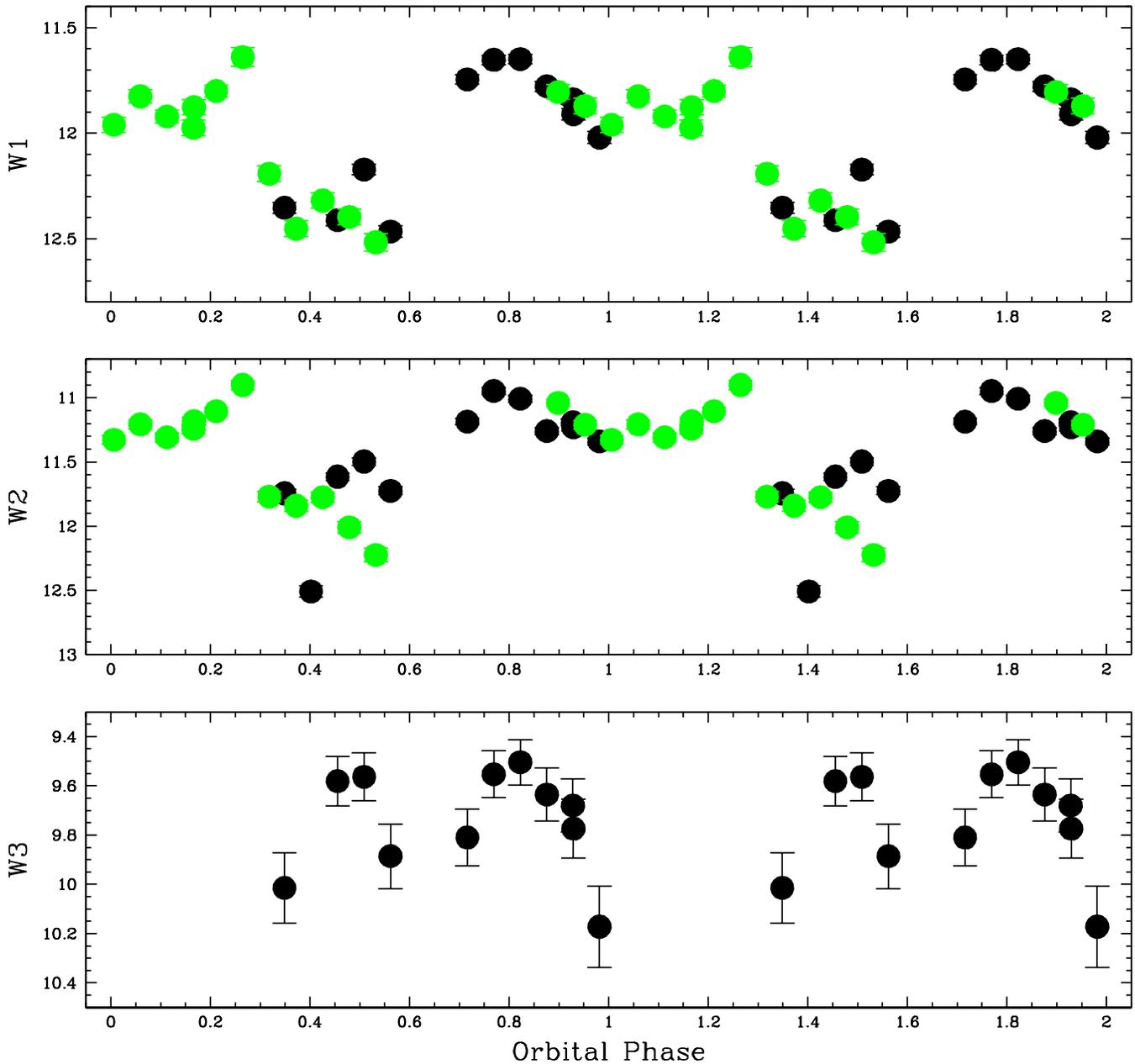
Figure 17. Light curves of BY Cam. The data plotted in green are from the *WISE* three-band Cryo single-exposure catalog. We have phased these data using the ephemeris listed in Schwarz et al. (2005).

emission in the *I* band that contaminates the primary minimum, which may be one reason that Schmidt et al. obtained a lower value for the inclination. It is also apparent that the *V*-band light curve is shaped by cyclotron emission. To get the $n = 1$ harmonic to explain the light curves in both bands requires AR UMa to have an effective field strength of $155 \leqslant B \leqslant 170$ MG. Such fields put the $n = 2$ harmonic in the *U* band. This result is consistent with the limit derived by Howell et al. (2001).

AR UMa was observed by *Spitzer* on two different epochs, during both of which the AAVSO database shows that AR UMa was in a similar visual state ($v \sim 16.5$). These observations occurred at phases 0.68 (2006 December) and 0.89 (2007 May), and the flux densities listed in Table 2 are consistent with the *W1* and *W2* light curves.

3.6. BL Hyi

Beuermann et al. (2007) summarize what is known about BL Hyi and present Zeeman tomography that shows a complex field distribution with two dominant regions of higher field strength. They find that an offset dipole with a polar field strength of 59.5 MG, inclined by $80°$ to the rotation axis, fits their phase-resolved spectroscopy. The optical light curve of BL Hyi is dominated by a bright phase that lasts for 40% of the orbit. Beuermann & Schwope (1989) model this as the main accretion spot that is located at a colatitude that puts it below the orbital plane and dominates the X-ray emission in the low state. At higher accretion rates, a second pole becomes active, and it is visible for most of the orbit. This pole predominantly emits soft X-rays.
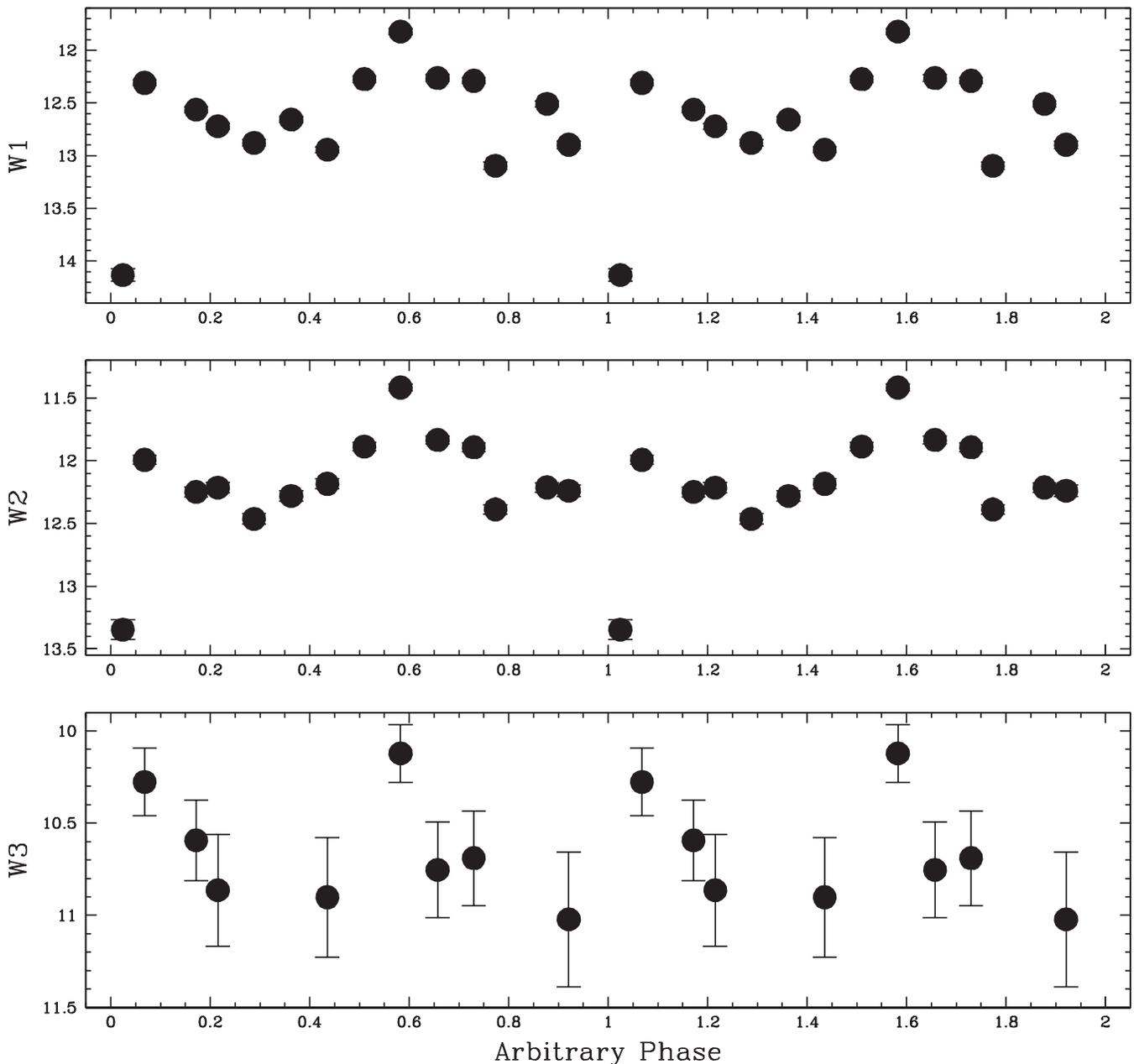
Figure 18. Light curves of CD Ind phased to the shorter period ephemeris listed in Vennes et al. (1996).

Wolff et al. (1999) present an ephemeris where $\phi = 0$ is defined as the "onset" of the optically bright phase. We have used this to phase the *WISE* light curves presented in Figure 16. With this phasing, the maxima in the *WISE* data occur at $\phi = 0$, and the bright phase lasts for 60% of an orbit. The *WISE* light curves are very similar to the white light data for BL Hyi in a low state presented by Cropper (1987). The circular polarization during a high state reached its maximum during the light curve minimum. We do not know the state of BL Hyi during the epoch of the *WISE* observations. The *WISE* data show variations over an orbit that exceed one magnitude in each of the bands. The deepest minimum occurs at $\phi = 0.75$, but a secondary minimum occurs near phase 0.35. It is quite possible that ellipsoidal variations from the late-type (M6/7, Schwope & Beuermann 1987) donor star are coloring the light curves and that both minima are partially due to this effect. This would

suggest an offset of $\Delta\phi = \pm 0.25$ to the Wolff et al. ephemeris to get to a true orbital phasing and that the orbital inclination must be toward the high end of the published range for this object ($20° \leqslant i \leqslant 70°$).

The large amplitude variations in all three bands indicate that cyclotron emission dominates. Ferrario et al. (1996) presented near-IR spectra of BL Hyi and found cyclotron humps centered at 1.3, 1.6, and 2.2 μm that suggested a field strength of 23 MG. Schwope et al. (1995a), however, observed "halo" Zeeman absorption lines that indicated a field strength of 12 MG. To get the large amplitude variations in *W*3 requires that the $n = 1$ harmonic falls in this bandpass. For field strengths above 14 MG, only a small fraction of the emission from the $n = 1$ harmonic is present in the *W*3 bandpass. A field strength of $B = 12$ MG is the best solution in that it has significant $n = 1$ emission in *W*3, with $n = 2$
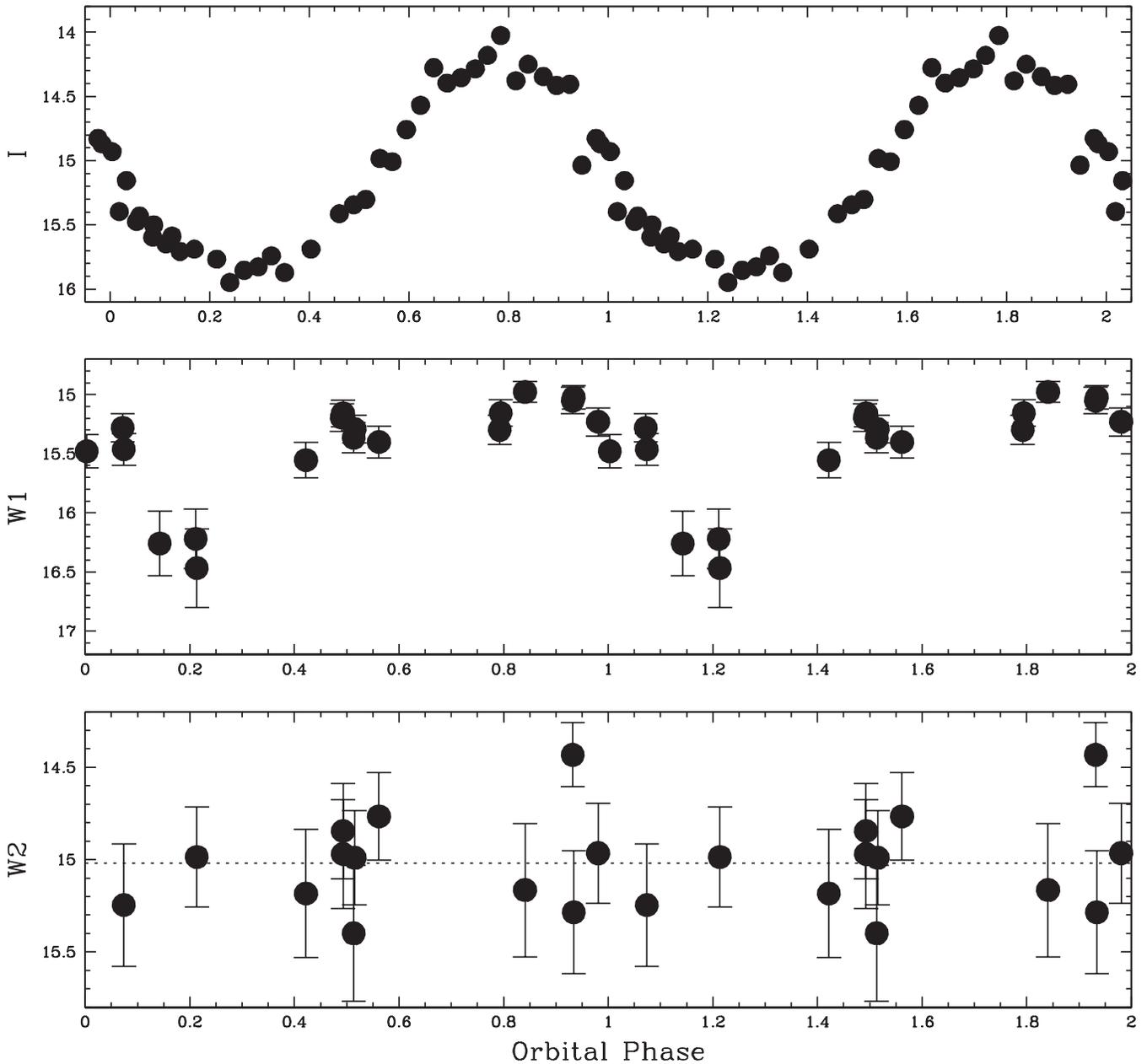
Figure 19. *WISE* light curves of CP Tuc compared to the *I*-band light curve of Thomas & Reinsch (1996). The mean *W*2 magnitude is indicated by a dotted line in the bottom panel.

emission captured in the *W*2 band, and $n = 3$ in *W*1. *The $n = 4$–6 harmonics from this field can then explain the near-IR spectra obtained by Ferrario et al. (1996).* It is important to note that while the *W*3 bandpass shares the phasing of the two minima, the morphology of this light curve is slightly different from the shorter-wavelength data sets, and the total amplitude of variability over an orbital period is smaller. Such differences could easily arise from the different angular distribution of the emission from the n = 1 harmonic.

3.7. BY Cam

BY Cam is a member of the small family of "asynchronous" polars, where the white dwarf in the system has a rotation period that differs from the orbital period. Unlike IPs, such systems do not appear to have accretion disks, and mass transfer occurs through an accretion stream. Schwarz et al. (2005) present a binary star ephemeris that we have used to phase the *WISE* data presented in Figure 17. In addition to the data obtained during the main cryogenic survey phase, there also exists a large number of three-band Cryo observations (plotted in green). The resulting light curves show large amplitude ($\Delta m \sim 1$ mag) variations in all three bandpasses. To get the three-band observations to overlap the four-band data, we adjusted the *W*1 magnitudes by -0.2 mag, and *W*2 by -0.3 mag. This difference could be due to an actual change in BY Cam or simply due to a different normalization for the three-band data. The AAVSO data indicate that BY Cam had $v \sim 15.3$ at the epoch of the four-band data; there are no corresponding visual estimates at the time of the three-band observations.
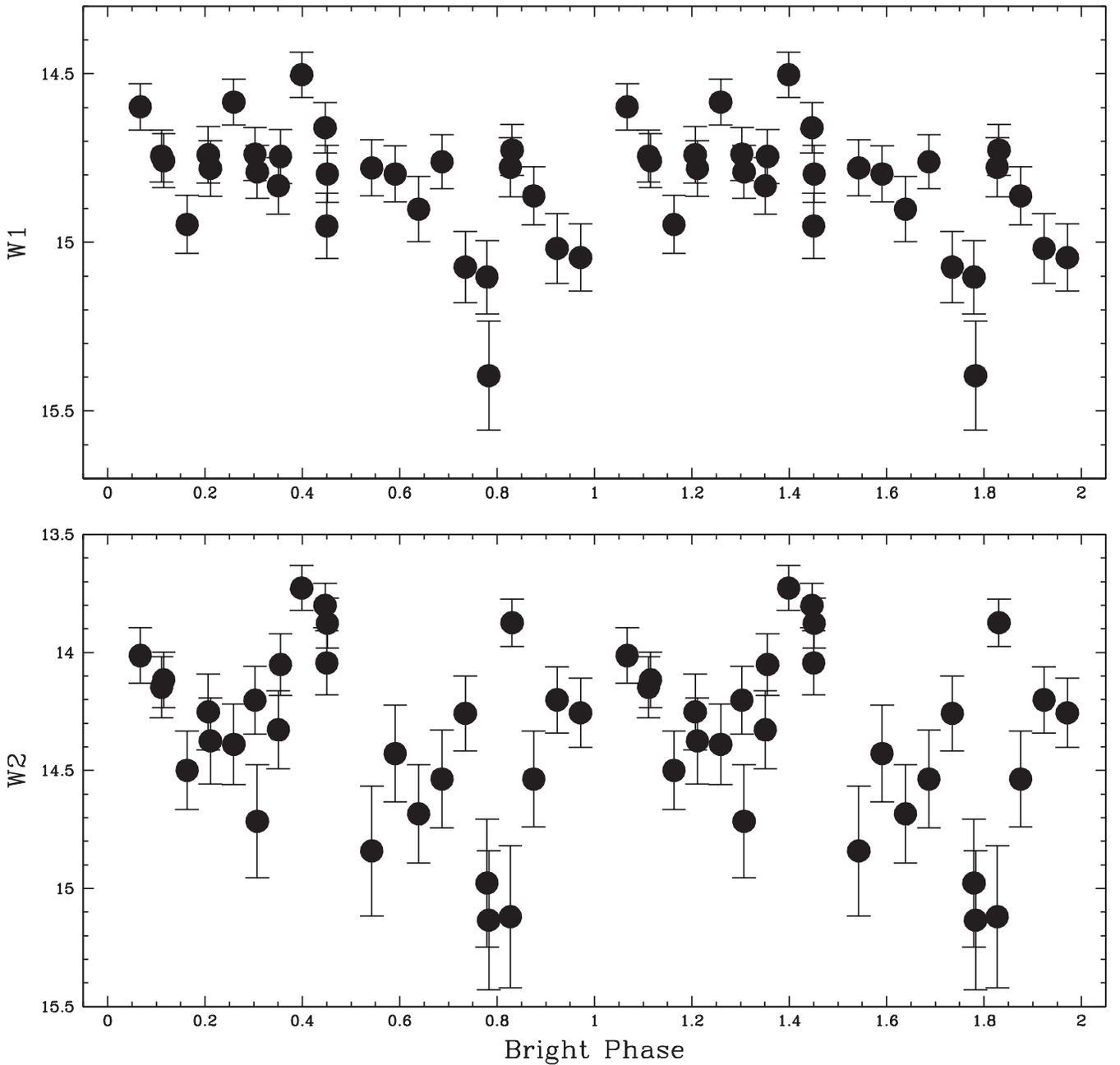
Figure 20. *WISE* light curves of CW Hyi phased to the "bright phase" ephemeris published by Schwope et al. (2002).

Superficially, the *W*1 and *W*2 light curves resemble the *K*-band light curve of AM Her (see Figure 1 in Campbell et al. 2008b), with ellipsoidal variations partially responsible for the light curve minima at $\phi = 0$ and 0.5. This suggests that these two bandpasses are dominated by cyclotron emission. The *W*3 data set is sparser, having maxima at phase 0.5 and 0.8. The latter peak is consistent with the other two bands, but the former falls during their primary minima. The lack of three-band Cryo data for *W*3 makes it difficult to intepret the 11.5 μm light curve. The large amplitude variability of BY Cam in the *W*3 bandpass suggests that cyclotron emission might be present, but this interpretation rests on the two minimum flux measurements. Cropper et al. (1989) estimated a field strength of 40.8 MG for BY Cam. Schwope (1995) tabulate the field strength as 28 MG. This latter field strength would allow for fundamental harmonic

cyclotron emission to appear in both the *W*1 and *W*2 bands, explaining the light curves.

Given the beating of the spin and orbital periods that is so prominent in optical data (see Honeycutt & Kafka 2005), it is somewhat surprising that the four-band and three-band data sets so closely resemble each other in both amplitude and phasing. The first four-band observation occurred on MJD 55267.243, and the first three-band observation took place on MJD 55458.635, or $\Delta t = 191.392$ days. Pavlenko et al. (2007) give the beat period as 14.568 days, and Honeycutt & Kafka (2005) give it as 14.54 days. These values suggest that the *WISE* observations occurred about 13.14 beat periods apart, perhaps sufficiently close to allow for similar morphologies and amplitudes in the cyclotron emission at the two epochs.
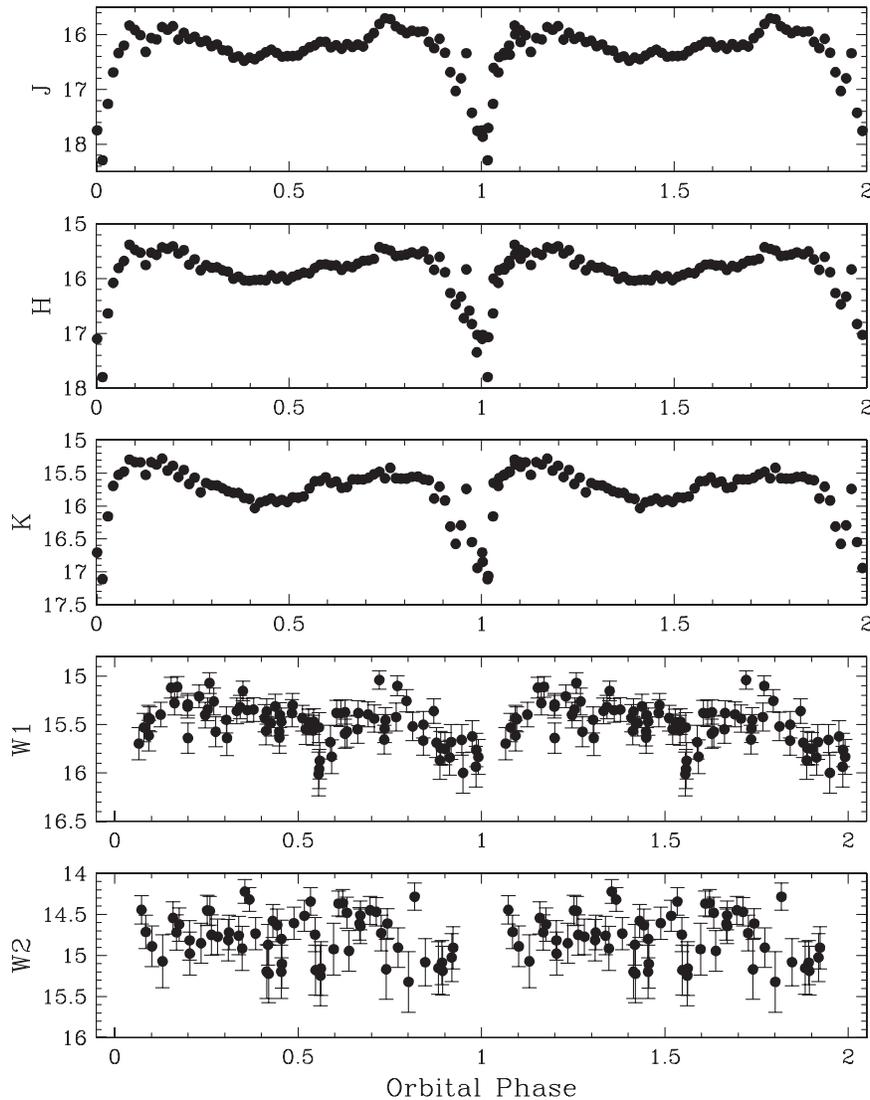
Figure 21. *JHK + WISE* light curves of EP Dra phased using the ephemeris by Schwope & Mengel (1997). The SQIID data are from 2004 July 30.

3.8. CD Ind

CD Ind appears to be an asynchronous polar. Vennes et al. (1996) found two probable orbital periods of 110.75 minutes, and its one-day alias of 102.83 minutes, from phase-resolved spectroscopic observations. As shown in Figure 18, phasing the *WISE* data to the shorter period results in the observed deep minimum falling close to phase zero. If the longer period is assumed to be the orbital period, then this minimum falls at phase 0.58. With the analysis of their light curve data and the periods found by Vennes et al., Schwope et al. (1997) suggest that CD Ind has a very small asynchronicity of 1%. They believe that the changing shape of the light curves may indicate a pole-swapping accretion mode. In this scenario, if the far, or southern pole, is accreting, it can be self-eclipsed. If the nearer pole is accreting, it is never eclipsed. The deep minima in the *WISE* light curves certainly seem to indicate a self-eclipse of the emission region.

Though no cyclotron features were detected in their spectra, Schwope et al. estimate a field strength of $B = 11 \pm 2$ MG based on arguments about the properties of an optically thin cyclotron continuum. All three of the *WISE*

bands show large amplitude variations. Ignoring the dip due to the self-eclipse, $\Delta W1 = 1.4$ mag, $\Delta W2 = 1.2$ mag, and $\Delta W3 = 1.0$ mag. Harkening back to our results for BL Hyi, it is clear that the *WISE* light curves are consistent with a field strength of $B \approx 11$ MG, as estimated by Schwope et al. The *W*3-band light curve is too sparse to examine the relative phasing of the three bands, but they share primary maxima and have a similar morphologies, except near phase zero. Unfortunately, the S/N ratio for the *W*3 data is too low for an in-depth comparison. The large amplitude of the variations in the *W*3 band implies that the $n = 1$ harmonic must be partially optically thick.

3.9. CP Tuc

CP Tuc is a short-period polar (89 minutes) whose visual light curve has a single broad maximum once each orbit. Thomas & Reinsch (1996) present a radial velocity curve analysis that supplies an orbital ephemeris for the system, to which we phased the *WISE* light curve data. Given the two magnitudes of variation in the *I* band, there has to be substantial cyclotron emission in the system, but the optical spectra do not
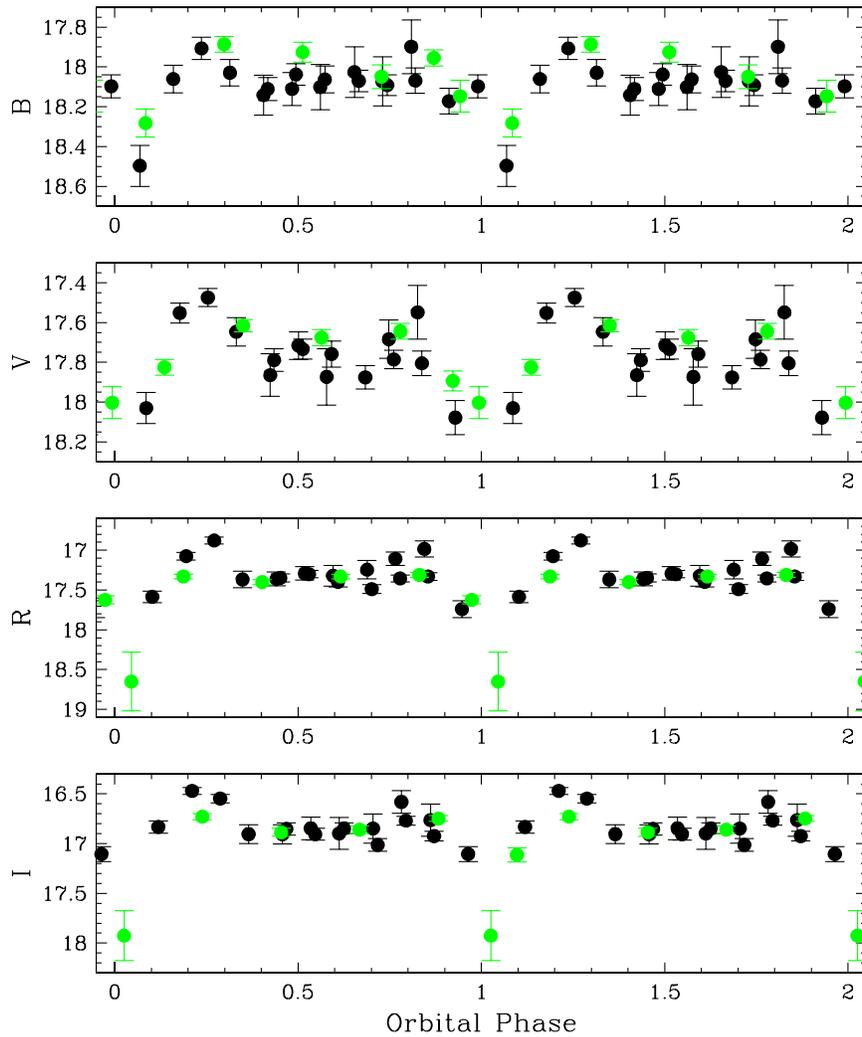
Figure 22. *BVRI* light curves of EP Dra. The filled black circles are for 2001 December 2, and the green circles are the 2005 March 2 observations.

reveal humps from discrete cyclotron harmonic emission. This suggests a low field strength, a small viewing angle to the accretion region, or a very high temperature. Thomas & Reinsch derive a shock temperature of 17 ± 3 keV and estimate a field strength of $B \lesssim 17$ MG.

We have extracted and plotted the Thomas & Reinsch I-band data along with the *WISE* light curves in Figure 19. The *W*1 light curve shows large amplitude variations ($\Delta W1 = 1.5$ mag), whereas the *W*2 shows no detectable variability (though the S/N ratios for the *W*2 data are quite low). The morphology of the *W*1 light curve is different from the *I* band, showing a broader maximum and a narrower minimum. This can be interpreted as being due to more highly beamed emission from the higher harmonics, as compared to the lower harmonic that is responsible for the *W*1 signal. As shown in Figure 1, a field with $B \approx 16$ MG would have the $n = 2$ harmonic in the *W*1 band, with nothing in *W*2, and is thus consistent with the estimate from Thomas & Reinsch (1996). Such a field then has the $n = 8$ harmonic centered in the *I* band. As shown in Figure 2, such a high harmonic from a high-temperature shock would be hard to discern, explaining the lack of discrete cyclotron features in the optical spectra of CP Tuc.

CP Tuc was not detected in the 2MASS PSC, though it is visible on the *K*-band image. Our reduction gives

$K_{2MASS} = 15.3 \pm 0.25$ at a phase of $\phi = 0.93$. CP Tuc was also detected serendipitously by *Spitzer* in the *S*1 and *S*2 bands (during warm operations) near phase $\phi = 0.37$. These *Spitzer* fluxes are perfectly consistent with the *WISE* light curves, even though the two sets of observations had $\Delta t = 2.6$ years.

3.10. CW Hyi

CW Hyi is a relatively long period polar, $P_{orb} = 3.03$ hr, that shows strong optical and polarimetric variability, but no discrete cyclotron features (Schwope et al. 2002). Schwope et al. believe that the cyclotron emission region remains visible throughout the orbit and that the variability is due to cyclotron beaming. They also give an ephemeris for CW Hyi where phase zero corresponds to the "center of the bright phase." We have phased the *WISE* light curves using this ephemeris (see Figure 20). Both the *W*1 and *W*2 light curves are complex, though the *W*1 light curve variations appear to be random and of modest amplitude. The *W*2 light curve shows variations with a much larger amplitude over an orbit, $\Delta W2 \approx 1.5$ mag, that has a brief maximum near $\phi = 0.4$ and a short-lived, deep minimum at $\phi = 0.8$.

Schwope et al. (2002) liken CW Hyi to EF Eri and presume that it has a similar field strength ($B \sim 13$ MG). It is clear from the light curves that we must have cyclotron emission in the *W*2
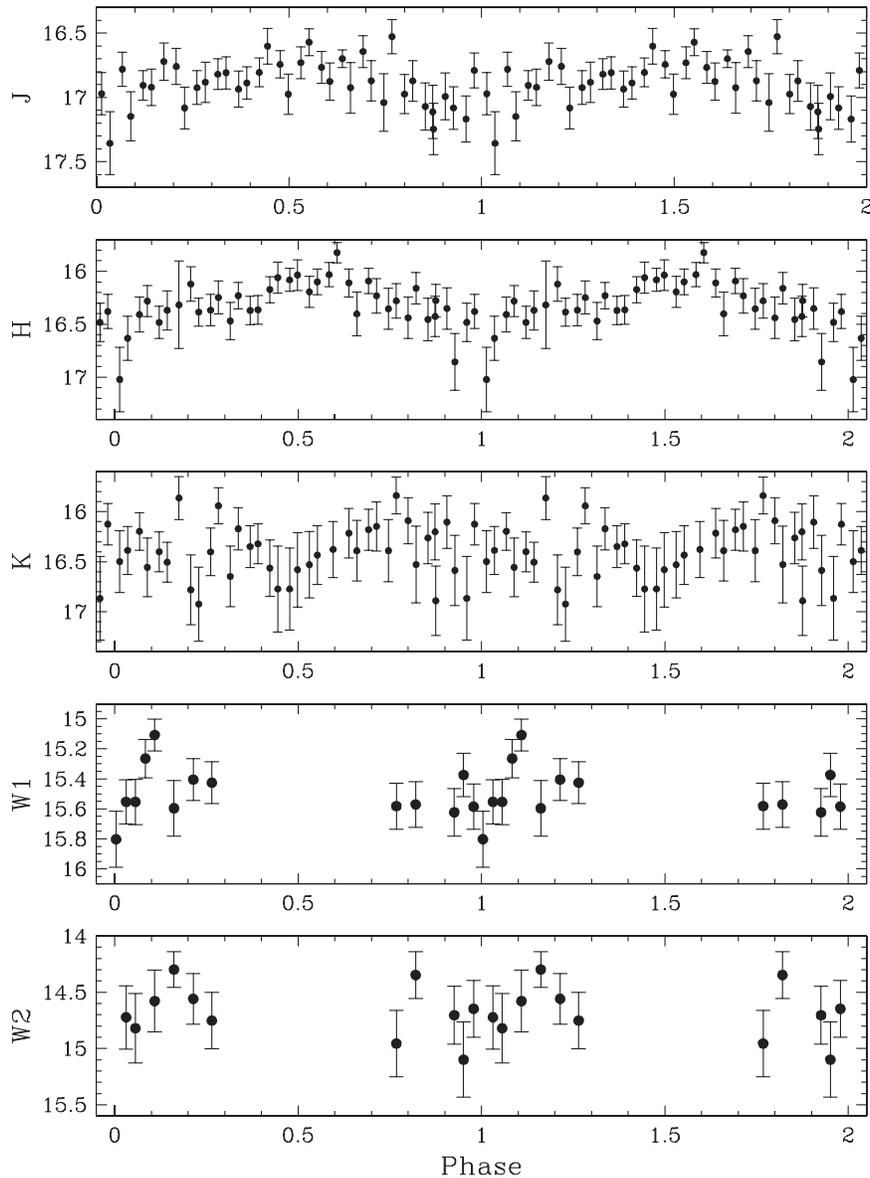
**Figure 23.** *JHK* (from Campbell et al. 2008b) and *WISE* light curves of EQ Cet.

bandpass, but very little in *W*1. As shown in Figure 1, fields with $B \sim 20$ MG can reproduce the observed variability. Note that Schwope et al. found that the TiO features of the secondary star were weakly visible in their spectra, which suggests that some of the observed variability in the *WISE* bandpasses are due to ellipsoidal modulations. CW Hyi was weakly detected in the W3 band, giving a surprisingly large color: $(W1 - W3) = 1.7$ mag. This excess is similar in size to that of BL Hyi, which has strong cyclotron emission in the *W*3 bandpass. A very low field model like that used for BL Hyi, however, would predict significant cyclotron emission in the *W*1 band. Thus, the origin of the *W*3 excess is probably not due to cyclotron emission.

3.11. EP Dra

EP Dra is a well-known eclipsing polar of short period. Schwope & Mengel (1997) derive an ephemeris for EP Dra from optical spectroscopy, and we have used it to phase the infrared photometry presented in Figure 21. Along with the

WISE data, we present *JHK* light curves obtained using SQIID on the KPNO 2.1 m telescope. In addition, we present *BVRI* light curves of EP Dra obtained with the NMSU 1 m in Figure 22 on two different epochs, separated by four years. The morphologies of the light curves in all nine of these bandpasses are very similar, though they all show a small offset from the phase zero of the Schwope & Mengel ephemeris. *WISE* actually did observe EP Dra during an eclipse, but the source was too faint to be detected. Bridge et al. (2003) present high time resolution photometry of the eclipses in EP Dra and find that the entire eclipse only lasts for 6.8 minutes (which is why our *V*-band observations missed the minima).

While the overall morphology of the light curves at all wavelengths is remarkably similar, there are subtle differences between the various bands. In both of the *WISE* bandpasses, there is a short-lived minimum at phase 0.57. In the *JHK* light curves there is a small brightening that is exactly coincident with this event. Nothing is seen in the optical light curves at this phase. The *BVRIJHK* light curves all show a prominent
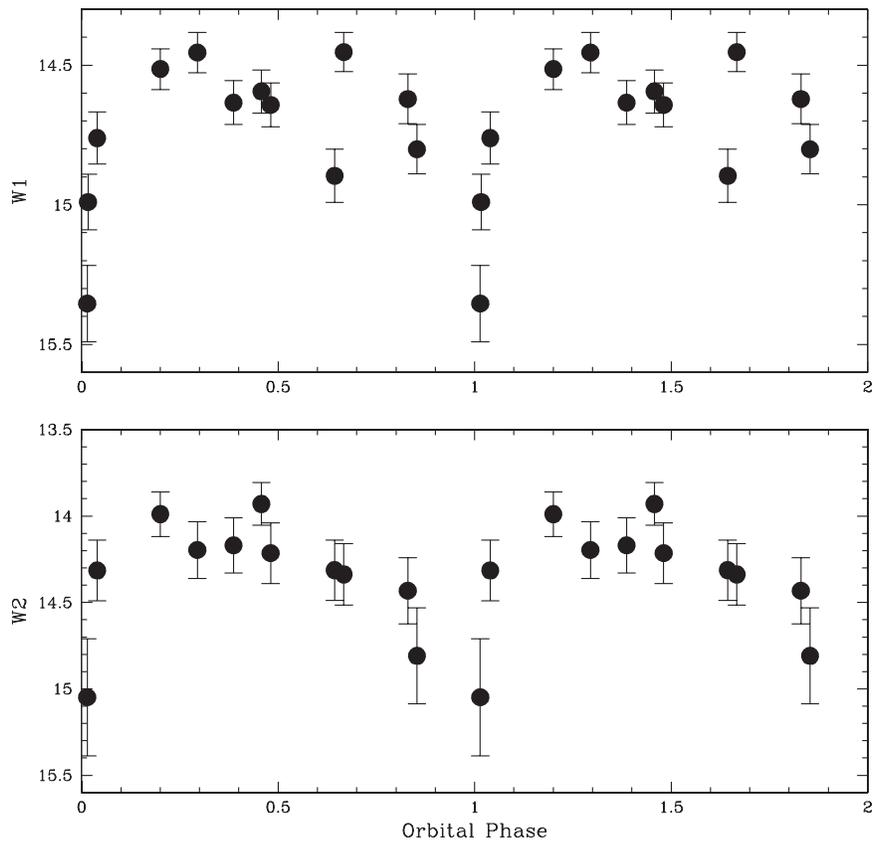
Figure 24. *WISE* light curves of FL Cet phased to the ephemeris listed in Schmidt et al. (2005a).
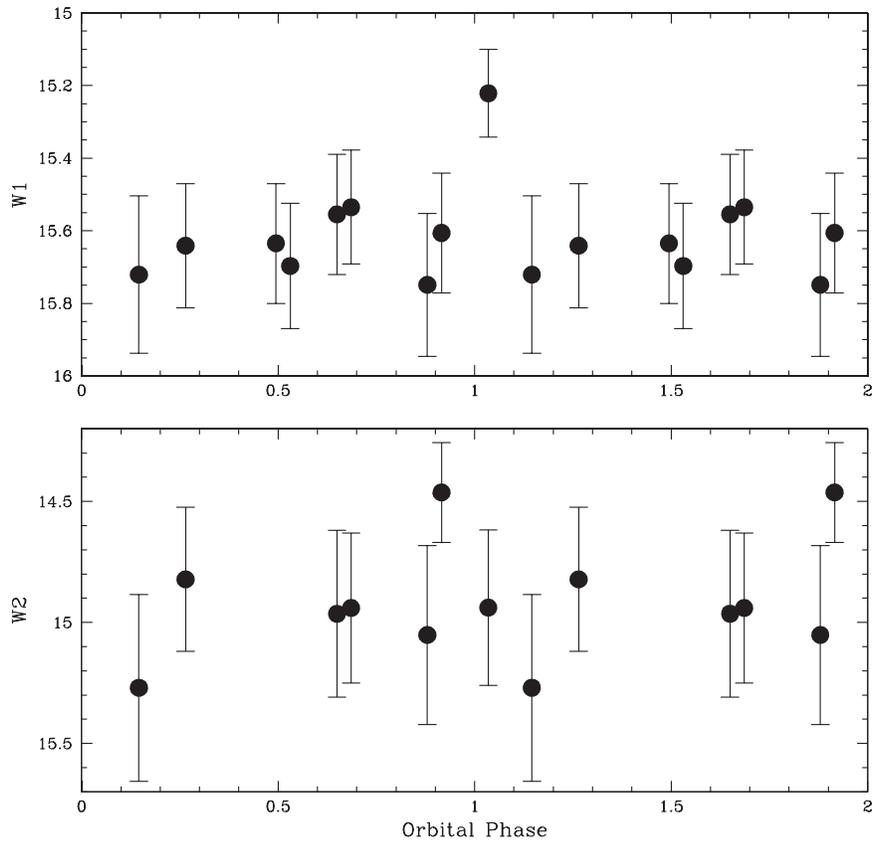
Figure 25. *WISE* light curves of GG Leo phased to the ephemeris in Burwitz et al. (1998).
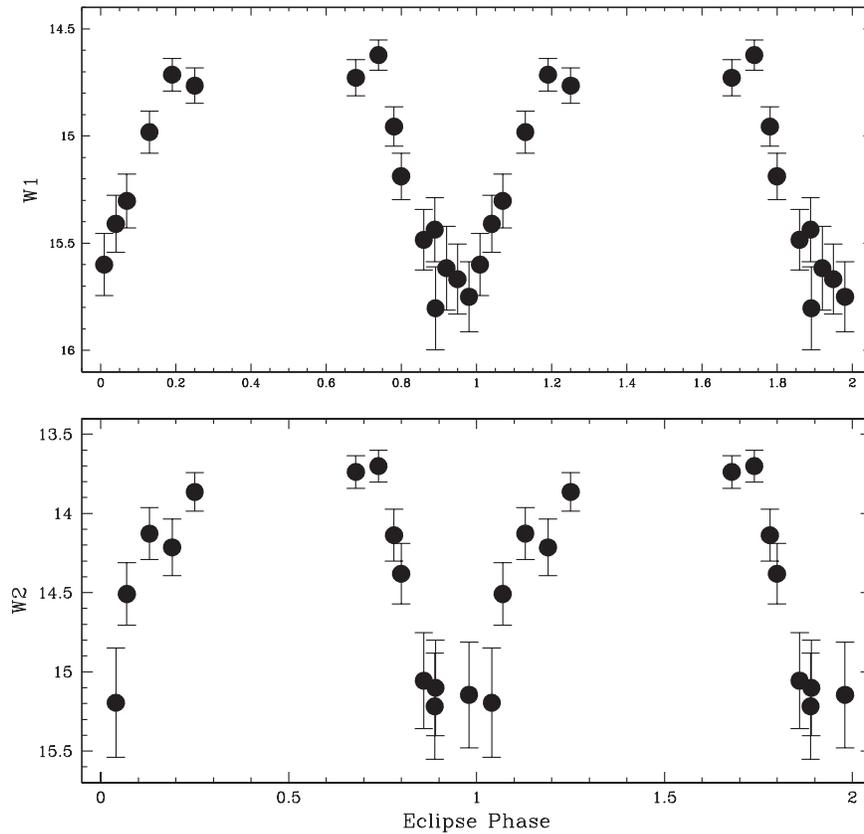
Figure 26. *WISE* light curves of HS Cam phased to the ephemeris by Tovmassian et al. (1997).

postminimum brightening. A smaller such feature occurs *before* the minimum in both the *J* and *V* bands. It is tempting to ascribe the morphology of the *JHK* light curves to ellipsoidal variations, but the ~2 mag depth of the main eclipse suggests that the luminosity in these bands is dominated by cyclotron/hot spot emission.

Schwope & Mengel (1997) detected Zeeman absorption lines in the accretion halo, which indicate a field strength of 16 MG. Such a field strength is consistent with the infrared light curve data. Clearly, *W*1 is shaped by the same emission present at shorter wavelengths, while *W*2 is only partially influenced by such emission. We believe that a slightly lower field strength would be a better match. If $B = 15$ MG, then the $n = 2$ harmonic would be strongest in the *W*1 bandpass and less prominent in *W*2 (see Figure 1). This could also explain the minima seen at $\phi = 0.57$ by presuming that this harmonic is partially optically thick at this phase. The corresponding maxima in the *JHK* bands are then from optically thin harmonics with $n \geqslant 3$. This implies that our viewing angle to the accretion region is at its maximum at $\phi = 0.57$. If symmetric, the other maximum would occur at $\phi = 0.07$. It is interesting that the *W*1 bandpass is depressed at this phase compared to the other, shorter-wavelength light curves, which are all near their peak brightnesses at this time.

The stability of EP Dra between the two epochs of optical observations is remarkable. This is reinforced by the match of the 2MASS data to our near-IR light curves, even though there were eight years between observations. Like CW Hyi, EP Dra was weakly detected in *W*3 and has a very large mid-IR excess: $(W1 - W3) = 2.42$ mag. Unlike CW Hyi, however, the lower field strength of EP Dra would lead to a small amount of cyclotron emission from the $n = 1$ harmonic in the *W*3 bandpass.

3.12. EQ Cet

Campbell et al. (2008b) present phase-resolved *JHK* spectroscopy of the short-period polar EQ Cet, from which they derive a field strength of 34 MG by modeling the observed cyclotron features. We use the phasing in that paper for the *WISE* light curves presented in Figure 23. A 34 MG field would not have cyclotron emission in the *K* band, and thus the light curve in that bandpass appears to be dominated by ellipsoidal variations from the secondary star. Unfortunately, the orbital period of EQ Cet (92.8 minutes) is similar to that of the *WISE* mission, and thus the phase coverage of the light curves is very poor, missing the times of maximum cyclotron emission that are visible in the *J* and *H* bands. A 34 MG field would have the $n = 1$ harmonic nearly centered in *W*1 and very little emission in *W*2.

3.13. FL Cet

FL Cet is a short-period eclipsing polar with $P_{orb} = 87$ minutes. Schmidt et al. (2005a) present an ephemeris for this object, and we have used it to phase the *WISE* light curves. Woudt et al. (2004) think FL Cet is a single-pole accretor with the spot hidden for half an orbit. Schmidt et al. present high-state optical spectra that appear to show cyclotron harmonics at 5600, 6550, and 7600 Å. Their low-state spectra show harmonics at 5180, 5590, 6210, 6860, and 7780 Å. From the latter they estimate $B = 29$ MG and $kT = 15$ keV. The *WISE* light curves shown in Figure 24 reveal a deep, sharp eclipse in
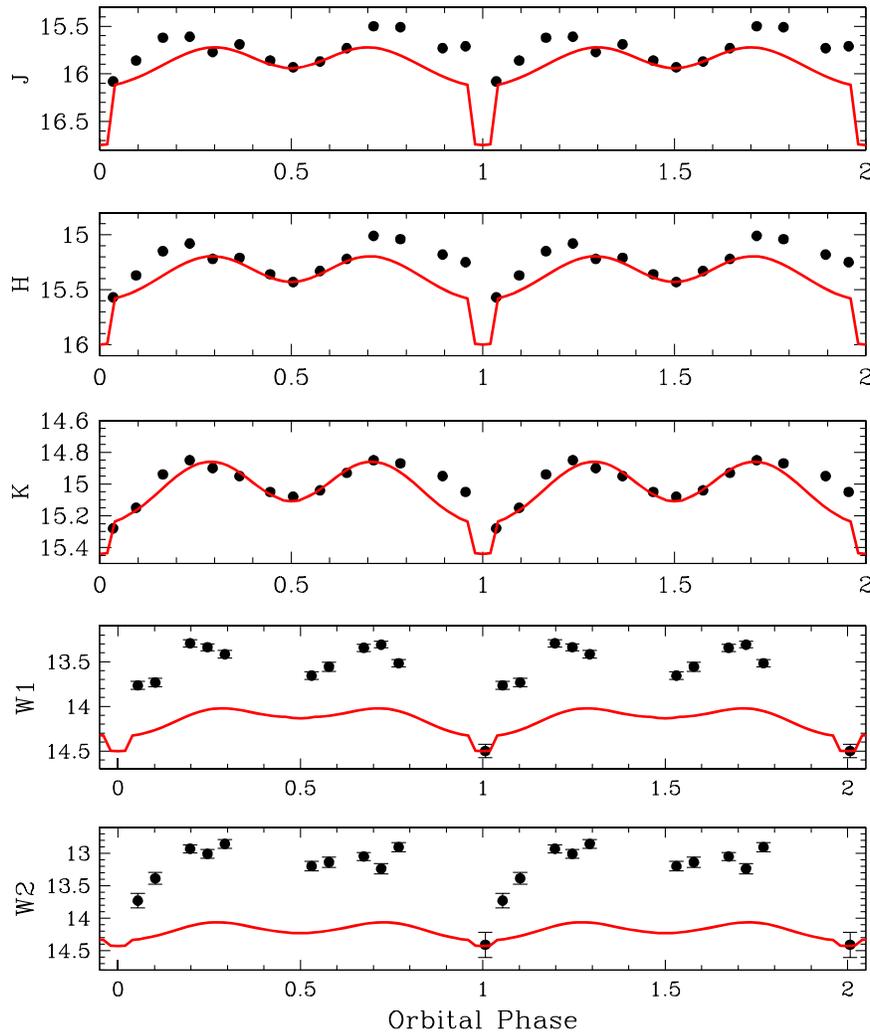
Figure 27. SQIID *JHK* + *WISE* light curves of HU Aqr phased to the ephemeris in Wittenmeyer et al. (2012). The *JHK* data were obtained during a low state, whereas the *WISE* observations probably occurred during a high state. The red solid line is an ellipsoidal variation model using the masses of the stellar components listed in Schwope et al. (2011).

*W*1 and a similar but broader event in *W*2. Clearly, there must be strong cyclotron emission in both bands to get such deep eclipses. A 29 MG field would have the $n = 1$ harmonic spanning both bandpasses, thus explaining the observations.

The *WISE* observations were actually obtained on two different epochs with three data points from 2010 January 13, and the rest were from 2010 July 19. The AAVSO has FL Cet at $v = 17.5$ during the first epoch, but no data for the second (though it was in a high state one month later). There is no offset between the two data sets, so we presume that FL Cet was low during all of the *WISE* observations. FL Cet was serendipitously observed with *Spitzer* on 2013 October 20. Due to the survey nature of those data, the phases are dramatically different between the two bands ($\phi_{S1} = 0.57$, $\phi_{S2} = 0.24$). Compared to the *WISE* fluxes at these phases, the *Spitzer* data caught FL Cet in an even lower state ($\Delta m \geqslant 1$ mag). As demonstrated by the large amount of SDSS photometry listed in Table 3, FL Cet was located within the SDSS II supernova survey region (see Frieman et al. 2008). These data appear to show that FL Cet was in a high state for much of the time from the end of 1998 until early 2003. However, this is contradicted by comparing to the 2MASS data (epoch 2000.7), which are much fainter than the UKIDSS database (epoch 2005.9),

showing that it did drop into low states during this period. Like several of the polars encountered above, FL Cet has a large *W*3 excess, $(W1 - W3) = 2.9$, that cannot be explained by cyclotron emission.

3.14. GG Leo

GG Leo is an ultrashort-period polar ($P_{orb} = 79.9$ minutes) for which Burwitz et al. (1998) derive an ephemeris from dips in the X-ray light curve. Their spectroscopy indicates an offset from the X-ray dip ephemeris to the binary star ephemeris of $\Delta\phi = 0.085$. We have phased the *WISE* data using this offset ephemeris, and the result is shown in Figure 25. GG Leo is faint in the mid-IR, so the error bars on the *WISE* data points are large. Clearly, however, there are no large-scale variations seen in these data. There is a lack of AAVSO data at the time of the *WISE* observations, but 10 days earlier, it had $V \geqslant 17.3$, suggesting it was in a low state. *Spitzer* data exist for this object, and the *S*1 and *S*2 flux densities agree with the mean values of the *W*1 and *W*2 data.

Brinkworth et al. (2007) combined the *Spitzer* data with *JHK* from 2MASS to construct an SED and concluded that GG Leo had a significant mid-IR excess due to dust emission. There are
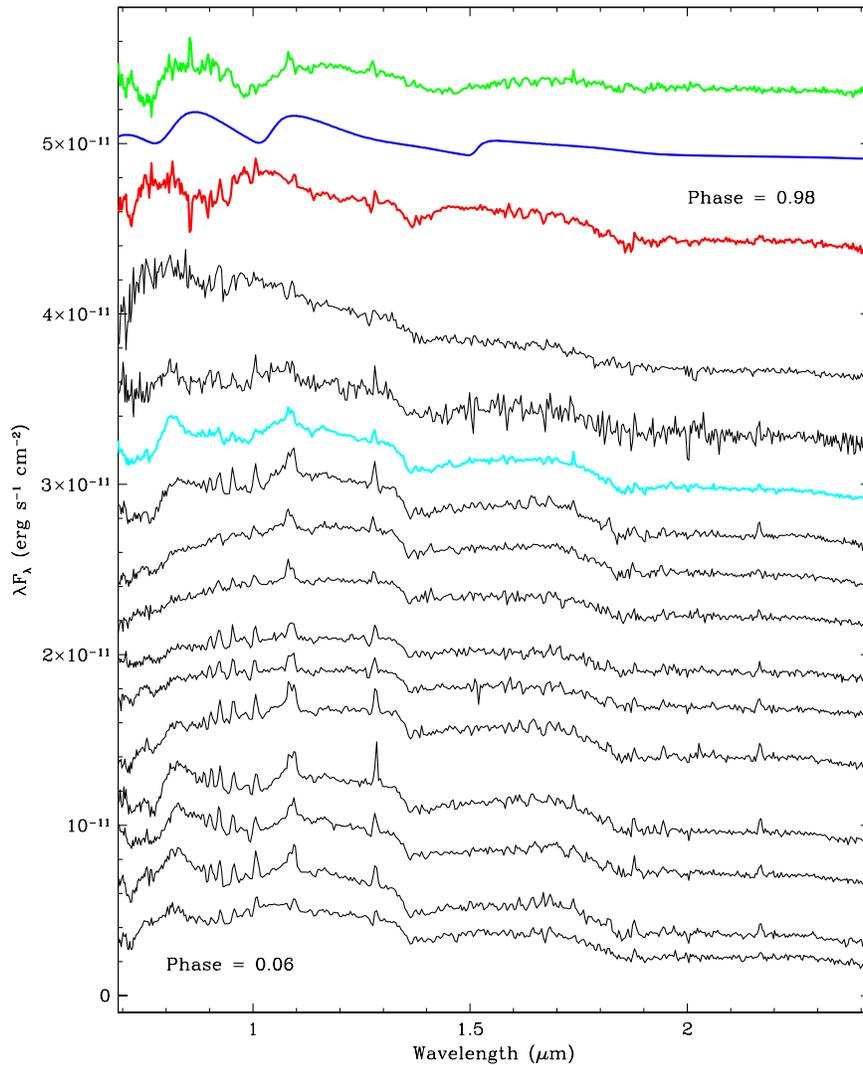
Figure 28. Phase-resolved spectroscopy of HU Aqr obtained with SpeX on the IRTF. The spectra increase in phase from bottom to top in increments of $\Delta\phi \sim 0.06$ (the spectrum at $\phi = 0.86$ was corrupted and is not present). HU Aqr was in a high state during these observations. We have subtracted the spectrum closest to the light curve minimum ($\phi = 0.98$, red) from a spectrum showing cyclotron emission ($\phi = 0.73$, cyan) to produce the secondary star-subtracted spectrum at the top (green). A cyclotron model with $B = 31.5$ MG is plotted in blue.

two problems with that conclusion. The first is that the 2MASS data were obtained at $\phi_{\text{X-ray}} = 0.63$, whereas the *Spitzer* data were obtained at $\phi_{\text{X-rray}} = 0.86$. The *V*- and *R*-band light curves presented by Burwitz et al. (their Figure 2) show that GG Leo is at or close to a maximum at phase 0.65, but near a minimum at phase 0.9. Thus, if there is cyclotron emission in the near-IR, GG Leo will certainly be much brighter ($\sim$1 mag) during the phase of the 2MASS observations when compared to that of the *Spitzer* data. Second, the 2MASS and *Spitzer* observations are not simultaneous. The UKIDSS database has GG Leo two magnitudes fainter in *J* and 1.1 mag fainter at *K* than it is in the 2MASS PSC. Without simultaneous data, it is dangerous to attribute the SED of GG Leo to dust.

Burwitz et al. concluded that the shape of the continuum in the optical spectra they obtained was consistent with cyclotron emission from a field with $B = 23 \pm 3$ MG and having $\theta = 55°$ and $kT \geqslant 19$. Such a field would have the $n = 1$ harmonic at 4.6 μm and the $n = 4$ to 2 harmonics in *J*, *H*, and *K*, respectively. The visual spectrum would be dominated by $n \geqslant 6$ harmonics, and with the derived viewing angle (see Figure 4)

and high temperature (see Figure 2), such harmonics would be indistinct. With $B = 23$ MG, there would be no harmonics in the *W*1 band, explaining its lack of variability. The *W*2 data set is sparse, and its S/N ratio is too low to determine if emission from the $n = 1$ harmonic is actually present. The mean magnitude of the *W*2 bandpass is somewhat brighter than *W*1, suggesting that there is excess emission in this band that could be due to cyclotron radiation.

3.15. HS Cam

HS Cam is an eclipsing short-period polar for which Tovmassian et al. (1997) have supplied an ephemeris, to which we have phased the remarkable *WISE* light curves (Figure 26). The visual light curves of HS Cam outside of the eclipse show limited variability, which Tovmassian et al. attribute to irradiation of the secondary star. The FWHM duration of the eclipses are 5 minutes, and in the *B*-band the system declines by nearly 4 mag. *WISE* did observe HS Cam at a phase of $\phi = 0.009$, but the source was not detected. The variations in the *W*2 bandpass almost attain $\Delta W2 = 2$ mag, and
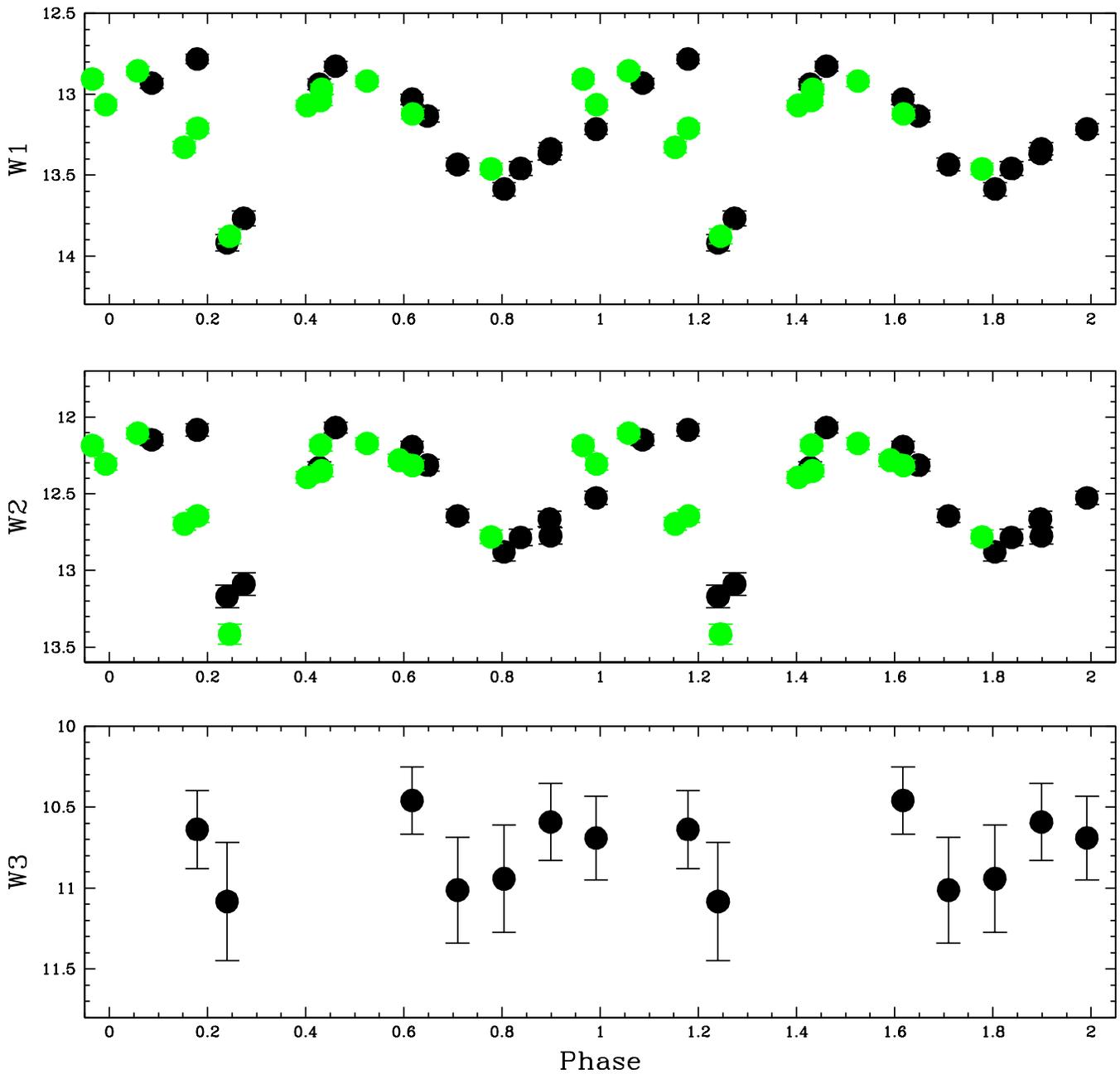
Figure 29. *WISE* light curves of IW Eri arbitrarily phased to an orbital period of 87.1 minutes. The green data points are from the three-band survey and have been shifted by +0.32 mag to make them overlap with the four-band data.

given that the maxima were obviously missed, the actual amplitude of the variations could be much larger. No cyclotron features were seen in the optical spectra, so the field strength is difficult to estimate. Note, however, that 2MASS observed this system at $\phi = 0.75$, and the source was not detected! This suggests a very low field strength. We recently observed this source with Near-Infrared Camera & Fabry-Perot Spectrometer (NICFPS) on the APO 3.5 m telescope at $\phi = 0.84$, near minimum light. We found HS Cam to be very faint and very red: $K = 15.65$ and $(J - K) = 1.99$. This is much too red to be a normal main sequence star, and it suggests that cyclotron emission is probably present in the K band. A field with $B \sim 8$ MG would have the $n = 3$ harmonic in $W2$, $n = 4$ harmonic in $W1$, and $n = 6$ and 7 in the K band. This would place the $n = 1$ and 2 harmonics in the $W3$ bandpass. HS Cam was not detected

at this wavelength, but this is not unexpected given the source faintness because to get a detection in $W3$ would require $(W1 - W3) \gtrsim 4$.

3.16. HU Aqr

HU Aqr is a very well known eclipsing polar for which circumbinary planets have been proposed to explain eclipse timing variations (see Qian et al. 2011). Wittenmyer et al. (2012) present a recent ephemeris for HU Aqr, and we use this to phase our infrared data. We combine *JHK* data obtained using SQIID (2001 December 2) with the *WISE* light curves and present them in Figure 27. HU Aqr was in a low state during the SQIID observations (it was in a high state during the 2MASS observations). We also obtained phase-resolved

Table 4
Near-infrared Data for Polars

Object	i/Y	J	H	K	Phase	Source
AI Tri	...	14.21 ± 0.03	13.92 ± 0.04	13.62 ± 0.04	0.48	2M
"	...	14.80 ± 0.03	14.24 ± 0.02	13.98 ± 0.02	0.00	APO
AM Her	...	11.70 ± 0.02	11.20 ± 0.02	11.00 ± 0.02	0.41	2M
AN UMa	...	15.60 ± 0.06	15.48 ± 0.11	15.07 ± 0.11	0.54	2M
AP CrB	...	14.71 ± 0.03	14.30 ± 0.05	13.89 ± 0.05	0.58	2M
"	15.31 ± 0.01	14.74 ± 0.01	14.15 ± 0.01	13.96 ± 0.01	...	UK
AR UMa	...	14.15 ± 0.02	13.60 ± 0.03	13.27 ± 0.04	0.93	2M
BL Hyi	...	14.32 ± 0.03	13.67 ± 0.03	13.25 ± 0.05	0.93	2M
"	13.46 ± 0.04	13.18 ± 0.08	...	12.67 ± 0.13	0.02	D
"	15.64 ± 0.06	14.15 ± 0.10	...	13.20 ± 0.18	0.05	D
BY Cam	...	13.96 ± 0.03	13.03 ± 0.03	12.48 ± 0.02	0.91	2M
CD Ind	...	13.82 ± 0.03	13.23 ± 0.03	12.97 ± 0.04	0.28	2M
CP Tuc	...	>15.7	...	15.32 ± 0.25	0.93	2M
CV Hyi	...	16.86 ± 0.17	16.41 ± 0.26	15.82 ± 0.32	...	2M
CW Hyi	...	16.81 ± 0.20	15.69 ± 0.15	15.82 ± 0.28	...	2M
EP Dra	...	16.27 ± 0.12	15.69 ± 0.15	15.50 ± 0.20	0.73	2M
EQ Cet	...	16.73 ± 0.14	16.32 ± 0.26	15.74 ± 0.25	0.26	2M
EU UMa	...	16.49 ± 0.11	16.01 ± 0.14	16.00 ± 0.23	...	2M
FL Cet	...	16.51 ± 0.14	16.49 ± 0.27	...	0.76	2M
"	15.92 ± 0.01	15.74 ± 0.01	16.00 ± 0.02	15.57 ± 0.02	...	UK
FL Cet	...	15.23 ± 0.16	14.71 ± 0.13	14.49 ± 0.04	0.60	APO
GG Leo	...	15.01 ± 0.04	14.77 ± 0.07	14.64 ± 0.10	0.72	2M
"	15.67 ± 0.01	17.04 ± 0.02	15.62 ± 0.01	15.68 ± 0.02	...	UK
HS Cam	...	...	...	...	0.75	2M
HS Cam	...	17.65 ± 0.21	16.94 ± 0.13	15.65 ± 0.05	0.84	APO
HU Aqr	...	14.18 ± 0.03	13.89 ± 0.04	13.63 ± 0.04	0.40	2M
"	14.17 ± 0.03	13.92 ± 0.11	...	13.51 ± 0.21	0.39	D
IW Eri	...	17.57 ± 0.26	16.69 ± 0.25	16.57 ± 0.36	0.19	2M
LW Cam	...	16.75 ± 0.14	16.61 ± 0.28	15.66 ± 0.23	0.12	2M
LW Cam	...	17.94 ± 0.20	17.92 ± 0.21	17.91 ± 0.27	0.61	APO
MR Ser	...	14.08 ± 0.02	13.78 ± 0.04	13.35 ± 0.04	0.47	2M
QQ Vul	...	13.58 ± 0.03	13.24 ± 0.04	13.06 ± 0.04	0.06	2M
QS Tel	...	14.29 ± 0.02	13.77 ± 0.04	13.53 ± 0.04	0.01	2M
ST LMi	...	13.51 ± 0.03	13.09 ± 0.04	12.91 ± 0.03	0.97	2M
UW Pic	...	15.63 ± 0.06	15.29 ± 0.09	14.89 ± 0.14	0.81	2M
"	14.99 ± 0.04	14.85 ± 0.13	...	...	0.72	D
UZ For	...	15.32 ± 0.04	14.90 ± 0.08	14.78 ± 0.12	0.89	2M
VV Pup	...	15.55 ± 0.07	14.91 ± 0.09	14.54 ± 0.09	0.43	2M
VY For	...	15.60 ± 0.05	15.00 ± 0.08	14.87 ± 0.14	0.55	2M
V347 Pav	...	16.20 ± 0.12	15.52 ± 0.15	14.99 ± 0.15	0.93	2M
"	17.30 ± 0.16	15.64 ± 0.19	...	...	0.94	D
"	17.30 ± 0.13	16.02 ± 0.23	...	...	0.85	D
V349 Pav	...	16.11 ± 0.09	16.23 ± 0.23	15.46 ± 0.23	0.59	2M
V381 Vel	16.62 ± 0.14	16.18 ± 0.18	...	...	...	2M
V388 Peg	...	16.20 ± 0.09	15.68 ± 0.10	15.54 ± 0.18	0.80	2M
V393 Pav	...	16.39 ± 0.12	15.68 ± 0.15	15.49 ± 0.20	0.01	2M
"	17.66 ± 0.16	15.94 ± 0.22	...	...	0.56	D
"	18.12 ± 0.18	...	...	...	0.14	D
V479 And	...	15.78 ± 0.08	15.22 ± 0.10	15.29 ± 0.16	0.83	2M
V516 Pup	...	16.26 ± 0.11	15.95 ± 0.20	15.31 ± 0.20	0.40	2M
V516 Pup	17.42 ± 0.12	16.37 ± 0.21	...	...	0.62	D
V834 Cen	...	13.47 ± 0.03	13.16 ± 0.02	12.77 ± 0.03	0.94	2M
"	15.74 ± 0.05	14.27 ± 0.12	...	13.54 ± 0.21	0.71	D
V884 Her	...	13.79 ± 0.03	13.29 ± 0.04	13.02 ± 0.03	0.98	2M
V895 Cen	...	13.98 ± 0.03	13.42 ± 0.03	13.15 ± 0.04	0.22	2M
"	15.17 ± 0.07	14.14 ± 0.08	...	13.14 ± 0.18	0.47	D
V1007 Her	...	17.19 ± 0.13	16.87 ± 0.16	16.38 ± 0.12	0.60	APO
V1033 Cen	...	13.53 ± 0.04	13.15 ± 0.05	12.94 ± 0.05	0.50	2M
"	...	14.26 ± 0.06	...	13.38 ± 0.24	0.22	D
V1043 Cen	...	12.82 ± 0.02	12.15 ± 0.02	11.93 ± 0.02	0.85	2M
"	14.09 ± 0.03	12.90 ± 0.05	...	12.04 ± 0.09	0.48	D
V1309 Ori	...	14.22 ± 0.03	13.66 ± 0.03	13.51 ± 0.05	0.00	2M
V1432 Aql	...	14.59 ± 0.04	14.12 ± 0.04	13.70 ± 0.05	0.85	2M
"	14.49 ± 0.03	14.06 ± 0.11	...	13.21 ± 0.16	0.65	D

Table 4
(Continued)

Object	i/Y	J	H	K	Phase	Source
V2301 Oph	…	14.44 ± 0.03	13.40 ± 0.03	12.60 ± 0.03	0.85	2M
WW Hor	…	16.00 ± 0.07	15.53 ± 0.10	14.89 ± 0.11	0.23	2M
WX LMi	…	13.43 ± 0.02	12.83 ± 0.02	12.49 ± 0.02	0.57	2M
HS0922+1333	…	13.45 ± 0.02	12.80 ± 0.02	12.54 ± 0.02	0.01	2M
RBS490	…	16.49 ± 0.13	16.46 ± 0.26	…	0.97	2M
RBS490	…	16.63 ± 0.12	16.64 ± 0.24	15.90 ± 0.11	0.03	APO
RXJ0154.0−5947	…	15.99 ± 0.09	15.66 ± 0.12	15.15 ± 0.16	…	2M
RXJ0502.8+1624	…	16.51 ± 0.12	15.57 ± 0.10	14.66 ± 0.08	…	2M
RXJ0649.8−0737	…	15.17 ± 0.03	14.58 ± 0.05	14.30 ± 0.06	…	2M
”	…	15.13 ± 0.01	14.55 ± 0.01	14.29 ± 0.01	…	UK
”	16.14 ± 0.07	15.10 ± 0.16	…	…	…	D
RXJ0859.1+0537	…	16.58 ± 0.15	16.04 ± 0.16	…	…	2M
”	…	16.50 ± 0.01	15.72 ± 0.01	15.51 ± 0.02	…	UK
RXJ0953.1+1458	…	16.91 ± 0.16	16.38 ± 0.25	16.09 ± 0.28	…	2M
RXJ1002−1925	…	…	…	16.08 ± 0.27	…	2M
RXJ1007.5−2017	…	16.30 ± 0.10	15.63 ± 0.12	15.22 ± 0.13	0.80	2M
”	16.60 ± 0.08	15.84 ± 0.19	…	…	0.67	D
RXJ2316−0527	…	15.22 ± 0.04	14.80 ± 0.06	14.64 ± 0.10	0.33	2M
”	15.10 ± 0.05	14.91 ± 0.16	…	13.62 ± 0.21	0.58	D
”	…	16.48 ± 0.01	16.00 ± 0.02	15.53 ± 0.02	…	UK
2QZ J142256.3−022108	…	…	17.51 ± 0.06	17.02 ± 0.07	…	UK
2QZ J142438.9−022739	…	…	15.91 ± 0.02	15.90 ± 0.11	…	UK
”	18.02 ± 0.16	…	…	…	…	D

spectra of HU Aqr using SpeX on the IRTF (2005 September 2), shown in Figure 28. HU Aqr had $K \sim 14.0$ at the time of the IRTF observations, a magnitude brighter than seen with SQIID. To isolate the cyclotron humps, we have subtracted the spectrum nearest minimum light ($\phi = 0.98$) from one of the spectra with strong cyclotron emission ($\phi = 0.73$) and plot it in green in Figure 28. We also include a CL cyclotron model (blue) with $B = 31.5$ MG in this figure. This value is different from the results of Schwope et al. (1993b), who found $B = 37$ MG during a low state.

Schwope et al. (2011) present the system parameters for HU Aqr, allowing us to construct a light curve model for our data set. With $M_1 = 0.8 \, M_\odot$ and $M_2 = 0.18 \, M_\odot$, we find a best-fit model with $T_1 = 18{,}000$ K, $T_2 = 2800$ K, and $i = 80°$. We had to adjust the phasing of the SQIID data by $\Delta\phi = +0.015$ and the *WISE* light curves by $\Delta\phi = +0.05$ to match the model light curve. Our value for the inclination is lower than the $i = 87°$ found by Schwope et al. (2011), but that could be due to our assumption that the entire K-band light curve is due to ellipsoidal variations. Obviously, there is a source of excess emission leading up to the eclipse in the K band, which is also seen in J and H. For field strengths near 31.5 MG (or 37 MG), no harmonics are centered in the K band. Because the excess at this wavelength occurs at the same phases as the cyclotron emission in the other bandpasses, we assume that the tail of the $n = 2$ harmonic is responsible for this effect.

As shown in Figure 27, the *WISE* light curves show a large, orbitally modulated excess above the ellipsoidal models, suggesting strong cyclotron emission. The peaks in the *WISE* light curves appear to occur at the same phases as those in the J and H bands, though the *WISE* data have poor phase coverage. A field strength near 32 MG would have the $n = 1$ harmonic straddling both $W1$ and $W2$, explaining the light curves. The limited amplitude of the variations in the *WISE* light curve data outside of the eclipse is consistent with emission from an

optically thin $n = 1$ harmonic. Unfortunately, we do not know the state of HU Aqr at the time of the *WISE* observations, though Bours et al. (2014) found it to be in a high state exactly two weeks after the *WISE* observations. HU Aqr has a significant $W3$ excess: $(W1 - W3) = 2.2$.

The morphology of the spectroscopic evolution over an orbit is interesting. Cyclotron emission is present almost immediately upon egress from the eclipse, grows in strength until $\phi = 0.26$, then suddenly disappears over the interval $0.33 \leqslant \phi \leqslant 0.67$. During this time, the spectra are dominated by features from the late-type secondary star. The cyclotron emission then returns for the rest of the orbit until $\phi = 0.92$. This evolution is in excellent agreement with the infrared light curves. After $\phi = 0.73$, the H I ($+$He I 1.0830 μm) emission lines weaken, suggesting that the line region becomes hidden before the cyclotron emission region. This is also the time when the K band has its largest excess above the ellipsoidal model, suggesting that the cyclotron emission has its most favorable viewing angle at this time (as compared to one-half orbit earlier).

3.17. IW Eri

IW Eri is a faint polar discovered in the *ROSAT* Bright Survey (RBS 541). Schwope et al. (2002) list two possible orbital periods: 87.1 and 81.82 minutes. After phasing the *WISE* light curves with both periods, we find that the 87.1 minute period produces a smoother light curve. The resulting light curves, including data from the three-band survey (see Figure 29), are unusual with two broad and deep minima. There appears to be a period where the cyclotron emission region is eclipsed. Outside of this deepest minimum, the full amplitude of the variations in the light curves is about 0.8 mag, similar to what is seen in the V band (see Schwope et al. 2002). IW Eri was not detected in the 2MASS PSC, but it is visible on the images, and in Table 4 we list the extracted JHK photometry for this source. IW Eri had $\langle V \rangle \sim 17.5$ when
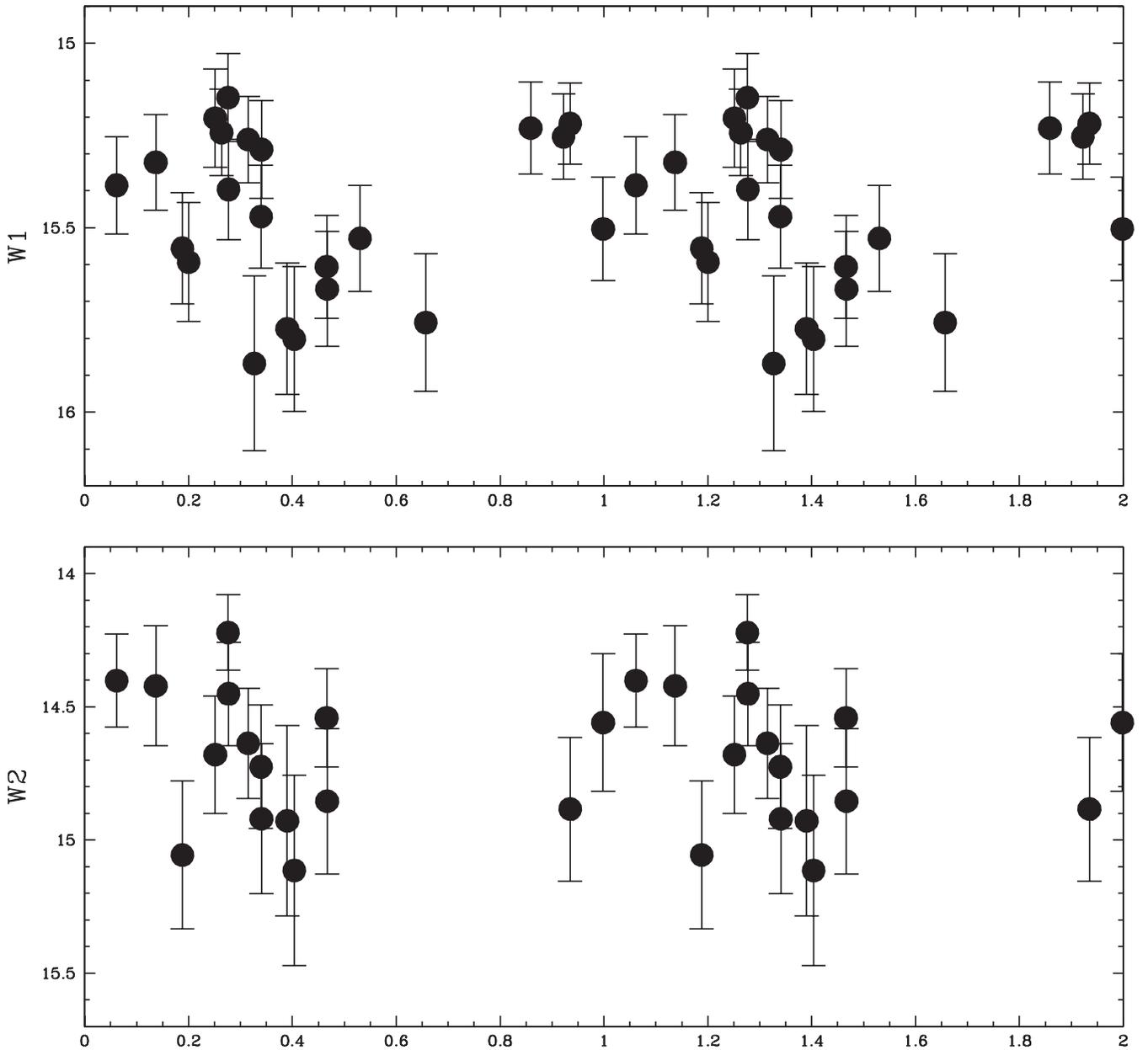
Figure 30. *WISE* light curves of MN Hya phased to the ephemeris of Buckley et al. (1998).

Schwope et al. observed it. Note that the 2MASS observations occurred three weeks after those visual data were acquired. Clearly, compared to those earlier data, IW Eri must have been in a high state when observed by *WISE* because it is difficult to envision any polar having $(K-W1) = 3.5$. The strong *WISE* variations suggest $B \leqslant 32$ MG. IW Eri has a modest *W3* excess: $(W1 - W3) = 1.7$.

3.18. LW Cam

Tovmassian et al. (2001) find an orbital period of $P_{orb} = 97.3$ minutes and liken LW Cam to BL Hyi. Unfortunately, this orbital period is similar to that of the *WISE* mission, so there is limited phase coverage. The 2MASS data ($\phi = 0.12$) were obtained within a few days of one of the observational data sets of Tovmassian et al., when the system was in a high state. With $(K_{2MASS}-W1) = -0.54$, it is certain the *WISE* data were

obtained during a much lower state. The *VRIJ* light curves presented by Tovmassian et al. are reminiscent of ST LMi (see Campbell et al. 2008a) and clearly show evidence for strong cyclotron emission (though the labeling of the ordinate axis on their *J*-band light curve of LW Cam cannot be correct). Our observations of LW Cam at APO ($\phi = 0.61$) show a source with blue near-IR colors. Comparison to the *J*-band light curve presented in Tovmassian et al. shows that this phase corresponds to minimum light. If LW Cam was in a true low state, like that observed by Tovmassian et al., the *WISE* fluxes would suggest the presence of mid-IR cyclotron emission, with it mostly confined to *W2*; this implies $B \sim 20$ MG.

3.19. MN Hya

Buckley et al. (1998) present evidence that MN Hya is an eclipsing, two-pole accretor with a relatively long orbital period
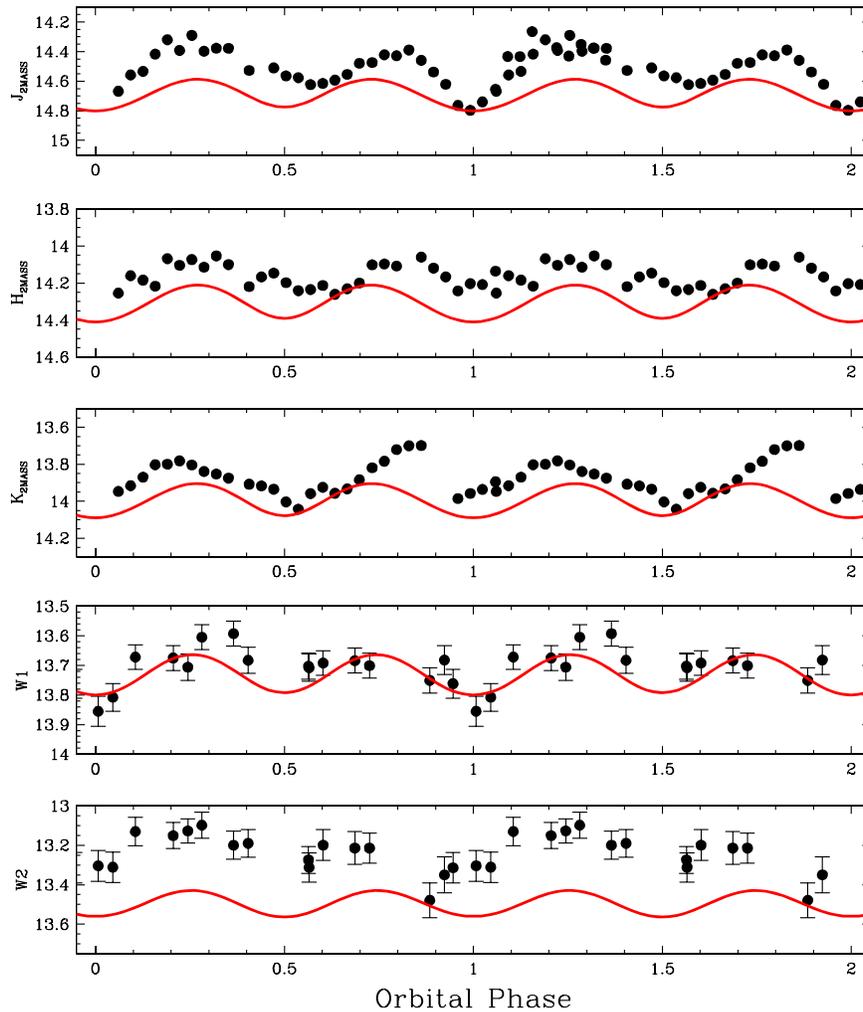
Figure 31. SQIID *JHK* and *WISE* light curves of MR Ser. The SQIID observations occurred during a low state in 2003, and the *WISE* data were obtained during a low state in 2010. The photometry has been phased to the ephemeris by Diaz & Cieslinski (2009). We generated light curve models for MR Ser (red). To properly phase the data to the models, we had to offset the *JHK* light curves by $\Delta\phi = -0.03$ and the *WISE* data by $\Delta\phi = -0.07$.

(3.39 hr). They suggest that one emission region is visible at all orbital phases, while the second, main cyclotron emitting region is below the orbital plane and is only visible for ∼40% of an orbit. Buckley et al. present an ephemeris for MN Hya, to which we have phased the *WISE* light curves (see Figure 30). The *WISE* light curves do not show an eclipse, even though one observation occurred exactly at phase zero. Such events are brief enough, and the error in the ephemeris is large enough, that such a short-lived event might have been missed. Both bandpasses show amplitudes of ∼1 mag, though these data are quite noisy. It does appear, however, that the bright phase in these data occurs near $\phi = 0.2$. This differs from Buckley et al., who find a single bright phase centered near $\phi = 0.7$. Unfortunately, the *WISE* data do not cover that phase. Buckley et al. estimate a field strength of $B = 20$ MG for the main pole. Such a field would have most of its cyclotron emission in the *W2* band. The similarity of the *WISE* light curve morphologies and the substantially brighter *W2* flux suggest that the field strength must be somewhat higher, $B \sim 28$ MG. However, with two-pole accretion and poor phase coverage, it is difficult to put too much confidence in this result.

3.20. MR Ser

MR Ser is a very well-known single pole accretor with $P_{\rm orb} = 1.89$ hr. Diaz & Cieslinski (2009) have updated the ephemeris published by Schwope et al. (1993a), and we phase our infrared data to their result. The AAVSO database shows that MR Ser was in a low state at the time of the *WISE* observations. We obtained *JHK* photometry of MR Ser on 2003 August 5 with SQIID on the KPNO 2.1 m. The Kafka & Honeycutt (2005) light curve for MR Ser shows that it was faint at this time (MR Ser was about 0.5 mag brighter in the 2MASS catalog, suggesting a high state). We present the combined *JHK* + *WISE* light curves in Figure 31. Schwope et al. (1993a) derived masses of the stellar components in MR Ser, finding $M_1 = 0.35$ $M_\odot$ and $M_2 = 0.13$ $M_\odot$. We generated light curve models using these inputs and plot the results in Figure 31. We find that the *W1* light curve is due to nearly pure ellipsoidal variations. The *JHK* and *W2* light curves show large excursions from this model, suggesting cyclotron emission.

We also used the NMSU 1 m to obtain two full orbits of *BVRI* photometry of MR Ser, shown in Figure 32, on 2004 April 13. There appears to have been an accretion event that
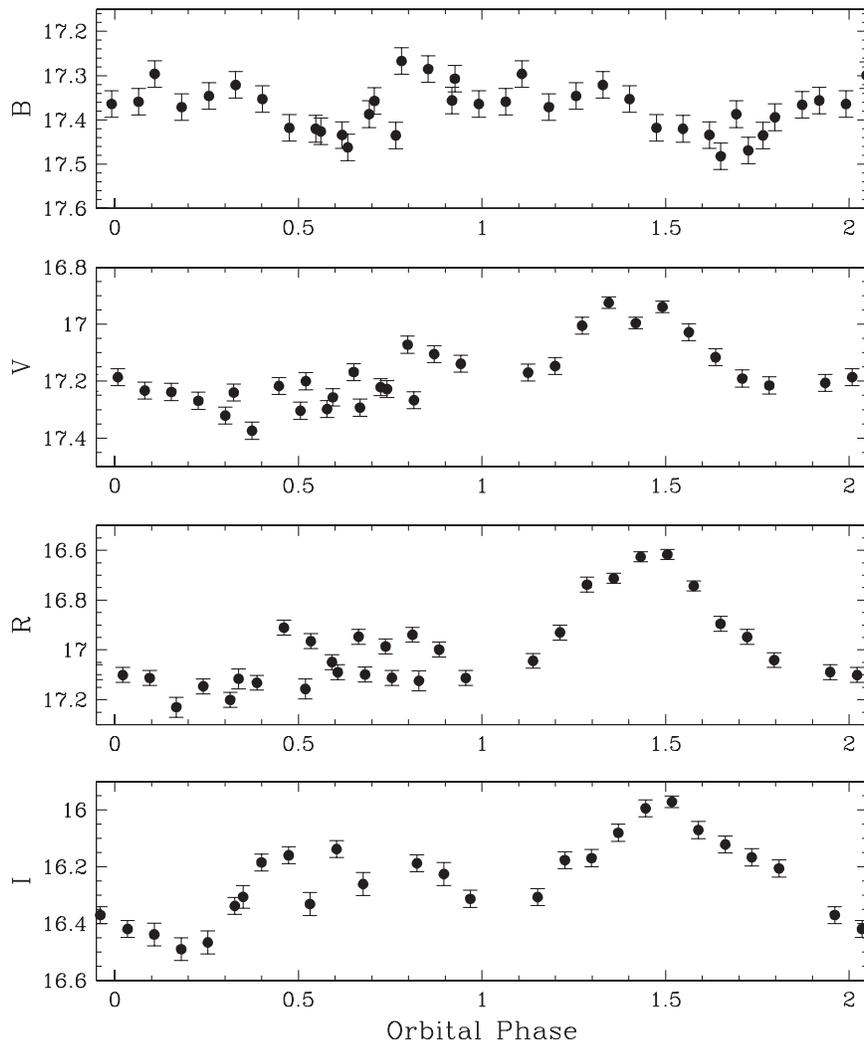
Figure 32. *BVRI* light curves of MR Ser obtained in 2004 on the NMSU 1 m telescope when the system was clearly in a low state. Two full orbits of data were obtained, showing that a flare occurred during the second orbit.

occurred during the second orbit that caused a flaring in the *VRI* photometry. This event was not seen in the *B* band. These optical observations caught MR Ser in an even lower state than observed by Schwope et al. (1993a). There is, however, no evidence for secondary star ellipsoidal variations in these light curves. This is due to the dilution from emission by the white dwarf and the accretion region. If the *K*-band flux at minimum light was due only to the donor star, with $(V - K) = 7.4$, this object would have $V \sim 21.4$. At $\phi = 0$, $V = 17.19$. Thus, there are four magnitudes of excess light in the *V* band that completely dilute the ellipsoidal variations at this wavelength.

We obtained phase-resolved spectroscopy of MR Ser over 58% of an orbit on 2005 February 7, covering $0.17 \leqslant \phi \leqslant 0.75$. These data, presented in Figure 33, show cyclotron harmonic emission throughout, with it being most prominent near phases 0.2 and 0.7. Note that while the top few spectra in Figure 33 suggest a much broader harmonic at 1.9 μm, the blue wing of this feature is due to an overcorrection of the very strong telluric water vapor absorption in this spectral region (as MR Ser transited the zenith, as seen from the IRTF, resulting in less telluric absorption than any of the standard stars observed that night). This is also an issue at 1.37 μm. Given the lack of an eclipse spectrum, and the fact that we have cyclotron humps throughout our data set, we cannot form a simple subtraction to

highlight the cyclotron emission. Instead, we plot a cyclotron model in Figure 33 with $B = 27.2$ MG. This model does a reasonable job in reproducing the observe humps. This value is slightly higher than the $B = 24.9$ MG value found by Schwope et al. (1993a) for the low-state cyclotron spectra they modeled, but it is similar to their value for the photospheric field strength: $B \sim 28$ MG. This field strength would predict strong cyclotron emission in the *J* (the $n = 3$ and 4 harmonics), *K* ($n = 2$), and *W*2 ($n = 1$) bands, with no cyclotron emission in the *W*1 band, consistent with the light curves. The small amplitude variations in the *W*2 band indicate a nearly constant source partially modulated by ellipsoidal variations. This suggests optically thin emission from the $n = 1$ harmonic. While H I Paα ($\lambda 1.87$ μm) emission is visible in our spectra, its profile and strength are strongly corrupted by telluric water vapor absorption.

MR Ser was observed by *Spitzer* on 2005 March 27, and we list the flux densities from our reduction of these data in Table 2. The AAVSO data had MR Ser at $v = 15.7$ four days later, suggesting MR Ser was in a high state. This is confirmed as the *S*1 flux is 67% larger than the *W*1 flux at the same phase. Brinkworth et al. believed that the unusual SED of MR Ser, with the mid-IR flux density peaking in the *S*2 and *S*3 bands, might be due to a blackbody with $T_{\rm eff} = 800$ K. Given the result
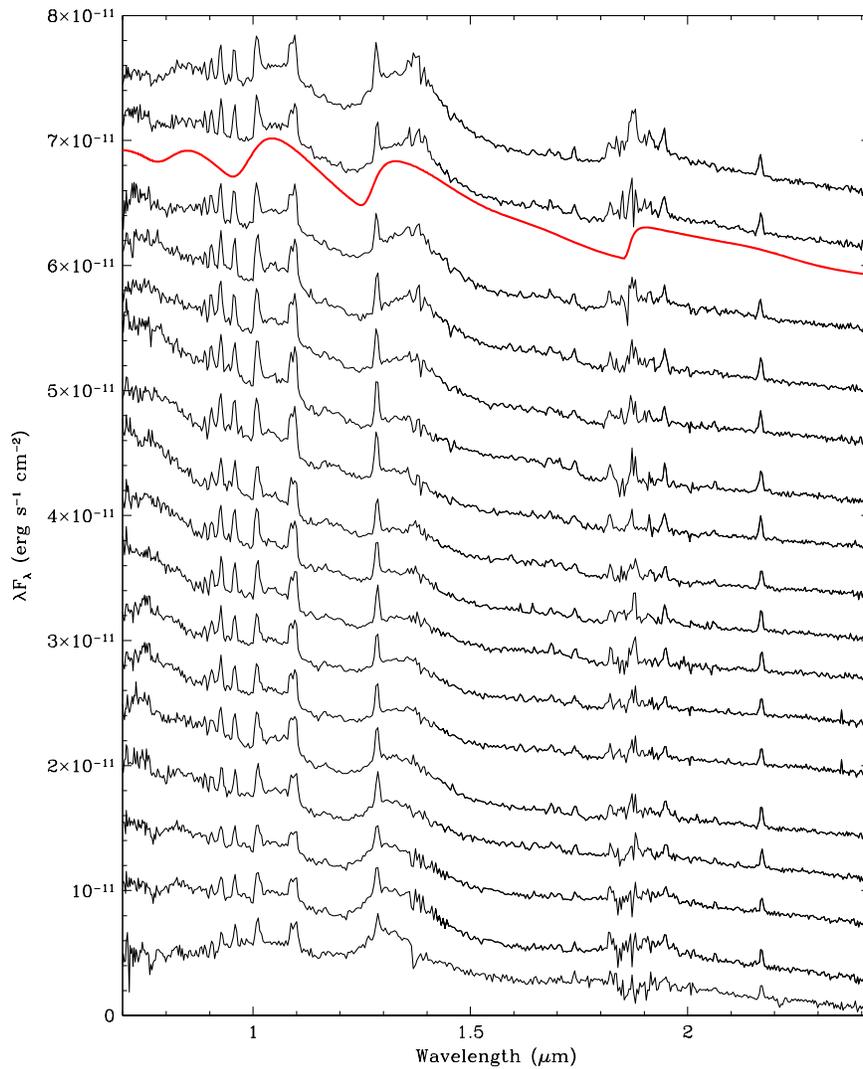
Figure 33. IRTF SpeX spectra for MR Ser covering phases 0.17 (bottom) to 0.75 (top) and separated by $\Delta\phi = 0.036$. The spectra have arbitrary flux offsets for clarity. As noted in the text, the blue wing (at 1.85 μm) of the broader cyclotron hump in the upper spectra (and merged with H I Paα) is actually due to undercorrection of the strong telluric water vapor absorption at this wavelength (compare to the spectra in the bottom of the plot, where this absorption is overcorrected). We plot a cyclotron model with $B = 27.2$ MG in red. All of the emission lines visible here are due to H I, except for the blend of He I (λ1.083 μm) with H I Paγ (λ1.094 μm).

above, we now know that this deviation was due to strong cyclotron emission from the $n = 1$ harmonic from a $\sim$27 MG field. The 2MASS *JHK* photometry at the phase of the *Spitzer* observations is also contaminated by cyclotron emission. Thus, combining the two data sets would lead to an unusual SED that is difficult to explain without considering the addition of a cyclotron component.

3.21. QQ Vul

QQ Vul is a long-period polar whose behavior is complex, and it remains unclear whether it is a one-pole or two-pole accretor (see Kafka & Honeycutt 2003 and references therein). Schwope et al. (2000) give an orbital ephemeris for the system, to which we have phased the *WISE* light curves. These light curves, presented in Figure 34, are peculiar, showing a broad dip near $\phi = 0.0$ and a slow brightening that peaks near $\phi = 0.75$. In fact, however, the *W*1 and *W*2 light curves are almost identical to the "Type 1" (*V*-band) light curves as defined in Kafka & Honeycutt

(2003). We obtained near-IR spectroscopy of QQ Vul on 2005 September 2, covering nearly one-half of an orbit, from phase 0.72 to phase 0.16 (see Figure 35). The AAVSO database indicates that QQ Vul had $V = 15.2$ at this time. The H I emission lines are strongest near $\phi = 0.75$ and gradually weaken until they nearly disappear at $\phi = 0$. Near this phase, the continuum is dominated by the secondary star, and we derive a spectral type of M4V, in agreement with that derived by Catalán et al. (1999). Near maximum light, the continuum gets much bluer, though features from the secondary star remain detectable. No discrete cyclotron humps are seen in these data.

3.22. QS Tel

QS Tel is a polar with a period (P_{orb} =2.3 hr) that puts it inside the CV period gap. Schwope et al. (1995b) derive an ephemeris for this object, and we have phased the *WISE* light curves (see Figure 36) using their result. The *W*1 light curve appears to show two maxima separated by 0.5 in phase. In
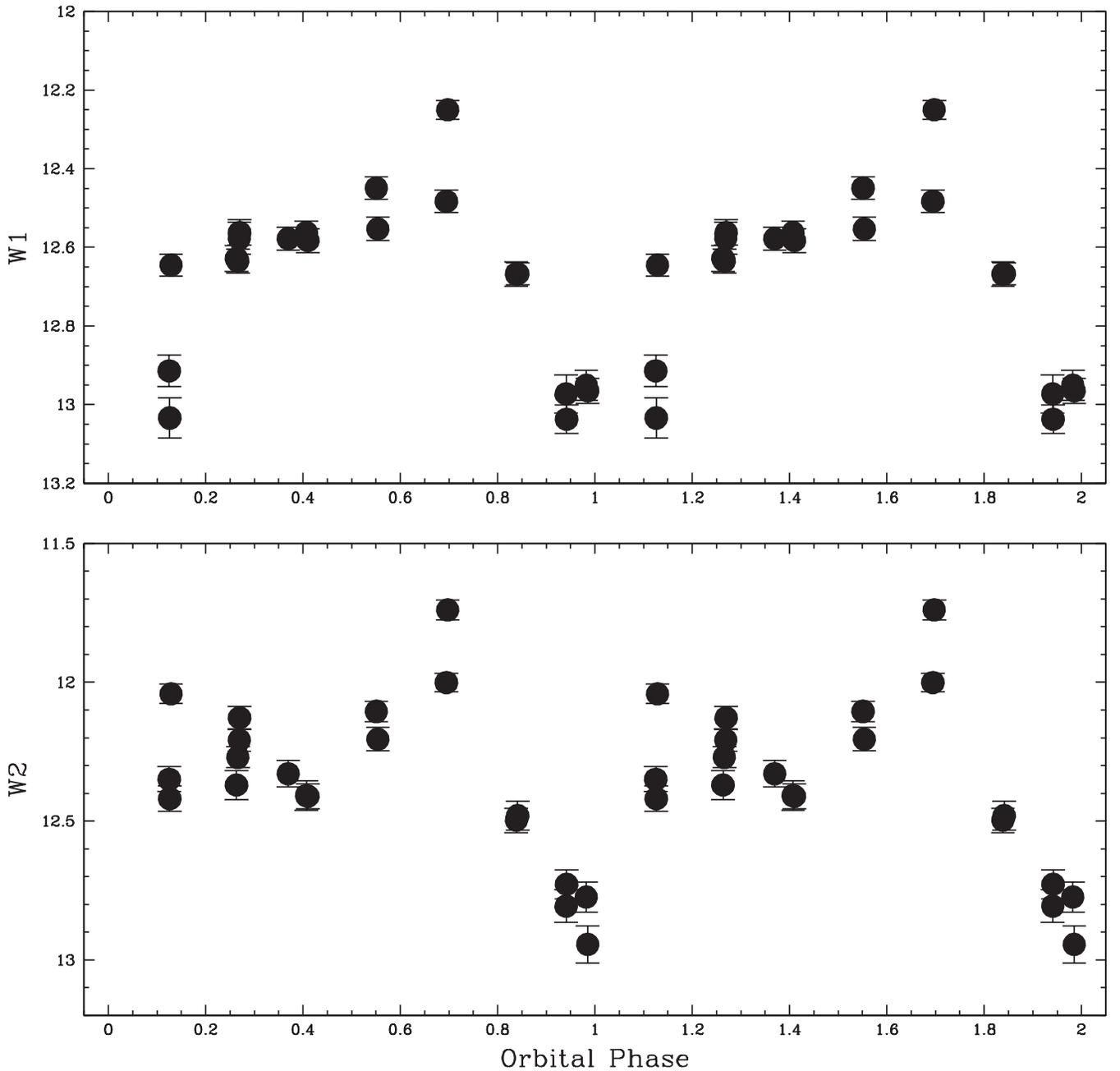
Figure 34. *WISE* light curves of QQ Vul phased to the ephemeris of Schwope et al. (2000). These light curves are nearly identical to the "Type 1" visual light curves in Kafka & Honeycutt (2005).

fact, the *W*1 light curve resembles the "intermediate state" *V*-band light curve presented by Schwope et al. (1995b). Schwope et al. found that there were two systems of cyclotron humps, one from a pole with $B \sim 70$ MG, and one with $B \sim 47$ MG. The phasing, amplitude, and morphology of the *W*1 light curve is very similar to that seen in the *V* band, suggesting they have a similar origin. Both of the field strengths derived for QS Tel, however, are much too high to have cyclotron emission in the *W*1 bandpass. It is thus interesting that the *W*2 light curve does not resemble the *W*1 light curve. There is obviously some emission process that is present in *W*1 but not in *W*2. If this is cyclotron emission, then $B \sim 35$ MG for one of the two poles. The small amplitude of the variations in *W*2 could be attributed to

ellipsoidal variations from a highly irradiated secondary star, though this would require a phase shift of $\Delta\phi = -0.25$ to put the deepest minimum at $\phi = 0$.

3.23. ST LMi

ST LMi is a well-known, short-period polar just below the CV period gap. Howell et al. (2000) give an ephemeris for this object, but it does a poor job of phasing up the infrared light curves. We present the *JHK* (from Campbell et al. 2008c) and the *WISE* light curves for ST LMi in Figure 37. Howell et al. (2000) list the system parameters for ST LMi, and we have used these to construct light curve models. To get the data to match the model light curves, we needed to adjust the phasing of the *JHK* data by $\Delta\phi = -0.21$
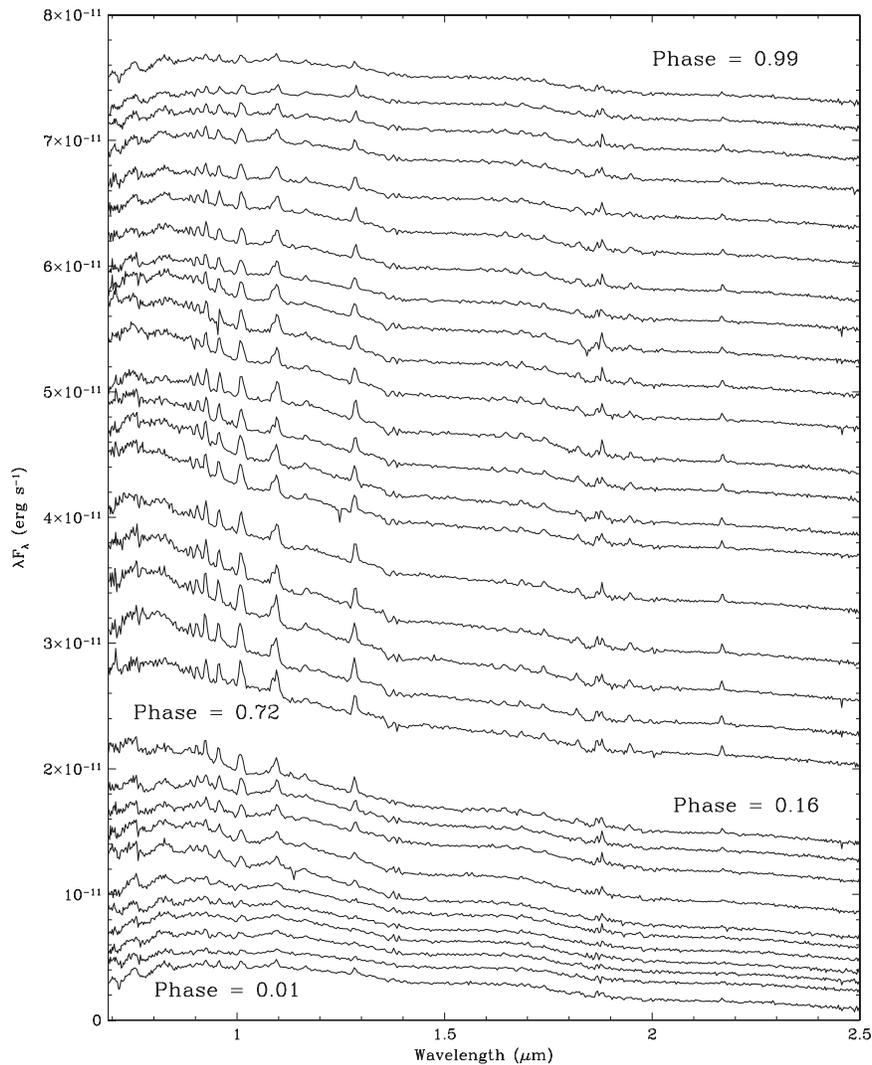
Figure 35. IRTF SpeX spectra for QQ Vul covered phases from 0.75 around to phase 0.16. The spectra have been ordered by phase bottom to top, separated by $\Delta\phi = 0.15$. The spectra have arbitrary flux offsets for clarity.

and the *WISE* data by $\Delta\phi = -0.18$. The *W*1 and *W*2 bandpasses appear to be completely dominated by ellipsoidal variations, and the *JHK* light curves have strong cyclotron emission. The *JHK* light curves were obtained on 2003 April 9, when the system was in a high state. The AAVSO data for the *WISE* epoch show that it was in a low state with $17.5 \leqslant V \leqslant 17.0$.

Campbell et al. (2008c) presented phase-resolved spectroscopy of ST LMi in a low state that showed weak cyclotron harmonics, from which they derived $B = 12$ MG. They also obtained near-IR spectra during an "extreme low state," and the system had no detectable cyclotron emission. A 12 MG field would have $n = 1$ in *W*3, $n = 2$ in *W*2, and $n = 3$ in *W*1. The lack of variability in these bandpasses, above that of the ellipsoidal variations, suggests that there was no cyclotron emission occurring during the epoch of the *WISE* observations. *Spitzer* observations of ST LMi were conducted on 2006 December 28, for which the AAVSO database suggests it had $V \sim 16$. The *S*1 and *S*2 fluxes were twice those detected by *WISE*, and they provide added evidence that ST LMi was in an extreme low state during the *WISE* mission. Using the same phasing offset noted above, the *Spitzer* data were obtained at

$\phi = 0.33$, close to the ellipsoidal maximum, but away from the main cyclotron emission phases.

3.24. UW Pic

UW Pic is another polar inside the period gap, with $P_{\rm orb} = 2.22$ hr. Reinsch et al. (1994) suggest that it has $B = 19$ MG, a field strength that would put cyclotron emission in the two shortest *WISE* bandpasses. We have used the ephemeris by Romero-Colmenero et al. (2003) to phase the *WISE* data presented in Figure 38, but we needed to offset them by $\Delta\phi = -0.074$ to match the morphology of their most recent light curve (see Figure 38). The phases of the near-IR data for UW Pic listed in Table 4 have not been offset. Note that there were two epochs of *WISE* observations: the four-band data obtained starting on 2010 February 28, and the three-band survey data obtained beginning 2010 September 8. It is obvious that UW Pic transitioned from a high state to a much lower state between these observational epochs. The four-band *W*3 light curve mimics the shorter wavelength light curves in that the source was detected during maximum, going undetected during their minima, but otherwise shows no significant variability. The three-band data shows limited variability, with only a weak
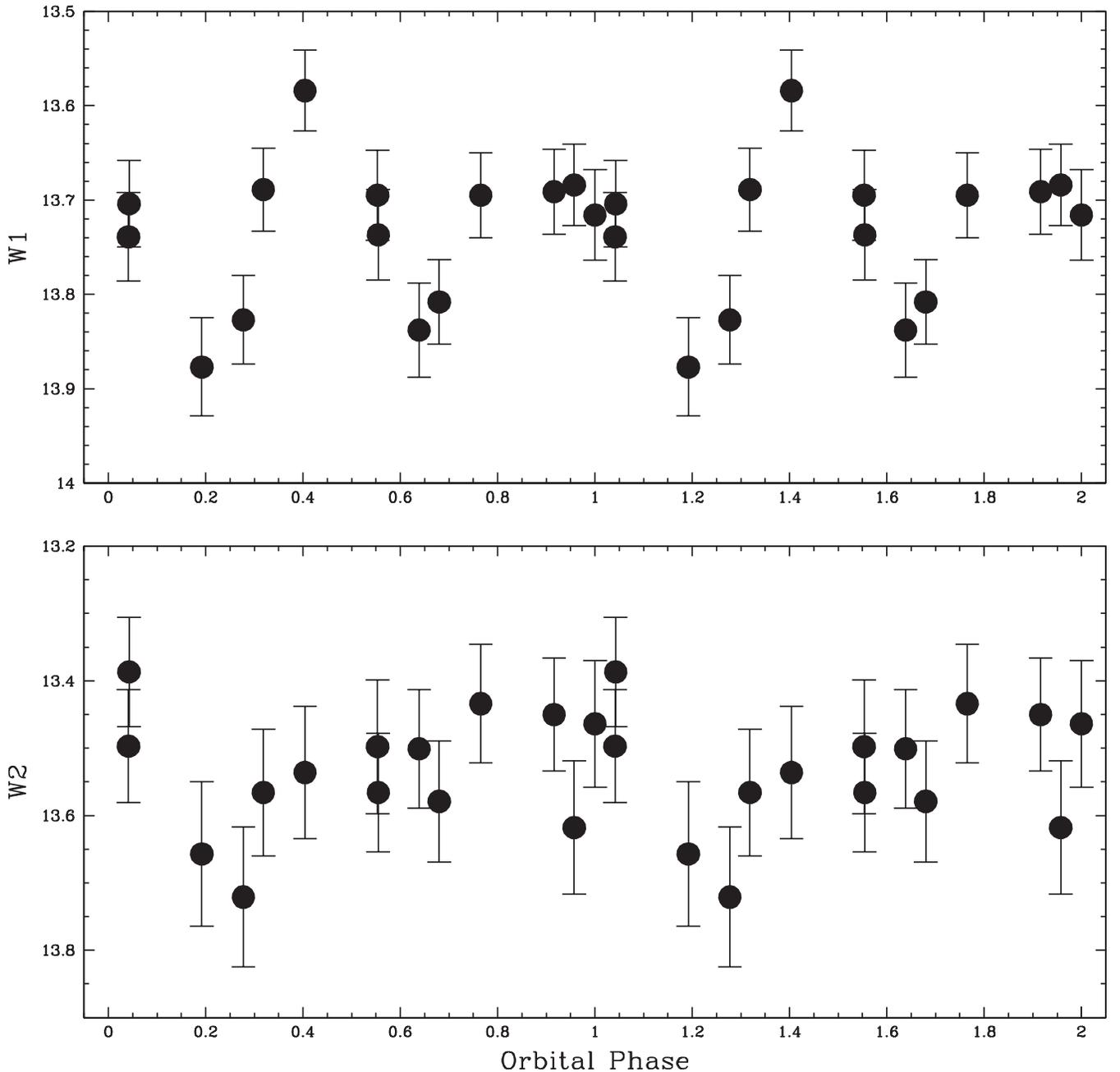
Figure 36. *WISE* light curves for QS Tel, phased to the ephemeris published in Schwope et al. (1995b).

minimum at $\phi = 0.75$ in the *W*1 band. If this is the same minimum as seen in the high state, it would argue that the orbital period for this system is incorrect. From the large amplitude variability, it is obvious that we have cyclotron emission in the two shorter *WISE* bandpasses. Reinsch et al. identified four cyclotron features in their spectra that they identify as the $n = 7$ to 10 harmonics from a 19 MG field. A 19 MG field, however, would not have significant *W*2 band emission. Reproducing the *WISE* data sets requires a field strength that is either higher ($B \sim 30$ MG) or lower ($B \sim 11$ MG). The fact that this faint source is detected in the W3 band is consistent with cyclotron emission in the *W*3 bandpass. Perhaps, as suggested by Romero-Colmenero et al., UW Pic is a two-pole accretor.

3.25. UZ For

UZ For is an eclipsing polar inside the period gap that appears to have two-pole accretion (Ferrario et al. 1989; Schwope et al. 1990). During the "bright phase," cyclotron harmonics from a field with $B \sim 55$ MG are seen. Ferrario et al. believe the second pole has $B = 28$ MG, whereas Schwope et al. find $B = 75$ MG (or 57 MG) for the secondary pole. Dai et al. (2010) present an updated ephemeris, to which we have phased the *WISE* light curves plotted in Figure 39. We added the *J*-band light curve from Ferrario et al. (1989) and constructed ellipsoidal variation models given the suggested parameters published in both Ferrario et al. and Schwope et al. (1990). We find that the best-fit model has $T_1 = 11{,}000$ K, $T_2 = 3300$ K, and $i = 80°$. Ferrario
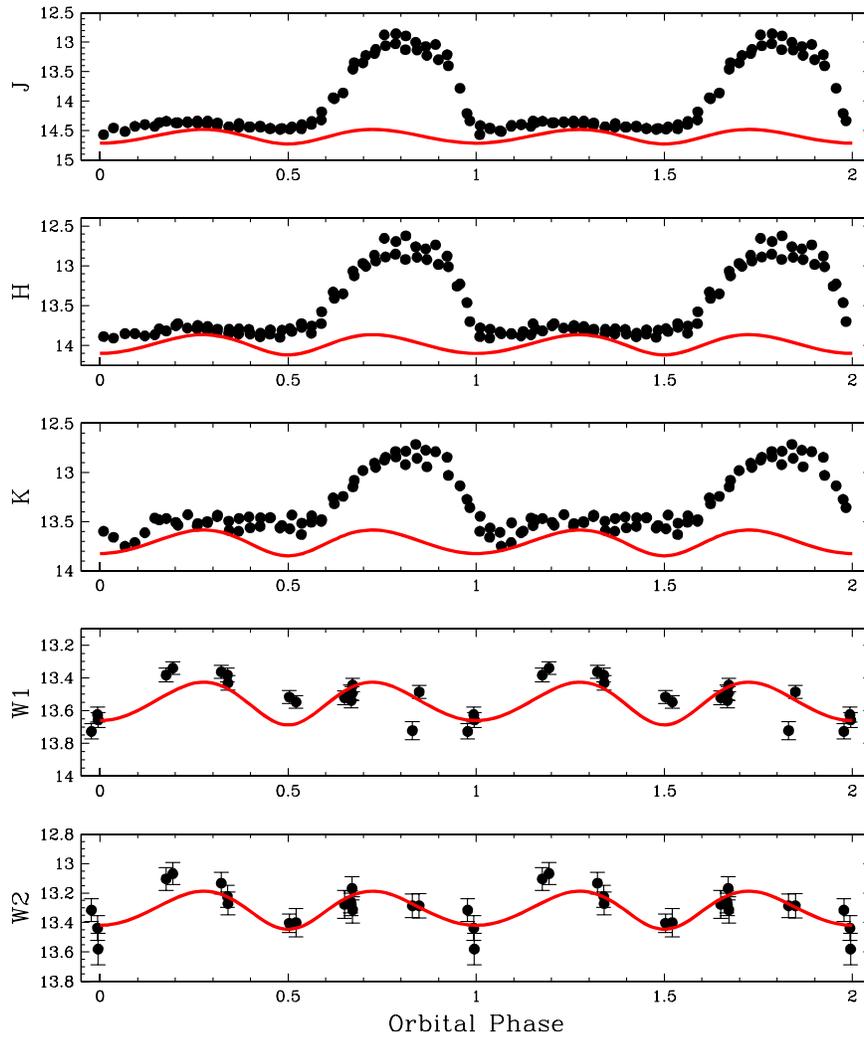
Figure 37. *JHK* (from Campbell et al. 2008c) and *WISE* light curves for ST LMi, phased to the ephemeris published in Howell et al. (2000). We have used the binary star parameters in that paper to construct a light curve model (red). As discussed in the text, the *JHK* data were offset from the Howell et al. phasing by $\Delta\phi = -0.21$ and the *WISE* data by $\Delta\phi = -0.18$.

et al. believed that the *J*-band light curve was almost completely due to ellipsoidal variations, but to get our model to work, we had to add in a small third light component to dilute the light curve to allow $i = 80°$. Given the poor fit of the model to the data between the eclipse and $\phi = 0.2$, the third light component may need to be increased.

The *WISE* light curves are complex and deviate from the ellipsoidal model at nearly every orbital phase. However, though poorly covered, the strongest deviation from the ellipsoidal model appears to occur between $\phi = 0.2$ and 0.4. The *J*-band light curve shows no deviation at this phase. The largest deviation in the *J* band occurs near phase 0.7, corresponding to the optical bright phase, and near the time of maximum (positive) circular polarization in the blue. The *WISE* light curves do not cover this phase. These light curve morphologies are consistent with the approximate strengths of the magnetic fields found by Ferrario et al., including optically thin fundamental harmonic emission from a 28 MG field. A 56 MG field would not have cyclotron emission in the *WISE* bandpasses, but it would have a feature on the blue side of the *J* band. The flip in the sign of the polarization noted by Ferrario et al. can then be explained as being due to the 28 MG pole.

We obtained a full orbit of spectroscopy of UZ For on 2005 September 3 using SpeX on the IRTF (see Figure 40). UZ For appears to have had $\langle K \rangle = 14.8$ at this time, in agreement with the 2MASS photometry. Note that the 2MASS *J*-band magnitude for UZ For was about one-half magnitude brighter than when observed by Ferrario et al. It is clear that the continuum at all orbital phases bears the imprint of the secondary star. At $\phi = 0.96$, the emission lines are weak, and the continuum is well represented by an M5V. Note that given the ephemeris deviation noted above, it is likely that this spectrum actually occurred very close to the eclipse phase because by $\phi = 0.03$ the emission lines have become quite strong again. At this latter phase, and in the range $0.70 \leqslant \phi \leqslant 0.92$, there is a strong excess present below 1.0 μm. This is the time of the cyclotron maximum from the high-strength pole, and we assign this excess to cyclotron emission from the $n \geqslant 2$ harmonics from the higher strength pole. There appears to be some evidence for a weak cyclotron harmonic in the *H* band at these phases, consistent with $n = 1$ for $B \sim 57$ MG. It is interesting that there is no evidence for cyclotron emission from this pole one-half orbit earlier, suggesting that it is hidden or that the viewing angle is very low.
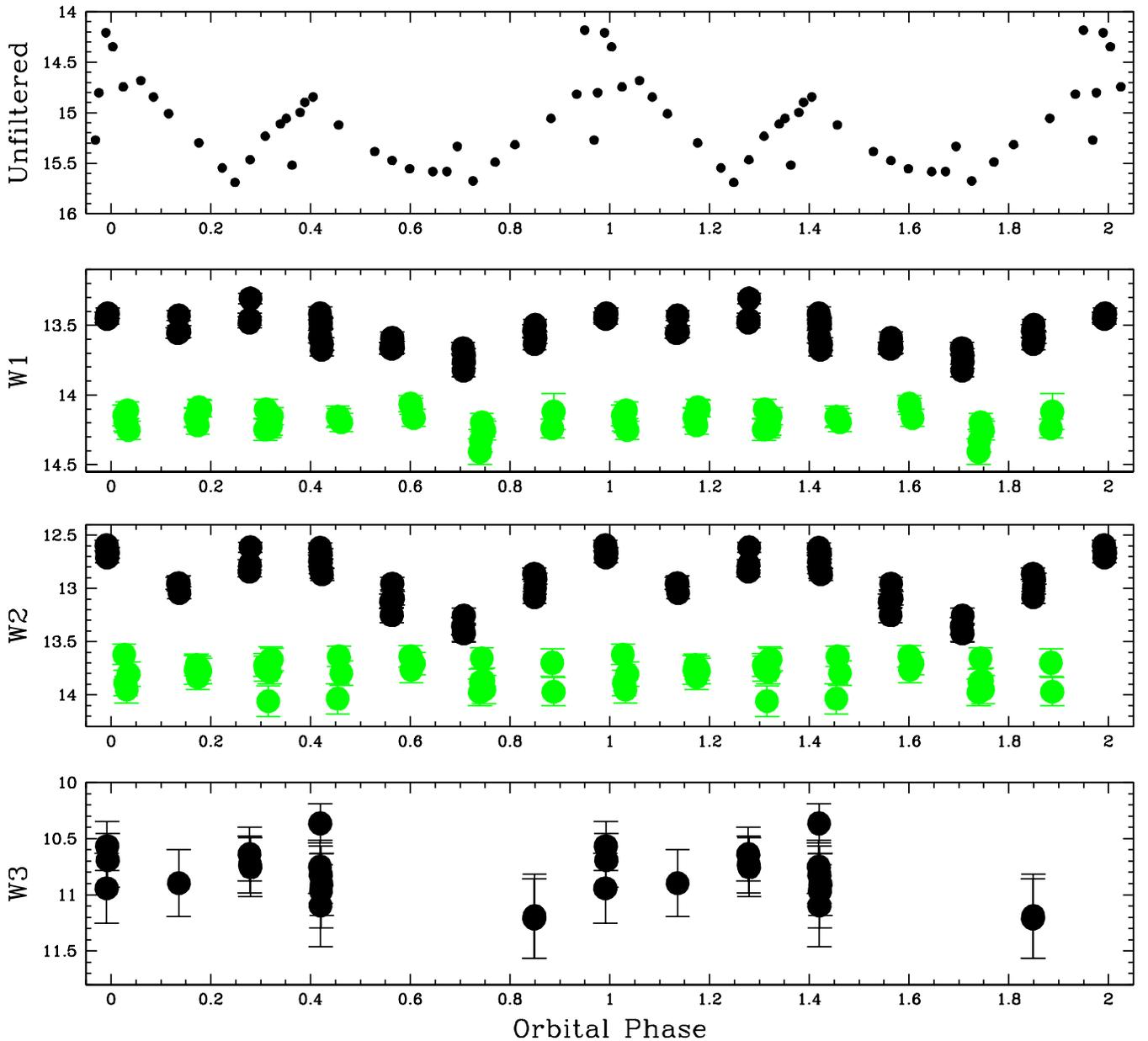
Figure 38. Top panel is the most recent (2001 December 19–20), unfiltered, visual light curve of UW Pic from Romero-Colmenero et al. (2003). The *WISE* light curves have been phased to the ephemeris in this paper, but they require an offset of $\Delta\phi = 0.074$ to best match the visual data set. The green circles are the *WISE* three-band data.

3.26. VV Pup

VV Pup was the first polar for which cyclotron features were seen in an optical spectrum (Visvanathan & Wickramasinghe 1979). Campbell et al. (2008b) present multiepoch optical and infrared spectroscopy of VV Pup covering a range of activity levels, from a very low optical state to a high state. In Figure 41 we present the *JHK* (from Campbell et al.) and *WISE* light curves phased to the ephemeris of Walker (1965). The *JHK* data were obtained during a high state. The AAVSO database does not have visual estimates at the time of the *WISE* observations, but a magnitude estimate listed in VSNET CV Circular 3051 shows that it was in a bright state 10 days prior. *Spitzer* data were also obtained for VV Pup, and they are listed in Table 2. The *WISE* fluxes are 1.5× higher than observed by *Spitzer*, during which the AAVSO had VV Pup at $v > 15.0$. It

appears that the *WISE* observations occurred during a high state. Howell et al. (2006b) present a radial velocity study of VV Pup, and using their parameters for the stellar masses, inclination, and secondary star *K*-band magnitude ($K = 15.3$, used to normalize the low-state flux), we are able to construct light curve models to compare to the high-state infrared data. We also obtained two full orbits of *BVRI* photometry of VV Pup on 2004 February 9 and 10 (see Figure 42). VV Pup was in a "mid-state" (see Campbell et al.) at this time, but the light curve morphology is the same as that originally reported by Walker (1965): a broad brightening centered on $\phi = 0$.

The peak of the visual light curve also corresponds to the time of maximum circular polarization (Liebert et al. 1978). Thus, at this time, we have our most direct view of the accretion region and hot spot on the surface of the white dwarf. Schwope & Beuermann (1997) model this pole with a high
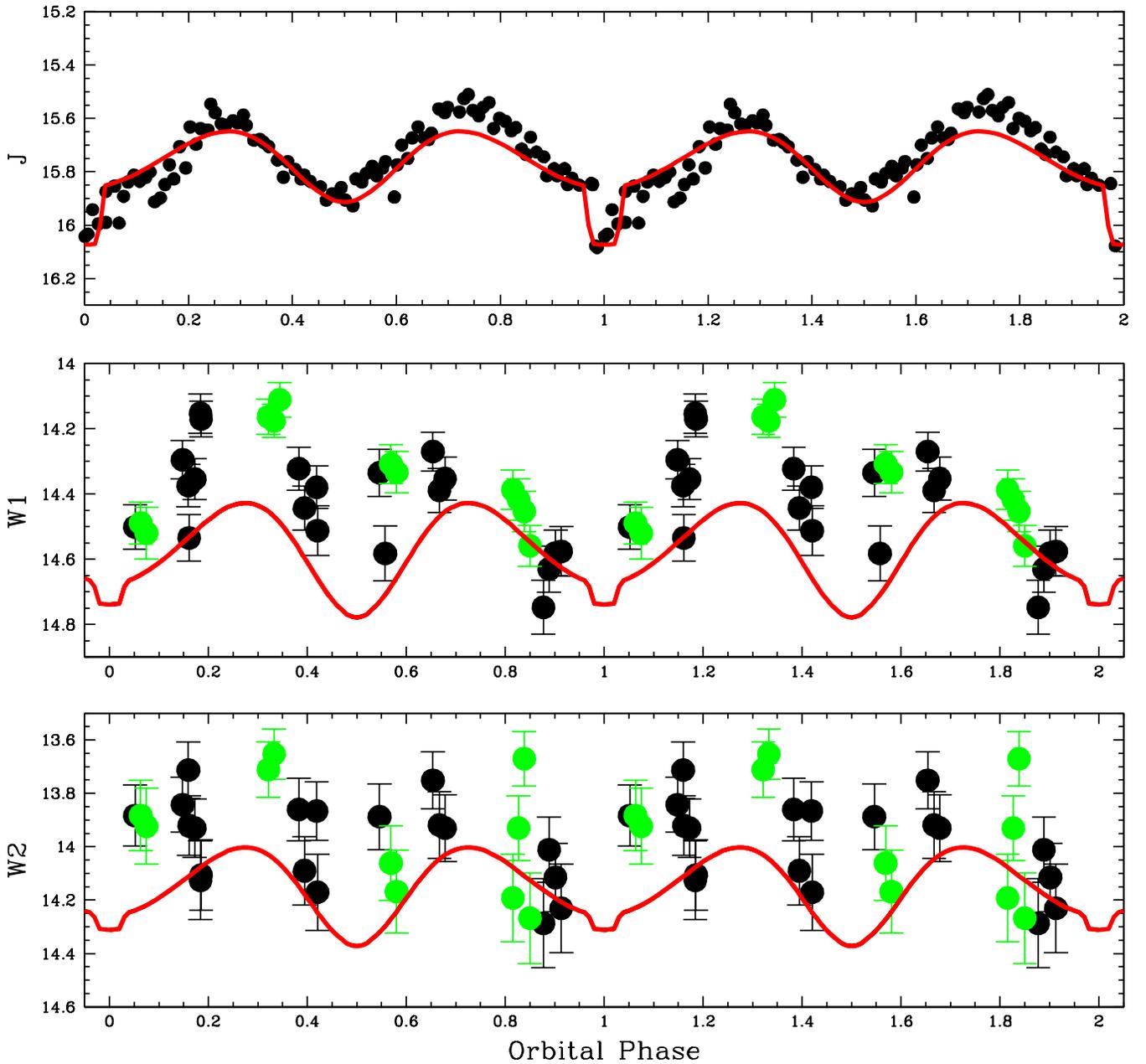
Figure 39. *WISE* light curves of UZ For phased to the ephemeris listed in Dai et al. (2010). The black filled circles are from the four-band survey, and the data in green are from the three-band survey. We added +0.1 mag to the three-band data to get them to overlap with the four-band photometry. The red solid curve is the light curve model we generated for this source.

southern colatitude that, when combined with the large orbital inclination of VV Pup ($i = 75°$), results in a self-eclipse for 60% of an orbit. Thus, the maximum cyclotron emission from this pole should occur between the phases of $\phi \sim 0.8$ and $\phi \sim 0.2$. This is borne out by the spectra presented in Campbell et al., where the $n = 7$–9 harmonics from a field with $B = 32$ MG are prominent in their low-state spectra. Between phases 0.2 and 0.8, weak harmonics are seen from the other pole. Campbell et al. assign these to a secondary pole with $B = 54$ MG, whereas Schwope & Beuermann attribute them to a region with $B = 57$ MG. Such a pole would not have significant cyclotron emission beyond the K band.

It is clear that, even in a high state, the influence of the ellipsoidal variations of the secondary star on the infrared light curves is quite substantial. The continuum level in all five

infrared bandpasses is about 1 mag above the levels expected in a low state, as demonstrated by the low-state light curve model shown in the bottom panel of Figure 41 (to construct the high-state light curves, we have added a "third light" component to the low-state model; in addition to elevating the total flux of the system, it also dilutes the ellipsoidal variations; see Harrison et al. 2013b). Like the optical bandpasses, the J-band light curve near $\phi = 0$ has a considerable cyclotron component, consistent with emission from a ~ 32 MG pole. The $n = 2$ harmonic from this pole would be located at the red end of the H band, and the tail would extend into the K band. There is clearly evidence for pre- and postphase zero cyclotron emission in the H and K bands, but at $\phi = 0$, there is no detectable emission. The minimum in these two bandpasses is consistent with the light curve model, leading us to surmise that we are
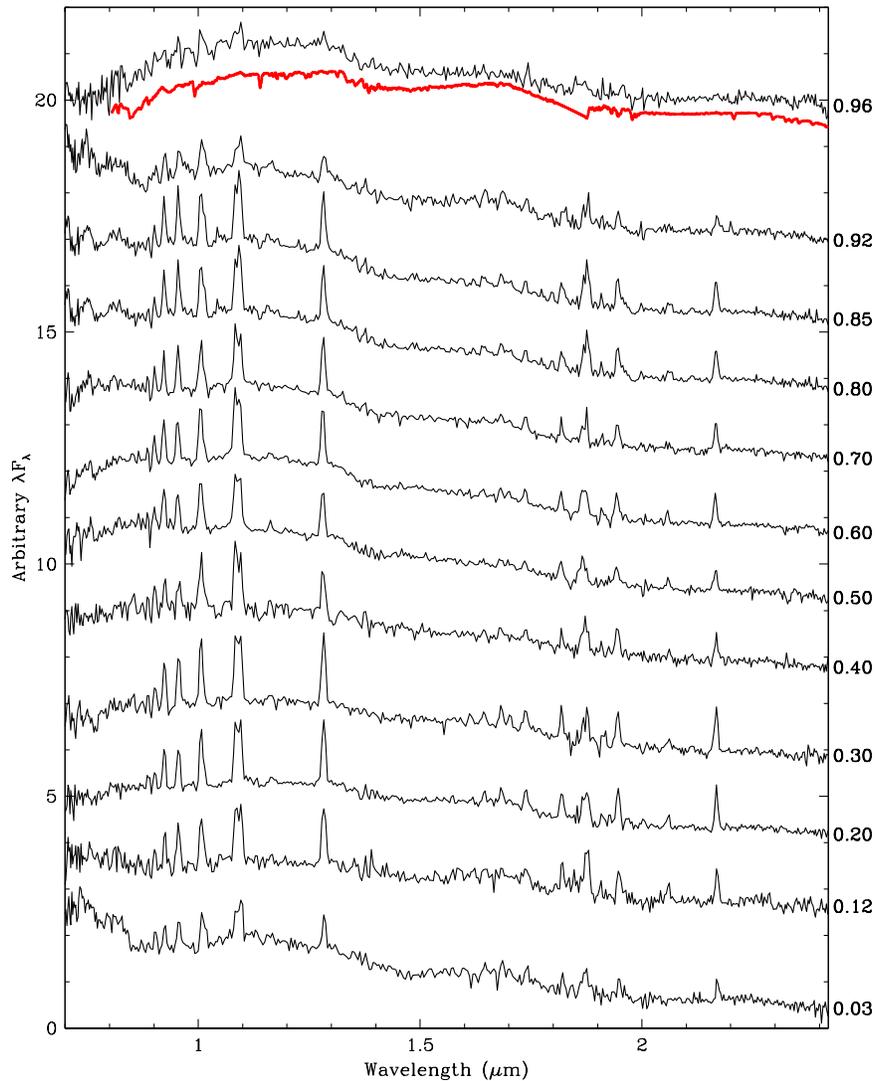
Figure 40. Near-IR spectra of UZ For over a full orbit obtained with SpeX on the IRTF. The predicted orbital phases are listed on the right-hand ordinate (though see text). The red spectrum is that of an M5V from the IRTF Spectral Library.

looking down the accretion column at this time. We also believe that the flat light curve, well above the ellipsoidal model, in the J band near $\phi = 0$ is due to hot spot emission filling in what would otherwise be a minimum in this bandpass. This would allow us to explain the JHK light curves as cyclotron emission from the 32 MG pole: the sharp cutoff at $\phi = 0.2$ that is obvious in both the J and K-band light curves is due to a self-eclipse. The spike/turn-on seen at $\phi = 0.8$ in the JHK data is also consistent with the return to visibility of this pole in the scenario described above. A 32 MG pole would have emission in both the $W1$ and $W2$ bands. The $W1$-band light curve at $\phi = 0$ shows a broad minimum, whereas the $W2$ light curve shows no such feature and is unlike the shorter wavelength light curves in this phase interval. We conclude that either the $n = 1$ harmonic from the 32 MG field is optically thick, leading to diminished emission in the $W1$ bandpass, or that the field strength is slightly lower than 32 MG. Note that Campbell et al. (2008b) found a field strength of $B = 30$ MG from their high-state near-IR spectra.

While we can explain the infrared light curves in the phase interval $0.8 \leqslant \phi \leqslant 0.2$, we cannot explain the remainder of the JHK or $WISE$ light curves using the higher field strength pole.

We clearly need a field strength similar to that of the primary pole. The minima at $\phi = 0.5$ in the JHK light curves suggest that, like the primary pole, we are looking down the column at this phase. In analogy with the primary pole, this cyclotron emission region undergoes self-eclipse at $\phi = 0.8$ and returns to view at $\phi = 0.2$, exactly antiphased to the primary pole. In contrast to the primary pole, the $WISE$ light curves do not show a deep minimum at $\phi = 0.5$, consistent with emission from the fundamental cyclotron harmonic of a pole with $B \sim 30$ MG.

As noted above, the strength of the secondary pole has been estimated to be $B \sim 54$ to 57 MG, and Schwope & Beuermann (1997) demonstrate that this pole was antiphased to the main accreting pole. The evidence for the presence of this high field strength appears to be very secure. It cannot, however, explain the infrared light curves. Either there are two poles of dramatically differing magnetic field strength inhabiting similar regions on the white dwarf, or the much higher field strength is somehow incorrect. In an attempt to constrain the field strength of the secondary pole, we obtained a phase-resolved set of blue spectra covering an entire orbital period for VV Pup on 2009 February 11 using the Blanco telescope
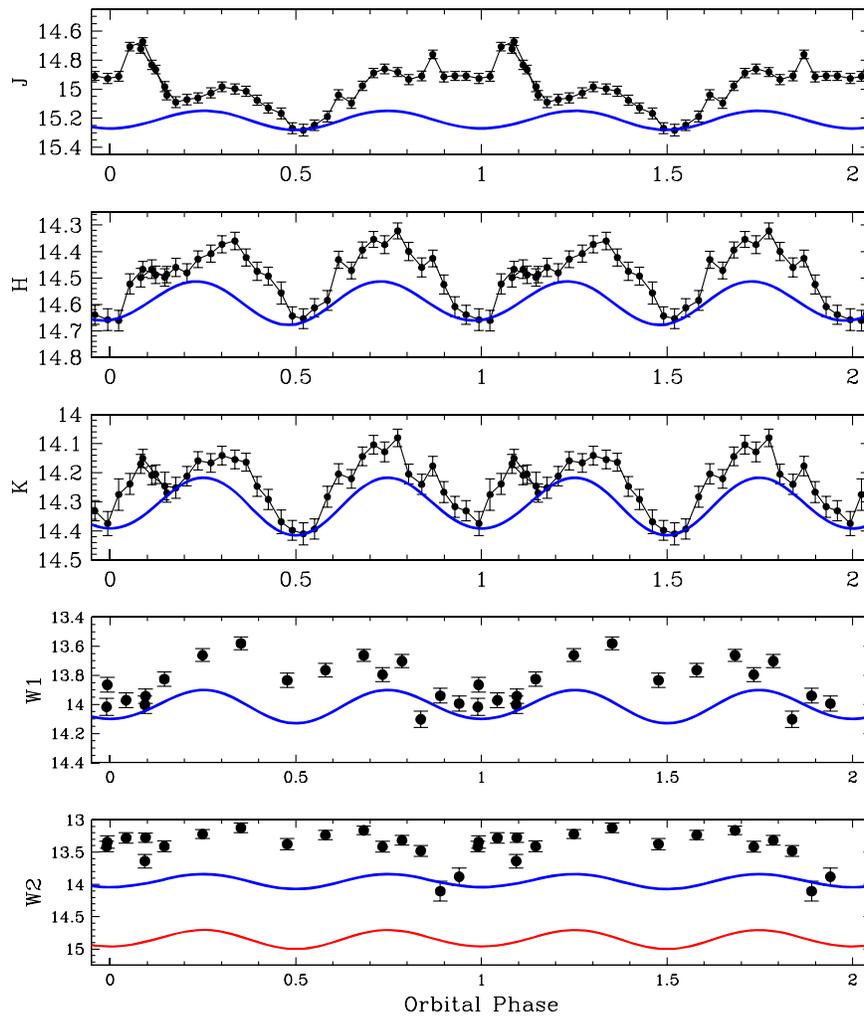
Figure 41. *JHK* (from Campbell et al. 2008b) and *WISE* light curves of VV Pup during a high state. The blue curves are a light curve model for the high state showing the presence of ellipsoidal variations. A low-state light curve model is presented in red in the bottom panel.

at CTIO. The AAVSO light curve database shows that VV Pup had $v \sim 16$ at this time. The spectra are presented in Figure 43 and clearly show the dramatic change in the continuum near $\phi = 0$, along with the superposition of the $n = 6$ and 7 harmonics from a field with $B \sim 30$ MG. There are essentially three spectra that cover the bright phase, and, like the light curves shown in Figure 42, they are skewed such that the rise to maximum is longer than the fall. To highlight the changes in the continuum over the orbit, we have clipped out the emission lines to enable us to construct a plot showing all of the spectra simultaneously. We do this to avoid having to subtract off a spectrum at a particular phase, which could lead to a corrupted continuum (it is obvious that there is no phase in our data set where cyclotron emission is not present). The spectra covering the phase interval $0.2 \leqslant \phi \leqslant 0.8$ show very little change in shape over the orbit, with a single, prominent cyclotron feature peaking near 5200 Å, essentially at the same wavelength as the $n = 7$ harmonic from the primary pole. This would be the $n = 4$ harmonic for a field strength of $B = 54$ MG, in agreement with Campbell et al. The $n = 5$ harmonic from this pole would peak near 4000 Å, consistent with the rising blue continuum in this region.

The $n = 3$ harmonic from such a pole would be to the red of our wavelength cutoff.

Thus, a high field strength pole is present on the white dwarf in VV Pup, and it may share a similar location on the white dwarf as the accretion region around a lower strength pole that is responsible for the infrared light curves in the phase interval $0.2 \leqslant \phi \leqslant 0.8$. It is curious that the strength of the $n = 4$ cyclotron harmonic from the 54 MG field shows very little change over the orbit. This is reinforced by the visual light curve data, which show that the minima are quite flat. Given the alignment between the $n = 4$ harmonic of the 54 MG pole and the $n = 7$ harmonic from the primary pole, we cannot actually determine if the former truly disappears at any point during the orbit. Mason et al. (2007) believe that this pole remains visible at all times. It is difficult to reconcile the optical/IR data set with a simple two-pole model. Even if one dismisses the *WISE* data as originating from a noncyclotron source, the variation seen in the *H* band cannot be produced by a 54 MG field. That the field structure on the white dwarf in VV Pup is complex is not a new conclusion. Mason et al. have shown that a dipolar field was inconsistent with the observed behavior of the phase-resolved Zeeman absorption features in the photosphere of the white dwarf in VV Pup.
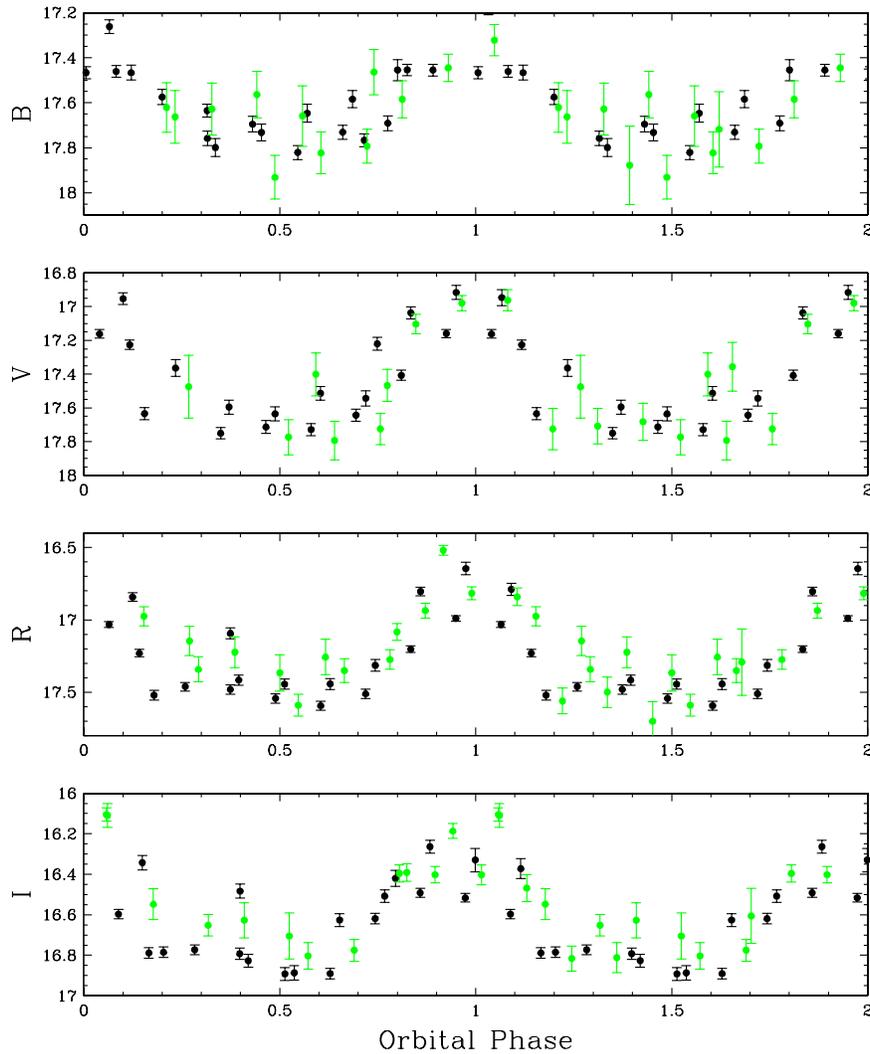
Figure 42. *BVRI* light curves of VV Pup on 2004 February 9 (black) and 2004 February 10 (green) phased to the ephemeris of Walker (1965).

3.27. VY For

Beuermann et al. (1989) provide an ephemeris for this long-period polar derived from a radial velocity study that finds a very low value for the semiamplitude of the secondary star. They suggest that this is probably due to a nearly face-on inclination, and they derived $i = 6°-12°$. In addition, they believe that the main accretion region probably never comes into view. We have phased the *WISE* light curves (see Figure 44) to the Beuermann et al. ephemeris after subtracting off 0.75 in phase so that $\phi = 0$ is the inferior conjunction of the secondary star. While noisy, the light curves do not look like ellipsoidal variations, which would be negligible for a very low orbital inclination. If the scenario outlined by Beuermann et al. attains, then the light curves of VY For provide insight into the mid-IR variability of polars without the contaminating effects of cyclotron emission, ellipsoidal variations, eclipses, or hot spot emission. The intrinsic, random variability of this source is limited in *W1* ($\Delta W1 \sim 0.2$ mag), but somewhat larger in *W2* ($\Delta W1 \sim 0.5$ mag). The only obvious source for this emission is the accretion stream. The fact that the variations are larger in *W2* than in *W1* demonstrates a flat spectral slope and where the dilution from the white dwarf + secondary star is greater in *W1* than it is in *W2*. This suggests free–free emission. Beuermann

et al. derive a spectral type of M4.5, and this is consistent with the mean ($W1 - W2$) color.

3.28. V347 Pav

Bailey et al. (1995) present multiband photometry and polarimetry of this object, as well as an ephemeris. Ramsay et al. (2004) provide an updated ephemeris where $\phi = 0$ is defined as the onset of the bright phase in the X-ray light curve. We phased all of the data to this latter ephemeris. Note that in the phasing of Bailey et al. the onset of the bright phase occurs at $\phi_{\mathrm{Bailey}} = 0.38$. In Figure 45 we present the *WISE* light curves along with the red ($\lambda 6500$–8400 Å bandpass) circular polarization and *I*-band light curves from Bailey et al. Note that V347 Pav was again observed by *WISE* 182 days later during the three-band survey, with little change in flux or light curve morphology. The bright phase in the X-ray and *I*-band light curves is similar, lasting for about 60% of an orbit. While the *WISE* data share the onset of the bright phase with the shorter wavelength light curves, the duration of the mid-IR bright phase is about 80% of an orbit. The positive circular polarization peaks at $\phi = 0.15$, and the *I*-band photometry peaks slightly earlier, near $\phi = 0.05$. Oddly, the negative polarization appears to peak only $\Delta\phi \sim 0.25$ phase earlier than
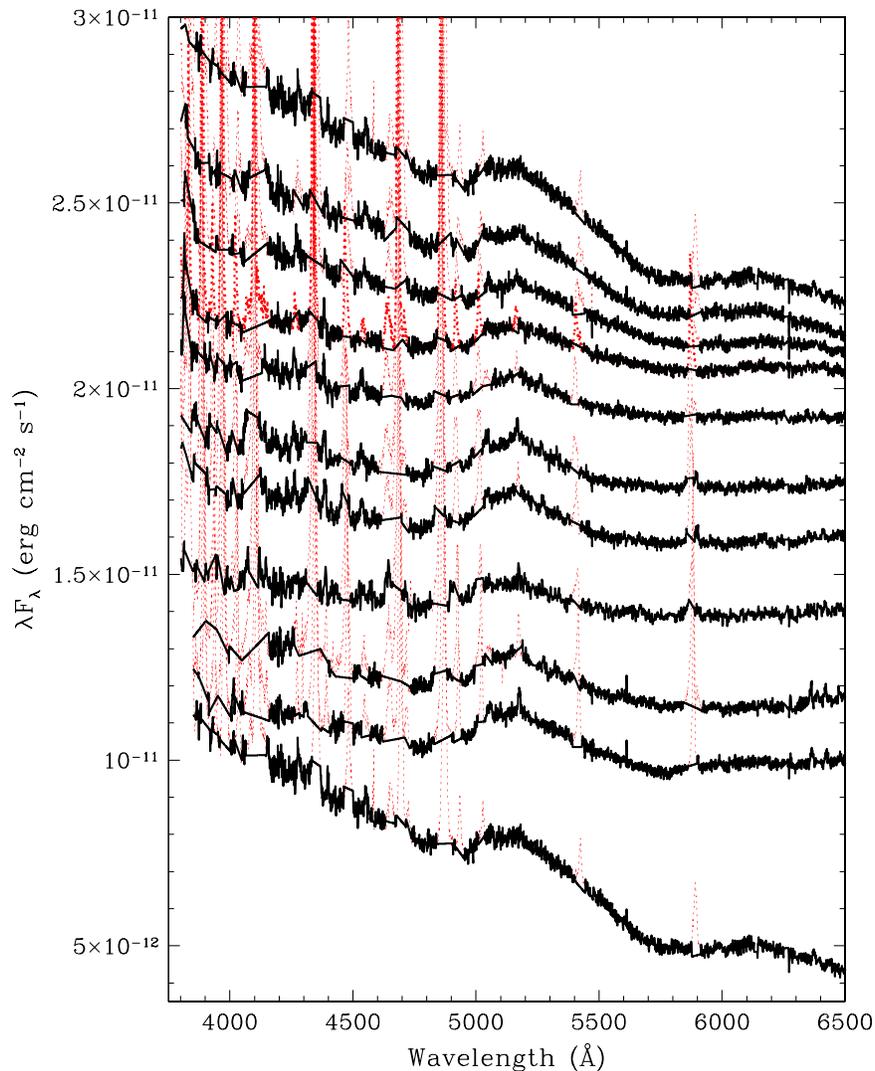
Figure 43. Phase-resolved set of blue optical spectra for VV Pup. The bottom spectrum had a phase of $\phi = 0.04$, and the spectra are incremented in phase by $\Delta\phi = 0.11$ from bottom to top. We plot the $\phi = 0.04$ spectrum again at the top. We produced spectra where all of the emission lines were patched over (black) so as to highlight the evolution of the continuum over an orbit. The spectra containing the line emission are plotted as red dotted lines.

the positive polarization, suggesting a peculiar geometry. Clearly, however, V347 Pav is a two-pole accretor.

In the geometry proposed by Bailey et al., the rise to maxima occurs when the southern pole appears from behind the limb, disappearing ~ 0.5 phase later. The combination of a high orbital inclination, $i = 60°$, and the magnetic colatitude keep this pole near the limb when it is in view, maximizing the cyclotron emission. Their geometry for the secondary pole has it spending about one-half of an orbit in view and passing almost directly under the line of sight. During this time, the X-ray emission has a flat minimum, but it does not completely disappear.

Bailey et al. suggest a field strength of 25 MG for the primary pole. The amplitude of the variations in W1 are greater than those in W2, suggesting that the offending cyclotron harmonic is predominantly located in that bandpass, with its tail extending into W2. This indicates that the field strength of this pole is either $B \sim 29$ MG or $B \sim 14$ MG. V347 Pav was observed with IRAC on *Spitzer* on two separate occasions: four-band imaging data on 2005 August 8, and light curves in the S2 and S4 bands on 2007 October 22. We present the latter

in Figure 46. Both light curves resemble those seen by *WISE*, except that the *Spitzer* data has better temporal resolution and higher S/N. These two light curves have minima at $\phi = 0.8$, suggesting a self-eclipse of the cyclotron emission region. The minimum in S2 is clearly flat bottomed and lasts about twice as long as that seen in S4. That the light curve morphology in S4 is similar to that seen in W1, W2, and S2 implies that some of the cyclotron emission in these bandpasses must emanate from a lower field strength pole, $B \lesssim 14$ MG.

If the center of the eclipse in S2 is when the primary pole is on the far side of the white dwarf, then this feature should be centered on the disk at $\phi = 0.3$. The X-ray light curve has a dip near this phase, which could be due to obscuration of the shock region by the accretion stream. There is a corresponding weak feature in the polarization light curve at this time. The *Spitzer* light curves show a brightening at this phase, tending to a maximum at $\phi = 0.4$. That both the S2 and S4 light curves look similar at this phase is in contrast to our earlier discussion, which would suggest that the emission from the two lowest harmonics should be nearly antiphased. This suggests a more
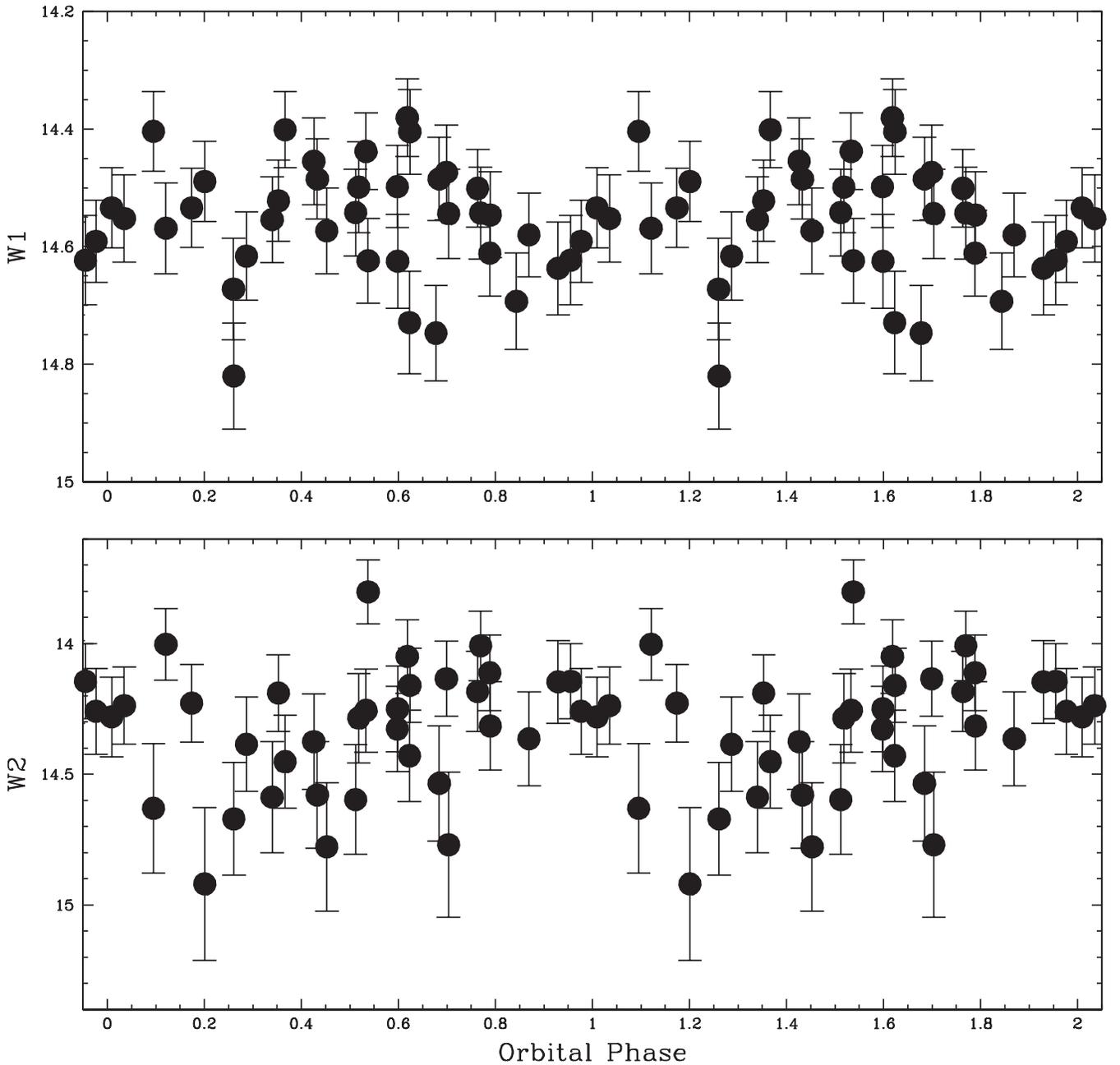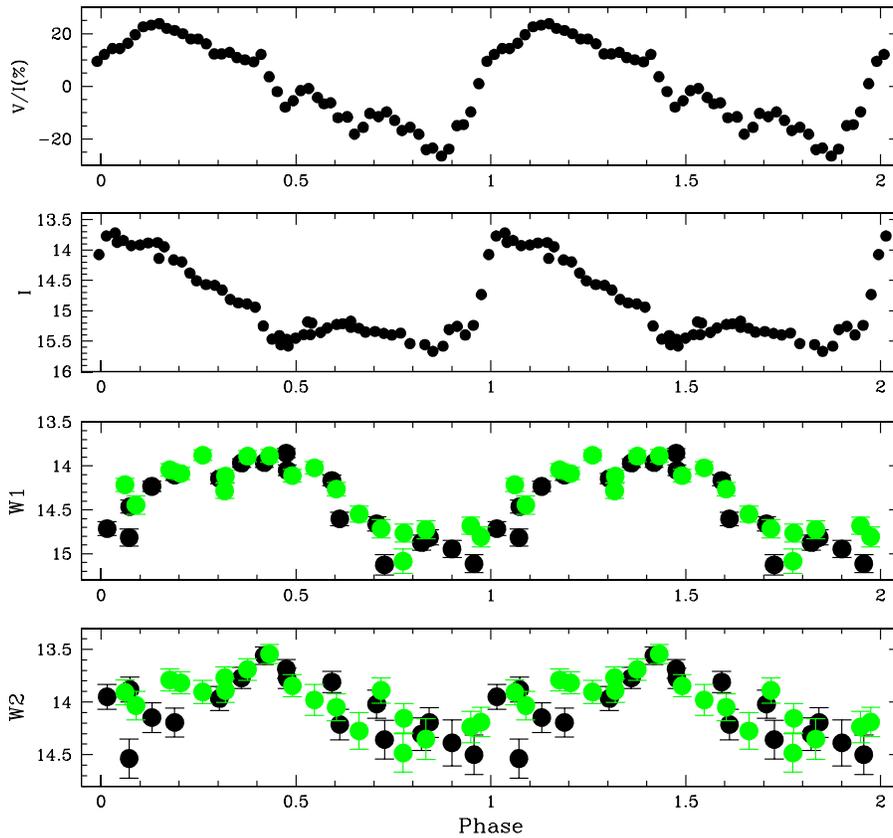
Figure 44. *WISE* light curves of VY For.

complex field distribution or that the S4 cyclotron emission is from a harmonic with $n > 1$.

It is difficult to believe that the large amplitude variations seen in the optical could come from a field with $B \leqslant 14$ MG because they would have to arise from harmonics with $n \geqslant 9$. It is interesting to note that, if we assume a dipolar structure with antipodal poles, the secondary pole would undergo a self-eclipse at $\phi = 0.5$, roughly the same phase as the dip in the mid-IR light curves that occurs within their broad maxima. The high viewing angles that would naturally arise on either side of this grazing event would result in strong cyclotron emission. Both the polarization and *I*-band light curves also show a dip at this phase. In this geometry, the secondary pole would be facing the observer near $\phi = 0.8$, and the minimum in S4 could be explained by the low viewing angle at this

phase if the cyclotron emission came from harmonics with $n > 1$.

We conclude that the most likely scenario for V347 Pup is that the primary accreting pole has a field strength near 29 MG, dominating the visual, *W*1, *W*2, and S2 light curves, and this pole undergoes a self-eclipse that is centered near $\phi = 0.8$. The secondary pole has a field strength near 7 MG, with emission from the $n = 2$ harmonic dominating the S4 band light curve. The higher harmonics from this field ($3 \leqslant n \leqslant 6$) would introduce additional maxima in the *W*1, *W*2, and S2 light curves. This model allows for the large negative circular polarization in the visual from high-number cyclotron harmonics, but these features would be optically thin and would create weak orbitally modulated broadband emission. Note that such emission would peak close to $\phi = 0$ and thus be

Figure 45. *WISE* light curves of V347 Pav combined with the red polarimetry and *I*-band light curve from Bailey et al. (1995). We have phased both sets of data to the ephemeris by Ramsay et al. (2004). The green filled circles are the *WISE* three-band data offset by $\Delta m = +0.1$ mag.

convolved with the rise in flux due to the cyclotron emission from the primary pole. Perhaps this emission is the reason for the *I*-band maximum leading that of the positive circular polarization. The premaxima rise in the bluest-band light curves presented by Bailey et al. is much more prolonged than seen in either the *I* or *H* band and is also consistent with this geometry.

The mean fluxes show that V347 Pav was 34% fainter during the *Spitzer* light curve observations than when observed by *WISE*. The *WISE* and *Spitzer* imaging data had nearly identical fluxes. No visual magnitude estimates for any of these observational epochs exist, though the AAVSO has V347 Pav at $V = 17.3$ roughly three weeks after the epoch of the *Spitzer* imaging observations. This is about one magnitude fainter than when Bailey et al. observed it. It appears likely that V347 Pav was in a low state during the *Spitzer* light curve observations. There are several epochs of near-IR photometry. At the time of the 2MASS observations (2000 June 4), V347 Pav was 0.66 mag fainter in *H* than when Bailey et al. observed it. There are two epochs of DENIS photometry, both near the light curve minimum. While the *I*-band magnitudes are relatively unchanged, the DENIS *J*-band magnitudes differ by 0.36 mag. This suggests cyclotron emission in the *J* band. Both of the DENIS data points are brighter than the 2MASS values, suggesting that V347 Pav was in a low state when observed by 2MASS.

3.29. V349 Pav

V349 Pav is a rarely observed polar in the CV period gap. Wickramasinghe et al. (1993) present an ephemeris for this object, and we have phased the *WISE* light curves to it (see Figure 47). Wickramasinghe et al. show that this system is a two-pole accretor where the dominant pole is located below the orbital plane, and it gives rise to a short-lived ($\Delta\phi \leqslant 0.4$) bright phase. They assume that the field strength is low, $B \sim 20$ MG. The *W*1 light curve shows small-scale variations that could be partially attributed to the stellar components in the system. The *W*2 light curve, however, shows a significant bright phase that lasts longer than those seen in the light curves presented by Wickramasinghe et al. (one of which we reproduce in Figure 47). The fact that the bright phases of the red and *W*2 light curves appear to have similar phasing is probably a coincidence, given the uncertainties in the ephemeris. The large amplitude in *W*2 and a similarly phased, but weaker feature in *W*1 suggest cyclotron emission from a $B \sim 28$ MG field. There are no visual magnitude estimates for any of the epochs of infrared data.

3.30. V379 Vir

Schmidt et al. (2003, 2005b) found that V379 Vir (= SDSS J121209.31+012627.7) is a short-period polar with a low field strength ($B = 7$ MG) and a possible brown dwarf secondary star. Burleigh et al. (2006) present an ephemeris where the zero phase is defined as the peak of the visual brightening. Debes et al. (2006) presented *JHK* light curves that showed large variations in the *K* band, but limited variability in *J* and *H*. The light curve in *K* had a distinctive "M" shape, with a sudden rise to the maximum and a sharp decline to the minimum. The *WISE* light curve data for V379 Vir are sparse, but do suggest large amplitude variations. V379 Vir was observed with IRAC on *Spitzer* in all four bands for a full orbit. We used MOPEX to
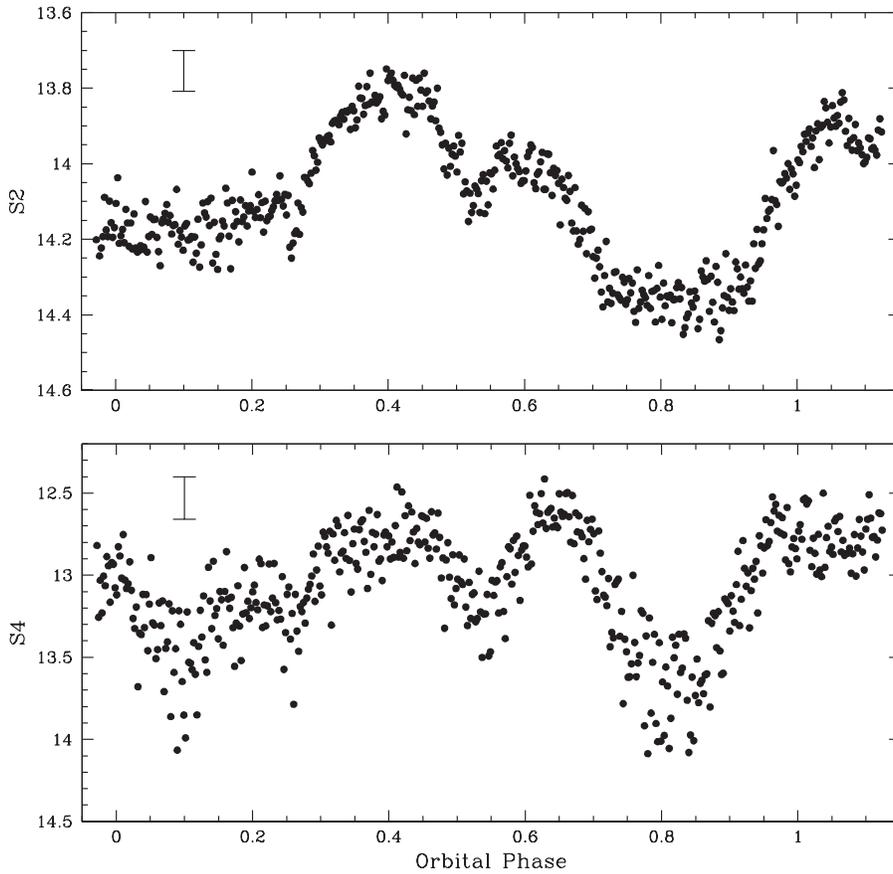
Figure 46. *Spitzer* light curves of V347 Pav. The light curves are not repeated so as to visualize details that cannot be seen in the *WISE* light curves. Typical photometric error bars are shown in the upper left of each panel.

produce this light curve by mosaicking three images together before extracting the flux densities. We present the light curve in Figure 48 and the mean flux densities in Table 2. In addition to the *Spitzer* data, we include the *K*-band light curve from Debes et al. offset in phase so that the bright phase aligns with the IRAC light curves.

Debes et al. proposed that the *K*-band light curve was due to cyclotron emission. This inference is obviously correct given the large amplitude variations seen in the mid-IR. The amplitudes in all four IRAC bandpasses are as large, or larger, than that seen in the *K* band. The variations seen in *S*1 and *S*2 are the largest amplitude cyclotron variations we have seen in the mid-IR light curves of any polar. A 7 MG field would have the $n = 2$ harmonic in *S*4, the $n = 3$ harmonic in *S*3, the $n = 4$ harmonic in *S*2, and the $n = 5$ and 6 harmonics in *S*1. The *K* band would contain both the $n = 7$ and 8 harmonics. Farihi et al. (2008) showed that cyclotron emission from a 7 MG field, when added to the spectrum of an L8 brown dwarf, could explain their *K*-band spectrum of V379 Vir.

The phasing of the cyclotron emission relative to the "pulse" phase of Burleigh et al. is interesting. Because the *Spitzer* observations occurred within 16 months of the establishment of the ephemeris for V379 Vir, the phasing cannot be off by more than $\Delta\phi = 0.1$. The usual assumption is that the visual brightening is due to a favorable viewing angle to the hot spot, and that generally the cyclotron emission should not be very strong at this time. However, the cyclotron emission at $\phi = 0$ remains close to its maximum value. Interestingly, all four light curves show a very small dip at $\phi = 0$. Overall, these light curves suggest that the viewing angle to the cyclotron emission region remains large throughout the orbit, and that it is a self-eclipse that causes the minima that last for 30% of the orbit. While the *K* and *S*1 minima are flat, the longer wavelength bands all show a rising slope from their faintest magnitudes. The duration of the minima are also wavelength dependent. Like encountered above, this implies that the lower harmonic cyclotron emission comes from a more extended region than does the higher harmonic emission.

3.31. V381 Vel

Very little is known about this system. Greiner & Schwarz (1998) present *ROSAT* observations that lead to a best-fit orbital period of $P_{orb} = 134$ minutes. Their optical spectra of this source showed strong cyclotron harmonic emission, which they ascribe to a field with $B = 52$ MG or, possibly, $B = 42$ MG. The *B*-band light curve of V381 Vel shows low amplitude ($\Delta B \sim 0.3$ mag) variations. The *WISE* data (not plotted) are unremarkable. The *W*1 light curve has the same morphology as the *B* band, with a single maximum, the duration of which lasts most of the orbit. The difference is that the amplitude is $\Delta W1 \sim 0.7$ mag. This is too large to be due to either a hot spot or ellipsoidal variations, so there might be cyclotron emission in this bandpass. The tail of the $n = 1$ harmonic from a field with $B = 42$ MG trickles into the *W*1 bandpass, though it is unlikely to be strong enough to cause the observed variations.
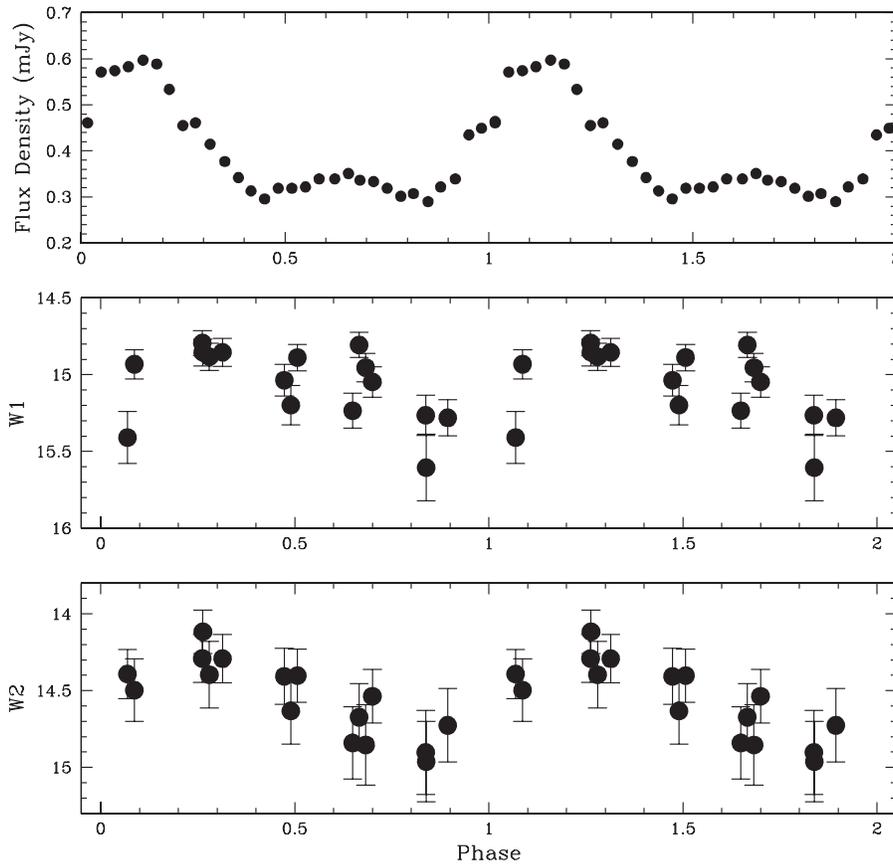
Figure 47. *WISE* and red (6500–8400Å) passband light curves of V349 Pav. The latter are from Wickramasinghe et al. (1993), and all are phased to the ephemeris in that paper.

3.32. V388 Peg

V388 Peg is a polar above the CV period gap. Tovmassian et al. (2000) present photometry, spectroscopy, and spectropolarimetry for this source and derive an ephemeris. The circular polarization reaches a maximum near phase 0.4, about the same phase as the peak in the visual light curves. The *B*-band data show a 1 mag brightening from minimum light, and the *R*-band shows nearly 2 mag of variation. Unfortunately, the binary period of V388 Peg is roughly twice that of the *WISE* orbital period, and thus the phase coverage of the data set is quite minimal (and therefore not plotted). The amplitude of the variations in *W*1 are of order 0.2 mag. While the data are noisy, the light curve in *W*2 indicates much larger variations: $\Delta W2 \sim$ 0.8 mag. No discrete harmonics were seen in the optical data set. An analysis of the spectropolarimetric data set led Tovmassian et al. to conclude that the field strength for the white dwarf in V388 Peg is near 20 MG. If the variations in *W*2 are ascribed to cyclotron emission, a slightly higher field strength would be necessary to exclude the $n = 2$ harmonic from the *W*1 band. This would put emission from $n = 6$ in the *R* band.

We obtained a full orbit of *JHK* phase-resolved spectroscopy of V388 Peg with SpeX on 2005 September 2. These data are shown in Figure 49. The mean *K* magnitude at the time of these observations was consistent with the 2MASS value. Having $(K_{2MASS}-W1) = 0.69$ suggests that V388 Peg was in a similar brightness state for the 2MASS, IRTF, and *WISE* observations. Near phase zero, the water vapor absorption (near 1.3 μm) from the donor star is clearly

present. The only other feature of note is the strongly changing continuum below 1 μm. From $\phi = 0.5$ to $\phi = 0.7$, the continuum gets much bluer. This could be due to a favorable viewing angle to the hot spot, though the emission lines are actually stronger earlier in the orbit. A 25 MG field would have harmonics centered in the *J*, *H*, and *K* bands, and there is no evidence for such features. A similar story attains for a 20 MG field, except that the $n = 3$ and $n = 4$ harmonics would fall near the telluric water vapor bands. Given the S/N of the IRTF data, these features would have been easily detected. Thus, either V388 Peg was in a high state during the SpeX observations and all of these harmonics were optically thick, or the magnetic field strength of the white dwarf in V388 Peg is much higher.

3.33. V393 Pav

V393 Pav is a short-period polar with a low field strength. Thomas et al. (1996) present an accurate ephemeris for this object, to which we have phased the *WISE* light curves shown in Figure 50. The phase coverage of the *WISE* data is not complete, covering 70% of the orbit. The *W*1 light curve shows a sharp peak at $\phi = 0.3$ with an amplitude of 0.7 mag. The *W*2 light curve is consistent with a nonvariable source. The *WISE* data do not cover the X-ray/optical bright phases, but the morphology of the *W*1 light curve is quite similar to the bright phase seen in the optical and X-ray light curves, except that it is shifted by $\Delta\phi = -0.5$. An analysis of the Zeeman absorption features in the optical spectrum by Thomas et al. suggests a field strength of $B = 16$ MG. Such a field would have the $n = 2$
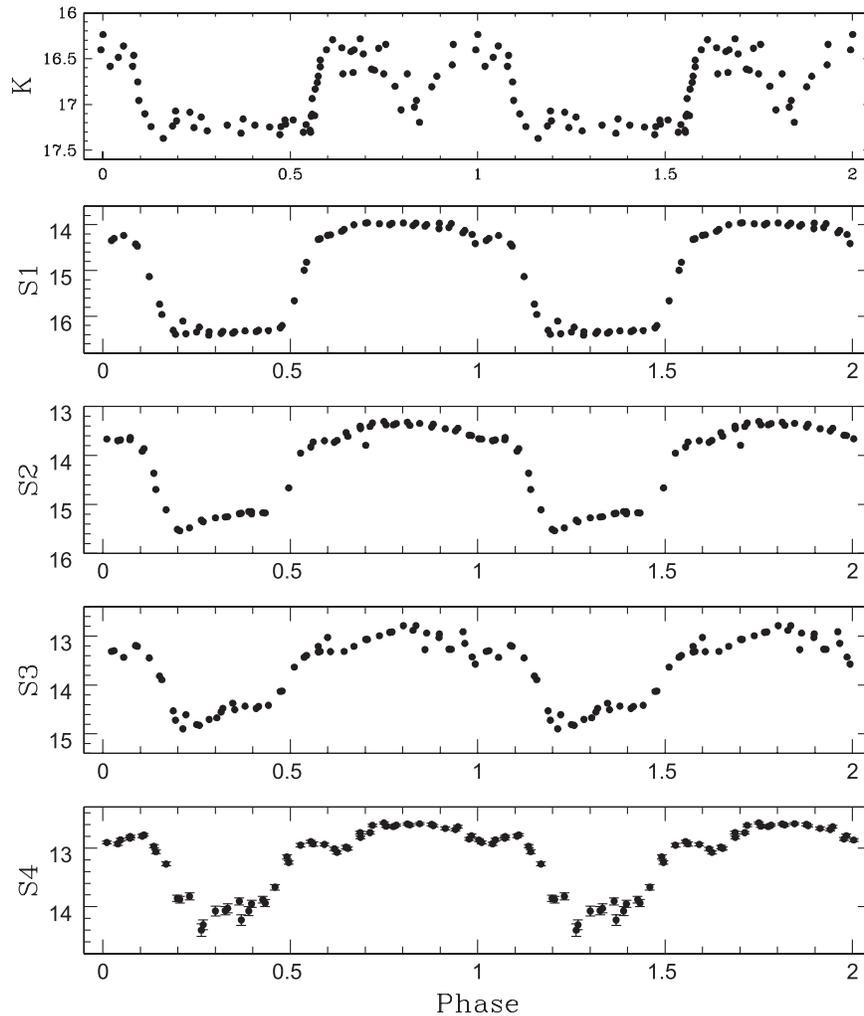
Figure 48. Infrared light curves for V379 Vir phased to the visual ephemeris in Burleigh et al. (2006). The *K*-band light curve in the top panel has been extracted from Debes et al. (2006) and has had its phase offset to match the *Spitzer* light curves. Note that only a subset of the extensive set of *K*-band data was extracted and plotted here.

harmonic in the *W*1 band, with nothing in the *W*2 band, consistent with the *WISE* results.

3.34. V479 And

V479 And was discovered in the SDSS survey (Szkody et al. 2005). It is unclear whether this object is actually a polar, though González-Buitrago et al. (2013) argue for the presence of UV cyclotron emission to explain their *Swift* observations of this system. If V479 And is a polar, it would have the longest orbital period, $P_{orb} = 14.3$ hr. González-Buitrago et al. present a binary orbital ephemeris for this system, and we have phased the *WISE* light curves using their result. The *W*1 light curve of V479 And appears to be almost identical to the *Swift* UV light curves (see Figure 51). The *W*2 data have a very low S/N, but these data are sufficient to suggest that the source is not highly variable at this wavelength. González-Buitrago et al. classify the secondary as a G8-K0IV, and the 2MASS and *WISE* colors are consistent with this range in spectral type. It seems unlikely that the identically phased small-amplitude variations seen in both the UV and *WISE* light curves could be due to cyclotron emission. A case for V479 And being a polar cannot be made from the existing data set.

3.35. V516 Pup

V516 Pup is polar in the period gap ($P_{orb} = 2.28$ hr) with a soft X-ray spectrum (Schwarz & Greiner 1999). The source shows a single minimum per orbit in the *B* and *V* bands, with a double-humped maximum similar in appearance to the *S*2 light curve of V347 Pav (see Figure 46), but having an amplitude of 2 mag. The *W*2 light curve (not shown) does not show any variability, whereas the *W*1 light curve is complex, with a full magnitude of variation. Schwarz & Greiner obtained optical spectra that showed three discrete harmonics to which they originate in a field strength with $B = 39 \pm 3$ MG. This result is consistent with the *WISE* data.

3.36. V834 Cen

V834 Cen is a well-known short-period polar. Schwope et al. (1993c) publish an ephemeris for this source based on a radial velocity study, as well as derive parameters for the underlying binary. There were two epochs of four-band data for V834 Cen: the first was obtained on 2010 February 3, and the second was obtained exactly six months later. We phase the first-epoch *WISE* data to the Schwope et al. ephemeris and combine it with *VJH* light curves from Bailey et al. (1983) to produce
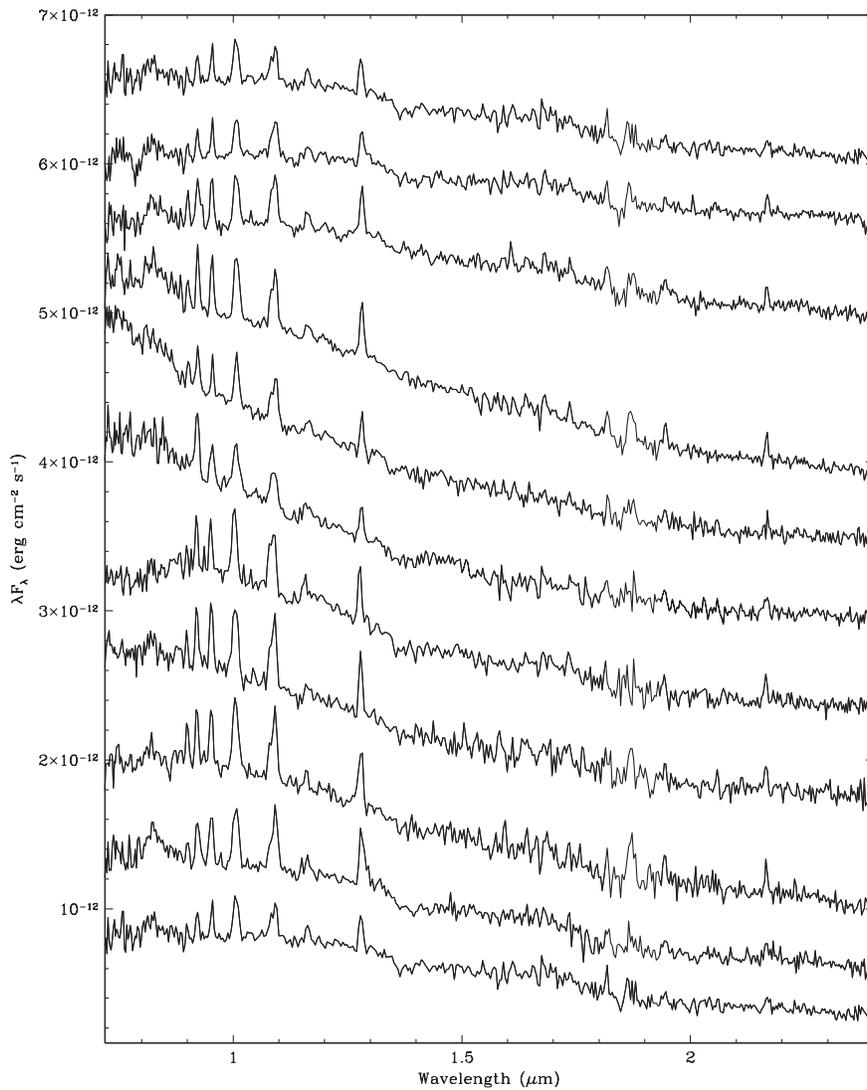
Figure 49. Phase-resolved near-IR spectra of V388 Peg. The phase zero spectrum is on the bottom and is repeated at the top. The spectra step by $\Delta\phi = 0.1$ in phase from bottom to top.

Figure 52. The W1 and W2 light curves are similar to the J- and H-band data from Bailey et al. The W3 light curve, however, shows large variations that are nearly antiphased to the shorter wavelength light curves. Schwope & Beuermann (1990) derived a field strength of 23 MG from both cyclotron and Zeeman features, and Potter et al. (2004) found $B = 31$ MG from modeling polarimetric observations. A field strength near 30 MG would have emission in the W1 and W2 bandpasses, but such emission should be antiphased to the shorter wavelength light curves, as it would originate from the cyclotron fundamental.

The W1 light curve superficially resembles one dominated by the ellipsoidal variations from an irradiated secondary star. Given the specifications of the binary as listed by both Schwope et al. (1993c) and Potter et al. (2004), we can construct ellipsoidal light curve models for V834 Cen to investigate this proposition. We plot both epochs of WISE data in Figure 53. Clearly, the cyclotron emission in the WISE bandpasses was weaker during the second epoch. If we assume that the W1 light curve is due to pure ellipsoidal variations in this fainter state, we find that the secondary has to have a late spectral type with $T_2 = 2300$ K ($\sim$M8), whereas the white

dwarf has $T_1 = 18{,}000$ K, with $i = 50°$. Although these results are within the bounds published for this source, they would result in V834 Cen being the closest polar: $d \approx 40$ pc. Unfortunately, we do not know whether V834 Cen was in a high or low state when either set of WISE data was obtained. Fortunately, there are abundant near-infrared data for this source, and we can assess the validity of the light curve modeling. The light curves presented in Bailey et al. show the system varying between $J = 14.3$ and 13.5. Sambruna et al. (1991) found similar values. The 2MASS observations, however, had $J = 13.5$ at minimum light, so nearly a magnitude brighter. Clearly, the system was in a high state when those data were obtained. The DENIS survey found the system at $J = 14.27$ when $\phi = 0.71$, a phase that is close to maximum light in that bandpass. Thus, V834 Cen was in a much lower state. At this time, $(J - K) = 0.72$, bluer than an M8 dwarf: $(J - K)_{M8V} = 1.1$. In the K-band light curve presented by Sambruna et al., the only real feature was a sharp dip at $\phi = 0$, during which the system fades to $K \sim 13.8$. There appears to be less cyclotron emission in this bandpass than in either J or H. In the J band, the modeled white dwarf and secondary star (red lines in Figure 53) have similar luminosities
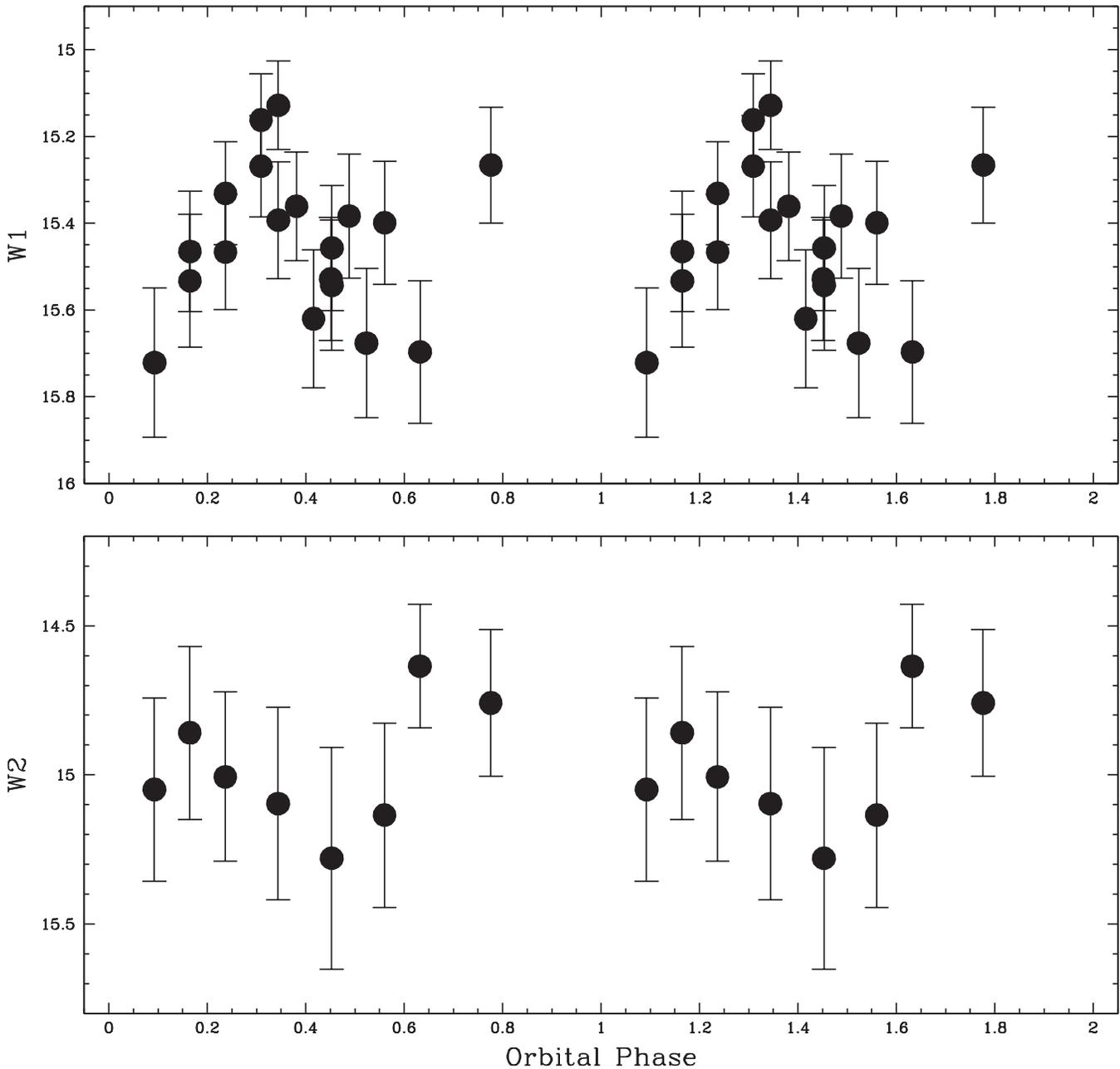
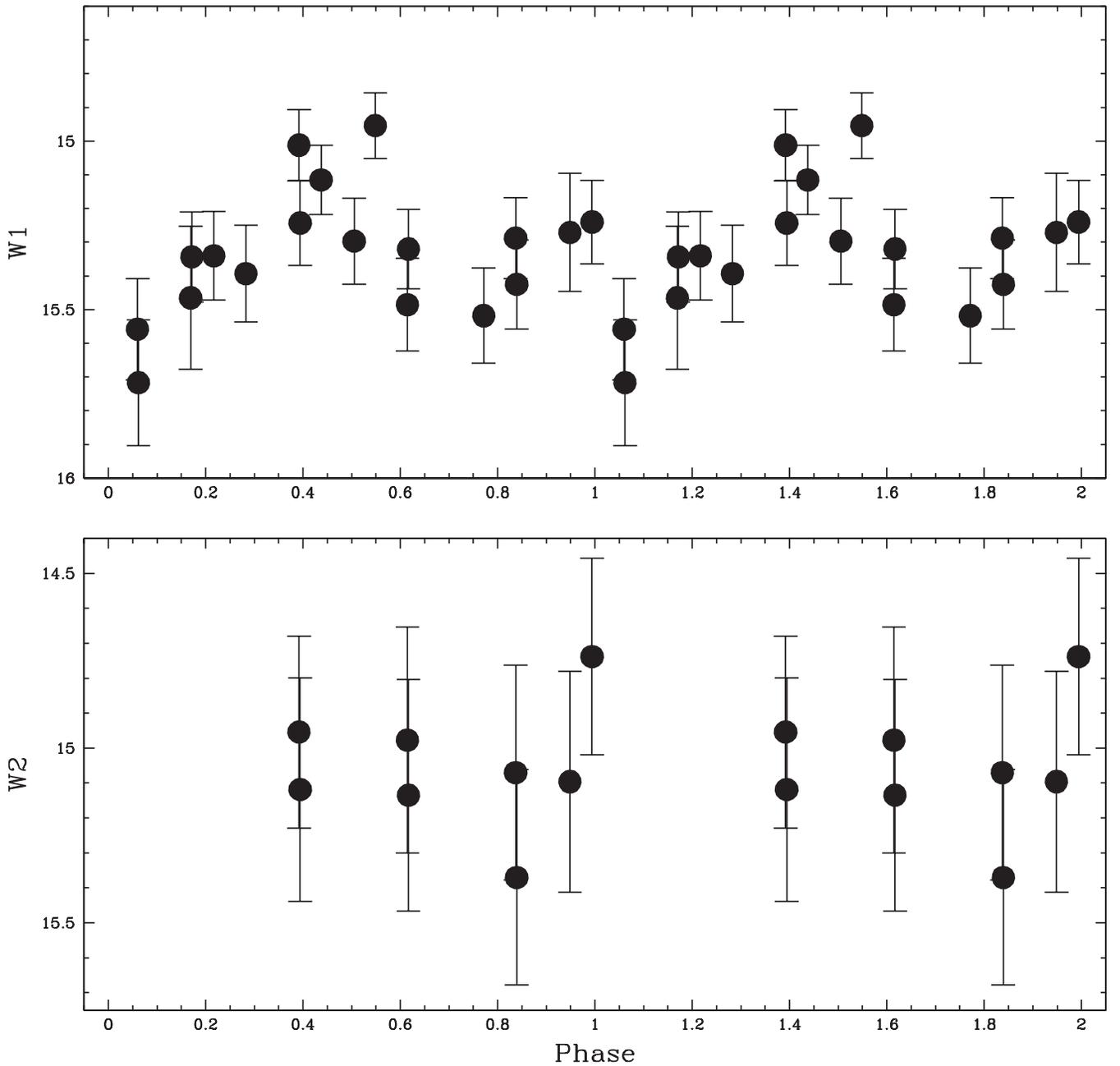**Figure 50.** *WISE* light curves of V393 Pav phased to the ephemeris given by Thomas et al. (1996).

$(L_1/L_2 = 1.1)$; in the K band the secondary dominates: $L_1/L_2 =$ 0.24. Assuming that the minimum is due to only the white dwarf plus the secondary star implies that $K_2 = 14.0$ and $W1 = 13.7$. V834 Cen is $\sim$0.6 mag brighter than this. Thus, even in the fainter state, there is considerable cyclotron emission present in the *WISE* bandpasses, and the ellipsoidal light curve model is invalid.

Bailey et al. (1983) believe that the minima in the light curves are when we are looking most directly down the accretion column. This geometry is consistent with all of the data if we assume that the field strength is much lower than previously assumed: $B \sim 11$ MG. Then the antiphasing of the $W3$ light curve would naturally arise from the $n = 1$ harmonic, while $W2$ and $W1$ emission would come from the $n = 2$ and 3 harmonics of this field, respectively. The issue with this field strength is that very high harmonic numbers ($n > 15$) would be

needed to reproduce the *V*-band variations, and that is implausible. We are left with proposing a model similar to VV Pup: two regions of dramatically differing field strength located at similar places on the white dwarf.

3.37. V884 Her

V884 Her is a short-period polar that Schmidt et al. (2001) believe harbors a high-field ($B = 150$ MG) white dwarf. Greiner et al. (1998a) provide a precise ephemeris for this object based on the timing of its X-ray dips, which they believe are due to an eclipse by the accretion stream. We extracted the *V*-band light curve for 1992 October from Greiner et al. to compare it to the *WISE* data in Figure 54. V884 Her was observed during both the four-band and three-band surveys, producing similar results. To get the *V*-band and *WISE* light

Figure 51. *WISE* light curves of V479 And phased to the binary orbital ephemeris in González-Buitrago et al. (2013).

curves to align, we had to adjust the *WISE* data by $\Delta\phi = -0.26$. This would require the orbital period to differ by about $2\,\sigma$ from what is listed in Greiner et al. The *V*-band magnitude was normalized assuming that the "nearby comparison star" used by Greiner et al. was star "C" in Szkody et al. (1995). Note that the APASS data listed in Table 3 appear to have caught V884 Her in a much brighter state ($V = 13.27$) than observed by either Szkody et al. or Greiner et al. The *W1* light curve is remarkably similar to the *V*-band data, suggesting a similar origin. The *W2* light curve shows a slightly stronger dip in the middle of the broad maximum than that seen in *W1*. The *W3* band shows no variations, but the source is surprisingly bright at this wavelength: $(W1 - W3) = 1.94$.

The *WISE* light curves are not consistent with a high field strength. While Schmidt et al. (2001) provide compelling

evidence for a field with $B \sim 150$ MG, if the *V*-band variations are due to cyclotron emission, then the *W1* and *W2* variations must also be due to cyclotron emission. This argues for a much lower field strength, $B \sim 30$ MG, for the region from which the mid-IR emission emanates. The dips near maximum light in the *WISE* data could then be due to a high viewing angle to the cyclotron emission region, a time when the emission from the $n = 1$ harmonic would be weakest. Perhaps, like several previous polars, the maxima in the *WISE* light curves are from an additional pole that has a longitude similar to the primary pole. The polarization behavior of V884 Her is complex, and Schmidt et al. suggest that either a secondary pole or a quadrapolar field geometry might be needed to fully explain the discrepancies they found in modeling their data with a single
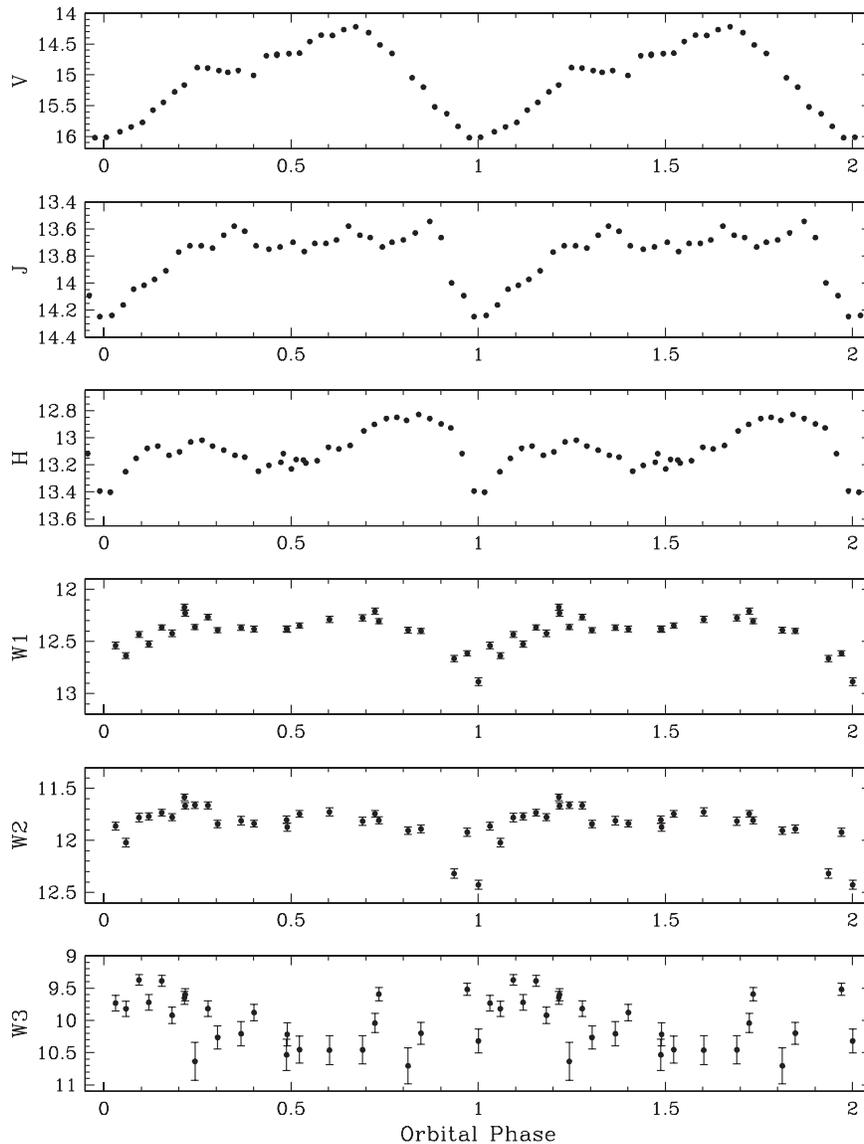
Figure 52. First-epoch *WISE* light curves of V834 Cen combined with *VJH* data from Bailey et al. (1983) phased to the ephemeris given by Schwope et al. (1993c).

field strength. Near-IR light curves of V884 Her would be useful in helping to resolve this conundrum.

3.38. V895 Cen

V895 Cen is a long-period eclipsing polar. Stobie et al. (1996) present an ephemeris based on white light eclipse timings, to which we phased the *WISE* data (see Figure 55). Note that the orbital period of V895 Cen is almost exactly three times that of the *WISE* orbit, resulting in very poor phase coverage. The *WISE* observations were also obtained on two distinct epochs, separated by 190 d. There was little apparent difference in the data between the two epochs. The 2MASS ($\phi = 0.22$) and DENIS ($\phi = 0.47$) data for V895 Cen were obtained within a few weeks of each other and are nearly identical. The multicolor optical light curves of V895 Cen in Stobie et al. show that the eclipse depth in the blue is much larger than in the red, suggesting that the spectral type of the secondary star is not too late. No cyclotron harmonics were present in their visual spectra.

We do not know the state of V895 Cen at the time of the *WISE* observations. Stobie et al. find that the $(R - I)$ color of the system during eclipse was consistent with an M2 dwarf. The 2MASS colors are $(J - H) = 0.56$ and $(H - K) = 0.27$, similar to that of an early M dwarf. The DENIS colors are $(I - J) = 1.03$ and $(J - K) = 1.00$; these are very close to that expected for an M2V. The mean *WISE* colors are $\langle (W1 - W2) \rangle = 0.15$ and $\langle (W1 - W3) \rangle = 0.68$. Using the 2MASS value, $(K - W1) = -0.06$. This suggests that the secondary dominates in the near-IR and out to *W2*. The *WISE* light curves are too sparse for light curve modeling, but the minimum at $\phi = 0.15$ is much too deep to be due to an eclipse of the white dwarf alone (as demonstrated by the lack of an eclipse in the *I*-band light curve of Stobie et al.). This suggests the eclipse of a cyclotron emitting region. With only three data points, the *W3* light curve is not very informative, but it does seem to mimic the *W1* and *W2* light curves. It seems likely that the white dwarf in the V895 Cen system has a very low magnetic field strength.
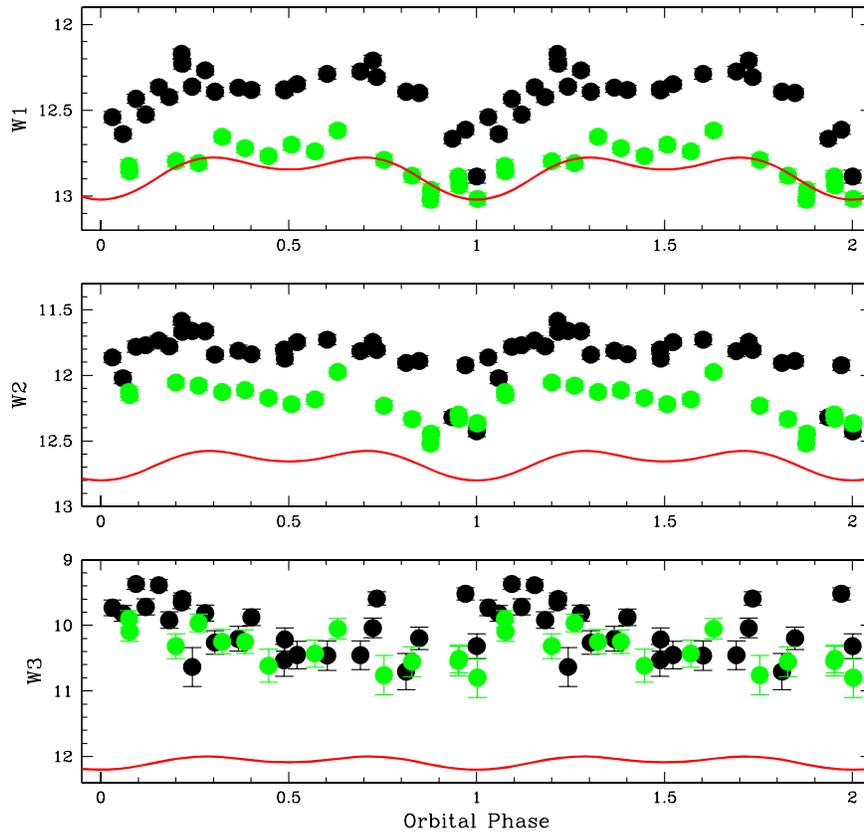
Figure 53. First (black) and second (green) epochs of *WISE* data for V834 Cen shifted in phase by $\Delta\phi = +0.02$. An attempt at a light curve model is shown in red. As described in the text, we find that the mid-IR is completely dominated by cyclotron emission (in reality, the red curves should be shifted downward by ~ 0.6 mag in all three panels).

3.39. V1007 Her

V1007 Her is a little-observed polar with a period that places it just below the period gap. Greiner et al. (1998b) have produced an ephemeris for this object whose phasing is tied to the "end of the bright phase." The X-ray and optical light curves are similar, with a single brightening once per orbit centered near $\phi = 0.7$ and lasting for one-half of the orbital period. As shown in the data tables, V1007 Her is very faint in the infrared. The *WISE* light curves, presented as Figure 56, are noisy. V1007 Her was observed during both the three-band and four-band surveys, with no apparent change in state. The *W*1 light curve is suggestive of ellipsoidal variations. The *W*2 light curve, however, appears more similar to the visual light curves, with a single weak maximum visible once per orbit. The mean infrared colors are not consistent with the luminosity being dominated by a late-type star, and they suggest that cyclotron emission is present. The cyclotron harmonics visible in their spectra of V1007 Her led Greiner et al. to conclude that the field strength was high: $B = 50$ MG. Such a field would not have emission in the *W*2 bandpass.

3.40. V1033 Cen

V1033 Cen is a longer-period polar that shows a single bright phase once per orbit. Rodrigues et al. (1998) present an ephemeris for this object that has phase zero at the peak of the bright phase. The orbital period of V1033 Cen is almost exactly twice the orbital period of *WISE*, so even though there were numerous measurements of this system (34), the

phase coverage of the data set is poor. These data do show that the system has no large-scale brightness changes over an orbit, but it does show small-scale changes ($\Delta m \sim 0.2$ mag) that occur from one orbit to the next. Rodrigues et al. believe that their polarimetry limits the field strength of the white dwarf in V1033 Cen to $15 \leqslant B \leqslant 40$ MG. Over most of this range in field strength, we would expect cyclotron emission to be present in the *WISE* bandpasses. We do not know the state of V1033 Cen at the epoch of the *WISE* observations; however, $(K_{2MASS} - \langle W1 \rangle) = 0.29$, while $(K_{DENIS} - \langle W1 \rangle) = 0.74$, suggesting that the *WISE* observations occurred during a higher state than that observed by DENIS. If so, the emission from low-harmonic cyclotron features could be optically thick and not strongly impress themselves on the mid-IR light curves.

3.41. V1043 Cen

V1043 Cen is a long-period polar that has a white dwarf with a surprisingly low temperature ($T_{eff} = 15,000$ K) given its orbital period (Gänsicke et al. 2000). Thomas et al. (2000) have established a very precise orbital ephemeris for this system, to which we have phased the *WISE* data. Thomas et al. also derive a field strength of 56 MG from the strong cyclotron features present in their optical spectra. There were two distinct epochs of *WISE* observations separated by 175 days. As shown in Figure 57, V1043 Cen brightened by about $\Delta m \sim 0.3$ mag between the two epochs. The first-epoch data appear to show a sharp minimum near $\phi = 0$ that is also present in the visual
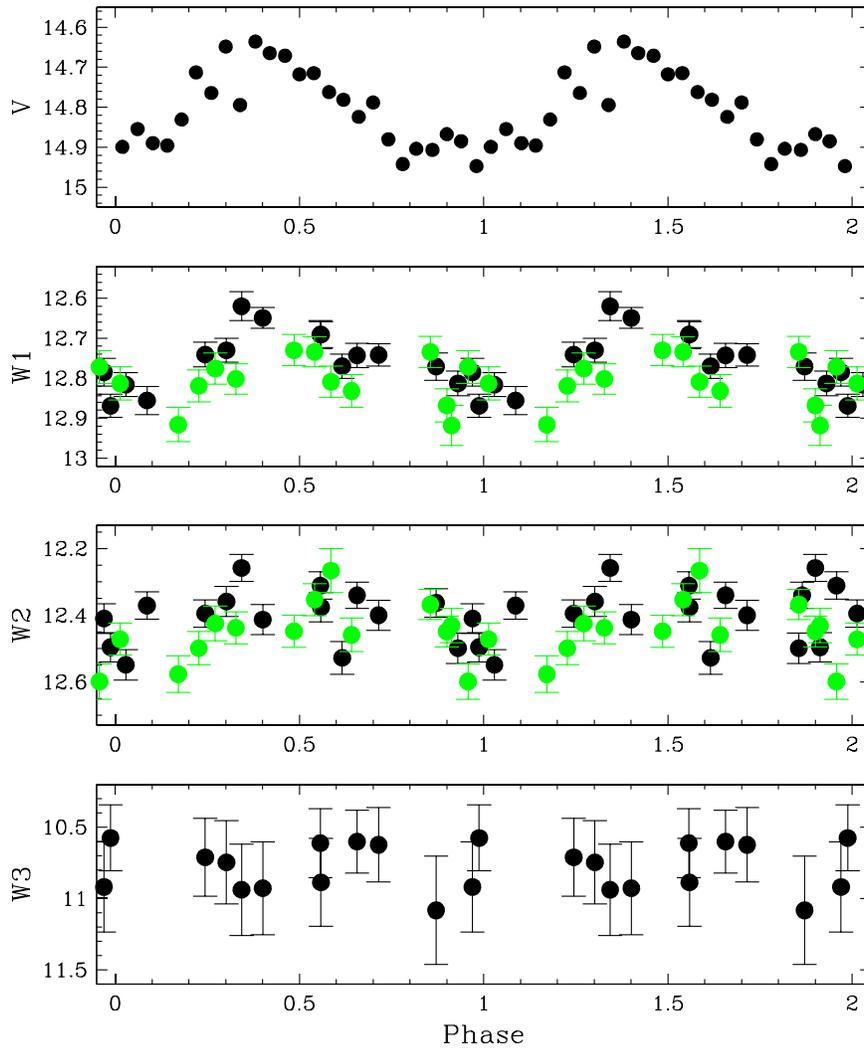
Figure 54. *WISE* data for V884 Her. The four-band data are plotted in black, and the three-band data in green. The *V*-band light curve is from Greiner et al. (1998). We had to shift the phasing of the *WISE* light curves by $\Delta\phi = -0.21$ to align them with the *V*-band data.

light curves. *Spitzer* observations of V1043 Cen were obtained and are similar in flux to the lower-state *WISE* observations. Gänsicke et al. have derived the temperatures and masses for the components in V1043 Cen, allowing us to produce an ellipsoidal light curve model. We normalize the light curve models by assuming that the minimum observed in *W*1 is when the cyclotron emission region is eclipsed. It is clear that ellipsoidal variations are affecting the observed light curves, but the *WISE* data are dominated by cyclotron emission throughout the orbit in both the *W*1 and *W*2 bandpasses. The higher-state *W*3 light curve shows considerable variation, but it does not appear to be periodic in nature. The lower-state *W*3 light curve is consistent with no variability.

The *W*1 and *W*2 light curves are similar to the *V*-band data presented by Thomas et al. The high field strength found by Thomas et al. cannot produce cyclotron emission in the *WISE* bandpasses. The slightly larger amplitude in the *W*2 band suggests a field strength of $B \sim 28$ MG. We believe that this lower field strength is consistent with the cyclotron humps in the spectra presented by Thomas et al. The largest feature they saw was centered near 6500 Å, which would be the $n = 3$ harmonic for a 56 MG field, but would be the $n = 6$ harmonic

for $B = 28$ MG. Their cyclotron model fits the next hump seen in their spectra (centered near 5000 Å) for most of the orbit, but near $\phi = 0.3$ this feature seems to be split into multiple components that resemble the increasingly compact series of the higher number cyclotron features. The transition to a single feature at other times in the orbit could simply be due to blurring caused by changes in the viewing angle (as demonstrated in Figure 5). Near-IR spectra would easily be able to resolve whether the lower magnetic field strength is correct.

3.42. V1309 Ori

V1309 Ori is currently the longest-period polar known, with $P_{orb} = 7.98$ hr. Staude et al. (2001) provide an ephemeris for this system, to which we have phased the *WISE* light curves. As shown in Figure 58, V1309 Ori was observed during both the four-band and three-band surveys. During the four-band epoch, the AAVSO database shows it to be in its "normal bright state" ($V \sim 16.5$), as defined by Reinsch et al. (2006). During the three-band observations, however, the AAVSO data show that V1309 Ori was in a lower state
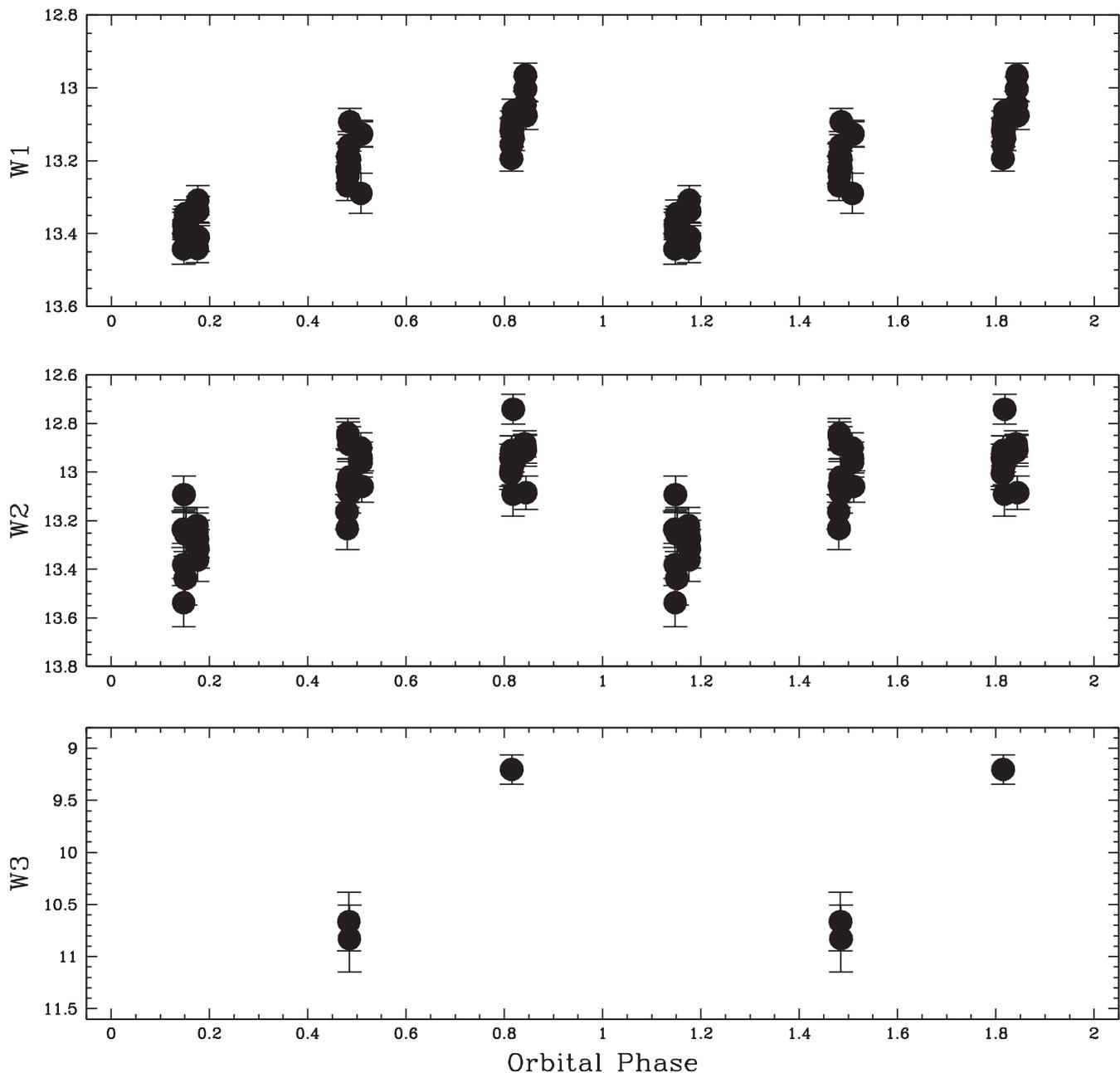
Figure 55. *WISE* data for V895 Cen phased to the ephemeris published by Stobie et al. (1996).

($V \sim 17.2$). The *WISE* light curves for both epochs appear identical. We have extracted the *JHK* light curves from Reinsch et al. and present them with the *WISE* data in Figure 58. The *JHK* data reveal a brief eclipse that also appears to be present in the *WISE* bands. At minimum light, ($W1 - W2$) = 0.0, consistent with the colors of a K7 dwarf (see Howell et al. 2010). *Spitzer* observed V1309 Ori at $\phi = 0.87$, and the *S*1 and *S*2 fluxes are nearly identical to the *W*1 and *W*2 values at that phase.

Given the parameters for the binary system listed in Staude et al., and assuming that the minimum at *W*1 is due to only the secondary star + white dwarf, we can construct ellipsoidal models for the infrared data set. The ellipsoidal models clearly demonstrate that, away from eclipse, the infrared light curves of V1309 Ori are dominated by cyclotron emission. While ellipsoidal variations influence the shape of these light curves, their effect is quite minimal. The *K*-band spectrum presented in Howell et al. (2010) was obtained at $\phi = 0.78$, not too far from the maximum in the light curve at this wavelength, yet no cyclotron features were visible. At the time of the spectroscopic observations, V1309 Ori had $K \sim 13.7$, approximately the same brightness as the ellipsoidal model at this phase. Apparently, there was no significant cyclotron emission present at the time of this spectrum. In modeling the optical/IR SED of V1309 Ori, Reinsch et al. assumed a field strength of 63 MG. Such a field cannot possibly explain their *JHK* light curves. To produce cyclotron emission in *JHK and* the *W*1 and *W*2 bands requires fields with $13 \leqslant B \leqslant 28$ MG. A field strength near 27 MG would also simultaneously explain the weak features at 5800
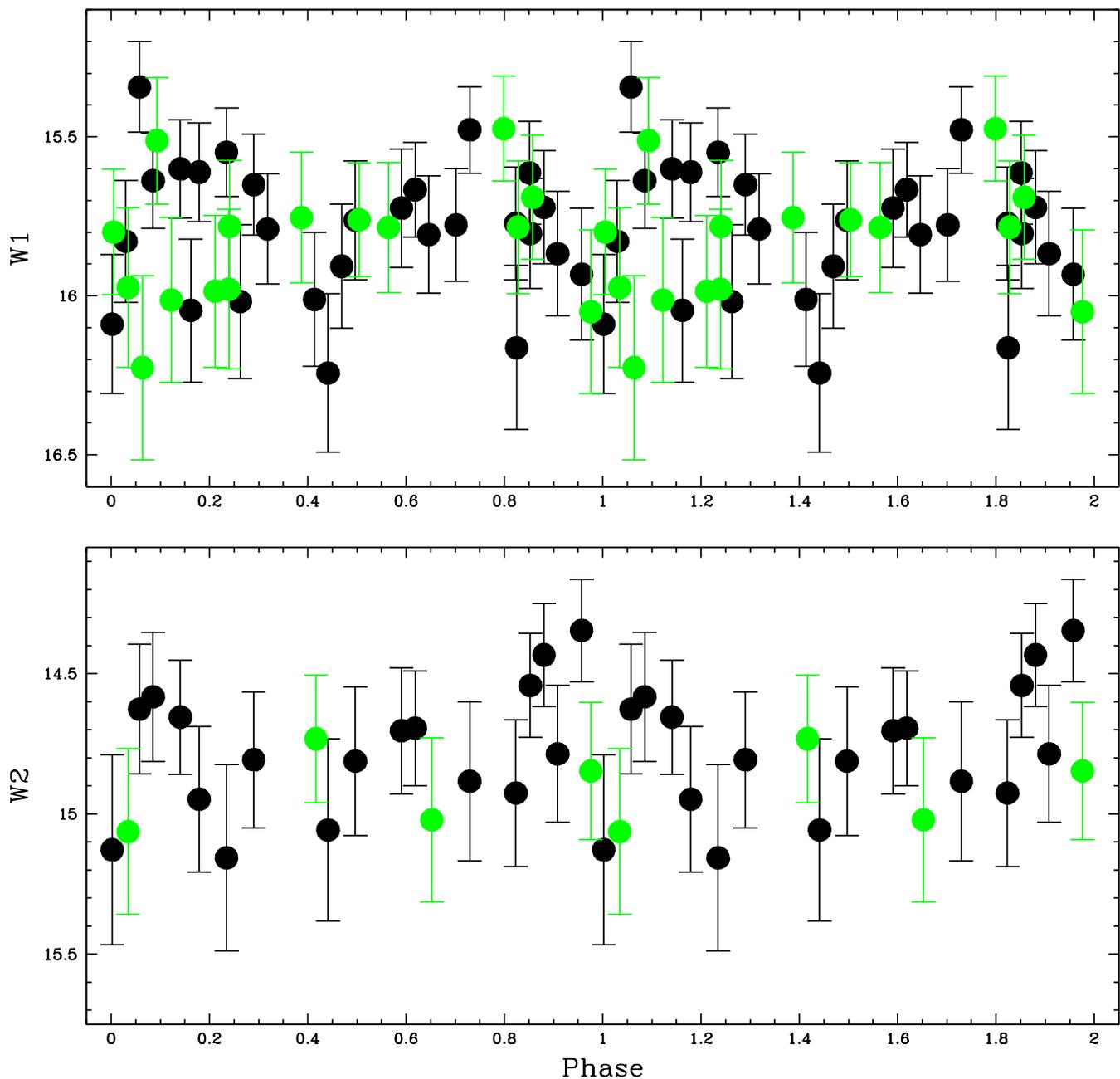
Figure 56. *WISE* four-band (black) and three-band (green) data for V1007 Her phased to the ephemeris of Greiner et al. (1998b).

and 8500 Å seen in the optical spectra obtained by Schafter et al. (1995), which have been attributed to cyclotron emission.

3.43. V1432 Aql

V1432 Aql is an asynchronous polar in which, unlike its brethren, the white dwarf is spinning more slowly than the orbital period. Patterson et al. (1995) found an eclipse period of 3.366 hr and a spin period of 3.375 hr. Andronov et al. (2006) updated these results and added a quadratic term to the spin ephemeris to account for the spin-up of the white dwarf. Andronov et al. derive a synchronization timescale of 97 years. We phased the *WISE* light curves using the orbital eclipse ephemeris of Andronov et al. and present them in Figure 59. We adjusted the *WISE* light curves by +0.133 in phase to move

the sharp minimum to $\phi = 0.0$. The *WISE* light curves show dramatic variability over an orbit, including an eclipse that is 2.5 mag deep. We obtained a full orbit of near-IR spectroscopy of V1432 Aql on 2005 September 3. We have extracted an *H*-band light curve for V1432 Aql from these data and include it as the top panel in Figure 59. We had to shift the *H*-band light curve by 0.05 in phase to place the minimum at $\phi = 0$. The resulting light curve closely resembles the *V*-band light curves presented in Patterson et al. (1995). Obviously, the same processes shaping the visual light curve are at work in the infrared.

In Figure 60, we plot the SpeX spectra phased to the Andronov et al. ephemeris, with steps of 0.05 in phase. Note that the second spectrum from the bottom in this plot corresponds to the *H*-band minimum and represents $\phi = 0$.
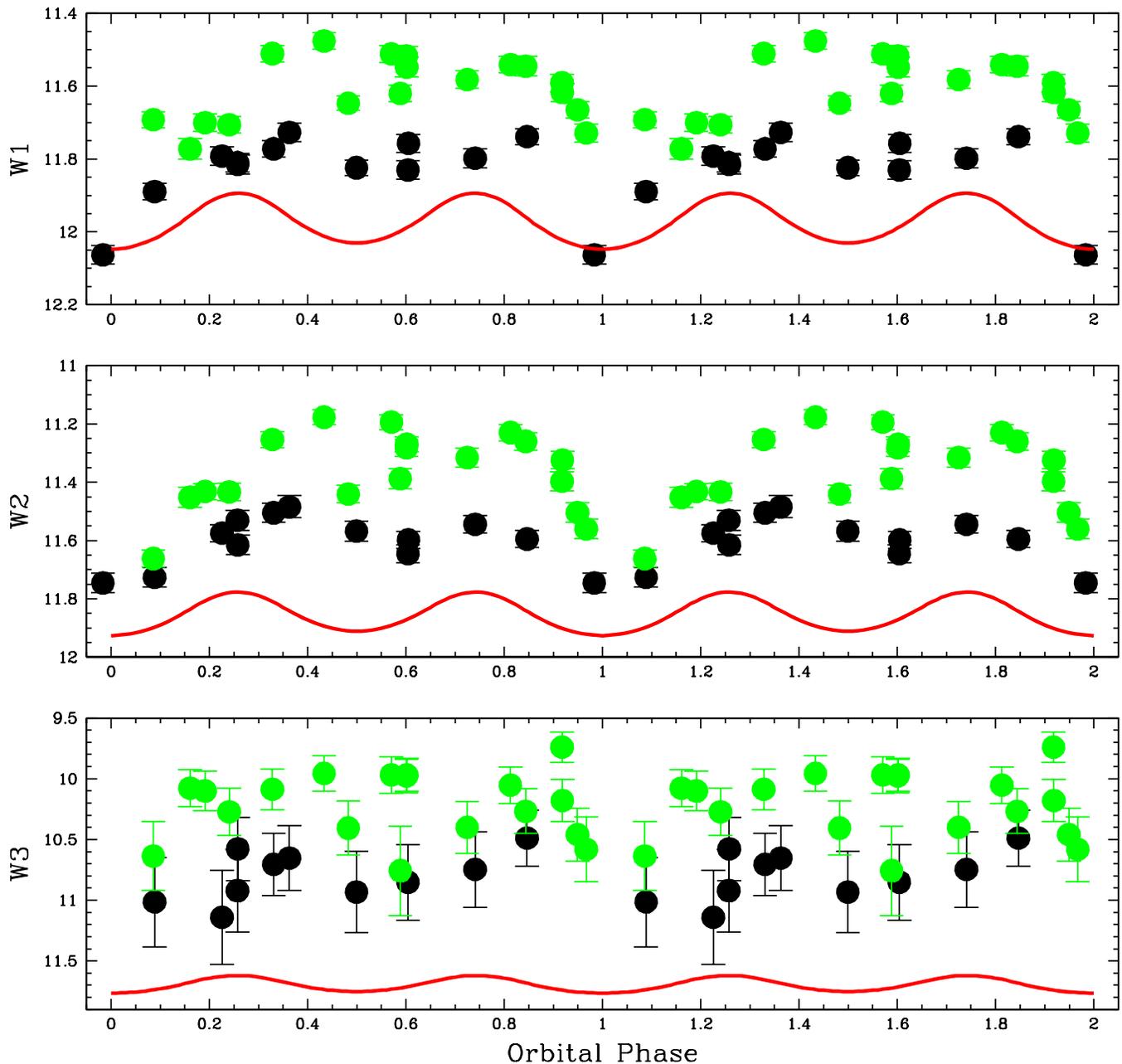
Figure 57. *WISE* observed V1043 Cen on two different epochs during the four-band survey. During the 175 days between the data sets, the system brightened. The first epoch is plotted in black, the second in green. As described in the text, we constructed ellipsoidal light curve models for V1043 Cen normalized to the minimum observed in the *W*1 bandpass.

The spectra show strong H I emission throughout and weaker He I emission. It is interesting that the line emission is actually weaker in the two spectra that immediately follow the eclipse than during the eclipse. The infrared spectra of 1432 Aql are also unusual in the strength of the He II emission at 1.16 μm and 2.19 μm. As noted for UZ For, this particular night at the IRTF was extremely dry, and the result was excellent telluric correction of the data set, as is demonstrated by the profile of H I Paα. Perhaps the most peculiar feature of these spectra is that the water vapor absorption features of the secondary star are clearly seen through most of the orbit, but are actually weakest near the eclipse and strongest near $\phi = 0.5$. Such a result makes no sense, implying that irradiation of the

secondary star by the primary somehow enhances the strength of the water vapor absorption features in the donor star.

3.44. V1500 Cyg

V1500 Cyg is believed to be an asynchronous polar of long period. The classical nova eruption that occurred in 1975 is what is believed to have knocked the system out of synchronization, and the timescale for it to again become phase locked is ~150 years (Schmidt & Stockman 1991). Because of the crowded field, V1500 Cyg was not detected by *WISE*. Harrison et al. (2013a) recently published new optical and infrared data for V1500 Cyg, modeling the light curves as being due to an irradiated secondary star (as done previously by
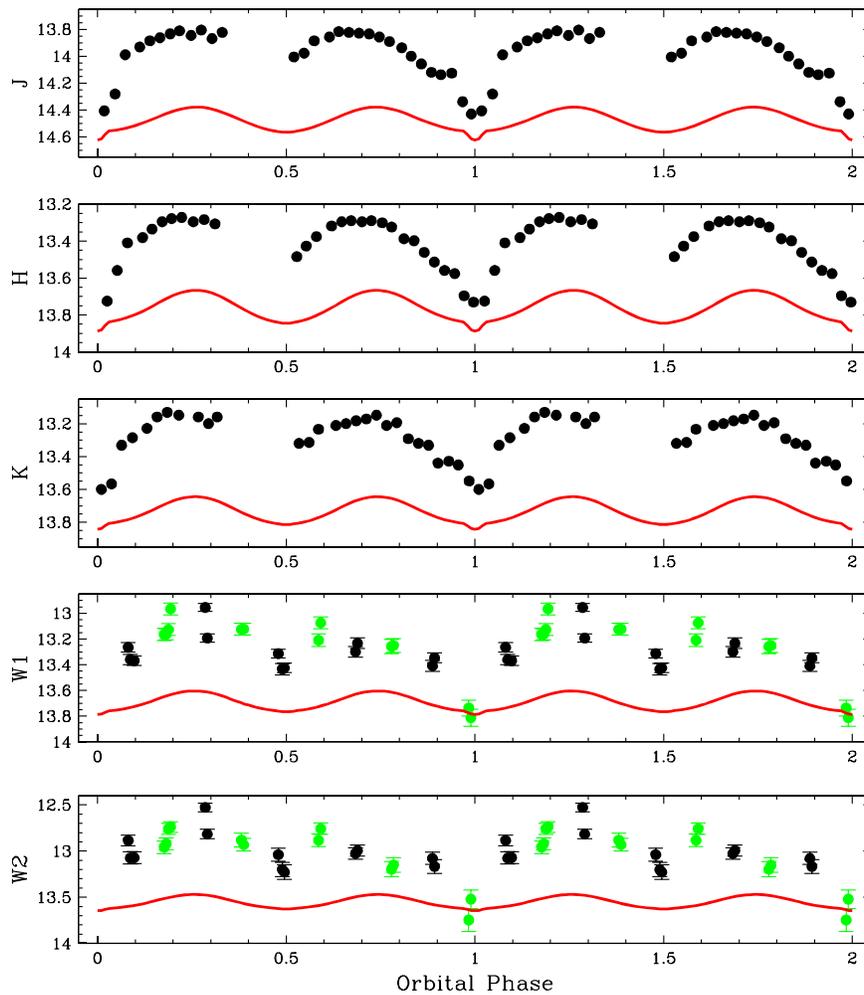
Figure 58. *WISE* four-band (black) and three-band (green) data for V1309 Ori phased to the ephemeris of Staude et al. (2001). The *JHK* light curves are from Reinsch et al. (2006). We have constructed an ellipsoidal light curve model for V1309 Ori (red) assuming that the two stellar components are the only sources responsible for flux during the *WISE* minima.

Schmidt et al. 1995). They suggested that there were asymmetries in its light curves that suggested the presence of cyclotron emission. Harrison et al. neglected to extract the *Spitzer* observations for V1500 Cyg. We do that here and list the results in Table 2. There were two epochs of data, a shallower survey data set, from which we could only extract the S1 flux density, and a pointed observation where we manually extracted the flux densities in all four IRAC bandpasses using IRAF. The last column in Table 2 lists both the predicted photometric and spin phases, respectively, calculated using the ephemerides in Schmidt et al. (1995).

Included in the *Spitzer* pointed observation of V1500 Cyg was a MIPS 24 μm image, presented in Figure 61. Given the low galactic latitude of V1500 Cyg ($b = -0°.07$), the 24 μm image is filled with patchy dust emission. Interestingly, V1500 Cyg is centered in an isolated bright patch that has an hourglass shape. Its long axis is aligned on an approximately north–south axis. The Hα image of the ejected shell of V1500 Cyg by Slavin et al. (1995) shows a clumpy shell with some emission along this axis. It is difficult to estimate the radius of this emission in the MIPS image, given that some of the brighter pixels could be unrelated field objects. A circle with a radius of 13″ encloses the majority of the feature. Slavin et al. found a mean radius of 3″ and no Hα

emission beyond 5″. The required expansion velocity was 1600 km s⁻¹, a value that is similar to expansion velocities derived by others for the bulk motion of the ejecta from this object (see Slavin et al.). The Hα images of V1500 Cyg were obtained 18 years after the outburst, whereas the MIPS observation occurred 28 years later. If the nebula seen in the MIPS image was ejected in 1975, it would require an expansion velocity of ≈3000 km s⁻¹. Helton et al. (2012) found that the [O IV] line at 25.9 μm was bright in the recent CNe they obtained *Spitzer* IRS spectra for, and such emission might explain the extended feature observed with MIPS. Helton et al. did not detect V1500 Cyg with the IRS, arriving at an upper limit of 51 mJy for the [O IV] line. Inside a five pixel radius aperture (12″.8), we find a flux of 2.31 mJy. Given that the IRS slit covered ∼25% of the nebula, the observed flux density is a factor of 10 below the upper limit derived by Helton et al.

3.45. V2301 Oph

V2301 Oph is an eclipsing short-period polar that appears to have a very low field strength. Ramsay & Cropper (2007) have published a quadratic ephemeris for this system, though the nonlinear term is very small. We have phased the *WISE* four-band and three-band data to this ephemeris.
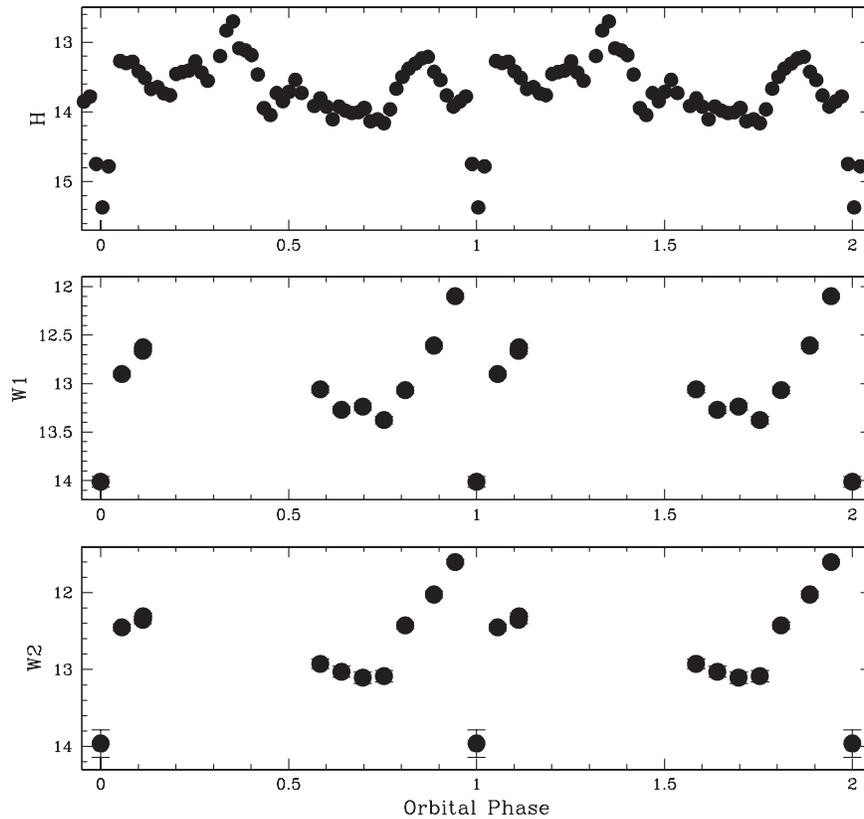
Figure 59. The *WISE* data for V1432 Aql phased to the ephemeris of Andronov et al. (2006). We have had to add +0.133 in phase to place the deep minimum at phase zero. In the top panel is an *H*-band light curve obtained from the spectra plotted in Figure 60. We added +0.05 in phase to this light curve in order to get the minimum to fall at $\phi = 0.0$.

The *WISE* light curves, presented in Figure 62, appear to have a number of deviant flux points, but a comparison of these data to that of a nearby star shows nothing unusual, suggesting that the discrepant points are real. Thus, V2301 Oph shows a remarkable level of interorbit variability of $\Delta m \sim 1$ mag in all three bandpasses. The AAVSO database indicates that V2301 Oph had $V \sim 16$ during both epochs of *WISE* observations, suggesting a high state. The extreme depth of the eclipse in the *WISE* light curves, the largest of any polar, also argues for a high state. The *W*3 light curve is quite complex, appearing to having on and off modes between orbits. In the bottom panel of Figure 62, we plot the *W*3 light curve with respect to MJD. When this is done, the light curve appears to show flaring activity, not unlike that seen for Z Cam (see Harrison 2014). In Z Cam, the *W*3 band variations were ascribed to synchrotron emission. The SDSS survey appears to have caught this object in a low state, given that those data were obtained near light curve maxima ($\phi_{SDSS} = 0.45$). An analysis of the Zeeman splitting of photospheric absorption lines led Ferrario et al. (1995) to suggest a mean field strength near 7 MG. The $n = 1$ harmonic from such a field would be located near the red edge of the *W*3 bandpass, while the $n = 3$–5 harmonics would be within the *W*1 and *W*2 bands. A field of 7 MG is consistent with both the red mean color ($\langle W1 \rangle - \langle W3 \rangle = 1.68$) and the *W*1 and *W*2 light curves being dominated by optically thick cyclotron emission. V2301 Oph has a *W*4 detection in the AllWISE catalog, but none of the four-band single exposure data points had S/N > 3.

3.46. WW Hor

WW Hor has an orbital period that puts it just below the CV period gap. Bailey et al. (1988) derived an ephemeris for this system, to which we phased the *WISE* data. We have extracted the *J*-band data from Bailey et al. and present it with the *W*1 and *W*2 light curves in Figure 63. Bailey et al. found that the colors during the eclipse were consistent with a late-type star (~M3). This is not true for the *WISE* data, suggesting that the deepest portion of the light curve minimum may have been missed. WW Hor shows 1.5 mag variations in the *J* band outside the eclipse, similar to what is seen in *W*1. The *W*1 band also appears to show a secondary minimum at $\phi = 0.5$ that is not seen in the *J* band. Perhaps this feature is due to a high viewing angle to the accretion region, which would diminish the emission from the fundamental cyclotron harmonic. There appears to be less variation in the *W*2 bandpass, though the gap in the light curve at $\phi = 0.5$ indicates that a minimum occurred at this time. Bailey et al. suggest a field strength of 25 MG, but the *WISE* light curves indicate that this is too low and that a slightly higher field strength is more realistic, being necessary to have cyclotron emission in both the *W*1 and *W*2 bands (the $n = 1$ harmonic is centered in the *W*2 band for $B = 25$ MG). We do not know whether WW Hor was in a high or a low state during the *WISE* observations, but the 2MASS *J*-band datum is identical to the photometry published by Bailey et al. at this phase ($\phi = 0.23$) and leads to ($K_{2MASS} - W1$) = 0.0. This suggests that at the epoch of the *WISE* observations, WW Hor was in a state similar to that seen when the *J*-band light curve was obtained.
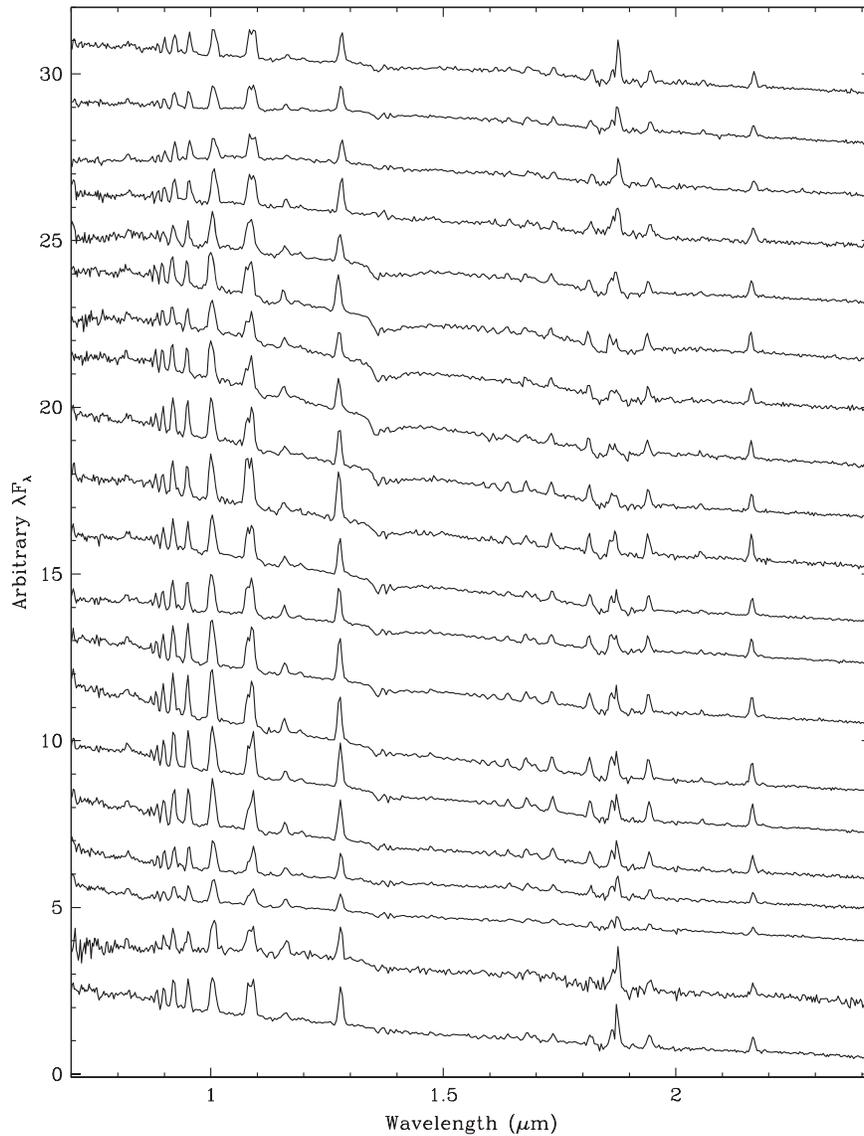
Figure 60. Near-IR spectra for V1432 Aql obtained with SpeX on the IRTF. These spectra have been phased using the ephemeris of Andronov et al. (2006), with the $\phi = 0$ spectrum at the bottom, with the phase incremented by +0.05 vertically. The $\phi = 0.05$ spectrum corresponds to the time of the eclipse, and we believe it was obtained closest to true phase zero.

3.47. WX LMi

WX LMi has been classified as a "prepolar," a system with a very low mass transfer rate, a cool white dwarf, and a secondary star that might not fill its Roche lobe (see Schmidt et al. 2005c). Vogel et al. (2007) obtained optical spectroscopy of the system and derived a binary orbital ephemeris. They also were able to accurately constrain the magnetic field strength of the two poles: 61.4 and 69.6 MG. The *WISE* light curves, phased to the Vogel et al. ephemeris, are shown in Figure 64. The *W*1 and *W*2 bandpasses appear to be dominated by ellipsoidal variations. Using the limits on the binary system derived by Vogel et al., we can model these data. Fixing the temperatures of the two components ($T_1 = 8000$ K, $T_2 = 3100$ K), we find $i = 53°$. This constrains the mass ratio (see Figure 3 in Vogel et al.) to be $q = 0.35$, leading to $M_1 = 0.70$ and $M_2 = 0.24$. The derived secondary star mass is consistent with the mass of a main sequence M4.5V. The final ellipsoidal model is plotted in red in Figure 64. The inclination we find is lower than reported elsewhere, suggesting the possibility of a

third light component that would act to dilute the amplitude of the variations seen in *W*1 and *W*2, causing us to underestimate the orbital inclination.

BVRI photometry of WX LMi was obtained with the NMSU 1 m telescope on 2009 April 29 and has been previously presented in Linnell et al. (2010), where it was combined with *GALEX* data. In their light curve models, Linnell et al. included two hot spots on the white dwarf that partially explained the combined UV and visual data sets. Using the parameters derived from modeling the *WISE* data, we can propagate the ellipsoidal models into the visual and re-model the *BVRI* data set. The result is presented in Figure 65 and highlights the strong cyclotron emission present in these bandpasses. The cyclotron emission is weakest in the *I* band, where the maximum is due to emission from the $n = 2$ harmonic from the 69.6 MG field. In our lower-inclination ellipsoidal light curve model, the secondary maximum (at $\phi = 0.78$) exceeds the predicted variation, suggesting weak cyclotron emission from the 61.4 MG pole, presumably from the tail of the $n = 3$
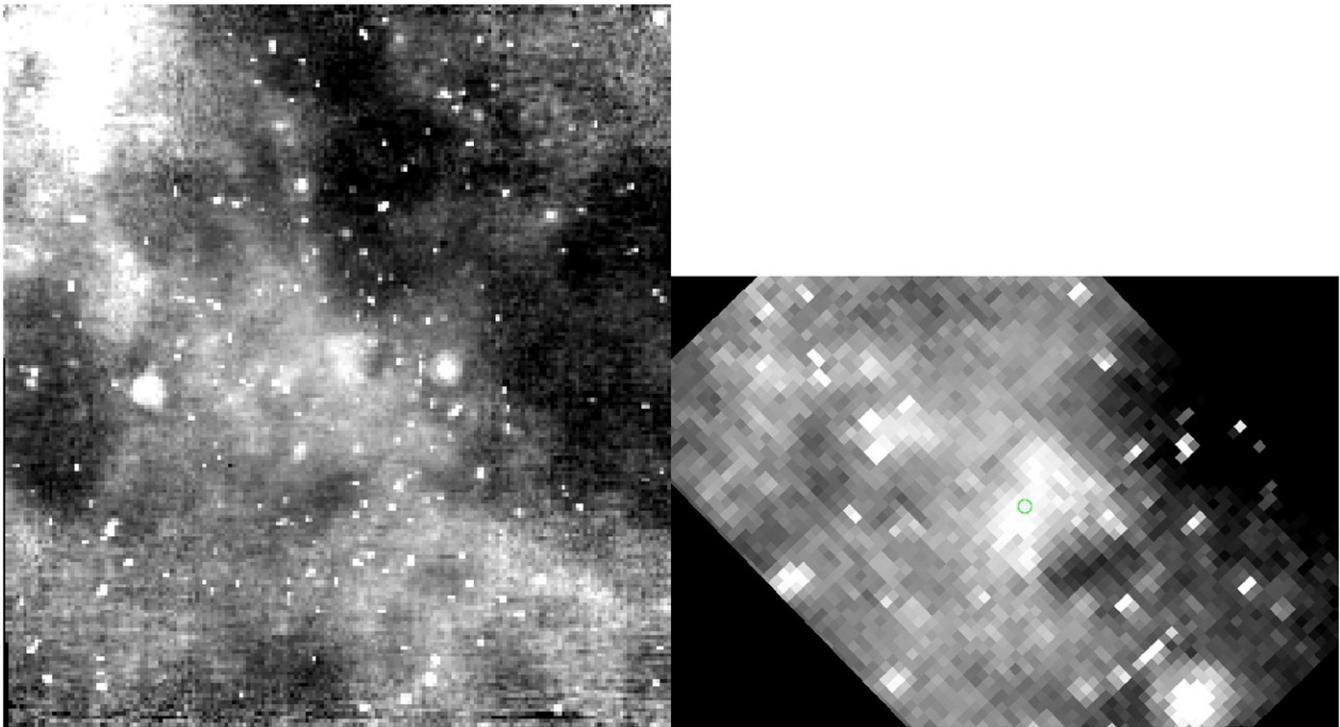
Figure 61. Left: the MIPS 24 μm image of the field of V1500 Cyg, showing the patchy dust. The image is $5\rlap{.}'4 \times 5\rlap{.}'4$ in size. V1500 Cyg is located at the center of the image, where there appears to be an hourglass-shaped emission feature. Right: a close-up of the region centered on V1500 Cyg, rotated so that north is up and east is to the left. The green circle is plotted at the astrometric position of V1500 Cyg.

harmonic that causes the strongest maximum in the R band. But the tail of the $n = 3$ harmonic from the 69.6 MG field causes the smaller R-band maxima centered near $\phi = 0.25$. The V band is dominated by cyclotron emission at all phases, due to the presence of the $n = 3$ harmonics from both fields. This also appears to be true for the B band, containing the $n = 4$ harmonic emission from both fields, because the deepest minimum at this wavelength has nearly the same phasing as those seen in the other bandpasses. *Small* hot spot emission cannot explain the nearly flat light curve in the B band. Linnell et al. employed very large hot spots located in the same hemisphere so as to reproduce the *GALEX* light curves. Such spots could help explain the nearly featureless B-band light curve.

Because prepolars are not expected to exhibit high states, we can use the infrared colors to both examine the issue of third light contamination and constrain the distance to WX LMi. The mean *WISE* color is $(\langle W1 \rangle - \langle W2 \rangle) = 0.20$, consistent with an M4/5V. The 2MASS data were obtained at superior conjunction and thus might be slightly contaminated by irradiation. At this phase, $(K–W1) = 0.17$, essentially identical to that of an M4V. It does not appear that there is a third light term that strongly affects the *WISE* fluxes, confirming the lower inclination that we find from the ellipsoidal modeling. From the infrared photometry we estimate $d = 102$ pc, consistent with the value found by Vogel et al.

3.48. HS0922+1333 (= Leo)

Vogel et al. (201) give a spectroscopic ephemeris for this long-period prepolar, and we have phased the *WISE* data to their result. Reimers & Hagen (2000) propose a two-pole system with field strengths of 66 and 81 MG. These field strengths would rule out cyclotron emission beyond the H band. The secondary star is prominent in optical spectroscopy, and the white dwarf is cool. The *WISE* light curves (not shown) reveal limited variability with minima near $\phi = 0$, consistent with ellipsoidal variations. HS0922+1333 was weakly detected in the W3 band, and the resultant $(W1 – W3) = 0.56$ color is consistent with an M3 spectral type to within the error bars of the data set.

3.49. RBS 490 (= Eri)

As its name suggests, RBS 490 was discovered in the *ROSAT* Bright Survey (Schwope et al. 2002). It had the hardest X-ray spectrum of the CVs discussed in Schwope et al., and they modeled it as thermal bremsstrahlung with $kT = 20$ keV. If RBS 490 is a polar, it would have the shortest orbital period known: $P_{\rm orb} = 46$ minutes. This unusual period was derived from a radial velocity study by Thorstensen et al. (2006), who also provide an ephemeris for this system. *WISE* observed RBS 490 during both the four-band and three-band surveys, with 190 days between epochs. Phasing the light curve data to the Thorstensen et al. ephemeris produces the result shown in Figure 66. The phase coverage is incomplete because the orbital period is roughly half that of *WISE*. However, it is clear that the three-band and four-band light curves are very similar, both showing large scale variations in the $W1$ and $W2$ bandpasses. We have already encountered the "M-like" light curve shape displayed by RBS 490 several times above. While the evidence for a polar from the X-ray and optical data sets is not especially strong, the large amplitude of the variations, and the repeatability of the mid-infrared light curve data on two widely separated epochs, strongly suggest cyclotron emission. Among the many
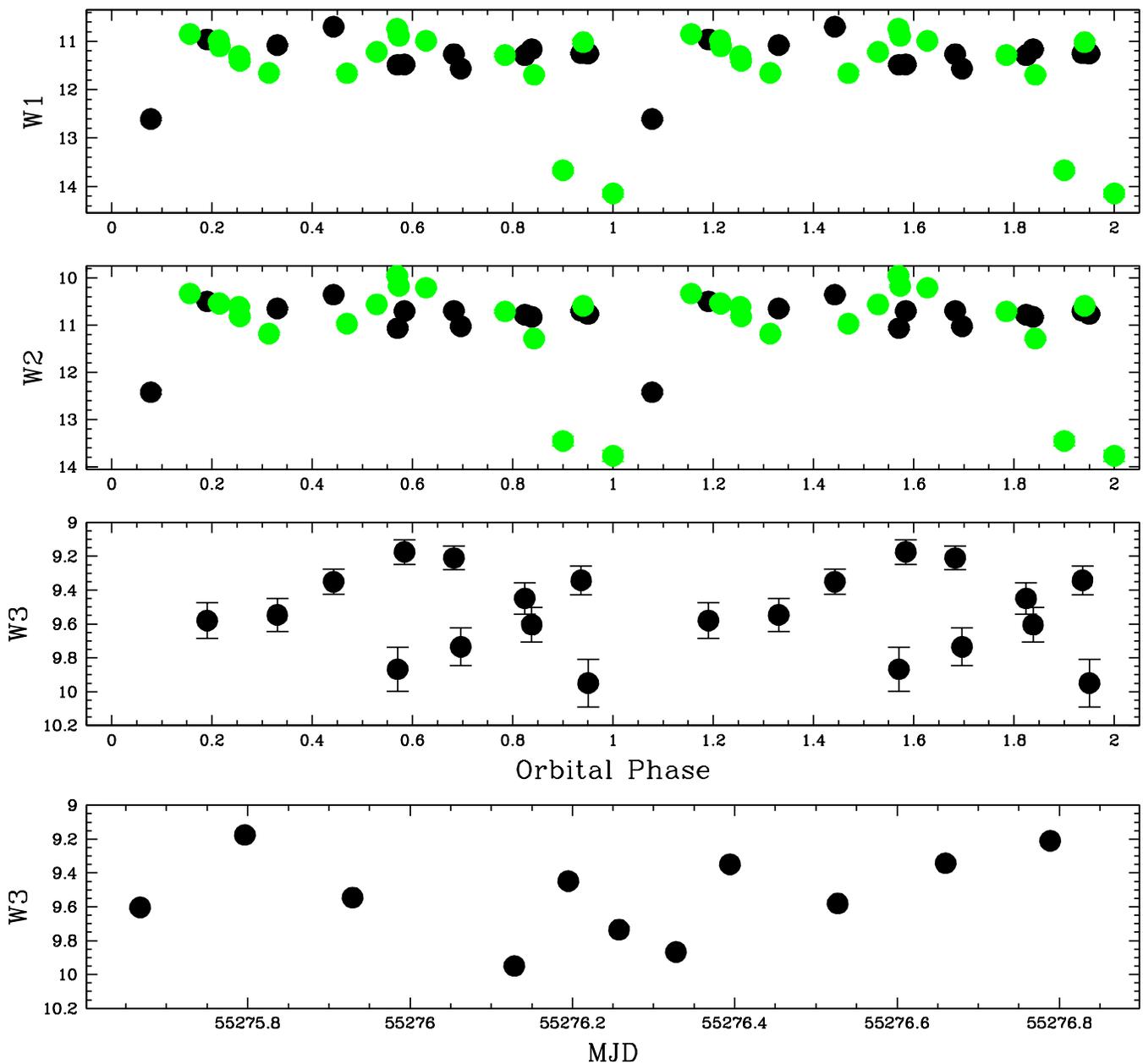
Figure 62. *WISE* light curves for V2301 Oph phased to the ephemeris by Ramsay & Cropper (2007). The four-band survey data are plotted in black, the B-band data in green. In the bottom panel, we present the *W*3 light curve plotted versus MJD.

peculiarities of this system is its detection in the *W*3 band. The *W*3 light curve is inadequate to determine if it has the same morphology as that seen in the shorter wavelength bandpasses. With $(\langle W1 \rangle - \langle W3 \rangle) = 3.93$, the system would be the "reddest" polar.

RBS 490 is a very faint source in the 2MASS database and was not detected in the *K* band. We obtained new *JHK* observations of RBS 490 on the APO 3.5 m telescope on 2014 October 30. While the predicted phases of the 2MASS and APO observations were very similar, the large epoch difference, combined with the low precision of the ephemeris, suggests that in reality these phases are unconstrained. The *J*- and *H*-band photometry for both epochs is, however, identical to within the error bars. The $(J-H)$ color is blue, but the $(H-K)$ color is very red. When combined with the *WISE*

results, this suggests that, like V379 Vir, the white dwarf in RBS 490 has a very low magnetic field strength.

While none of the photometry for this system is simultaneous, it does not appear that RBS 490 undergoes large changes in brightness. Thorstensen et al. present *UBVI* data for RBS 490 on two different epochs, and with that and the *JHK*, *GALEX*, and *WISE* data sets, we can construct its SED. The line-of-sight extinction[12] at the position of RBS 490 is very low, $A_V \sim 0.1$ mag, but sufficient to warrant correcting the *GALEX* fluxes. The resulting SED, shown in Figure 67, is unusual, showing a steeper decline in the near-IR than if it were dominated by a cool M-type donor star. In fact, to model this SED required the sum of two relatively hot blackbodies:

---

[12] http://irsa.ipac.caltech.edu/applications/DUST/
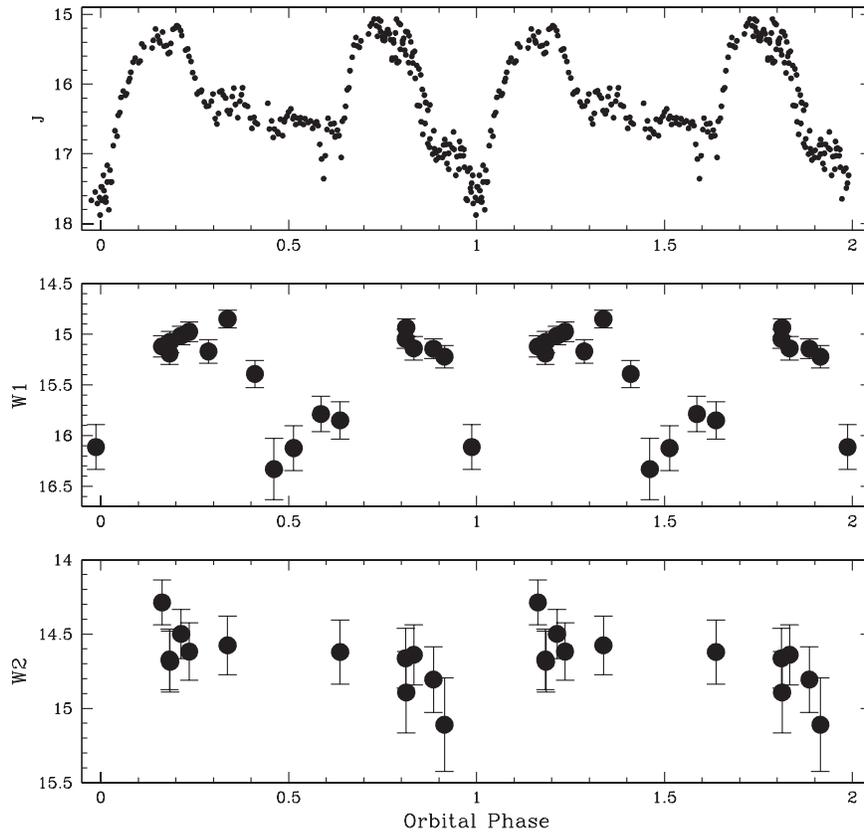
Figure 63. *J*-band light curve of WW Hor (top) from Bailey et al. (1988) compared to the *WISE* data, using their ephemeris.

$T_1 = 25{,}000$ K, and $T_2 = 5200$ K. We cannot get a cooler secondary star to reproduce the observations. This situation is reminiscent of EI Psc, a nonmagnetic CV with an orbital period of 64 minutes, also below the theoretical CV period limit for main sequence objects of normal composition (see Thorstensen et al. 2002, and references therein). The secondary star in EI Psc has a spectral type of mid-*K* and even reveals normal ellipsoidal variations consistent with this spectral type (Harrison et al. 2009). Thorstensen et al. (2002) suggest that the donor star in EI Psc may be hydrogen deficient, and such objects might be able to evolve to very short periods while maintaining higher photospheric temperatures (see Baraffe & Kolb 2000). The lack of CO features in its *K*-band spectrum is consistent with this interpretation.

Starting at *K*, there is a considerable, long wavelength excess. As we showed above, the *W*1 and *W*2 bands exhibit >1 mag variations over an orbit, and they repeat on two widely separated epochs. These are almost certainly due to cyclotron emission. Whether *W*3 is from cyclotron emission, or from the mechanism that creates the large *W*3 band excesses in the other polars, is unknown. For demonstration purposes, we have added a CL model cyclotron spectrum with $B = 11.5$ MG ($\log \Lambda = -0.5$, $\Theta = 80°$, and $kT = 20$ keV) to the two-blackbody model. Until we have fully phase-resolved light curves in the near- and mid-IR, it will be difficult to properly constrain the SED of RBS 490.

3.50. RXJ0502.8+1624 (= Tau 4)

RXJ0502.8+1624 is a suspected polar of unknown orbital period. Howell et al. (2008) present a series of *K*-band spectra that covered 87 minutes, but the very obvious stream eclipse

they saw did not repeat. No features from the secondary star were seen, suggesting a short-period system. The *WISE* observations spanned one full day, opening the possibility of determining the orbital period. We searched for periods with $P_{\rm orb} \leqslant 24$ hr, and only those near 1.5 and 3 hr produce symmetric light curves. We plot the *WISE* data phased to the 90-minute period in Figure 68. The variations in the *WISE* data are small, suggesting either a lack of cyclotron emission at this time or a field strength above 35 MG. Howell et al. did see evidence for two cyclotron humps in their *K*-band spectra, but they were not well enough defined to enable a rough estimate for the field strength. Howell et al. suggest that RXJ0502.8 +1624 might have been in a high state at the time of their observations as the spectra had $K \sim 13.7$, compared to the 2MASS value: $K = 14.66$. This suggestion is confirmed because the All Sky Automated Survey (ASAS)[13] observations (tabulated for this source here: http://ooruri.kusastro.kyoto-u. ac.jp/mailarchive/vsnet-recent-ip/5926) show it having $V = 13.91$ at the epoch of the *Keck* spectra, while it was at $V \sim 14.5$, or fainter, on many other occasions. The color derived from the mean *WISE* magnitude and the *K*-band value reported by Howell et al. is $(K–W1) = -0.19$, which suggests that RXJ0502.8+1624 was probably in a lower state when observed by *WISE*.

3.51. RXJ0649.8–0737 (= Mon)

Motch et al. (1998) suggest that RXJ0649.8–0737 is a polar with a period of 4.4 hr. This period phases the *WISE* light curves quite nicely, with the *W*1 light curve roughly consistent

---

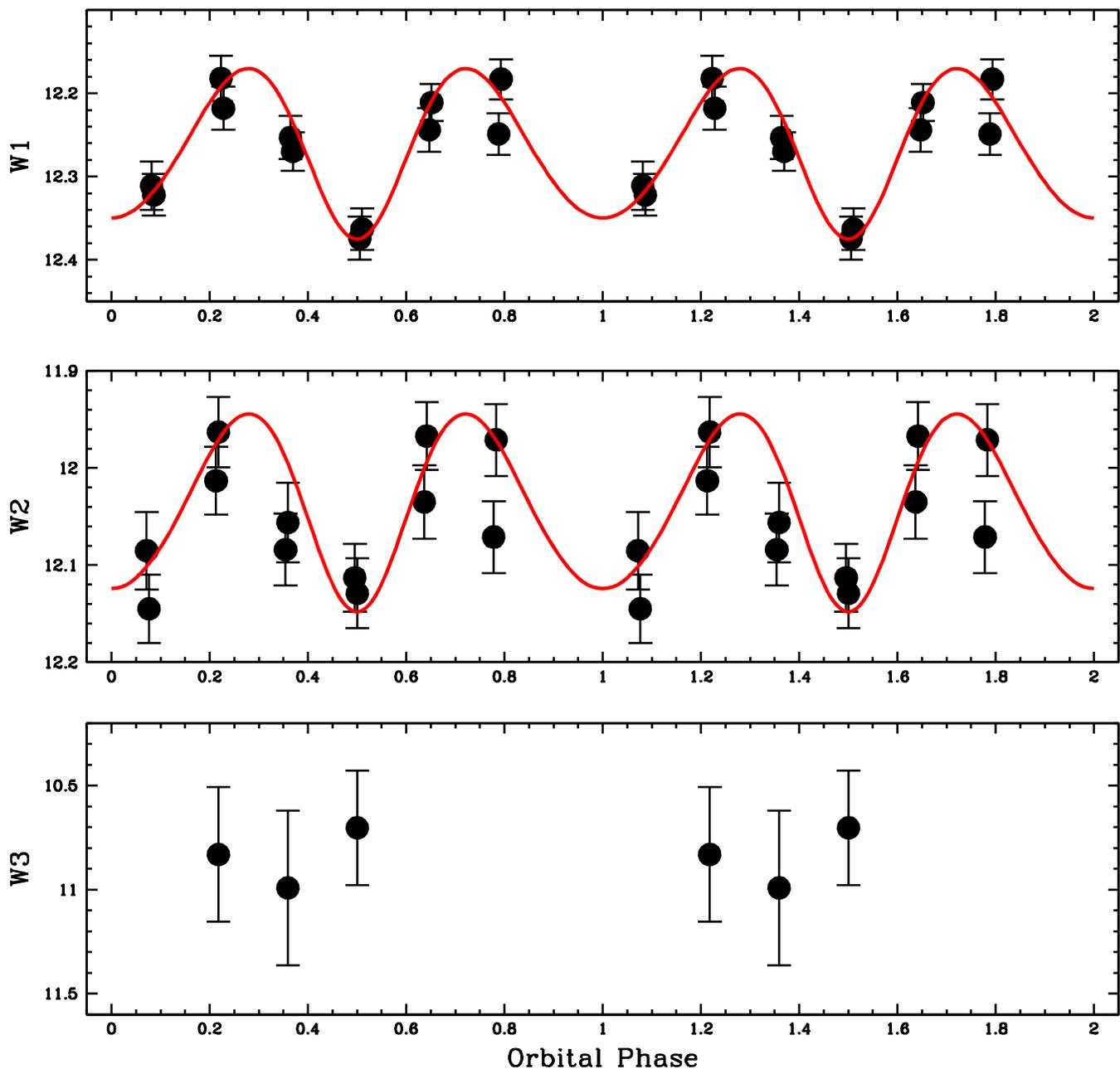[13] http://www.astrouw.edu.pl/asas/

Figure 64. *WISE* light curves of WX LMi phased to the ephemeris in Vogel et al. (2007). An ellipsoidal light curve model is plotted in red.

with ellipsoidal variations (see Figure 69). The *W2* light curve, however, appears to show a deeper, shorter-lived minimum than in *W1*. This light curve is more consistent with strong cyclotron emission in this bandpass, suggesting a field strength of $B \leqslant 26$ MG. The 2MASS and UKIDSS *K* magnitudes are identical and give $(K - \langle W1 \rangle) = -0.03$, suggesting that RXJ0649.8−0737 was in a similar state on all three epochs. The DENIS survey has the source at a similar level in the *J* band as the other two near-IR surveys. The near-IR colors are consistent with an early M-type star that might be expected at the proposed orbital period of this system.

3.52. RXJ0859.1+0537 (= Hya)

RXJ0859.1+0537 was identified as a polar by Beuermann et al. (1999). Szkody et al. (2005) list the period as 1.1 hr, and

this phases the *WISE W1* light curve reasonably well (not plotted). The source is not variable in *W2*, but shows a single bright phase ($\Delta W1 = 0.4$ mag) once per orbit in *W1*. If this is cyclotron emission, than the field strength is either $\geqslant 35$ MG or $\leqslant 20$ MG. The UKIDSS data for two widely separated epochs show an object with identical *JHK* colors, and these are similar to what was found by 2MASS. The lack of variability in the near-IR suggests lower field strengths. The two epochs of SDSS data show substantial differences in brightness.

3.53. RXJ0953.1+1458 (= Leo)

Beuermann & Burwitz (1995) give the period of this system as 102 minutes, and phasing the *WISE* data to this period (not plotted) reveals a single maximum and minimum per orbit with an amplitude of $\Delta W1 = 0.5$ mag. While the 2MASS colors are
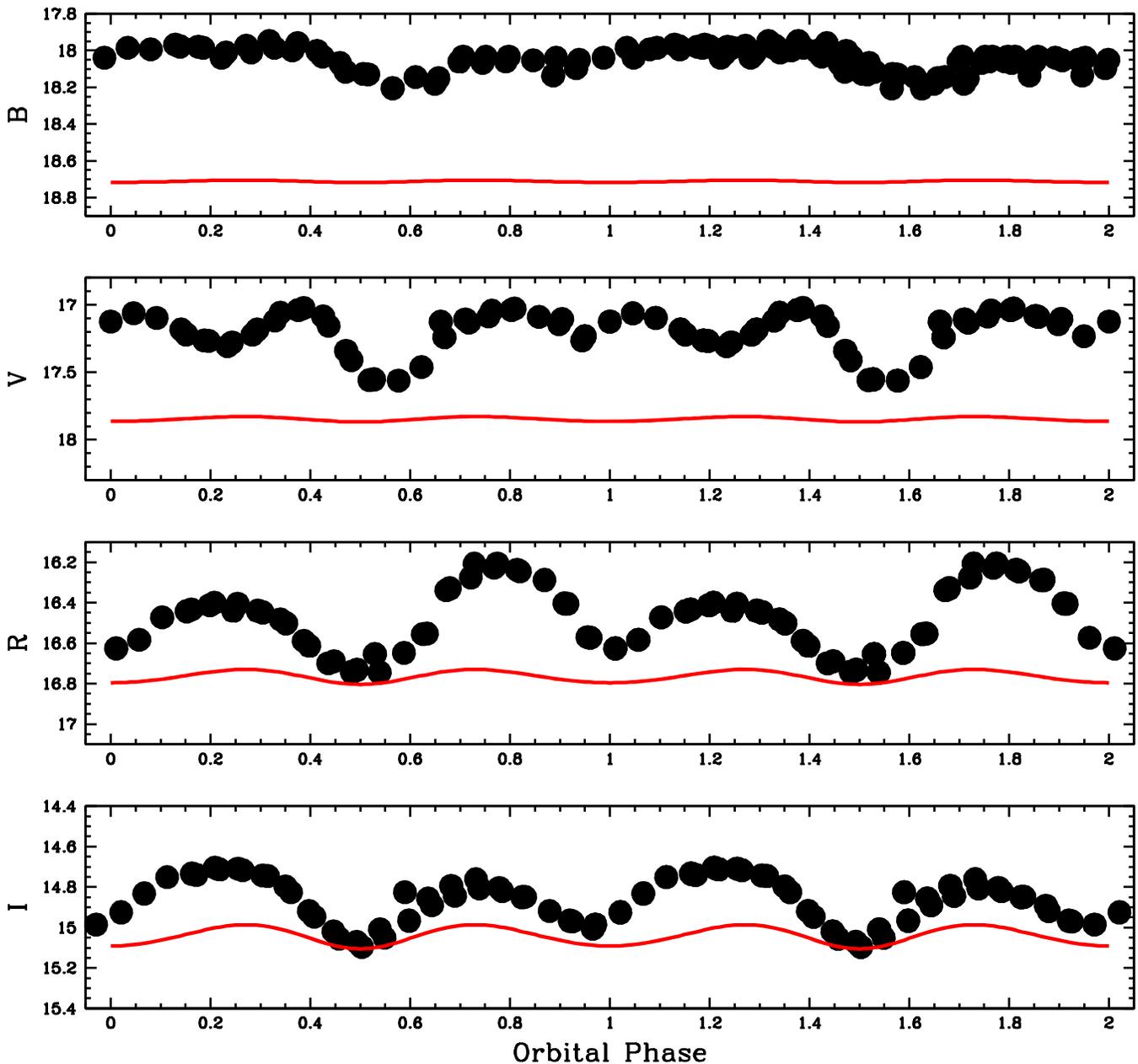
Figure 65. *BVRI* light curves of WX LMi from Linnell et al. (2010), with the same ellipsoidal light curve model as in Figure 64, propagated to these bandpasses (in red).

consistent with a mid-M-type star, the mean *WISE* colors are much too red, suggesting the possibility of cyclotron emission from a field with $B \leqslant 30$ MG.

3.54. RXJ1002–1925 (= Hya)

Beuermann & Burwitz (1995) find an orbital period of 107 minutes for RXJ1002–1925, and Ramsay & Cropper (2003) present X-ray and UV light curves that show a single bright phase once per orbit. The *WISE* light curves (not shown) have low S/N for this source, but they also exhibit a single bright phase once per orbit in both bandpasses, with similar amplitudes ($\Delta W1 \approx \Delta W2 \approx 0.8$ mag). Thus, the source resembles AI Tri and suggests a field strength of $B \sim 32$ MG. RXJ1002–1925 was not listed in the 2MASS PSC, though we were able to extract a K magnitude from the 2MASS images and

list it in Table 4. The *WISE* color is large: $(\langle W1 \rangle - \langle W2 \rangle) = 0.59 \pm 0.14$, also suggestive of cyclotron emission.

3.55. RXJ1007.5–2017 (= Hya)

Thomas et al. (2012) present an ephemeris for this long-period polar derived from *I*-band photometry, and we phased the *WISE* data to this result. The cyclotron harmonics seen in the spectra of RXJ1007.5–2017 led Thomas et al. to estimate $B = 94$ MG. Thus, this object should not have cyclotron emission in the infrared beyond the *J* band. The *WISE* light curves show limited variability, but they do exhibit considerable orbit-to-orbit changes. These variations do not resemble the *I*-band data in Thomas et al. This source is not especially faint in the mid-IR, so the lack of obvious ellipsoidal variations in the *WISE* data is curious. The mean *WISE* color is quite red:
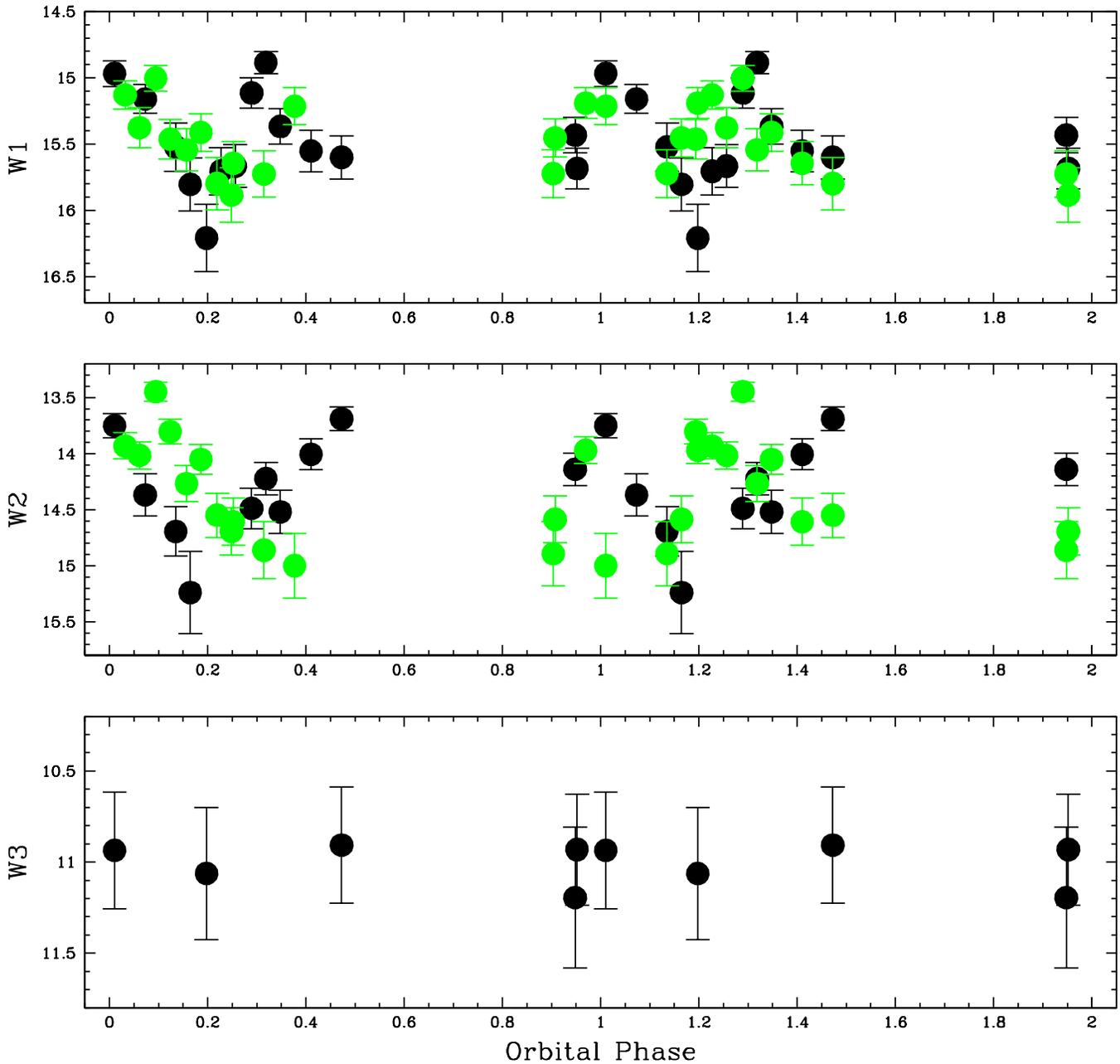
Figure 66. *WISE* four-band (black) and three-band (green) light curves of RBS 490 phased to the ephemeris of Thorstensen et al. (2006). The precision of the ephemeris, combined with the ultrashort orbital period of this system (46 minutes), means that the actual phasing is unconstrained.

$(\langle W1 \rangle - \langle W2 \rangle) = 0.53 \pm 0.07$, though $(K_{2MASS} - \langle W1 \rangle) = 0.07 \pm 0.14$ is consistent with the M3 donor star spectral type found by Thomas et al.

3.56. RXJ2316–0527 (= Aqr 5)

Rodrigues et al. (2006) have used optical and infrared photometry to establish an ephemeris for RXJ2316–0527 where $\phi = 0$ is the time of minimum light. We phased the *WISE* data to this ephemeris, but even though the source is not very faint in the mid-IR, the resulting light curves do not resemble those at shorter wavelengths. The *W1* light curve is essentially nonvariable, whereas the *W2* light curve is complex and has a total amplitude of $\Delta W2 = 1$ mag. Rodrigues et al. found that RXJ2316–0527 had significant

circular polarization that did not change sign over an orbit. They derived a field strength for this source of $20 \leqslant B \leqslant 30$ MG. Such fields would certainly have cyclotron emission in the *WISE* bandpasses, and such emission could create the *W2* light curve. The *RIH* light curves of RXJ2316–0527 are very similar to those seen in V1500 Cyg and suggest a highly irradiated secondary star. Indeed, Rodrigues et al. were able to find suitable models for the observed light curves with a hot white dwarf ($T_1 = 55{,}000$ K) heating a cool secondary star ($T_2 = 3300$ K), a result that is almost identical to that found for V1500 Cyg by Harrison et al. (2013a). The 2MASS *H*-band measurement ($\phi = 0.33$, near maximum light) is consistent with the *H*-band light curve in Rodrigues et al., suggesting a similar state. The DENIS survey ($\phi = 0.58$, also during the light curve maximum) appears
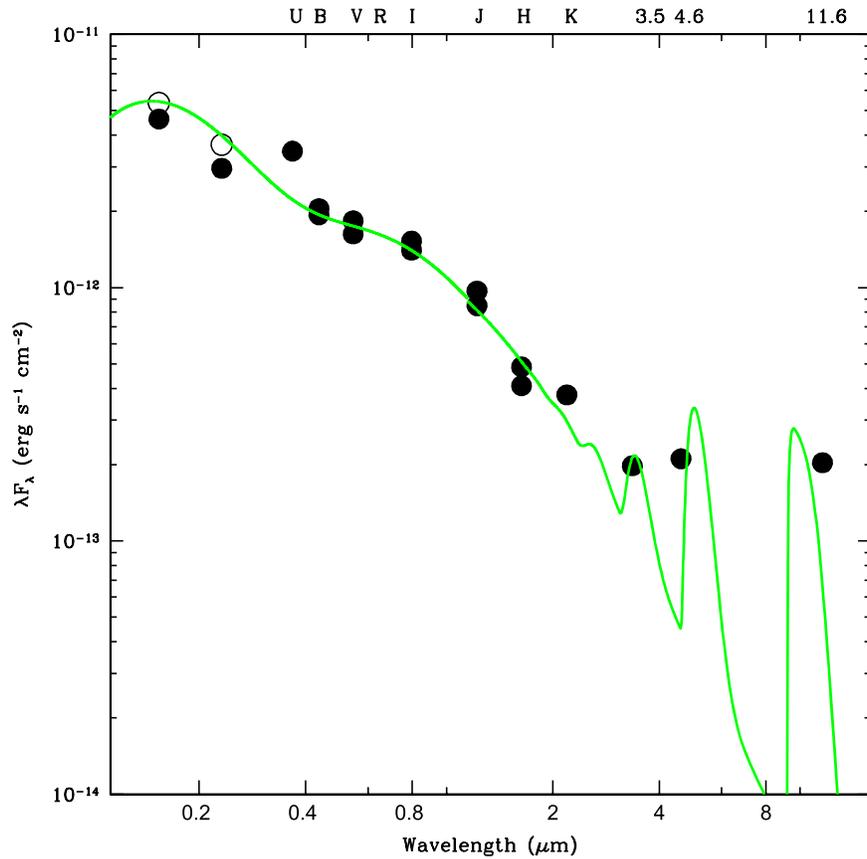
Figure 67. Spectral energy distribution of RBS 490. We have dereddened the *GALEX* data by $A_V = 0.1$ (open circles), but we ignored this small amount of reddening at all other wavelengths. The *UBVI* data on two different epochs are from Thorstensen et al. (2006). The *JHK* data are from 2MASS and our own recent observations of this system. We also plot the mean *WISE* data from Table 1. We have fit the SED with the sum of two blackbodies ($T_1 = 25{,}000$ K, $T_2 = 5{,}200$ K) and a constant-Λ cyclotron model for $B = 11.5$ MG (green). See Figure 1 for the *WISE* bandpass transmission curves.

to have caught it in a different state, where it was 0.3 mag brighter in *J* and 1.0 mag brighter in *K*! It is unclear what state the system was in during the *WISE* observations. The colors are peculiar with $(K_{2MASS} - W1)_{\phi=0.33} = -0.36 \pm 0.12$, while $(\langle W1 \rangle - \langle W2 \rangle) = 0.40 \pm 0.07$. The latter is too red to be due to a cool secondary star. A simple explanation is that there is cyclotron emission in the *K* and *W2* bands and not in *W1*. This implies a field strength near 25 MG, within the range proposed by Rodrigues et al.

3.57. 1RXSJ060033.1–270918 (= Lep)

This object is listed as an AM Her in Downes et al. (2001), and the Ritter & Kolb (2003) catalog lists the orbital period as 0.0757 days. 1RXSJ060033.1–270918 was observed during both the four-band and three-band surveys. Phasing the data to the Ritter & Kolb period results in the light curve shown in Figure 70. The source seems to show a single brightening once per orbit of modest amplitude ($\Delta W1 \sim 0.3$ mag) in *W1*, and no variation in *W2*. The four- and three-band data phase-up well, so the orbital period appears to be correct. If the bright phase is associated with cyclotron emission, the field strength is $B \leqslant 38$ MG.

3.58. 2QZ J142256.3–022108 (= Vir)

2QZ J142256.3–022108 was confirmed as a polar by Marsh et al. (2002), who quote a period of 3.37 hr with the possibility

of one-day aliases. Hilton et al. (2009) find a period of 4 hr. Phasing the *WISE* data to the 4 hr period results in a cleaner light curve (not shown) than at the shorter period. The *W1* light curve shows a short-lived 0.5 mag brightening once per orbit. The source was only detected twice in the *W2* bandpass in the single-exposure database. The amplitude of the *W1* variation suggests cyclotron emission and field strengths of $B \leqslant 38$ MG.

3.59. 2QZ J142438.9–022739 (= Vir)

Marsh et al. (2002) also confirm 2QZ J142438.9–022739 as a polar and list the period as 0.1555 days, again with several one cycle per day aliases possible. Phasing the data with this period results in a nonsymmetric light curve. We found that using an orbital period of 0.160 days results in a smoother light curve (not shown), but one that remains quite noisy. 2QZ J142438.9–022739 shows dramatic variability at all wavelengths in the SDSS database. Like the previous two targets, the variations in *W1* suggest cyclotron emission from a field with $B \leqslant 38$ MG.

3.60. Blends

There are several sources listed in Table 1 that were bright enough to be detected by *WISE*, but which were blended with nearby objects. These polars are indicated in the last column of Table 1 with the word "Blend." CV Hyi is the first of these sources. Even though this source is heavily blended, there do
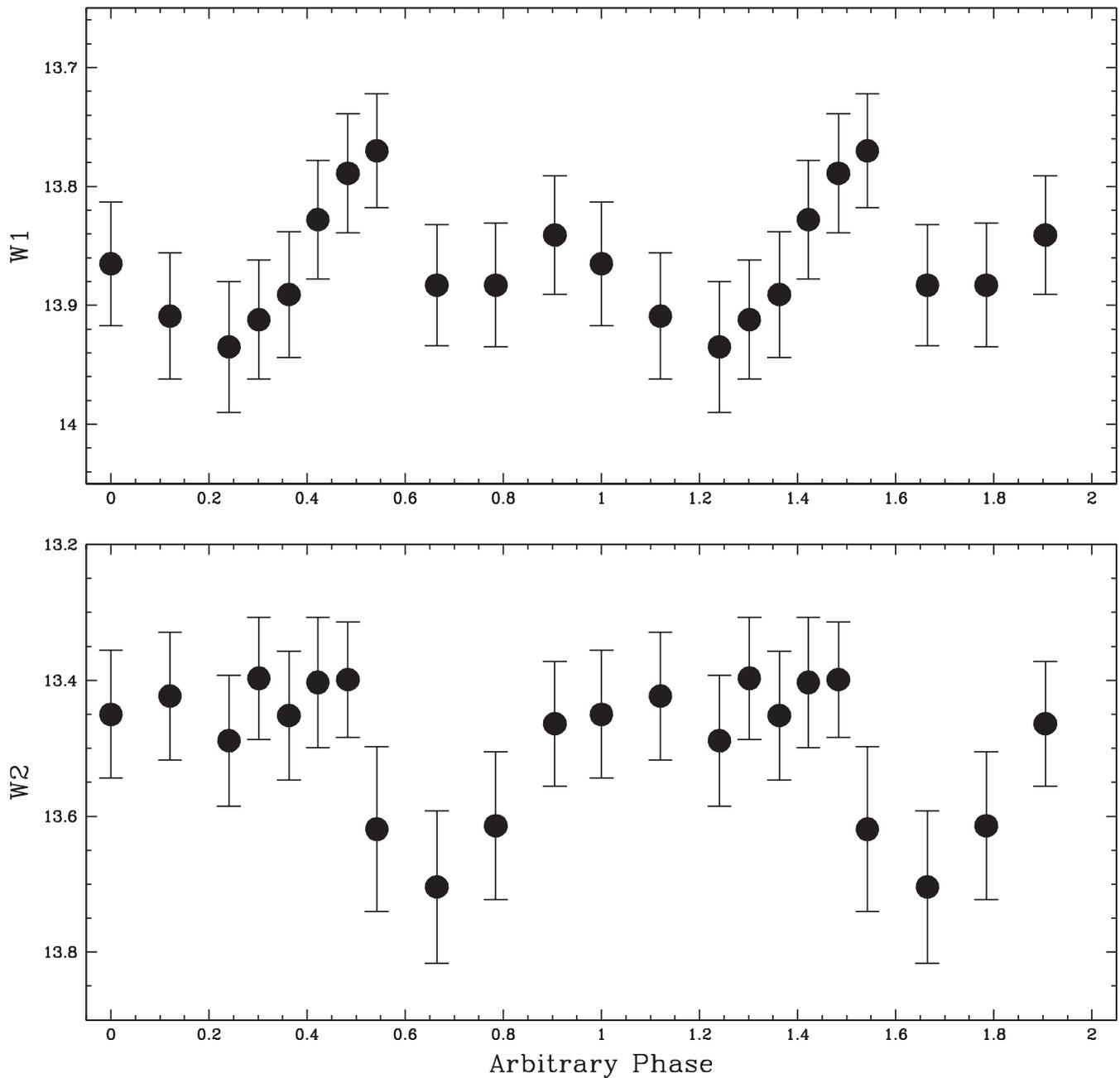
Figure 68. *WISE* data for RXJ0502.8+1624 phased to an orbital period of 90 minutes. The orbital period for this source is unknown, but periods of 90 and 180 minutes produce smooth *WISE* light curves.

appear to be variations present of sufficient amplitude to affect the light curve of its nearby (presumably nonvariable) neighbor. A similar story is true for HY Eri. The coordinates of the single-exposure light curve data are scattered in RA and Declination, and it is impossible to decipher which source they are associated with. Clearly, however, there is a variable source here. The position of HY Eri in the Allwise Point Source catalog *is* associated with the correct object, though its fluxes are suspect. RXJ0154.0–5947 is blended with a much brighter source, but there is a single-exposure detection that appears to be associated with this source. The magnitudes listed in Table 1 for RXJ0154.0–5947 are from this single detection in the four-band light curve data.

4. DISCUSSION AND CONCLUSIONS

We have extracted single-exposure *WISE* light curve data for a large sample of polars to estimate both field strengths, and we show that low-harmonic cyclotron emission appears to be a common feature of these objects. Although the derivations of field strengths from photometry alone cannot lead to very precise constraints, they certainly can provide insight that can be employed when planning future observations. In some cases, such as AI Tri, the existing multiwavelength data set is sufficient to provide tight constraints on the field strength for one of the cyclotron emission regions, as well as provide limits on the strength of the secondary pole. Clearly, large-amplitude, periodic variations in the *WISE* bandpasses imply cyclotron
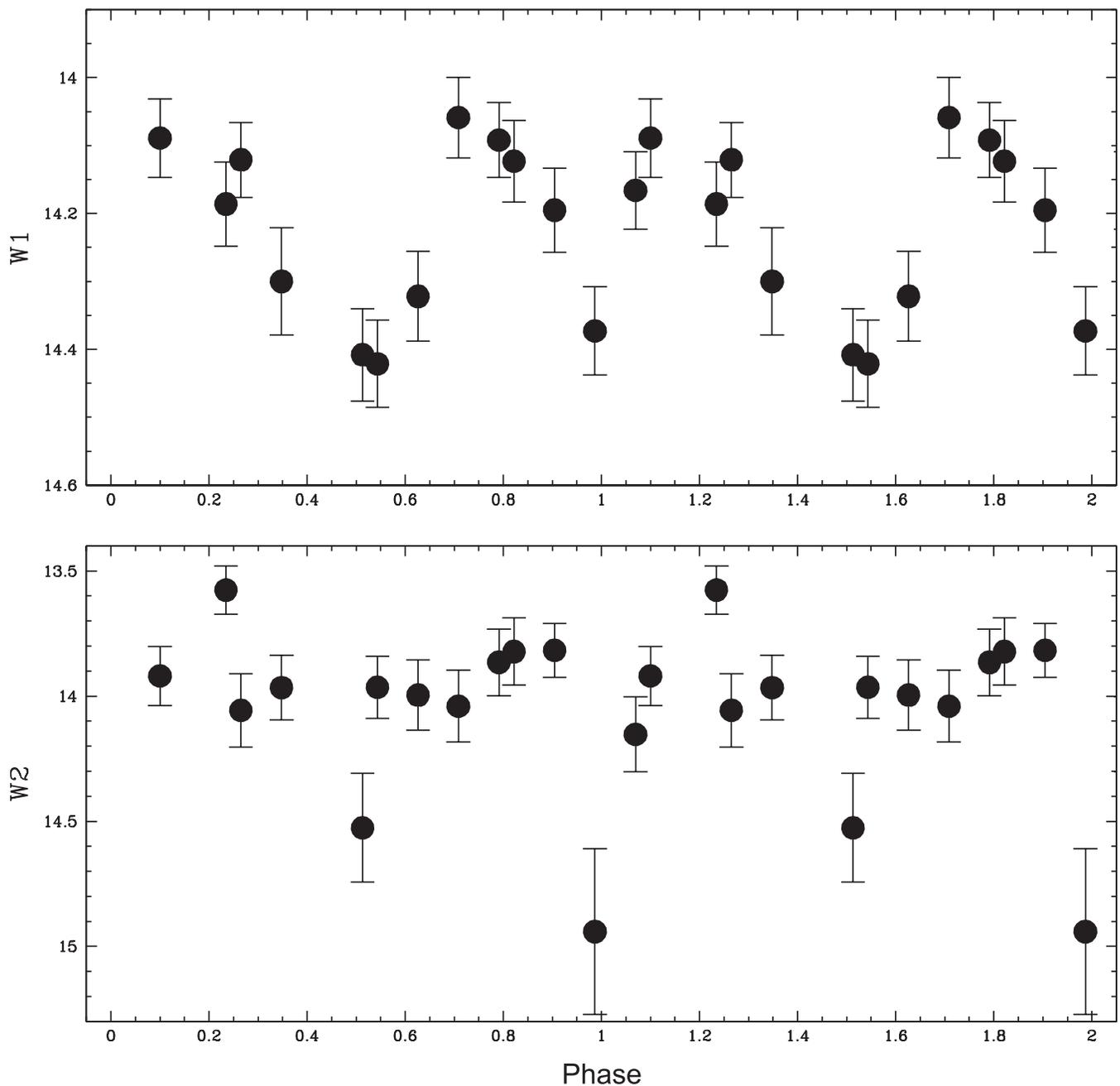
Figure 69. *WISE* data for RXJ0649.8–0737 phased to its suggested orbital period of 4.4 hr (Motch et al. 1998) and plotted to put the deepest minimum near $\phi = 0.0$.

emission. Thus, with this assumption, even low S/N light curve data can yield limits on the field strengths for a number of polars where no such estimates exist. Additionally, we have found that many of the published field strengths for polars are clearly inconsistent with the *WISE* light curve data. It is possible that for a few of these objects cyclotron emission from a second, lower field strength pole could explain the observations. However, the presence of phasing and morphology in the *WISE* light curves identical to those seen at shorter wavelengths is only logically consistent with a field strength different than that which had been previously derived for the source. Alternatively, as noted above for several sources, two regions of dramatically different field strength could be located at similar longitudes.

We summarize our conclusions about the field strengths of the program polars in Table 6. While the majority of these were derived from the *WISE* light curve data, some of these values have been estimated through the incorporation of data sets at other wavelengths. This is *always* true for any field strengths we derived where $B \geqslant 38$ MG. The second column of this table lists the previously published field strengths for these objects. The references to these values are contained within the discussion section for each of the objects and will not be repeated here. The third column lists our new estimates for the dominant field strength. When there is information on both poles, the data for the two poles are separated by a "/." When our results were consistent with previously published results, we simply mirror the previous result. For several polars, there
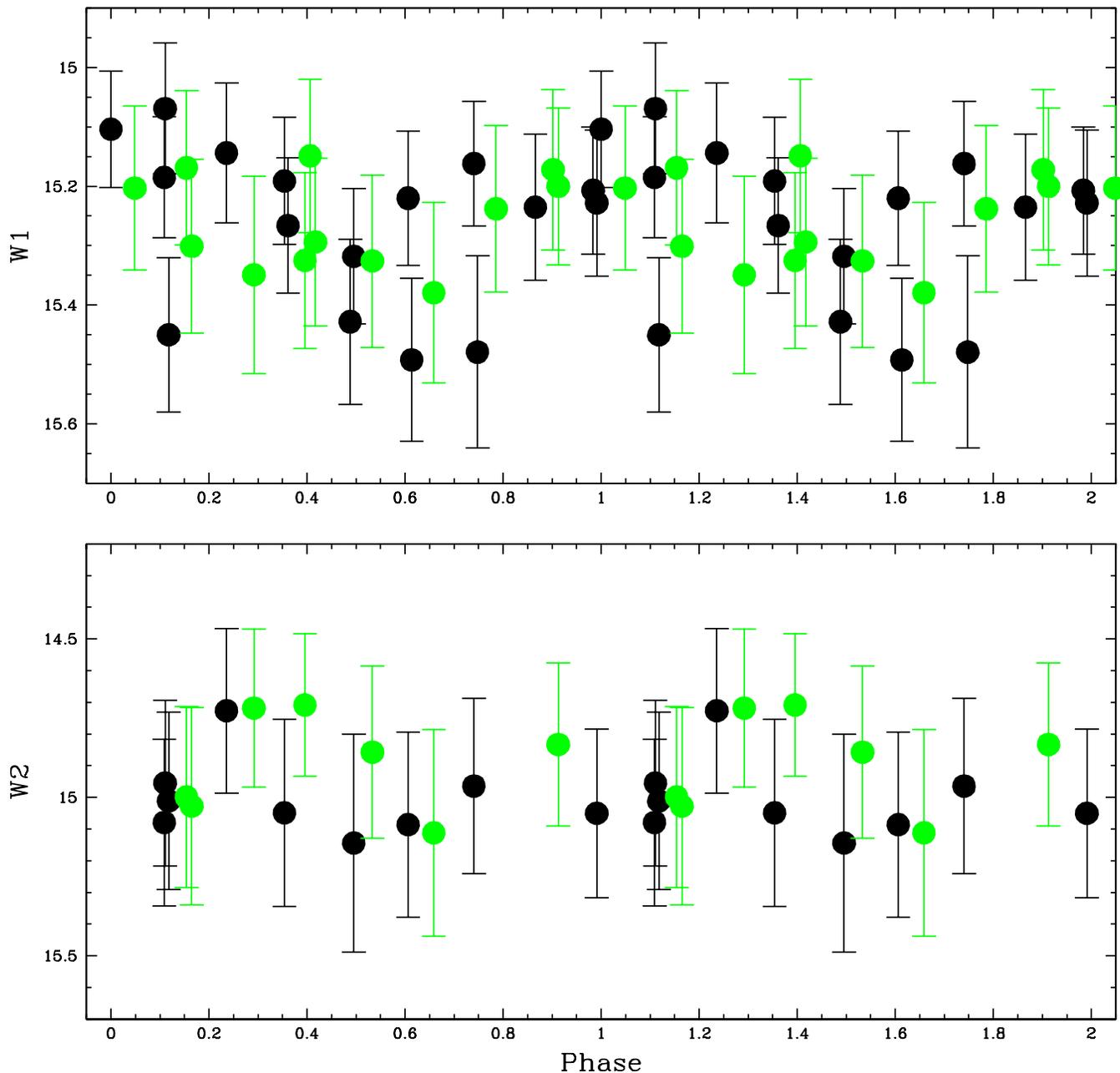
Figure 70. *WISE* four-band (black) and three-band (green) data for 1RXSJ0600-270918 phased to an orbital period of 0.0757 days.

Table 5
Herschel Data for AM Her

Obs. Date (UT)	70 μm (mJy)	160 μm (mJy)
2011 May 27 15:21:29	4.78 ± 0.68	7.73 ± 2.00

appear to be two field strengths present at the same phase as the "secondary pole." We list these field strengths separated by an ampersand. The fourth column lists whether cyclotron emission from the fundamental harmonic was suspected, and whether the amplitude of the variability (typically, $\Delta m \geqslant 0.7$ mag) indicated whether the fundamental harmonic appeared to be optically thin or partially optically thick. There were a few cases, such as V1432 Aql, where the light curves suggested that

the harmonics were completely optically thick, but to get significant orbitally modulated variation in the flux from the cyclotron fundamental requires it to be *partially* thick. The final column lists the state of the system at the time of the *WISE* observations. Colons indicate uncertain values.

As noted in the introduction, the presence of large-amplitude variations in the high-state *W*3 light curve of AM Her was surprising, and it implies that fundamental harmonic cyclotron emission can exist regardless of the mass transfer rate. This result is reinforced by the results listed in Table 6. There are a number of polars that were in high states in which apparent cyclotron emission from the $n = 1$ harmonic was observed. In fact, Table 6 shows that, for every system in which the fundamental harmonic cyclotron emission fell within the *WISE* bandpasses, large amplitude variability was detected. This suggests that the common assumption that polar accretion

Table 6
Polar Field Strengths

Object	B_1/B_2 (Published)	B_1/B_2 (WISE)	$n = 1?$ (Thick or Thin)	State
AI Tri	32, 38/40–41	32/73	Yes, thin	Intermediate
AM Her	13.6	12	Yes, thick	High
AN UMa	32	32	Yes, thin	Low
AR UMa	155	155–170	…	…
BL Hyi	12, 23	12	Yes, thin	…
BY Cam	40, 28	28	Yes, thin	…
CD Ind	11	11	Yes, thick	…
CP Tuc	17	~16	…	…
CW Hyi	13:	~20	Yes, thick	…
EP Dra	16	15	…	Low
EQ Cet	34	34	Yes, …	Low
FL Cet	29	29	Yes, thick	Low
GG Leo	23 ± 3	23	…	Low
HS Cam	…	8:	…	…
HU Aqr	37	31.5	Yes, thin	High?
IW Eri	…	⩽32	Yes, thin	High
LW Cam	…	~20	…	Low
MN Hya	20	28:	Yes, thin	…
MR Ser	25.8–28	27.2	Yes:, thin	Low
QS Tel	70, 47	35	Yes, thin	…
UW Pic	19	11:	…	High
UZ For	55/28, 75, 57	57/28	Yes, thick/thin	High?
VV Pup	32/54	30/54 & 30	Yes, thick	High
V347 Pav	25	29/7	Yes, …	Low
V349 Pav	20	28	Yes, thick	…
V379 Vir	7	7	…	…
V381 Vel	52, 42	⩽42	Yes, thin	…
V393 Pav	16	16	…	…
V516 Pav	39	39	Yes, thin	…
V834 Cen	23, 31/?	30 & 11	Yes, thick	…
V884 Her	150	150 & 30	Yes:, thick	…
V895 Cen	…	⩽13	…	…
V1007 Her	50	⩽30	Yes, thick	…
V1033 Cen	15–40	⩾36	…	…
V1043 Cen	56	28	Yes, thin	…
V1309 Ori	63	~27	Yes, thick	…
V2301 Oph	7	7	…	High
WW Hor	25	~30	Yes, thick	…
RBS490	…	11.5:	…	…
RXJ0649.8–0737	…	⩽26	…	…
RXJ0859.1+0537	…	⩾35, ⩽20	…	…
RXJ0953.1+1458	…	⩽30	…	…
RXJ1002–1925	…	32	Yes, thin	…
RXJ2316–0527	20–30	25	…	…
2QZ J142256.3–022108	…	⩽38	…	…
2QZ J142438.9–022739	…	⩽38	…	…

columns are completely optically thick in the lowest cyclotron harmonics is incorrect. As noted in Schmidt et al. (2001), such emission "presumably arises in a low-ṁ tail of low optical depth."

4.1. The Strong W3 Excesses of Polars

One of the surprising results from this survey is the relative brightness of these objects at 11.5 μm (though the error bars on the W3 fluxes for many of these systems are quite large). While circumbinary dust was invoked to explain the odd SEDs of polars observed by *Spitzer* (e.g., Howell et al. 2006a; Brinkworth et al. 2007; Hoard et al. 2007), we have shown in the preceding that the unusual SEDs of each of the polars in

those studies resulted from cyclotron emission. The origin of the W3 "excesses" seen here is not as obvious. Figure 1 shows that there are only a few polars that have colors consistent with main sequence stars. As shown in Table 6, nine of the targets with fields low enough to put the fundamental harmonic in W3 were detected in this bandpass. Only two faint systems with low fields, HS Cam and V379 Vir, were not detected in W3. What is interesting (see Figure 1) is that all of the systems where we expect cyclotron emission to be present in the W3 bandpass, except ST LMi, tend to be the redder systems in (W1 − W2), while spanning the observed color range in (W2 − W3). All are found on the right-hand side of the color–color diagram. As discussed above, at the time of the *WISE*
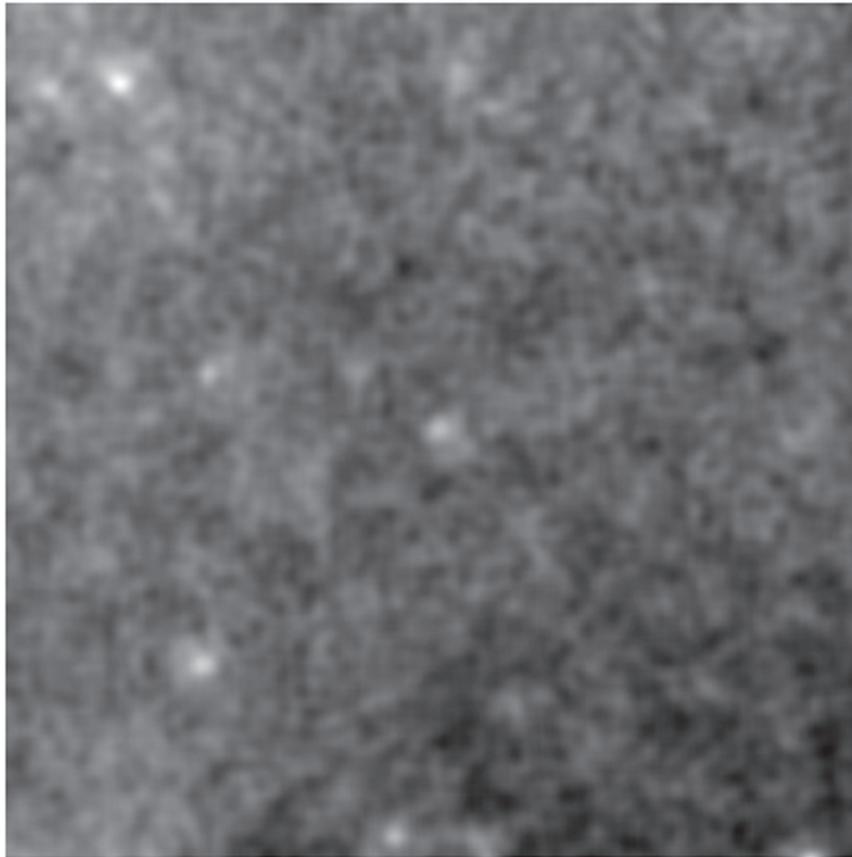
Figure 71. *WISE W*4-band image for V834 Cen (center).

observations, ST LMi did not appear to have *the expected cyclotron emission* present in either the *W*1 or *W*2 bands, suggesting that it was in an extreme low state. We conclude that the *W*3 excesses seen in most polars are probably not due to cyclotron emission from low field regions. This finding is amplified by the *W*3 light curves of several higher field sources (e.g., AI Tri, V884 Her), where there was little evidence for variability.

One possible source of long wavelength emission is bremsstrahlung from the accretion stream. We have two prepolars in our sample of objects, WX LMi and HS0922 +1333. These objects are expected to have very low mass transfer rates and thus are expected to have the weakest accretion streams. Fortunately, both of these prepolars have field strengths that preclude cyclotron emission in the *WISE* bandpasses. HS0922+1333 has a (*W*2 − *W*3) color consistent with its secondary star, while WX LMi has (*W*2 − *W*3) = 0.77. These two objects join V895 Cen (a low-field polar with suspected cyclotron emission in the *WISE* bandpasses) in having the bluest *WISE* colors. The accretion stream explanation for the long wavelength excesses is strengthened by observations of VY For and V1043 Cen. If the Beuermann et al. (1989) scenario for the system geometry of VY For is correct, the only obvious variable source in the mid-IR for this system would be the accretion stream. In V1043 Cen, the *W*3 light curve during its low state was nonvariable, but in the high state, this light curve showed random, large-scale variability ($\Delta W3 > 1$ mag). This change in behavior could be explained as an increase in a clumpy mass flow through the accretion stream. This type of variability is also one method to rule out

circumbinary dust emission, as it is difficult to imagine how large changes on short timescales can be accomplished with realistic dust distributions.

There were three polars detected in the *W*4 band: AM Her, V834 Cen, and V2301 Oph. These sources could provide insight into whether bremsstrahlung can explain the *W*3 excesses. They have the following (*W*3 − *W*4) colors, respectively: 1.07, 1.74, and 1.07. We explored the SED of AM Her in Figure 11 and found that a free–free component could explain the long-wavelength fluxes of this source. Obviously, such an explanation is viable for V2301 Oph. We believe that the mean (*W*3 − *W*4) color for V834 Cen is suspect. As shown in Figure 53, V834 Cen underwent a transition in brightness between the two four-band epochs of observation. The mean *W*1, *W*2, and *W*3 magnitudes dropped by 0.4 mag between the two sets of data. Since we believe that all three bands are contaminated by cyclotron emission, it is not clear if the *W*4 band flux would show the same decline if it was not also associated with cyclotron emission. The *W*3-band light curve also shows a large range in brightness over an orbit. During the faintest portion of the light curve, *W*3 = 11.5. The typical 3σ limit for a *W*4 detection is *W*4 = 8.6. If the color remained constant over the orbit, V834 Cen would be well below the *W*4 detection limit for at least a third of the orbit. Therefore it seems likely that the *W*4 flux is probably weighted by the brightest portions of the light curve of V834 Cen, and it is difficult to estimate the true (*W*3 − *W*4) color. Additionally, the *WISE W*4 imaging data, shown in Figure 71, suggest that there are several faint sources located near V834 Cen that could corrupt the cataloged fluxes. Thus, it is probable that all three of the

polars detected in the *W*4 bandpass could have SEDs that are consistent with a weak ($\sim$1% $L_{\rm opt}$) bremsstrahlung component.

Another possible source for the long-wavelength excesses is synchrotron or gyrosynchrotron emission. Mason & Gray (2007) summarize the radio detections of four polars (AM Her, AR UMa, V834 Cen, and ST LMi). Only AM Her has been shown to be a persistent radio source. Chanmuam & Dulk (1982) observed a very large, 100% circularly polarized flare at 4.9 GHz from AM Her, which they ascribed to a gyrosynchrotron source. Both Chanmugam & Dulk and Mason & Gray suggest that this gyrosynchrotron emission arises near the surface of the secondary star in these systems, where fields of a few thousand Gauss are expected to occur. Gyrosynchrotron radiation in the mid-IR, however, does not appear to be plausible. Recent observations of both IPs and nonmagnetic CVs in the mid-IR (Harrison et al. 2007, 2010; Harrison 2014) have provided evidence for synchrotron emission from these sources. In the case of each of those objects, however, accretion disks are present. As discussed in Harrison (2014), such structures are believed to play an integral role in the formation of the magnetic fields that both confine and accelerate material in the relativistic outflows observed for X-ray binaries. It is not clear if the conditions required for synchrotron emission exist within the typical polar. In any case, such emission has a more transient nature and, except for V2301 Oph (see Figure 62), none of the *W*3 light curves appeared to show the large-scale flaring events that have been attributed to synchrotron emission in the other CVs. It is interesting that V2301 Oph was one of the three polars detected in the *W*4 band.

Whatever the nature of the *W*3 excesses from these objects, it is clear that mid-IR observations of polars are extremely worthwhile. Future observations with the *James Webb Space Telescope* should be able to resolve any outstanding mysteries, while being capable of supplying phase-resolved mid-IR spectroscopy that will allow for the derivation of the properties in the regions that produce low-harmonic cyclotron emission. Such observations are crucial for understanding how mass is accreted by magnetic white dwarfs, especially where the field topology is more complex than a simple dipole.

REFERENCES

Andronov, I. L., Baklanov, A. V., & Burwitz, V. 2006, A&A, 452, 941
Arnaud, K. A. 1996, in ASP Conf. Ser. 101, Astronomical Data Analysis Software and Systems V, ed. G. Jacoby & J. Barnes (San Francisco, CA: ASP), 19
Bailey, J., Axon, D. J., Hough, J. H., et al. 1983, MNRAS, 205, 1
Bailey, J. A., Ferrario, L., Wickramasinghe, D. T., Buckley, D. A. H., & Hough, J. H. 1995, MNRAS, 272, 579
Balog, Z., Müller, T., Laas, U., et al. 2014, ExA, 37, 129
Baraffe, I., & Kolb, U. 2000, MNRAS, 318, 345
Beuermann, K., & Burwitz, V. 1995, in ASP Conf. Ser. 85 Magnetic Cataclysmic Variables, ed. D. A. H. Buckley & B. Warner (San Francisco, CA: ASP), 99
Beuermann, K., Euchner, F., Reinsch, K., Jordan, S., & Gänsicke, B. T. 2007, A&A, 463, 647
Beuermann, K., Thomas, H.-C., Giommi, P., Tagliaferri, G., & Schwope, A. D. 1989, A&A, 219, L7
Beuermann, K., Thomas, H.-C., Reinsch, K., et al. 1999, A&A, 347, 47
Beuermann, K. S., & Schwope, A. D. 1989, A&A, 223, 179
Bonnet-Bidaud, J. M., Mouchet, M., Somova, T. A., & Somov, N. N. 1996, A&A, 306, 199
Bours, M. C. P., Marsh, T. R., Breedt, E., et al. 2014, MNRAS, 445, 1924
Bridge, C. M., Cropper, M., Ramsay, G., de Bruijne, J. H. J., Reynolds, A. P., & Perryman, M. A. C. 2003, MNRAS, 341, 863
Brinkworth, C. S., Hoard, D. W., Wachter, S., et al. 2007, ApJ, 659, 1541
Buckley, D. A. H., Ferrario, L., Wickramasinghe, D. T., & Bailey, J. A. 1998, MNRAS, 295, 899
Burleigh, M. R., Marsh, T. R., Gänsicke, B. T., Goad, M. R., et al. 2006, MNRAS, 373, 1416
Burwitz, V., Reinsch, K., Schwope, A. D., & Hakala, P. J. 1998, A&A, 331, 262
Campbell, R. K. 2008, PhD thesis, New Mexico State Univ.
Campbell, R. K., Harrison, T. E., & Kafka, S. 2008a, ApJ, 683, 409
Campbell, R. K., Harrison, T. E., Mason, E., Howell, S. B., & Schowpe, A. D. 2008b, ApJ, 678, 1304
Campbell, R. K., Harrison, T. E., Schowpe, A. D., & Howell, S. B. 2008c, ApJ, 672, 531
Catalán, M. S., Schwope, A. D., & Smith, R. C. 1999, MNRAS, 310, 123
Chanmugam, G., & Dulk, G. A. 1981, ApJ, 244, 569
Chanmugam, G., & Dulk, G. A. 1982, ApJL, 255, 107
Cropper, M. 1987, MNRAS, 228, 389
Cropper, M., Mason, K. O., Allington-Smith, J. R., Branduardi-Raymont, G., et al. 1989, MNRAS, 236, 29
Dai, Z.-B., Quian, S.-B., Fernández, L., & Baume, G. L. 2010, MNRAS, 409, 1195
Debes, J. H., López-Morales, M., Bonanos, A. Z., & Weinberger, A. J. 2006, ApJ, 647, 147
Diaz, M. P., & Cieslinski, D. 2009, AJ, 137, 296
Downes, R. A., Webbink, R. F., Shara, M. M., et al. 2001, PASP, 113, 764
Epchtein, N., de Batz, B., Copet, E., et al. 1994, ApSS, 217, 3
Farihi, J., Burleigh, M. R., & Hoard, D. W. 2008, ApJ, 674, 421
Fazio, G. G., Hora, J. L., Allen, L. E., et al. 2004, ApJS, 154, 10
Ferrario, L., Bailey, J., & Wickramasinghe, D. 1996, MNRAS, 282, 218
Ferrario, L., Wickramasinghe, D. T., Bailey, J., & Buckley, D. 1995, MNRAS, 273, 17
Ferrario, L., Wickramasinghe, D. T., Bailey, J., Touhy, I. R., & Hough, J. H. 1989, ApJ, 337, 832
Ferrario, L., Wickramasinghe, D. T., & Schmidt, G. 2003, MNRAS, 338, 340
Fischer, A., & Beuermann, K. 2001, A&A, 373, 211
Frieman, J. A., Bassett, B., Becker, A., et al. 2008, AJ, 135, 338
Gänsicke, B. T., Beuermann, K., de Martino, D., & Thomas, H.-C. 2000, A&A, 354, 605

Gänsicke, B. T., Jordan, S., Beuermann, K., et al. 2004, ApJ, 613, 141
Gänsicke, B. T., Schmidt, G. D., Jordan, S., & Szkody, P. 2001, ApJ, 555, 380
González-Buitrago, D., Tovmassian, G., Zharikov, S., et al. 2013, A&A, 553, 28
Greiner, J., Remillard, R. A., & Motch, C. 1998a, A&A, 336, 191
Greiner, J., & Schwarz, R. 1998, A&A, 340, 129
Greiner, J., Schwarz, R., & Wenzel, W. 1998b, MNRAS, 296, 437
Harrison, T. E. 2014, ApJL, 791, L18
Harrison, T. E., Bornak, J., Howell, S. B., et al. 2009, AJ, 137, 4061
Harrison, T. E., Bornak, J., Rupen, M. P., & Howell, S. B. 2010, ApJ, 710, 325
Harrison, T. E., Campbell, R. D., & Lyke, J. E. 2013a, AJ, 146, 37
Harrison, T. E., Campbell, R. K., Howell, S. B., Cordova, F. A., & Schwope, A. D. 2007, ApJ, 656, 444
Harrison, T. E., Gelino, D. M., Buxton, M., & Fost, T. 2014, AJ, 148, 22
Harrison, T. E., Hamilton, R. T., Tappert, C., Hoffman, D. I., & Campbell, R. K. 2013b, AJ, 145, 19
Harrison, T. E., Howell, S. B., Szkody, P., & Cordova, F. A. 2005, ApJ, 632, L123
Howell, S. B., Ciardi, D. R., Dhillon, V. S., & Skidmore, W. 2000, ApJ, 530, 904
Howell, S. B., Harrison, T. E., Szkody, P., & Silvestri, N. M. 2010, AJ, 139, 1771
Helton, L. A., Gehrz, R. D., Woodward, C. E., et al. 2012, ApJ, 755, 37
Henden, A., & Munari, U. 2014, CoSka, 43, 518
Hilton, E. J., Szkody, P., Mukadam, A., et al. 2009, AJ, 137, 3606
Hoard, D. W., Howell, S. B., Brinkworth, C. S., Ciardi, D. R., & Wachter, S. 2007, ApJ, 671, 734
Honeycutt, R. K., & Kafka, S. 2005, MNRAS, 364, 917
Howell, S. B., Brinkworth, C., Hoard, D. W., et al. 2006a, ApJ, 646, 65
Howell, S. B., Gelino, D. M., & Harrison, T. E. 2001, AJ, 121, 482
Howell, S. B., Harrison, T. E., Campbell, R. K., Cordova, F. A., & Szkody, P. 2006b, AJ, 131, 2216
Howell, S. B., Harrison, T. E., Huber, M. E., et al. 2008, AJ, 136, 2541
Hubeny, I. 1988, CoPhC, 52, 103
Ibar, E., Ivison, R. J., Cava, A., et al. 2010, MNRAS, 409, 38
Jarret, T. H., Cohen, M., Masci, F., et al. 2011, ApJ, 735, 112
Kafka, S., & Honeycutt, R. K. 2003, AJ, 125, 2188
Kafka, S., & Honeycutt, R. K. 2005, AJ, 130, 742
Katajainen, S., Scaltriti, F., Piirola, V., Lehto, H. J., & Anderlucci, E. 2001, A&A, 372, 945
Krzesinski, J., Kleinmann, S. J., Nitta, A., Hügelmeyer, S., et al. 2009, A&A, 508, 339
Lawrence, A., Warren, S. J., Almaini, O., et al. 2007, MNRAS, 379, 1599
Liebert, J., Stockman, H. S., Angel, J. R. P., et al. 1978, ApJ, 225, 201
Linnell, A. P., Szkody, P., Plotkin, R. M., et al. 2010, ApJ, 713, 1183
Makovoz, D., Roby, T., Khan, I., & Booth, H. 2006, Proc. SPIE, 6274, 10
Marsh, T. R., Morales-Rueda, L., Steeghs, D., et al. 2002, in ASP Conf. Ser. 261, The Physics of Cataclysmic Variables and Related Objects, ed. B. T. Gänsicke, K. Beuermann & K. Reinsch (San Francisco, CA: ASP), 200
Mason, E., Wickramasinghe, D., Howell, S. B., & Szkody, P. 2007, A&A, 467, 281
Mason, P. A., & Gray, C. L. 2007, ApJ, 660, 662
Motch, C., Guillot, P., Haberl, F., et al. 1998, A&AS, 132, 341
Patterson, J., Skillman, D. R., Thorstensen, J., & Hellier, C. 1995, PASP, 107, 307
Pavlenko, E., Babina, J., & Andreev, M. 2007, in ASP Conf. Ser. 372, 5th European Workshop on White Dwarfs (San Francisco, CA: ASP), 537
Pavlenko, E., Shugarov, S. Yu, Katysheva, N. A., et al. 2007, in ASP Conf. Ser. 372, White Dwarfs, ed. R. Napiwotzki & M. R. Burleigh (San Francisco, CA: ASP), 511
Potter, S. B., Romero-Colmenero, E., Watson, C. A., Buckley, D. A. H., & Phillips, A. 2004, MNRAS, 348, 316
Predehl, P., & Schmitt, J. H. M. M. 1995, A&A, 293, 889
Qian, S.-B., Liu, L., Liao, W.-P., Li, L.-J., et al. 2011, MNRAS, 414, 16
Ramaty, R. 1969, ApJ, 158, 753
Ramsay, G., & Cropper, M. 2003, MNRAS, 338, 219
Ramsay, G., & Cropper, M. 2007, MNRAS, 379, 1209
Ramsay, G., Cropper, M., Mason, K. O., Cordova, F. A., & Priedhorsky, W. 2004, MNRAS, 347, 95
Ramseyer, T. F. 1994, ApJ, 425, 243
Reimers, D., & Hagen, H.-J. 2000, A&A, 358, L45
Reinsch, K., Burwitz, V., Beuermann, K., Schwope, A. D., & Thomas, H.-C. 1994, A&A, 291, L27
Reinsch, K., Kim, Y., & Beuermann, K. 2006, A&A, 457, 1043
Rieke, G. H., Young, E. T., Cadien, J., et al. 2004, Proc. SPIE, 5487, 50
Ritter, H., & Kolb, U. 2003, A&A, 404, 301

Rodrigues, C. V., Cieslinski, D., & Steiner, J. E. 1998, A&A, 335, 979
Rodrigues, C. V., Jablonski, F. J., D'Amico, F., et al. 2006, MNRAS, 369, 1972
Romero-Colmenero, E., Potter, S. B., Buckley, D. A. H., Barrett, P. E., & Vrielmann, S. 2003, MNRAS, 339, 685
Sambruna, R. M., Chiappetti, L., Treves, A., et al. 1991, ApJ, 374, 744
Schafter, A. W., Reinsch, K., Beuermann, K., et al. 1995, ApJ, 443, 319
Schmidt, G. D., Ferrario, L., Wickramasinghe, D. T., & Smith, P. S. 2001, ApJ, 553, 823
Schmidt, G. D., Harris, H. C., Liebert, J., Eisenstein, D. J., et al. 2003, ApJ, 595, 1101
Schmidt, G. D., Liebert, J., & Stockman, H. S. 1995, ApJ, 441, 414
Schmidt, G. D., & Stockman, H. S. 1991, ApJ, 371, 749
Schmidt, G. D., Szkody, P., Homer, L., et al. 2005a, ApJ, 620, 422
Schmidt, G. D., Szkody, P., Silvestri, N. M., Cushing, M. C., et al. 2005b, ApJ, 630, 173
Schmidt, G. D., Szkody, P., Smith, P. S., et al. 1996, ApJ, 473, 483
Schmidt, G. D., Szkody, P., Vanlandingham, K. M., et al. 2005b, ApJ, 630, 1037
Schmidt, G. D., Szkody, P., Vanlandingham, K. M., et al. 2005c, ApJ, 630, 1037
Schwarz, R., & Greiner, J. 1999, ASPC, 157, 139
Schwarz, R., Schwope, A. D., Beuermann, K., et al. 1998, A&A, 338, 465
Schwarz, R., Schwope, A. D., Staude, A., & Remillard, R. A. 2005, A&A, 444, 213
Schwope, A., & Beuermann, K. 1987, ApSS, 131, 637
Schwope, A. D. 1990, RvMA, 3, 44
Schwope, A. D. 1995, RvMA, 8, 125
Scwhope, A. D., & Beuermann, K. 1990, A&A, 238, 173
Schwope, A. D., & Beuermann, K. 1997, AN, 318, 111
Schwope, A. D., Beuermann, K., & Jordan, S. 1995a, A&A, 301, 447
Schwope, A. D., Beuermann, K., Jordan, S., & Thomas, H.-C. 1993a, A&A, 278, 487
Schwope, A. D., Beuermann, K., & Thomas, H.-C. 1990, A&A, 230, 120
Schwope, A. D., Brunner, H., Buckley, D., et al. 2002, A&A, 396, 895
Schwope, A. D., Buckley, D. A. H., O'Donoghue, D., et al. 1997, A&A, 326, 195
Schwope, A. D., Catalán, M. S., Beuermann, K., et al. 2000, MNRAS, 313, 533
Schwope, A. D., Horne, K., Steeghs, D., & Still, M. 2011, A&A, 531, 34
Schwope, A. D., & Mengel, S. 1997, AN, 318, 25
Schwope, A. D., Schreiber, M. R., & Szkody, P. 2006, A&A, 452, 955
Schwope, A. D., Staude, A., Koester, D., & Vogel, J. 2007, A&A, 469, 1027
Schwope, A. D., Thomas, H.-C., & Beuermann, K. 1993b, A&A, 271, L25
Schwope, A. D., Thomas, H.-C., Beuermann, K., et al. 1995b, A&A, 293, 764
Schwope, A. D., Thomas, H.-C., Beuermann, K., & Reinsch, K. 1993c, A&A, 267, 103
Skrutskie, M. F., Cutri, R. M., Stiening, R., Weinberg, M. D., et al. 2006, AJ, 131, 1163
Shafter, A. W., Reinsch, K., Beuermann, K., Misselt, K. A., et al. 1995, ApJ, 443, 319
Slavin, A. J., O'Brien, T. J. O., & Dunlop, J. S. 1995, MNRAS, 276, 353
Staude, A., Schwope, A. D., & Schwarz, R. 2001, A&A, 374, 588
Stobie, R. S., Okeke, P. N., Buckley, D. A. H., & O'Donoghue, D. 1996, MNRAS, 283, L127
Szkody, P., Henden, A., Fraser, O. J., et al. 2005, AJ, 129, 2386
Szkody, P., Silber, A., Hoard, D. W., et al. 1995, ApJL, 455, L43
Thomas, H.-C., Beuermann, K., Burwitz, V., Reinsch, K., & Schwope, A. D. 2000, A&A, 353, 646
Thomas, H.-C., Beuermann, K., Reinsch, K., et al. 2012, A&A, 546, 104
Thomas, H.-C., Beuermann, K., Schwope, A. D., & Burwitz, V. 1996, A&A, 313, 833
Thomas, H.-C., & Reinsch, K. 1996, A&A, 315, L1
Thorstensen, J. R., & Fenton, W. H. 2002, PASP, 114, 74
Thorstensen, J. R., Fenton, W. H., Patterson, J. O., et al. 2002, ApJL, 567, L49
Thorstensen, J. R., Lépine, S., & Shara, M. 2006, PASP, 118, 1238
Tovmassian, G. H., Greiner, J., Schwope, A. D., et al. 2000, ApJ, 537, 927
Tovmassian, G. H., Greiner, J., Zickgraf, F.-J., et al. 1997, A&A, 328, 571
Tovmassian, G. H., Szkody, P., Greiner, J., et al. 2001, A&A, 379, 199
Traulsen, I., Reinsch, K., Schwarz, R., et al. 2010, A&A, 516, 76
Vennes, S., Wickramasinghe, D. T., Thorstensen, J. R., et al. 1996, A&A, 100, 7
Visvanathan, N., & Wickramasinghe, D. T. 1979, Natur, 261, 47
Vogel, J., Schwope, A. D., & Gänsicke, B. T. 2007, A&A, 464, 647
Vogel, J., Schwope, A. D., & Schwarz, R. 2011, A&A, 530, 117

Walker, M. 1965, MiKon, 57, 1

Wickramasinghe, D. T., Ferrario, L., Bailey, J. A., et al. 1993, MNRAS, 265, L29

Wilson, R. E., & Devinney, E. J. 1971, ApJ, 166, 605

Wittenmyer, R. A., Horner, J., Marshall, J. P., Butters, O. W., & Tinney, C. G. 2012, MNRAS, 419, 3258

Wolff, M. T., Wood, K. S., Imamura, J. N., et al. 1999, ApJ, 526, 435

Woudt, P. A., Warner, B., & Pretorius, M. L. 2004, MNRAS, 351, 1015

Wright, E. L., Eisenhardt, P. R. M., Mainzer, A. K., et al. 2010, AJ, 140, 1868

York, D. G., Adelman, J., Anderson, J. E., et al. 2000, AJ, 120, 1579

Yuan, H. B., Liu, X. W., & Xiang, M. S. 2013, MNRAS, 430, 2188